Titre: Title:	Développement et analyse du procédé d'injection flexible pour la mise en forme de pièces composites fortement courbées
Auteur: Author:	Philippe Causse
Date:	2011
Type:	Mémoire ou thèse / Dissertation or Thesis
Référence: Citation:	Causse, P. (2011). Développement et analyse du procédé d'injection flexible pour la mise en forme de pièces composites fortement courbées [Ph.D. thesis, École Polytechnique de Montréal]. PolyPublie. https://publications.polymtl.ca/699/

URL de PolyPublie: PolyPublie URL:	https://publications.polymtl.ca/699/
Directeurs de recherche: Advisors:	François Trochu, & Eduardo-Antonio-Julian Ruiz
Programme: Program:	Génie mécanique

UNIVERSITÉ DE MONTRÉAL

DÉVELOPPEMENT ET ANALYSE DU PROCÉDÉ D'INJECTION FLEXIBLE POUR LA MISE EN FORME DE PIÈCES COMPOSITES FORTEMENT COURBÉES

PHILIPPE CAUSSE

DÉPARTEMENT DE GÉNIE MÉCANIQUE

ÉCOLE POLYTECHNIQUE DE MONTRÉAL

THÈSE PRÉSENTÉE EN VUE DE L'OBTENTION

DU DIPLÔME DE PHILOSOPHIAE DOCTOR

(GÉNIE MÉCANIQUE)

DÉCEMBRE 2011

UNIVERSITÉ DE MONTRÉAL

ÉCOLE POLYTECHNIQUE DE MONTRÉAL

Cette thèse intitulée:

DÉVELOPPEMENT ET ANALYSE DU PROCÉDÉ D'INJECTION FLEXIBLE POUR LA MISE EN FORME DE PIÈCES COMPOSITES FORTEMENT COURBÉES

Présentée par : CAUSSE Philippe

en vue de l'obtention du diplôme de : Philosophiae Doctor

a été dûment acceptée par le jury d'examen constitué de :

M. TURENNE Sylvain, Ph.D., président

M. TROCHU François, Ph.D., membre et directeur de recherche

M. RUIZ Eduardo Antonio Julian, Ph.D., membre et codirecteur de recherche

M. BOUKHILI Rachid, Ph.D., membre

M. PHAM Tan, Ph.D., membre

REMERCIEMENTS

Je tiens à remercier en premier lieu le professeur François Trochu de m'avoir donné l'opportunité de réaliser ce travail de thèse sous sa supervision. Ses intuitions et sa vision globale de la recherche ont grandement contribué à la réalisation de ce projet. J'apprécie tout particulièrement la confiance et la liberté d'action qu'il m'a accordées au cours de ces années de travail. Je remercie également mon codirecteur de recherche le professeur Eduardo Ruiz pour le dynamisme, la créativité et l'optimisme dont il a toujours fait preuve au cours de nos longues discussions. Je mesure aujourd'hui pleinement la pertinence des conseils qu'il m'a prodigués tout au long de mon travail.

J'ai eu la chance de réaliser ce travail de recherche au sein de l'équipe dynamique et chaleureuse de la Chaire sur les Composites à Haute Performance. Les collaborations et nombreux échanges réalisés avec tous les membres de ce laboratoire m'ont grandement aidé dans ma démarche de recherche. Je remercie particulièrement Bruno, Éric, Tarik, François, Paul, Mouhcine, Julian, Alex, ainsi que les stagiaires que j'ai eu la chance d'encadrer: David, Charles et Hermann.

Enfin, cette thèse n'aurait pas été possible sans toutes les personnes formidables que j'ai la chance de côtoyer dans ma vie de tous les jours. Merci donc à Julie, ma famille et mes amis.

RÉSUMÉ

Les polymères thermodurcissables renforcés par des fibres continues possèdent un potentiel unanimement reconnu pour la conception de pièces structurales à haute performance. Au cours des dernières décennies, ces matériaux composites ont notamment avantageusement remplacé les métaux et alliages dans de nombreuses applications aéronautiques. L'utilisation de tels composites reste en revanche limitée dans le secteur automobile. Les procédés de mise en forme usuels nécessitent des temps de cycle relativement longs qui sont en effet incompatibles avec la production en grande série.

L'injection flexible est une nouvelle méthode de mise en forme par injection sur renfort. Ce procédé vise principalement à abaisser le temps de fabrication pour augmenter les cadences de production. Le principe de fonctionnement repose sur l'utilisation d'un outillage dont la géométrie varie au cours du cycle de fabrication. Le procédé fait ainsi intervenir une membrane flexible et un fluide de compaction permettant d'imposer une déformation contrôlée à une des deux parois du moule. L'injection flexible est développée à l'École Polytechnique de Montréal depuis 2003 au sein de la Chaire sur les Composites à Haute Performance. Les travaux déjà réalisés ont démontré le potentiel du procédé en termes de gain de temps et de qualité d'imprégnation pour des géométries simples. Le présent travail de thèse vise à poursuivre le développement en étudiant le cas particulier d'une géométrie fortement courbée. L'objectif général est d'identifier les paramètres de fabrication importants afin de formuler des recommandations pour l'application future du procédé à des pièces réelles. Le projet a été réalisé en trois étapes principales décrites ci-après.

Dans un premier temps, un montage expérimental a été mis au point pour fabriquer un panneau rectangulaire en forme de marche d'escalier. Cette étape a notamment nécessité la sélection d'une membrane flexible ainsi que d'une stratégie d'étanchéité adéquate. Par ailleurs, une procédure de préformage utilisant un agent liant thermodurcissable a été développée pour préparer des préformes fibreuses permettant l'implémentation du procédé à la forme géométrique considérée.

Cette méthodologie a par la suite été utilisée pour fabriquer une première série de pièces avec une résine vinylester et un renfort multidirectionnel en fibres de verre. Des coupes longitudinales réalisées dans la partie centrale des spécimens ont été inspectées visuellement et traitées par analyse d'images pour caractériser la qualité de la mise en forme. Les résultats démontrent tout d'abord que le procédé permet une consolidation uniforme des parties planes dans toutes les directions de l'espace. En revanche, des défauts de fabrication tels que des variations d'épaisseur et des zones riches en résine sont présents dans les parties courbées de la structure. Ce comportement spécifique est attribué aux modes de déformation de la membrane et du renfort fibreux dans les zones courbées. La géométrie initiale de la préforme a notamment une forte influence sur la qualité de la pièce finale. Il est de plus suggéré qu'une modification de la géométrie de préformage permet d'atténuer l'intensité des différents défauts de fabrication.

La deuxième partie du travail visait à mieux comprendre les mécanismes de formation de défauts dus au comportement spécifique de la préforme dans les zones courbées. Pour ce faire, une deuxième série d'expériences a été réalisée avec un tissu de verre quasi unidirectionnel afin de mieux contrôler l'architecture de la préforme. La qualité de la mise en forme dans les parties courbées des pièces a été caractérisée expérimentalement et les observations ont été comparées aux prédictions obtenues à l'aide d'un modèle numérique simplifié. Pour développer cet outil de simulation, la déformation du renfort fibreux a tout d'abord été étudiée au cours des différentes étapes du cycle de production dans le cas d'une géométrie plane. Cette analyse a permis de proposer une loi de compaction transverse tenant compte de l'effet de l'agent liant thermodurcissable sur le comportement mécanique de la préforme. Ce modèle a par la suite été implémenté dans un logiciel commercial de calcul par éléments finis afin de simuler la déformation des fibres de l'étape initiale de préformage jusqu'à la mise en forme finale du composite. Un essai de caractérisation simple a par ailleurs été développé pour analyser le comportement du tissu lors du préformage courbé et construire la géométrie initiale du modèle éléments finis. Dans l'ensemble, les observations expérimentales et les simulations numériques sont en accord et montrent que l'étape de préformage a une influence majeure sur la qualité de la pièce finale. Il est notamment démontré qu'une sélection adéquate des conditions de préformage (i.e. géométrie du moule de préformage et pression de préformage) permet de fabriquer la pièce en forme d'escalier sans défaut apparent.

La dernière partie de l'étude s'est intéressée à la déformation résiduelle des pièces mises en forme lors de la deuxième série de fabrication. Une procédure a été mise au point pour mesurer la distorsion thermoélastique de la structure courbée en enregistrant le changement de forme de l'échantillon au cours d'une simple expérience de refroidissement. Les résultats expérimentaux ont été comparés aux prédictions obtenues par différents modèles afin de mieux comprendre l'influence de la qualité de mise en forme. Ce travail montre que les défauts de fabrication localisés dans les parties courbées du composite peuvent modifier la composante thermoélastique de la distorsion due à la dilatation différentielle. Premièrement, les variations d'épaisseur changent localement les coefficients de dilatation thermique du composite en modifiant le taux de fibres dans les zones courbées. Deuxièmement, les zones riches en résine introduisent des concentrations de contrainte dans la structure lorsque la température varie du fait de leur dilatation thermique élevée. Les analyses suggèrent aussi que l'impact des défauts de mise en forme n'est pas le même sur la déformation résiduelle due au retrait de la résine. Il est par ailleurs souligné que la consolidation de la préforme dans les parties courbées introduit des contraintes sur les fibres susceptibles d'agir comme une source de distorsion additionnelle.

De façon générale, le travail démontre que le procédé d'injection flexible peut être utilisé pour mettre en forme des composites à haute performance dans le cas de géométries fortement courbées. Cependant, la qualité de la mise en forme dépend grandement de la façon dont la membrane flexible et la préforme fibreuse se déforment dans les zones de courbure importante. Le développement de membranes tridimensionnelles et la mise au point de procédures de préformage robustes sont d'ailleurs identifiés comme des axes de recherche prioritaires en vue de l'application future du procédé à des pièces réelles de géométries complexes.

ABSTRACT

Thermosetting polymers reinforced by continuous fibers possess a widely recognized potential for the design of advanced primary structures. Over the last decades, these composite materials have notably replaced metallic materials in many aeronautical applications. The use of such high performance composites is however limited in the automotive industry. Because of the relatively long cycle times required, existing processing techniques are indeed not suited for high production volume.

Flexible Injection is a recently proposed Liquid Composite Molding process. The main objective of this method is to increase the production rate of thermoset composites by reducing the overall cycle time. During the manufacturing cycle, the process imposes a controlled deformation to one side of the tooling using a flexible membrane and a compaction fluid. Flexible Injection has been under development at École Polytechnique de Montréal within the Chair on high performance composites since 2003. Past work demonstrated the potential of the process to speed up the manufacturing and ensure a good impregnation of the fibers in the case of simple geometries. In an effort to pursue the development, this thesis studies the specific case of strongly curved geometries. The main objective is to identify the key processing parameters in order to formulate appropriate recommendations for future implementation with real industrial components. Three main stages were carried out during the research.

Firstly, an experimental setup has been designed to process a rectangular stair-shaped composite panel. This step required adopting an adequate sealing strategy and selecting an appropriate material for the flexible membrane. Furthermore, a preforming procedure was specially devised to prepare semi-rigid fibrous preforms suited for the desired geometry. The developed methodology was applied to produce a first series of parts out of vinyl ester resin and multiaxial glass fiber fabric. Longitudinal cross-sections of the fabricated specimens were then inspected visually and treated by image analysis to assess the quality of the processing. Results show that the process provides a uniform consolidation of the flat sections along any direction. However,

manufacturing defects such as thickness variations and resin rich zones are created in the corners of the structure. This behavior is caused by the specific deformation of the membrane and of the fiber bed in the curved areas. The initial geometry of the preform is a key parameter having a strong impact on the quality of the final part. It is also suggested that the magnitude of the different defects can be reduced by modifying the geometry of the preforming tool.

The second part of the project investigated further the mechanisms that generate preform induced manufacturing defects. During this study, new manufacturing experiments were conducted with a quasi unidirectional glass fiber fabric to control precisely the architecture of the preform. Experimental observations of the processing quality in the corners of the specimens were compared with the predictions made by a simplified numerical model. To develop this simulation tool, the deformation of the fiber bed was first analyzed during the different stages of the production cycle in the specific case of planar geometry. Such analysis allowed proposing a transverse compaction model that takes into account the effect of the thermosetting binder on the mechanical behavior of the preform. This model was then implemented in a finite element software to simulate the fibers deformation from initial preforming to final processing of the composite. A simple characterization test was developed to analyze the corner preforming behavior of the fabric and build the initial geometry of the finite element model. Overall, experimental observations and numerical simulations are in good agreement and show the major influence of the preforming stage on the quality of the final product. In particular, it is shown that the preforming conditions (i.e., geometry of the preforming tool and preforming pressure) have to be selected according to the targeted fiber fraction to produce a defect-free stair-shaped component.

The last part of the work studied the residual distortion of the specimens processed during the second manufacturing program. A procedure was devised to measure the thermoelastic spring-in of the curved structure by recording the change in shape of the sample during a simple cool down experiment. The experimental results were compared with the predictions made by different modeling approaches to investigate further the influence of the layup quality. This study shows that manufacturing defects located at the corner of the composite can impact the thermoelastic

component of distortion caused by differential thermal expansion. Firstly, thickness variations affect locally the coefficients of thermal expansion of the composite by changing the fiber volume fraction in the curved areas. Secondly, resin rich zones create stress concentration in the structure when the temperature varies because of their important coefficient of thermal expansion. Results also suggest that the impact of processing defects can be different for the shrinkage-induced distortion. It is also noted that fiber stresses due to consolidation of the preform in the curved regions can act as an additional cause of distortion.

Overall, the thesis shows that the flexible injection technique can effectively produce high performance composites with strongly curved geometries. However, the quality of the processing strongly depends on the deformation of both flexible membrane and fibrous preform in the curved areas. Developing three-dimensional flexible membranes and devising robust preforming procedures are indeed indentified as key aspects for future development of the process in the case of real parts of complex geometry.

TABLE DES MATIÈRES

LISTE DES TABLEAUX

LISTE DES FIGURES

LISTE DES SIGLES ET ABRÉVIATIONS

CTE	Coefficient of Thermal Expansion
FI	Flexible Injection
LCM	Liquid Composite Molding
RTM	Resin Transfer Molding
r_p	rayon de préformage interne
R_p	rayon de préformage externe
p_c	pression de compaction
p_i	pression d'injection
p_p	pression de préformage
S_{th}	thermoelastic spring-in
σ_f	contrainte effective sur les fibres
V_f	taux volumique de fibres

INTRODUCTION

Les matériaux composites à matrice polymère renforcés de fibres continues possèdent des propriétés mécaniques leur permettant de rivaliser avec les matériaux métalliques plus traditionnels tout en offrant une meilleure résistance à la corrosion et un gain de poids substantiel. Dans le domaine aéronautique, ces deux avantages ont permis aux composites de s'imposer en tant que matériaux privilégiés pour la conception de pièces structurales. À titre d'exemple, les matériaux composites représentent plus de 50% du poids total de l'appareil dans les récents programmes *Dreamliner 787* de Boeing et *A350* d'Airbus (Kelly, 2008). Le succès des composites à haute performance dans le secteur aéronautique a nécessité plusieurs dizaines d'années de travail afin de développer des techniques de fabrication robustes et économiquement viables. Pour les composites à matrice thermodurcissable, les principales méthodes de fabrication sont la mise en forme par autoclave et le moulage par transfert de résine (RTM pour « Resin Transfer Molding »). Aujourd'hui, ces techniques sont aussi utilisées dans le secteur automobile principalement pour les applications de très haut de gamme telles que les voitures de super tourisme. Par exemple, le récent modèle *Aventador* de Lamborghini possède un châssis monocoque en fibres de carbone alliant une rigidité et une légèreté exceptionnelles. L'application de ce type de technologie à des véhicules de grande série engendrerait une diminution de la masse permettant des gains énergétiques considérables (Helms et Lambrecht, 2007). Malheureusement, une telle implémentation n'est à l'heure actuelle pas rentable d'un point de vue économique. Les deux principaux obstacles sont le coût des constituants (notamment des fibres de carbone) ainsi que l'absence de procédé adapté pour les hauts volumes de production (Musselman, 2006; Sehanobish, 2009). En raison de temps de cycle trop longs, les matériaux composites ne peuvent en effet pas rivaliser avec les matériaux métalliques pour des applications structurales nécessitant plusieurs dizaines de milliers de pièces par an.

L'injection flexible est une méthode de mise en forme récemment proposée et brevetée (Ruiz et Trochu, 2011) visant à augmenter les cadences de production des composites thermodurcissables. Ce procédé est actuellement en cours de développement au sein de la Chaire sur les Composites à Haute Performance (CCHP) de l'École Polytechnique de Montréal. S'inscrivant dans le cadre de

ce projet global, cette thèse s'intéresse particulièrement à la fabrication de pièces composites fortement courbées. Le travail cherche à comprendre les caractéristiques spécifiques de ce type de géométrie afin de formuler des recommandations concrètes pour l'application future du procédé à des pièces réelles de géométries complexes. La thèse est organisée en 6 chapitres. Une revue de littérature est tout d'abord présentée afin de cerner les enjeux et la problématique du projet. Les principales conclusions de cette étape sont utilisées au chapitre 2 pour définir l'hypothèse de travail ainsi que les objectifs spécifiques du projet de recherche. Ces objectifs sont réalisés grâce à trois articles de journaux publiés ou soumis présentés dans les chapitres 3 à 5. Les principaux enseignements ainsi que les limitations du travail sont discutés dans le dernier chapitre afin de formuler des recommandations pour la poursuite des travaux.

CHAPITRE 1 REVUE DE LITTÉRATURE

La revue bibliographique présentée dans ce chapitre comprend trois parties principales. L'ensemble des travaux déjà réalisés pour le développement du procédé d'injection flexible est dans un premier temps synthétisé. La deuxième partie discute de la mise en forme de pièces fortement courbées par les procédés existants tels que l'autoclave et le RTM. Finalement, la problématique de la distorsion de composites courbés est abordée dans la dernière section. Les principales causes du phénomène ainsi que les méthodes d'analyse utilisées dans la littérature scientifique y sont tour à tour détaillées.

1.1 Le procédé d'injection flexible

1.1.1 Principe de fonctionnement

L'injection flexible est une nouvelle méthode de mise en forme de composites appartenant à la famille des procédés de fabrication par injection sur renfort fibreux ou « Liquid Composite Molding » (LCM). L'originalité de cette technique réside dans le fait qu'elle autorise une déformation contrôlée d'une des parois du moule au cours du cycle de fabrication. Ceci est réalisé par une membrane flexible placée entre les deux parties du moule (cf. Figure 1-1). Cette membrane sépare la cavité totale de l'outillage en deux chambres isolées : une cavité d'injection située sous la membrane et contenant le renfort fibreux et une cavité de compaction au dessus de la membrane. Les différentes étapes de fabrication illustrées sur la Figure 1-1 sont décrites ci-après :

- ***Étape 1 : Drapage et fermeture du moule.***

  La préforme fibreuse est tout d'abord installée dans la cavité d'injection, la membrane est déposée sur le moule inférieur et le montage est fermé. L'air présent dans les deux chambres est par la suite évacué par application d'une pression de vide. Selon la hauteur de la cavité totale du montage, les fibres peuvent la remplir entièrement ou seulement en partie.

- ***Étape 2 : Injection.***

  Une résine thermodurcissable liquide est injectée sous pression dans la cavité d'injection. Dans le cas d'une préforme moins épaisse que la cavité totale, l'écoulement de la résine peut s'effectuer à travers l'interstice libre au dessus du renfort fibreux.

- ***Étape 3 : Compaction.***

  Après injection du volume de résine souhaité, le port d'entrée de résine est fermé et un fluide de compaction est introduit sous pression dans la cavité supérieure. Le remplissage de la cavité de compaction entraîne une déformation de la membrane et permet de compléter l'imprégnation des fibres.

- ***Étape 4 : Cuisson.***

  Les évents du fluide et de la résine sont fermés et une pression de compaction est maintenue sur le fluide au cours de la polymérisation de la résine.

- ***Étape 5 : Démoulage***

  Lorsque la cuisson est terminée, le fluide de compaction est évacué par application d'une pression de vide, le moule est ouvert et la pièce est démoulée.

.

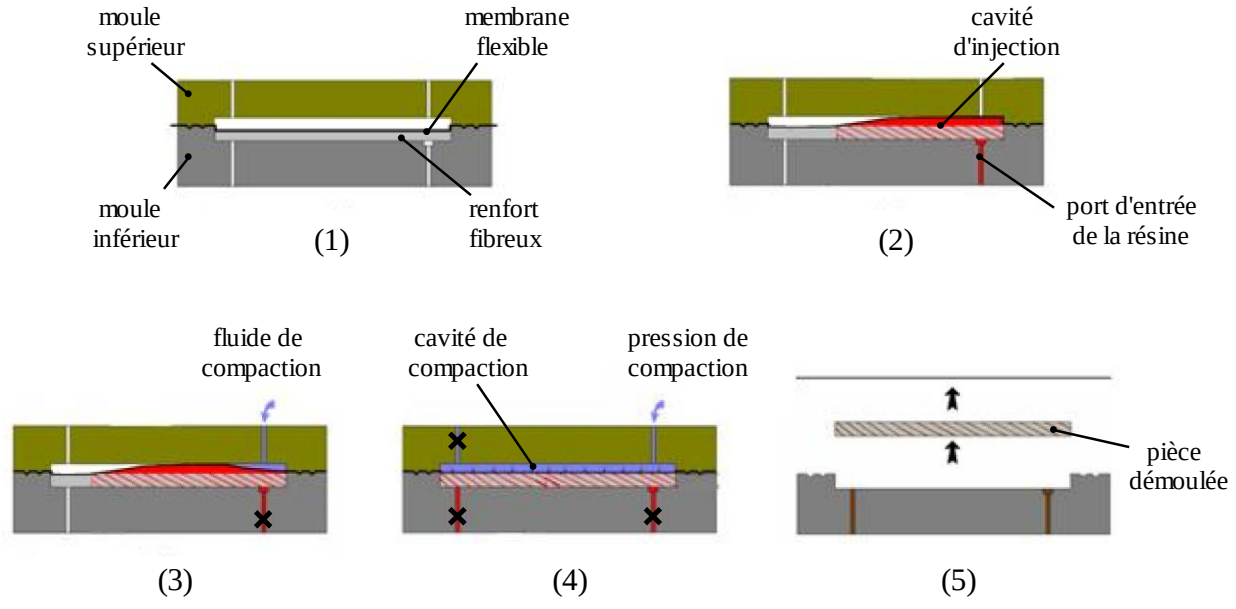

Figure 1-1 : Principales étapes de fabrication par injection flexible (cf. texte pour détails).

L'Injection flexible possède les avantages classiques des procédés d'injection en moule fermé comme la faible émanation de volatiles et le potentiel pour l'automatisation. Comparativement au RTM, le procédé apporte trois principaux avantages. Premièrement, l'écoulement de la résine au dessus de la préforme suivi d'une imprégnation transverse des fibres permet de réduire significativement le temps de remplissage. Par ailleurs, ce schéma de remplissage rend l'injection flexible beaucoup moins sensible aux effets de bord que le procédé RTM. Enfin, l'application d'une pression de compaction tout au long de la phase de polymérisation permet d'améliorer l'imprégnation du renfort et de produire des pièces à haut taux volumique de fibres et possédant un taux de porosité faible.

1.1.2 État du développement

Travaux expérimentaux

Les premiers travaux de développement du procédé ont été réalisés dès 2003 par Briones (2005). L'étape initiale de ce travail a consisté à concevoir le premier moule de fabrication pour l'injection flexible. Cet outillage, baptisé « Polyflex I », possède une géométrie plane (cf. Figure 1-2). Ce moule a été fabriqué en matériau transparent afin de permettre la visualisation de l'avancement des fluides dans la cavité. Plusieurs plans d'expériences ont été réalisés pour étudier l'influence des paramètres de fabrication (pression et viscosité du fluide de compaction, taux volumique de fibres,…) sur le temps d'imprégnation total. Dans le but de limiter le temps d'expérimentation, la résine a été remplacée par un fluide inerte (i.e. une huile silicone). Aucune pièce composite n'a donc été mise en forme au cours de ces travaux. Toutes les expériences ont été réalisées avec un mat aléatoire en fibres de verre continues. Avec un tel choix de renfort, le taux volumique de fibres maximum est resté limité à 30 %. Une des principales observations de Briones a été l'existence d'un point de croisement des fluides à partir duquel le fluide de compaction dépasse le front de résine dans la cavité. Ce phénomène néfaste entrainant une forte diminution de la vitesse d'imprégnation a été identifié comme un point à améliorer. Dans le meilleur des cas étudiés, le temps d'imprégnation total a néanmoins pu être diminué d'un facteur 5 par rapport au temps théorique obtenu avec le procédé RTM. Ces premiers résultats ont donc bien démontré le potentiel de l'injection flexible pour diminuer le temps de fabrication.

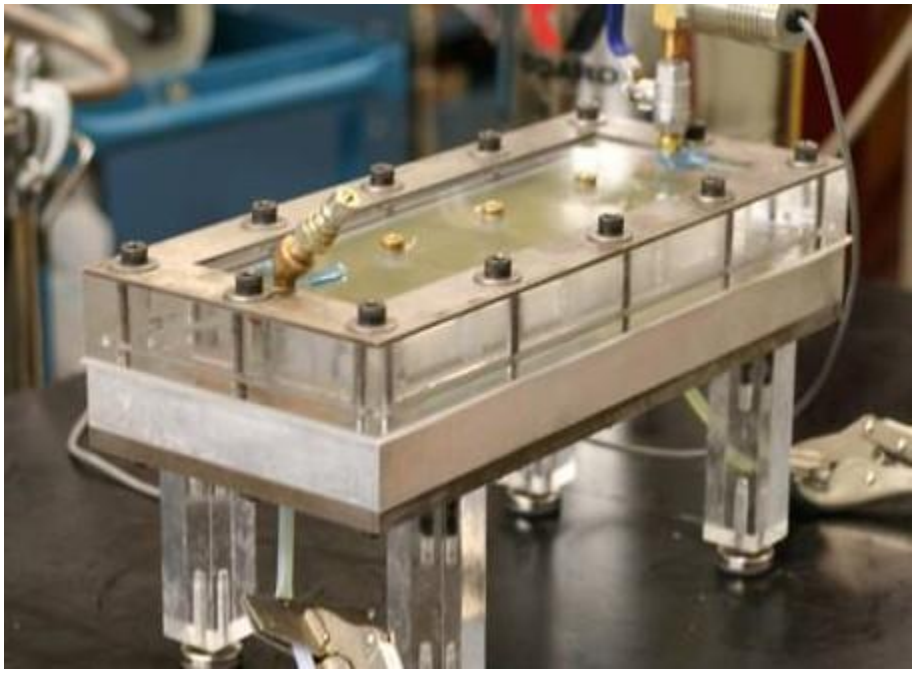

Figure 1-2 : Moule de première génération “Polyflex I”.

Le moule de première génération a par la suite été utilisé lors de deux travaux de maîtrise supplémentaires (Allard, 2006; Daqoune, 2007). Allard a tout d’abord poursuivi les travaux de Briones en utilisant une résine polyester pour fabriquer les premières pièces réelles. La variabilité de l’épaisseur des spécimens fabriqués a été caractérisée par mesure manuelle à l’aide d’un micromètre. Ces analyses ont permis de constater une diminution sensible de l’épaisseur à partir de la ligne de croisement des fluides. Allard a aussi utilisé un système de compaction plus perfectionné permettant d’appliquer un profil de pression cyclique avec une fréquence maximale de 0.8 Hz. Ce dispositif a contribué à diminuer le temps d’imprégnation (jusqu’à 8 fois plus rapide que le RTM) mais n’a pas permis d’éliminer le phénomène de croisement des fluides. Enfin, Allard a étudié l’impact du préformage à l’aide d’un agent liant thermodurcissable pour diminuer l’épaisseur naturelle du renfort sec et promouvoir un écoulement de la résine dans l’interstice libre au dessus de la préforme. Aucune amélioration significative du temps de cycle n’a été observée avec cette configuration. Cependant, Allard souligne à raison que cette conclusion n’est peut être valide que pour un renfort de type mat aléatoire possédant un taux de fibres naturel faible et une perméabilité planaire élevée. Par la suite, un comportement radicalement différent a été observé par Daqoune lors de la mise en œuvre du procédé avec des

renforts tissés multidirectionnels (Daqoune, 2007). La perméabilité de ce type de renfort est en effet beaucoup plus faible que celle d'un mat aléatoire. Un écoulement de la résine dans l'interstice libre suivi d'une imprégnation transverse devient alors beaucoup plus avantageux pour accélérer la mise en forme. Tout d'abord, le phénomène de croisement des fluides dans la cavité est éliminé. De plus, l'utilisation de renforts multidirectionnels permet d'atteindre des taux volumiques de fibres beaucoup plus élevés qu'avec un mat aléatoire (jusqu'à 58% dans les travaux de Daqoune). Dans une telle situation, l'injection flexible s'avère beaucoup plus rapide que le procédé RTM. Dans le meilleur des cas étudiés, une diminution du temps de remplissage total d'un facteur 35 a ainsi été observée. L'épaisseur de l'interstice libre a une grande influence sur le temps d'injection et sur l'homogénéité de l'épaisseur de la pièce finale. Par conséquent, Daqoune suggère qu'il existe une hauteur totale de cavité optimale permettant d'accélérer le procédé tout en assurant une qualité d'imprégnation satisfaisante. Dans ses travaux, Daqoune n'a cependant pas utilisé de technique de caractérisation rigoureuse de l'imprégnation du renfort comme par exemple la pyrolyse de la matrice. La qualité générale des pièces fabriquées a en effet été estimée par inspection visuelle. Cette méthode simple a néanmoins permis d'illustrer l'influence de l'application d'une pression de vide dans la chambre d'injection sur l'imprégnation du tissu. Tel que représenté sur la Figure 1-3, l'augmentation de la pression de vide permet d'améliorer la qualité générale de la pièce. Une telle observation est bien évidemment intuitive puisqu'une pression de vide plus élevée entraîne une baisse de la quantité d'air présent dans la cavité avant l'injection diminuant ainsi le volume total des porosités dans la pièce finale.

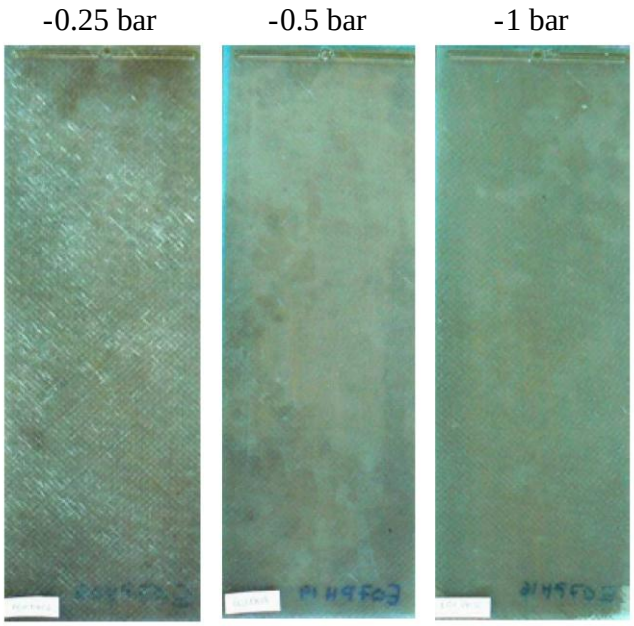

Figure 1-3 : Influence de la pression de vide dans la chambre d'injection sur l'aspect visuel de pièces planes (Daqoune, 2007).

L'injection flexible a ensuite été étudiée avec des moules de fabrication chauffés (Abdellaoui, 2008). Deux nouveaux montages permettant une température de fabrication de 100ºC ont été développés au cours de ce projet. Un moule de géométrie simple (i.e. plane) a d'abord permis d'évaluer l'effet d'un profil de compaction cyclique à haute fréquence (jusqu'à 30 Hz). Des valeurs de fréquence optimales permettant de diminuer le temps d'imprégnation et d'uniformiser l'épaisseur de la pièce ont été identifiées. Cependant, ces résultats ne s'appliquent qu'au type de renfort fibreux utilisé dans ce travail et ne peuvent donc pas être extrapolés à un cadre plus général. Des travaux supplémentaires semblent nécessaires pour mieux comprendre les mécanismes physiques expliquant l'influence d'un profil de compaction cyclique sur la mise en œuvre de l'injection flexible. Abdellaoui a par ailleurs étudié la possibilité d'un contrôle en température réalisé grâce au fluide de compaction. La faisabilité d'un tel contrôle a été démontré au cours de la phase de cuisson du composite ainsi que lors du refroidissement du montage avant le démoulage. Les expériences réalisées ont mis en évidence l'importance de la conductivité thermique de la membrane flexible pour assurer un contrôle performant. La méthodologie proposée a été appliquée dans le cas d'une pièce tridimensionnelle légèrement courbée

représentant un toit de *Corvette* à l'échelle ¼. Cette pièce représentée sur la Figure 1-4 a été le premier spécimen à géométrie non plane réalisé par injection flexible.

Figure 1-4 : Première pièce de géométrie non plane fabriquée par injection flexible: le toit de *Corvette* à l'échelle ¼.

Les plus récents travaux sur l'injection flexible ont porté sur la fabrication de panneaux composites auto-raidis par des nervures en forme d'omega (Rifay, 2010). Au cours de ce travail, deux types de pièces composites ont été étudiés: un panneau possédant un raidisseur simple et un panneau plus complexe incorporant un raidisseur en forme de croix. L'application du procédé à ce type de géométrie a notamment été rendue possible grâce aux recommandations formulées à la fin de la présente thèse. Les travaux de Rifay sont donc discutés plus en détail dans le chapitre 6 du document.

Travaux de modélisation

Jusqu'à présent, l'analyse expérimentale a constitué la majeure partie des travaux de développement de l'injection flexible. Des tentatives de modélisation ont cependant aussi été

entreprises notamment par Touraine (2005). L'objectif principal de cette étude était de reproduire les résultats expérimentaux de Briones à l'aide d'un modèle éléments finis en 2 dimensions. Le modèle numérique développé utilise des représentations différentes pour les deux fluides intervenant dans le procédé: écoulement de Stokes pour le fluide de compaction et écoulement de Darcy en milieu poreux déformable pour la résine. Afin de simplifier le problème, la rigidité de la membrane a été négligée lors du couplage des deux écoulements. Une autre simplification importante concerne le comportement en compaction du renfort fibreux, considéré comme élastique et représenté par une simple loi de puissance. Les prédictions réalisées coïncident relativement bien avec les résultats expérimentaux jusqu'à la fermeture de l'évent du fluide du compaction. En revanche, des différences très importantes ont été constatées lors la dernière étape d'imprégnation (entre la fermeture de l'évent de compaction et celle de l'évent de résine). Touraine attribue ces écarts au comportement fortement non linéaire du renfort et recommande une meilleure représentation du comportement en compaction dans l'analyse. Cette limitation illustre bien la difficulté de modéliser de façon adéquate un procédé aussi complexe que l'injection flexible et explique en partie le choix de privilégier une approche expérimentale pour le développement du procédé.

1.2 Mise en forme de pièces composites courbées

L'injection flexible n'a encore jamais été utilisée pour fabriquer des pièces fortement courbées. En revanche, ce type de géométrie a déjà fait l'objet de nombreuses études dans le cas de procédés de fabrication plus anciens. La section suivante présente un résumé de ces travaux pour le procédé par autoclave et le RTM afin d'illustrer les difficultés de fabrication liées à l'utilisation de faibles rayons de courbure. Comme il sera présenté, le comportement des renforts fibreux est un paramètre fondamental lors de la mise en forme. Une brève présentation de la spécificité mécanique de ce type de matériau est donc proposée dans une première sous-section.

1.2.1 Comportement mécanique des renforts fibreux

Les renforts à fibres continues se présentent sous la forme de plis plans. Un pli de renfort est constitué d'un ensemble de mèches (ou torons) pouvant être tissées ou liées par un fil de couture.

Chacune des mèches est elle-même constituée de plusieurs milliers de fibres dont le diamètre est de l'ordre de quelques micromètres. Cette architecture particulière entraîne un comportement mécanique macroscopique complexe fortement orthotrope, viscoélastique et non linéaire même lorsque le matériau de base est élastique isotrope (comme le verre par exemple). L'étude du comportement mécanique des renforts fibreux est un domaine de recherche vaste et très actif depuis de nombreuses années. Le paragraphe suivant ne vise pas à résumer cette problématique de façon exhaustive mais à présenter des exemples de caractérisation courants afin d'illustrer le comportement spécifique des renforts fibreux.

Comportement en compaction

Au cours de la mise en forme, le tissu subit généralement une compression à travers l'épaisseur (ou compaction) afin de contrôler le taux volumique de fibres du composite. Pour évaluer les forces de fermeture en moule rigide ou le taux de fibres maximal pouvant être atteint avec un moule flexible, il est très important de connaitre la relation entre la pression appliquée et le taux volumique de fibres. La compaction d'un renfort fibreux est un phénomène viscoélastique non linéaire généralement étudié à l'aide d'essais mécaniques sur des échantillons plans. La Figure 1-5 illustre par exemple le comportement hystérétique et le décalage progressif des courbes de compaction au cours d'un essai cyclique à vitesse de déplacement constante. Lorsque le temps de cycle n'est pas un critère majeur, ce comportement peut par exemple être mis à profit pour augmenter le taux de fibres maximal lorsque la pression de mise en forme est limitée (Niggemann et al., 2008). Un autre essai couramment utilisé consiste à maintenir un taux volumique de fibres constant et à enregistrer l'évolution de la contrainte effective sur les fibres au cours du temps. Des courbes de relaxation typiques obtenues avec cette procédure sont illustrées sur la Figure 1-6.

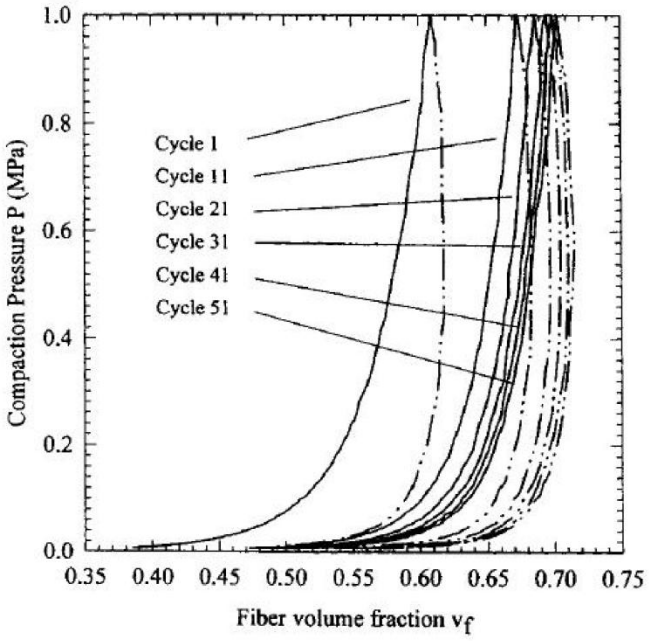

Figure 1-5 : Essai de compaction cyclique (Robitaille et Gauvin, 1999).

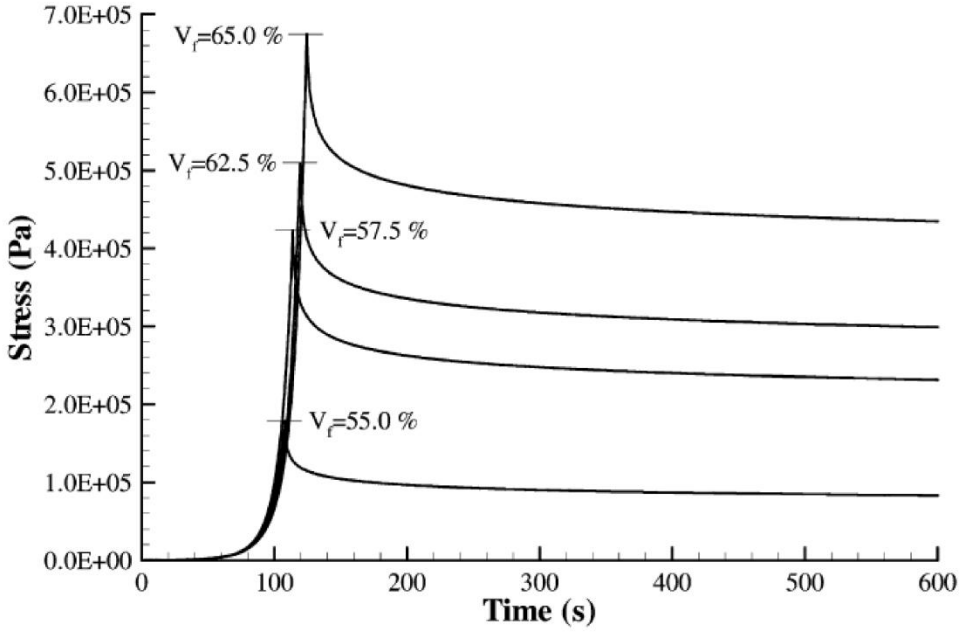

Figure 1-6 : Essais de relaxation d'un renfort fibreux (Bickerton et al., 2003).

La réponse en compaction d'un renfort fibreux dépend fortement de la vitesse de chargement, du nombre de plis utilisés ainsi que de l'effet lubrifiant de la résine pour un renfort imprégné (Bickerton et al., 2003; Robitaille et Gauvin, 1998a, 1998b). La caractérisation complète de la réponse en compaction nécessite donc la réalisation d'un nombre très élevé d'essais expérimentaux. Par ailleurs, la modélisation rigoureuse d'un tel comportement s'avère délicate. Des modèles viscoélastiques ont déjà permis de reproduire de façon convenable les résultats typiques présentés précédemment (Kelly et al., 2006). Pour des raisons de simplicité, il est cependant courant d'utiliser une loi élastique non linéaire reliant le taux volumique de fibres à la pression appliquée (Gutowski et al., 1987; Robitaille et Gauvin, 1998b; Toll et Manson, 1994)

Cisaillement planaire et drapabilité

Pour fabriquer une pièce complexe, les plis de renfort initialement plans doivent être drapés sur une surface non plane. Cette opération nécessite un cisaillement planaire important du tissu. Afin d'évaluer le comportement en cisaillement, des essais de caractérisation en cadre rigide (« picture frame test » sur Figure 1-7a) ou d'extension de biais (« bias extension test ») ont notamment été développés. Ces procédures sont particulièrement efficaces pour caractériser le comportement de renforts tissés mais peuvent s'avérer limitées pour des renforts liés par un fil de couture. Les mécanismes de déformation de ces derniers font en effet intervenir des phénomènes de glissement incompatibles avec les hypothèses cinématiques sous-jacentes à un cisaillement pur (Bel et al., 2011).

Les essais de caractérisation du cisaillement planaire permettent de recueillir des données primordiales pour la simulation du drapage de formes complexes (Figure 1-7b). Historiquement, les premiers modèles numériques développés considéraient le cisaillement planaire comme principal mode de déformation des renforts. Les méthodes numériques proposées plus récemment utilisent des modèles plus raffinés incluant notamment les propriétés en flexion et en traction du tissu (Boisse et al., 2011) et les effets de glissement entre les plis (Chen et al., 2011). Des progrès peuvent cependant être encore accomplis pour permettre une représentation fidèle de tous les mécanismes de déformation du renfort. Par exemple, la compréhension du couplage entre le cisaillement planaire et le comportement en compaction reste à améliorer.

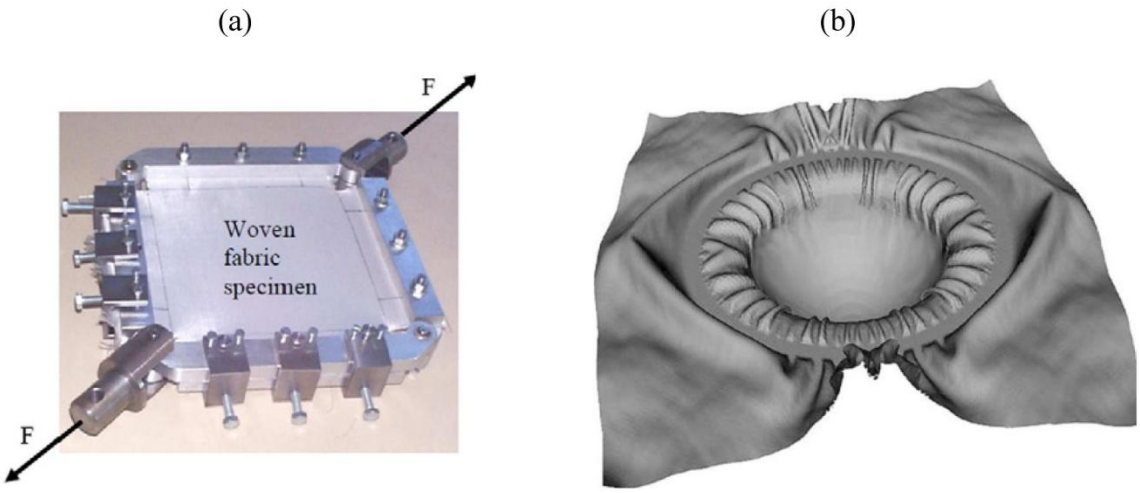

Figure 1-7 : Caractérisation du cisaillement planaire (a) et exemple de simulation de drapage sur hémisphère d'un renfort tissé (b) (Boisse et al., 2011).

1.2.2 Le procédé de fabrication par autoclave

Contrairement à l'injection flexible, la mise en forme par autoclave utilise un renfort fibreux pré-imprégné de résine. Cependant, les deux méthodes possèdent un point commun fondamental: la forme finale de la pièce résulte de la consolidation sous paroi flexible d'un renfort fibreux saturé par la résine. Tel qu'illustré dans la section suivante, de nombreuses études réalisées sur le procédé par autoclave ont démontré que les géométries courbées possèdent un comportement en consolidation différent des parties planes pouvant mener à l'apparition de défauts de mise en forme.

Observations expérimentales

La Figure 1-8 présente les deux types de défaut de fabrication couramment observés dans les zones fortement courbées lors de la mise en forme par autoclave. Le premier type de défaut, souvent visible à l'œil nu, est une région entièrement constituée de résine pure (Figure 1-8a). Deux mécanismes peuvent être à l'origine d'une telle imperfection. Tout d'abord, des plis (« wrinkles ») peuvent apparaitre sur la surface du tissu lorsque ce dernier doit adopter une géométrie courbée (Potter, 2002; Potter, 2004). Lors de l'application de la pression de

consolidation, la résine migre vers cette zone de faible perméabilité et une région riche en résine est créée (Feih et Shercliff, 2005; Hubert et Poursartip, 2001). Le deuxième mécanisme générant des régions de résine pure concerne spécifiquement la fabrication avec un moule concave. Dans cette situation, les fibres ont tendance à ne pas adopter la forme du moule dans la section courbée et à « couper au plus court » au dessus de la courbure. L'espace libre entre le moule rigide et le renfort aboutit finalement à la création d'une zone riche en résine sur la partie extérieure de la courbe. Ce phénomène appelé « fiber bridging » a été observé a de nombreuses reprises (Wisnom et al., 2006; Wisnom et al., 2001; Yang et al., 1996). En raison de ce comportement, l'utilisation d'un moule concave est généralement considérée comme plus délicate que la fabrication sur un moule convexe.

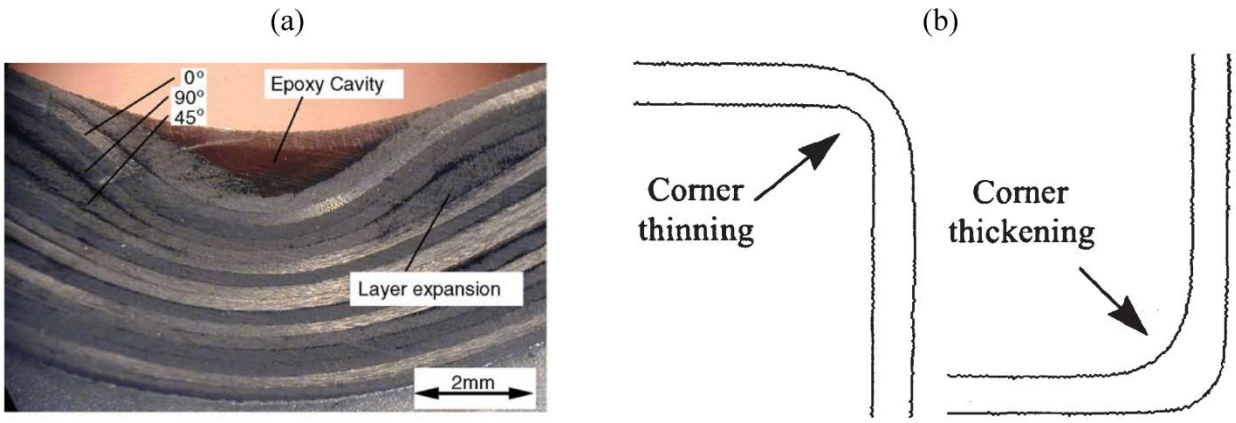

Figure 1-8 : Exemples de défauts de fabrication observés sur des pièces fortement courbées fabriquées en autoclave: (a) zone riche en résine (Feih et Shercliff, 2005); (b) variations d'épaisseurs (Hubert et Poursartip, 2001).

L'absence de région riche en résine n'implique pas nécessairement une répartition parfaitement homogène des fibres et de la matrice dans le composite. Des variations d'épaisseur dans les parties courbées (Figure 1-8b) ont en effet pu être observées par analyse d'image ou à l'aide d'une simple mesure par micromètre. Avec un même empilement, une sous-épaisseur pour une fabrication sur moule convexe et une surépaisseur sur moule concave ont par exemple été reportées (Hubert et Poursartip, 2001; Wiersma et al., 1998). D'autres études ont fait état d'une

surépaisseur de la partie courbée lors de la fabrication avec un moule convexe (Li et al., 2009a; Naji et Hoa, 1999). L'architecture du tissu joue un rôle important sur l'épaisseur finale des parties courbées. De plus fortes variations d'épaisseur ont ainsi observées lorsque les fibres sont perpendiculaires au plan contenant la courbure comparativement à des échantillons contenant des fibres parallèles à la section courbée (Li et al., 2009a; Oakeshott, 2003). Cette caractéristique est due à la rigidité des fibres présentes dans le plan de la section courbée qui limitent fortement la compaction du tissu dans la courbure (Hubert et Poursartip, 2001).

L'utilisation d'un faible rayon de courbure est un facteur aggravant favorisant la création de défauts de fabrication. Cette conclusion relativement intuitive a été notamment confirmée par une étude statistique menée sur plus de dix mille pièces aéronautiques caractérisées à l'aide de techniques non destructives (Wang et al., 2009). Des observations similaires ont aussi été effectuées lors d'études sur la mise en forme de spécimens en L. Des variations d'épaisseur plus prononcées ont par exemple été observées en diminuant le rayon de courbure lors de la fabrication sur un moule convexe (Li et al., 2009a). Dans le cas d'un moule concave, une augmentation de la zone riche en résine due au « fiber bridging » lors de la diminution du rayon du moule concave a aussi été observée (Jain et al., 1997).

Modélisation de la consolidation de pièces courbées

La modélisation de la mise en forme par autoclave fait intervenir différents phénomènes physiques: écoulement de la résine à travers le renfort, déformation du renfort fibreux, réaction de polymérisation, échange de chaleur entre la pièce et l'outillage, développement de contraintes résiduelles dans la pièce. De plus, la nature flexible du moule entraîne un couplage fort entre l'écoulement de la résine et la déformation du renfort. Depuis les travaux de Gutowski (1987), le phénomène de consolidation est généralement représenté par la loi de Terzaghi initialement proposée en mécanique des sols. Cette approche stipule que la contrainte sur le renfort saturé est répartie entre la contrainte effective sur le renfort fibreux et la pression de la résine. La résolution du problème de consolidation nécessite donc une loi de comportement mécanique du renfort et un modèle pour l'écoulement de la résine. Ce dernier est généralement modélisé comme un écoulement en milieu poreux régi par la loi de Darcy. Étant donné la nature déformable du milieu

poreux, la variation de la perméabilité en fonction du taux volumique de fibres doit de plus être considérée (Gutowski et al., 1987).

Les premiers travaux de modélisation du procédé par autoclave se sont principalement intéressés au cas d'une géométrie plane (Gutowski et al., 1987; Loos et Springer, 1983). Dans un article de revue couvrant la littérature jusqu'en 1996, Hubert et Poursartip firent remarquer que le couplage entre l'écoulement de la résine et la déformation du renfort devait être étudié de façon plus approfondie dans le cas de géométries complexes (Hubert et Poursartip, 1998). Ce constat a motivé le développement d'outils de simulation adaptés comme le logiciel COMPRO développé à l'université de la Colombie Britannique (Fernlund et al., 2002b; Hubert et al., 1999; Johnston et al., 2001). Le module de compaction du logiciel COMPRO considère un comportement isotrope transverse du renfort fibreux dans lequel le couplage dû aux effets de Poisson est négligé (Hubert et al., 1999). Ce type de modélisation a par la suite été repris par d'autres chercheurs (Li et al., 2008; Li et Tucker III, 2002). Plusieurs études paramétriques réalisées avec ces outils numériques ont identifié l'influence primordiale du comportement en cisaillement sur la forme finale de la section courbée (Hubert et al., 1999; Li et Tucker III, 2002; Li et al., 2009b). Tel qu'illustré sur la Figure 1-9, l'augmentation du module de cisaillement à travers l'épaisseur du renfort fibreux entraîne une diminution de la consolidation de la partie courbée et affecte aussi l'épaisseur des parties planes entourant la courbure.

Les simulations numériques peuvent très utiles pour mieux comprendre le phénomène de consolidation des formes courbées. Des prédictions en accord avec les expériences ont notamment été obtenues avec ce genre d'approche (Hubert et al., 1999; Li et al., 2009a). Certaines limitations doivent cependant être soulignées. Les modèles numériques présentés précédemment utilisent une représentation homogène du renfort ne faisant pas de distinction entre le cisaillement à l'intérieur d'un pli et le cisaillement entre les plis principalement dicté par le glissement des différentes couches. Le module de cisaillement à travers l'épaisseur est par ailleurs difficile à estimer expérimentalement. Enfin, les simulations sont effectuées à partir d'une géométrie initiale idéale ne tenant pas compte d'éventuels défauts dans l'empilement pouvant être introduits lors de la mise en place du tissu sur le moule.

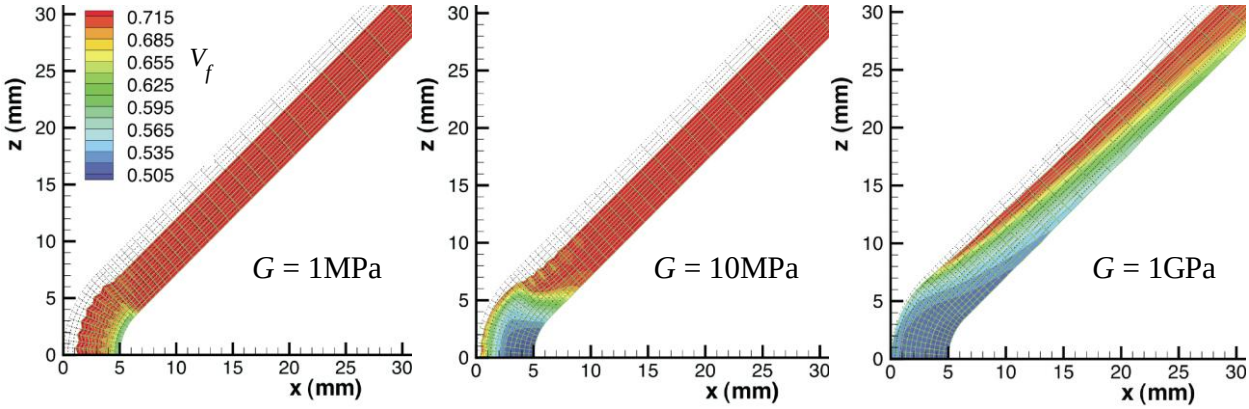

Figure 1-9 : Influence du comportement en cisaillement à travers l'épaisseur sur la consolidation d'un composite courbée prédite par simulation numérique (Li et Tucker III, 2002).

Stratégies d'amélioration de la qualité

Le placement initial des plis de pré-imprégnés sur le moule est une étape essentielle à la réussite de la mise en forme. Par exemple, un empilement manuel réalisé avec précaution permet d'éviter la formation de plis sur le renfort (Brillant et Hubert, 2010). Une stratégie plus systématique pour améliorer la mise en forme consiste à placer sous le film flexible une plaque de compression rigide (ou « caul sheet ») reproduisant la géométrie de la pièce à fabriquer. Pour assurer une bonne correction, le dimensionnement de la plaque est une donnée essentielle (Yang et al., 1996). La flexibilité de la plaque de compression joue aussi un rôle très important sur la correction apportée (Fernlund et al., 2002a). Comme illustré sur la Figure 1-10, des plaques de rigidité différentes n'entraînent pas les mêmes corrections des variations d'épaisseur. Afin de mieux comprendre cette observation, Gu et al. (2010) on utilisé un film sensible à la pression placé entre le composite et le moule. Ce dispositif a permis d'illustrer l'influence de la rigidité du moule flexible sur le profil de pression effectivement transmis au composite.

Une autre stratégie d'amélioration de la qualité consiste à placer des coussinets en caoutchouc sur les partie courbées afin d'augmenter localement la pression transmise au composite. Ce type de dispositif a notamment été utilisé pour fabriquer des pièces d'épaisseur quasi-uniforme en dehors

de l'autoclave, avec une pression de consolidation correspondant simplement à la pression atmosphérique (Brillant et Hubert, 2010).

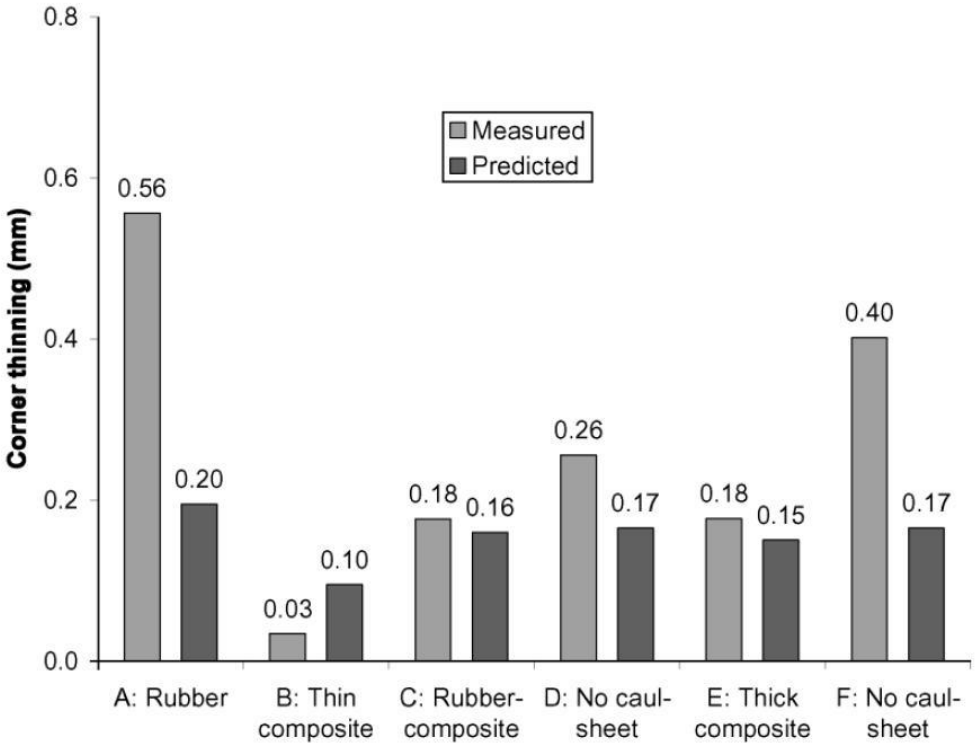

Figure 1-10 : Impact de l'utilisation de différentes plaques de compression sur la diminution de l'épaisseur d'une section courbée mise en forme avec un moule convexe (Fernlund et al., 2002a).

1.2.3 Procédés à moule rigide: le RTM

Avec le procédé RTM, l'épaisseur de la pièce est directement dictée par la cavité du moule rigide. Il ne peut donc pas y avoir de variation d'épaisseur indésirable. En revanche, plusieurs ouvrages de référence mentionnent que l'utilisation de rayons de courbure trop faibles peut entraîner l'apparition de zones riches en résine dans les parties courbées des pièces (Cauchois, 1997; Gutowski, 1997; Potter, 1997). Cet effet est illustré schématiquement sur la Figure 1-11. Lors de la fermeture du moule, les plis de tissu secs tendent à devenir plus compactés sur le rayon intérieur et créent ainsi un espace libre sur le côté extérieur de la zone courbée. Au cours de l'injection, cet espace est rempli par la résine et une zone riche en résine est créée sur la pièce.

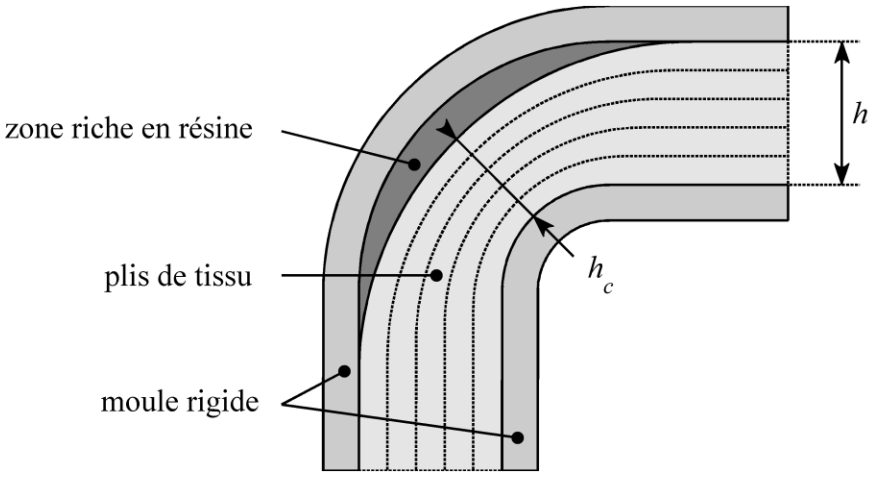

Figure 1-11 : Création d'une région riche en résine sur des pièces fortement courbées fabriquées par RTM.

Gao et Young (2002) ont étudié l'influence de plusieurs paramètres de fabrication sur la création de zones riches en résine sur des éprouvettes en L fabriquées par RTM. Une analyse microscopique de coupes longitudinales des pièces fabriquées a été utilisée pour quantifier le rapport h_c/h comparant l'épaisseur des fibres au centre de la courbure avec l'épaisseur totale de la cavité. Les expériences réalisées ont montré une diminution de ce rapport lorsque l'angle au centre de la partie courbée et l'épaisseur de la cavité augmentaient et lorsque le taux de fibres diminuait. Les tendances observées ont aussi pu être reproduites à l'aide d'un modèle géométrique simplifié considérant des fibres inextensibles et incluant un facteur de glissement empirique. L'influence de l'angle de courbure et du taux volumique de fibres a été confirmée par une autre étude expérimentale plus récente (Dong, 2011). Ces travaux ont aussi évalué l'impact de l'architecture du tissu et du rayon de courbure. Une amplification du phénomène a ainsi été observée pour une diminution du rayon de courbure et pour des fibres orientées dans la direction circonférentielle. Un modèle mécanique simplifié supposant notamment un comportement transverse élastique non linéaire en loi de puissance a de plus été proposé pour reproduire les observations expérimentales.

Certaines études ont par ailleurs montré que la formation de ce type de défaut pouvait être évitée grâce à une stratégie de préformage adaptée. En utilisant un préformage sous paroi flexible, des canaux en U possédant une répartition homogène des fibres dans les parties courbées ont pu être fabriqués par le procédé RTM (Holmberg et Berglund, 1997). L'utilisation d'un outil de préformage différent du moule de fabrication a aussi été recommandée pour d'autres procédés à moule rigide comme le SRIM (« Structural Reaction Injection Molding ») afin d'éviter l'apparition de défauts de fabrication (Arndt, 1991).

1.3 Déformation résiduelle de pièces courbées

La fabrication d'un composite à matrice thermodurcissable s'accompagne inévitablement de l'apparition de contraintes résiduelles. Dans certains cas, ces contraintes peuvent être suffisamment élevées pour créer des fissures dans la matrice et entraîner la délamination de la pièce (Ruiz et Trochu, 2005b; Svanberg, 2002). Cette situation peut notamment se produire lors de la mise en forme de pièces épaisses pour lesquelles l'exothermie de la polymérisation entraîne une forte augmentation de la température. Le risque de délamination est moins élevé pour des pièces minces. Cependant, les contraintes résiduelles peuvent entraîner une distorsion de la géométrie après démoulage. La section suivante présente un résumé des travaux portant sur la distorsion résiduelle de pièces courbées. La synthèse se limite aux cas de pièces minces pour lesquelles la température et le degré de cuisson peuvent être considérés constants à travers l'épaisseur de la pièce.

1.3.1 Le phénomène de « Spring-in »

Le démoulage d'une pièce courbée s'accompagne d'une augmentation de la courbure de sorte que la géométrie finale ne correspond plus à celle du moule. Ce phénomène illustré sur la Figure 1-12 pour une géométrie en L est communément appelé « spring-in ». L'angle de distorsion (ou angle de « spring-in ») $\Delta\theta$ d'une pièce en angle droit est typiquement compris entre 1º et 2º. Bien que relativement faible, une telle déformation peut poser d'importants problèmes lors de la phase d'assemblage et nécessiter une compensation de l'orientation des surfaces utiles (Fernlund et al., 2003; Jeffreys et Leaney, 2000).

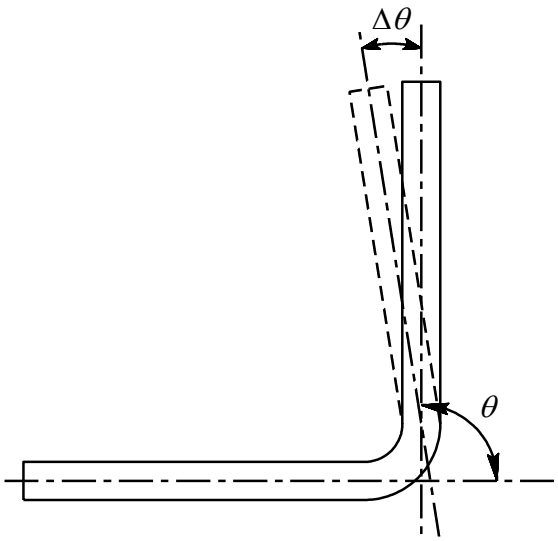

Figure 1-12 : Illustration du phénomène de “spring-in” d’un composite en L.

Un des premiers exemples illustrant la distorsion spécifique des composites courbés concernait la déformation résiduelle en forme d’os de chien (« dog-boning ») d’un tube rectangulaire (Hammond et Farrell, 1978). Depuis, de très nombreux travaux de recherche ont été réalisés pour comprendre, prédire et éventuellement corriger ce phénomène.

1.3.2 Origines de la distorsion

Dilatation thermique

Les polymères thermodurcissables et les fibres utilisés pour la fabrication de matériaux composites possèdent des propriétés de dilatation thermique sensiblement différentes. Le coefficient de dilatation thermique linéaire des résines est généralement compris entre 3.10^{-5}/ºC et 10^{-4}/ºC. En comparaison, cette valeur est de 5.10^{-6}/ºC pour les fibres de verre. Les fibres de carbone ont quant à elles un comportement isotrope transverse avec des coefficients de dilatation thermique de l’ordre de 10^{-5}/ºC dans la direction radiale et pouvant même être négatif (jusqu’à -10^{-6}/ºC) dans la direction longitudinale. Lors d’un changement de température du composite, des contraintes thermiques se développent donc à l’interface des fibres et de la matrice. C’est notamment le cas lors du refroidissement de la pièce après une mise en forme à haute

température. Dans le cas d'un laminé plan symétrique, un changement de température n'a pas d'impact sur la forme de la pièce car le champ des contraintes se développant au niveau microscopique est en équilibre à l'échelle macroscopique. En revanche, pour un empilement non symétrique ou pour une géométrie non plane, un changement de température crée un gradient de contraintes à l'échelle macroscopique entrainant nécessairement une déformation du composite.

Retrait volumique de cuisson

Au cours de la polymérisation, des liaisons chimiques sont créées entre les monomères de résine. Ce réarrangement moléculaire entraîne une diminution progressive du volume spécifique appelé retrait. À titre indicatif, pour des résines de type vinylester comme celle qui sera utilisée dans la suite du travail, le retrait volumique total se situe entre 7 et 10% (Cao et Lee, 2003). Lors de la mise en forme, les fibres restent quant à elles stables et ne subissent aucun changement de volume. Dès lors, le retrait chimique entraîne l'apparition de contraintes résiduelles à l'interface fibre/matrice comme dans le cas de la dilatation thermique. Pour transmettre des contraintes, la matrice doit être suffisamment rigide et donc avoir atteint un degré de cuisson suffisant. Seule une partie du retrait total participe ainsi à l'apparition de contraintes résiduelles.

Contraintes introduites sur les fibres lors de la mise en forme

Les contraintes résiduelles dues à la dilatation thermique et au retrait chimique se développent dans le composite lorsque la résine est à l'état solide (caoutchouteux ou vitreux). La procédure de mise en forme peut aussi introduire des contraintes sur les fibres lorsque la résine est encore à l'état liquide. Lors du démoulage de la pièce, ces contraintes sont transmises à la résine et peuvent contribuer à déformation résiduelle. L'exemple le plus étudié de contrainte fibreuse contribuant à la distorsion est le mécanisme d'interaction moule/pièce qui sera présenté dans la section suivante.

1.3.3 Mécanismes de déformation résiduelle

Anisotropie

Un matériau composite possède des propriétés fortement anisotropes car l'effet de renfort des fibres est plus important dans le plan de la pièce qu'à travers son épaisseur. Dès lors, un changement de volume différentiel entres les fibres et la matrice (dû à la dilatation thermique ou au retrait chimique) entraîne une expansion à travers l'épaisseur plus importante que l'expansion dans le plan. Pour une géométrie plane, cette expansion différentielle n'a pas d'impact sur la forme générale de la pièce. En revanche, l'expansion anisotrope combinée à une géométrie courbée entraîne une modification de la courbure de la pièce tel qu'illustré sur la Figure 1-13.

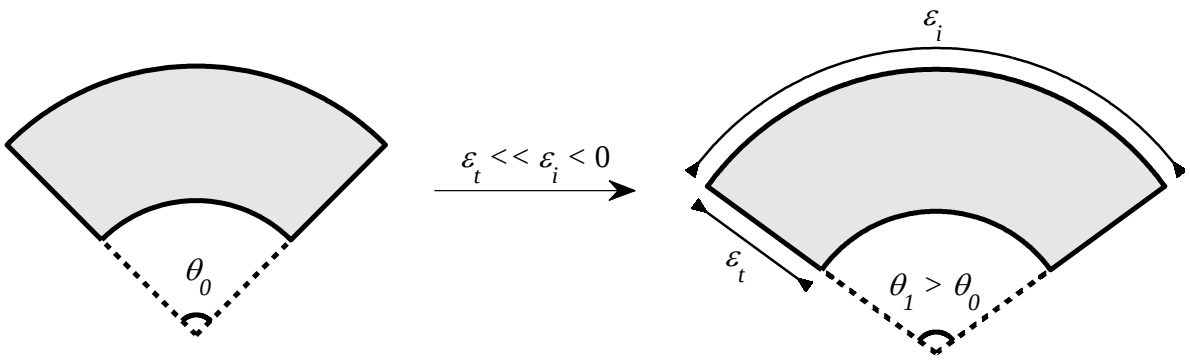

Figure 1-13 : Expansion anisotrope entrainant la distorsion des structures courbées.

Répartition non homogène des fibres et de la matrice

Lors de la mise en forme par autoclave, une partie de la résine peut être extraite du renfort pré-imprégné à l'aide d'un milieu drainant placé sous la paroi flexible. Cet écoulement de résine est susceptible de créer un gradient de taux de fibres à travers l'épaisseur de la pièce. Des analyses par microscopie ont notamment permis de relever l'existence d'une couche à faible taux de fibres du côté du moule rigide et une couche à plus haut taux de fibres du côté de la paroi flexible (Radford, 1993; Yang et Huang, 1997). Le composite n'est alors plus totalement symétrique et une courbure convexe (du moule vers la membrane) se développe lors du démoulage de la pièce comme illustré sur la Figure 1-14. Pour un composite en L, ce gauchissement modifie la valeur

effective de la distorsion en fonction de la nature convexe ou concave du moule de fabrication (Radford, 1995; Yang et al., 2003).

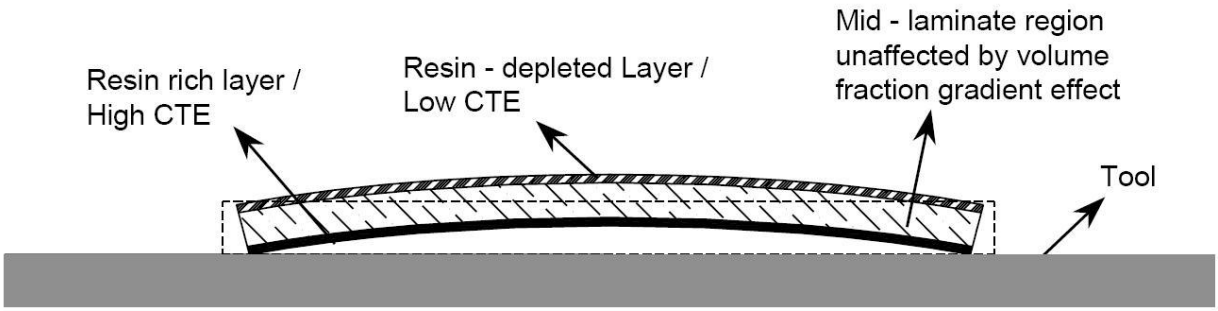

Figure 1-14 : Phénomène de gauchissement causé par un gradient de taux de fibres à travers l'épaisseur du composite (Bapanapalli et Smith, 2005).

Des défauts de fabrication entrainant une distribution non homogène de la matrice et des fibres dans la zone courbée influence aussi la distorsion résiduelle. Par exemple, Wiersma et al. (1998) ont observé une distorsion plus importante pour des pièces comportant une surépaisseur dans la courbure. Un comportement similaire a aussi été observé pour des composites à matrice thermodurcissable (Salomi et al., 2008). Des travaux numériques ont aussi souligné l'influence potentielle des régions riches en résine sur la déformation de pièces courbées comme des raidisseurs en T (Dong et al., 2004a, 2004b). Cependant, il a été récemment remarqué qu'aucune étude visant à quantifier de façon systématique l'impact des défauts de fabrication sur la distorsion n'a jusqu'à maintenant était publiée (Dong, 2011).

Interaction moule/pièce

Le cycle de cuisson utilisé en autoclave commence généralement par l'application de la pression de consolidation suivie d'une montée en température. Au cours de cette phase de chauffage, le moule et le renfort pré-imprégné se dilatent de façon différente. Par exemple l'aluminium et l'acier pouvant être utilisés pour la fabrication des moules ont un coefficient de dilatation thermique de l'ordre de 10^{-5}/ºC, soit bien supérieur à celui des fibres. Par frottement, les fibres en

contact avec le moule sont alors chargées en tension et l'ensemble de l'empilement est cisaillé à travers son épaisseur. Cet effet d'interaction moule/pièce est illustré sur la Figure 1-15a dans le cas d'un composite plan. Après démoulage, les contraintes fibreuses sont libérées et un gauchissement apparaît sur le composite (Figure 1-15b).

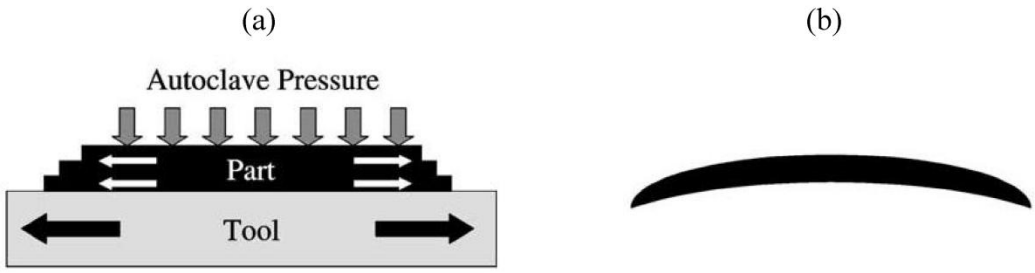

Figure 1-15 : Illustration du mécanisme d'interaction moule/pièce pour un composite plan (Twigg et al., 2004a): (a) cisaillement de la préforme au cours de la montée en température; (b) gauchissement de la pièce après démoulage.

L'influence de l'interaction moule/pièce sur la déformation dépend de la rigidité de la pièce: l'effet diminue lorsque l'épaisseur augmente (Cann et Adams, 2001; Darrow Jr et Smith, 2002). Le transfert de contraintes du moule à la pièce est aussi dépendant de la nature de l'empilement et du traitement de surface utilisé pour le démoulage (Radford, 2010). Il faut aussi remarquer que le gauchissement dû à l'interaction moule/pièce (Figure 1-15b) et celui dû au gradient de taux de fibres (Figure 1-14) sont similaires et peuvent être difficiles à analyser séparément. L'impact subséquent de l'interaction moule/pièce sur la distorsion effective d'une pièce en L dépend donc lui aussi de la nature du moule. Comme illustré sur la Figure 1-16, un moule convexe tend à amplifier la distorsion alors qu'un moule concave en limite les effets apparents. Ce mécanisme de distorsion peut être atténué en utilisant un matériau à faible dilatation thermique (comme de l'invar) pour la fabrication de l'outillage (Bapanapalli et Smith, 2005; Huang et Yang, 1997a) .

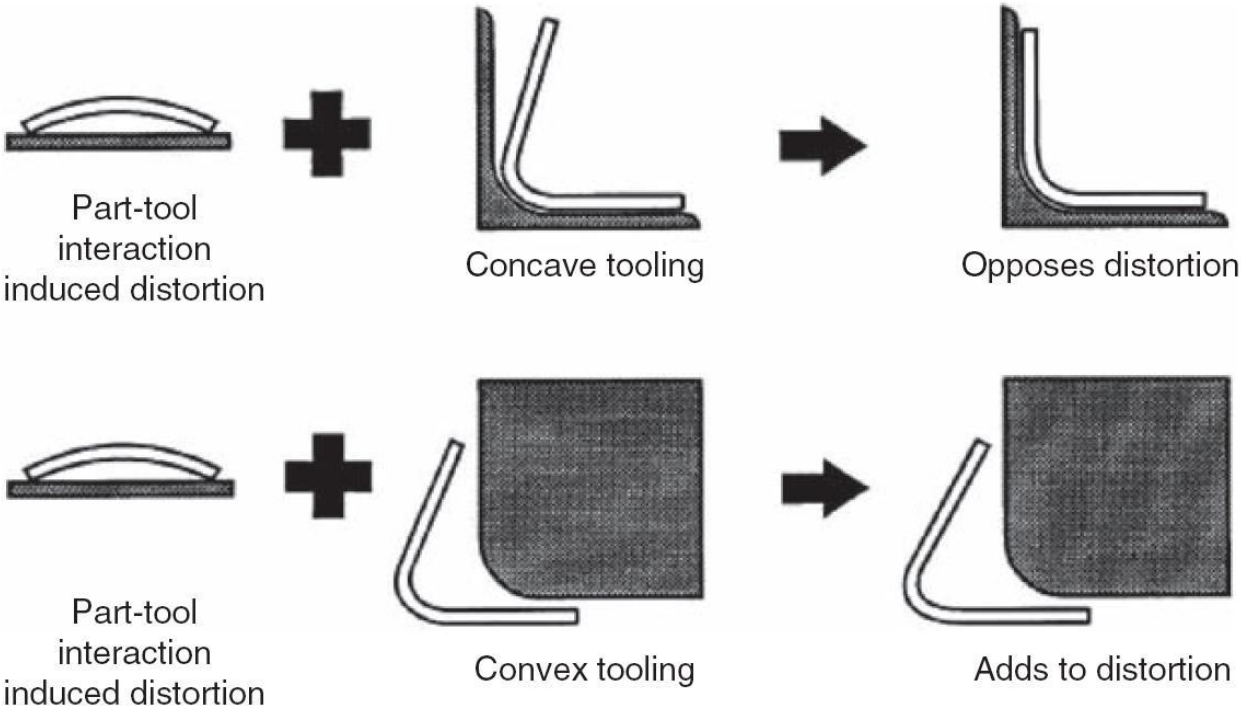

Figure 1-16 : Influence de l'interaction moule/pièce sur la distorsion effective d'un composite en L (Radford, 2010).

Contrainte fibreuse due à la consolidation courbée

En dehors des mécanismes de dilatation, la simple application d'une pression de consolidation introduit des contraintes sur le renfort fibreux. Dans le cas d'une pièce plane, la contrainte effective est principalement une contrainte en compression à travers l'épaisseur de la pièce n'ayant aucun impact sur la distorsion. Pour un composite courbé, l'application de la pression de mise en forme peut en revanche entraîner l'apparition de contraintes planaires dans le composite. Ce mécanisme illustré sur la Figure 1-17 dans le cas d'un moule concave a déjà été proposé comme source de distorsion potentielle (Ersoy et al., 2005b; Potter et al., 2005). Cependant, aucun travail publié n'a essayé de quantifier la déformation additionnelle pouvant être générée par ce mécanisme.

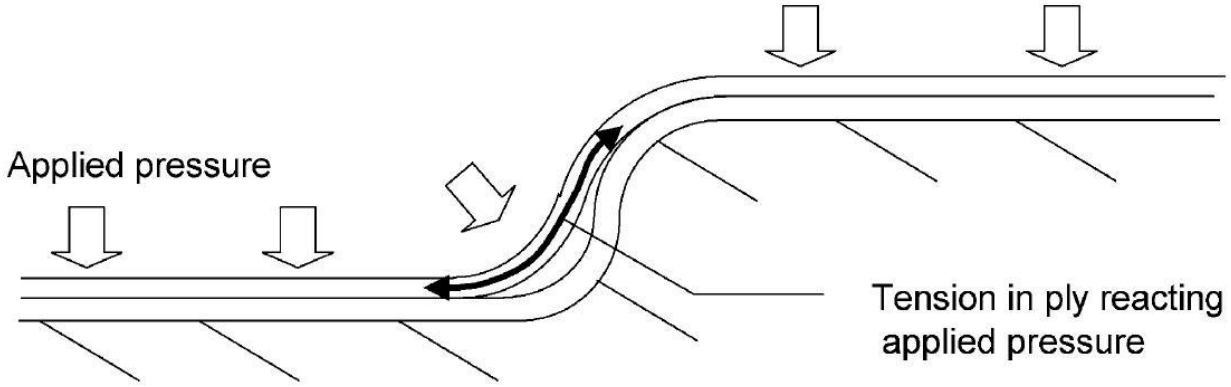

Figure 1-17 : Illustration schématique de l'introduction de contraintes planaires sur le renfort fibreux lors de la consolidation sur un moule concave (Potter et al., 2005).

1.3.4 Prédiction de la distorsion

Approches analytiques

La méthode de prédiction la plus citée dans la littérature est une formule analytique initialement proposée par Radford (1987) permettant d'évaluer la distorsion d'une pièce courbée d'angle θ:

$$\frac{\Delta\theta}{\theta} = \frac{(\alpha_i - \alpha_t)\Delta T}{1+\alpha_t \Delta T} - \frac{\phi_i - \phi_t}{1+\phi_t} \tag{2.1}$$

où ΔT est le changement de température (généralement un refroidissement de la température de mise en forme jusqu'à la température ambiante); α_i et α_t sont les coefficients de dilatation thermique dans le plan et à travers l'épaisseur; ϕ_i et ϕ_t sont les contractions dues au retrait chimique dans le plan et à travers l'épaisseur.

L'équation (2.1) a été utilisée dans plusieurs travaux en considérant des coefficients de dilatation et de contraction chimique constants. Cette approche a notamment permis de reproduire plusieurs résultats expérimentaux comme la proportionnalité entre l'angle de distorsion et l'angle total pour des angles variant de 15 à 135° (Huang et Yang, 1997b) ou l'évolution linéaire de l'angle de distorsion en fonction de la température (Radford et Diefendorf, 1993; Radford et Rennick, 2000). D'autres études ont apporté des modifications à l'équation (2.1) pour inclure une

dépendance en température des coefficients de dilatation (Ersoy et al., 2005a; Salomi et al., 2008; Yoon et Kim, 2001).

Les coefficients de dilatation thermique peuvent être directement mesurés sur des échantillons composites (Fu et Radford, 1999; Yoon et Kim, 2001) ou estimés par analyse micromécanique. Pour un composite unidirectionnel, des relations analytiques ont été proposées pour déterminer les coefficients de dilatation longitudinal et transverse à partir des propriétés de chaque constituant. Les plus souvent utilisées sont les formules proposées par Schapery (1968) mais d'autre méthodes analytiques existent (Karadeniz et Kumlutas, 2007). À partir des propriétés caractéristiques d'un pli unidirectionnel, les coefficients de dilatation thermique d'un empilement multidirectionnel peuvent enfin être déterminés à l'aide d'une analyse tridimensionnelle du laminé (Dong, 2009a; Goetschel et Radford, 1997). Un autre approche consiste à utiliser une analyse micromécanique par éléments finis pour estimer les différents coefficients de dilatation sur un volume unitaire représentatif (Dong, 2008; Islam et al., 2001). Les contractions dues au retrait chimique peuvent aussi être estimées à partir de relations micromécaniques bien que cette approche soit plus délicate (Nelson et Cairns, 1989). En effet, le pourcentage du retrait total intervenant effectivement dans la distorsion est difficile à déterminer à priori. Pour pallier cette limitation, des procédures de mesure in situ ont été proposées afin d'estimer l'expansion du composite au cours de la cuisson (Garstka et al., 2007). D'autres travaux ont ajusté la valeur du retrait chimique effectif a posteriori en ajustant les prédictions de l'équation (2.1) avec les mesures expérimentales de l'angle de distorsion (Radford, 1995). Enfin, plusieurs études ont introduit un coefficient de dilatation effectif incluant les effets de la dilatation thermique et du retrait chimique (Bapanapalli et Smith, 2005; Dong, 2009a; Hsiao et Gangireddy, 2008).

Le principal désavantage de l'équation (2.1) est qu'elle ne prend pas en compte les effets de l'interaction moule/pièce. Bien qu'elles soient moins souvent utilisées, d'autres approches analytiques ont été proposées notamment en modifiant la théorie des laminés pour inclure une déformation à travers l'épaisseur du composite (Jain et Mai, 1996, 1997). Plus récemment, Arafath et al. (2009) ont développé une formulation analytique permettant d'inclure les effets de

l'interaction moule/pièce dans l'analyse. Ce travail se limite cependant au cas de composites minces possédant un rapport rayon sur épaisseur supérieur à 8.

Travaux de simulation numérique

Les approches analytiques discutées précédemment peuvent être étendues à des géométries courbées plus générales qu'un simple L (Dong, 2009b), mais ne peuvent pas s'appliquer à des géométries complexes comportant notamment des doubles courbures. Dans ce genre de situation, l'analyse numérique fondée sur le calcul par éléments finis est la seule option disponible pour prédire la déformation résiduelle. La distorsion de composite courbées a notamment été étudiée à l'aide de logiciels commerciaux de simulation ou à l'aide d'outils numériques spécialement développés (Johnston et al., 2001; Zhu et al., 2001). L'utilisation d'un logiciel commercial permet de réduire le temps de développement et aussi d'implémenter des lois de comportement complexes à l'aide de sous-routines usager (Clifford et al., 2006; Ersoy et al., 2010b; Svanberg et Holmberg, 2004a). L'utilisation d'un code « maison » offre quant à elle une plus grande liberté pour la modélisation mais nécessite en contrepartie des efforts de développement plus importants.

Les premières utilisations de la méthode des éléments finis pour prédire la distorsion ont utilisé des lois de comportement simples (linéaire élastique) et ne s'intéressaient qu'à la déformation induite par la dilatation (Radford, 1987; Zahlan et O'Neill, 1989). Au fils des années, des analyses plus détaillées ont été développées pour incorporer notamment :

- un développement graduel des propriétés mécaniques et thermiques au cours de la cuisson (Johnston et al., 2001; Oakeshott, 2003; Svanberg et Holmberg, 2004b);
- une modélisation viscoélastique du comportement (Clifford et al., 2006; Wiersma et al., 1998; Zhu et al., 2001);
- une représentation entièrement tridimensionnelle (Bapanapalli et Smith, 2005; Clifford et al., 2006; Svanberg et al., 2005)
- la prise en compte d'hétérogénéités de fabrication comme des gradients de taux de fibres (Darrow Jr et Smith, 2002) ou des variations d'épaisseur (Oakeshott, 2003).

Une des principales difficultés de la prédiction de la distorsion par éléments finis reste la modélisation du phénomène d'interaction moule/pièce. Dans le logiciel COMPRO, il a été proposé d'ajouter une couche à faible cisaillement pour simuler l'interface entre le composite et l'outillage (Fernlund et al., 2002b). Bien qu'intéressante, cette approche reste limitée car elle nécessite d'ajuster les propriétés de la couche de cisaillement en fonction de la longueur de la pièce (Twigg et al., 2004b). Il faut enfin souligner que malgré l'évolution constante de la puissance des ordinateurs, le temps de calcul peut encore s'avérer important pour les simulations tridimensionnelles de pièces aéronautiques réelles de grande taille. Afin de diminuer les temps de calcul, Fernlund et al. (2003) ont couplé un code simulation 2D des contraintes résiduelles (COMPRO) à un logiciel commercial d'analyse structurelle 3D (Abaqus). Cette approche permet effectivement d'accélérer la résolution tout en conservant une bonne précision des prédictions. Cependant, les auteurs admettent que cette méthodologie peut être difficile à implémenter pour certaines géométries et demande plus d'étapes qu'une analyse tridimensionnelle directe.

1.3.5 Mesure de la distorsion

Quelques études ont utilisé des techniques très simples pour mesurer l'angle de distorsion comme tracer le profil de la pièce sur une feuille de papier (Hsiao et Gangireddy, 2008; Yoon et Kim, 2001). Bien que très facile à implémenter, la précision d'une telle mesure peut s'avérer insuffisante pour obtenir des résultats exploitables. A l'opposé, d'autres travaux ont utilisé des machines de mesure tridimensionnelle perfectionnées (Oakeshott, 2003; Salomi et al., 2008; Yang et al., 2003). Un tel équipement fournit une mesure très précise mais nécessite un investissement important. Enfin, certains auteurs ont développé des techniques d'analyse d'images à partir de simples photographies (Bapanapalli et Smith, 2005; Darrow Jr et Smith, 2002) ou d'images scannées des pièces (Albert et Fernlund, 2002). Ce type de procédure est une bonne option pour obtenir une précision convenable tout en limitant les coûts expérimentaux. Il faut enfin remarquer que la forme de l'échantillon étudié peut avoir une influence sur la mesure de l'angle distorsion. Pour un composite en L, un faible gauchissement des parties planes peut par exemple modifier la mesure de l'angle de distorsion de façon significative (Albert et Fernlund, 2002).

Mesurer précisément l'angle de distorsion après démoulage est une étape essentielle de tout travail expérimental étudiant la déformation résiduelle. Cependant la valeur totale de cet angle ne donne aucune information sur les contributions relatives des différentes sources de distorsion. Afin de mieux comprendre l'importance de chaque mécanisme de déformation, une procédure particulièrement intéressante a été proposée par Radford et Diefendorf (1993). L'approche consiste à enregistrer l'évolution de la forme de l'échantillon en fonction de sa température à l'aide d'un montage spécialement développé (Figure 1-18a). Ce dispositif placé dans une enceinte à température contrôlée utilise un ensemble de miroirs et de rayons laser ainsi qu'un moteur électrique imposant une rotation précise à l'assemblage. La Figure 1-18b montre un résultat de mesure typique. Tel qu'indiqué sur ce schéma, la distorsion totale est séparée en une composante thermoélastique due à la dilatation différentielle et une composante non-thermoélastique due aux effets irréversibles du retrait chimique et de l'interaction moule/pièce. Cette méthodologie a par la suite été reprise dans plusieurs études visant à estimer les contributions de chacune des sources de déformation afin d'en corriger les effets (Radford, 2010; Radford et Rennick, 2000).

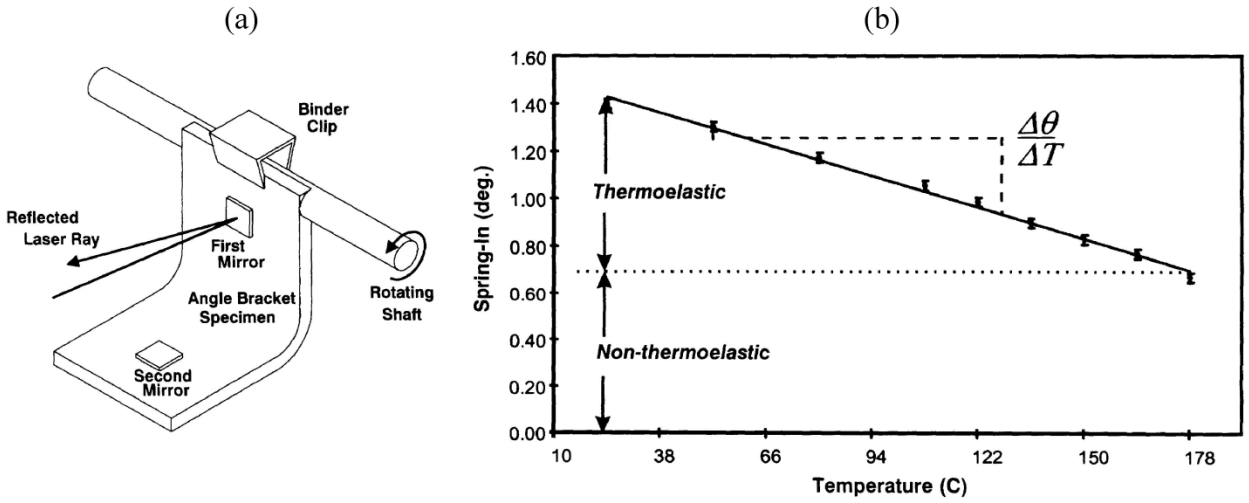

Figure 1-18 : Séparation des composantes thermoélastique et non thermoélastique de la déformation (Radford et Rennick, 2000): (a) montage expérimental de mesure de l'angle de distorsion; (b) exemple de résultats.

1.3.6 Stratégie de correction

A l'heure actuelle, il n'existe aucun outil de prototypage virtuel « clé en main » pour concevoir une pièce composite et déterminer les paramètres de fabrication adéquats afin d'obtenir une géométrie finale parfaitement maitrisée. En revanche, plusieurs approches ont été proposées afin de corriger les effets néfastes de la distorsion résiduelle. Cette dernière partie de la recherche bibliographique résume les différentes options envisageables.

Conception de moules avec compensation de la distorsion

La méthode la plus intuitive pour corriger les déformations résiduelles consiste simplement à adapter la géométrie du moule de fabrication. Cette approche a notamment été utilisée pour fabriquer des nervures aéronautiques en U possédant un angle de 90º à température ambiante (Jain et al., 1998). Déterminer la géométrie du moule peut s'avérer plus difficile dans le cas d'une structure plus complexe. Par exemple, Capehart et al. (2007) ont eu recours à une procédure itérative de simulations par éléments finis afin de déterminer la géométrie du moule permettant de fabriquer une carrosserie de porte automobile avec la géométrie souhaitée. Enfin, il convient de remarquer que cette stratégie ne permet que de corriger la forme de la pièce à une température donnée. Si la température évolue au cours de l'utilisation, une déformation thermoélastique de la structure ne peut pas être évitée par compensation de la géométrie du moule.

Orientation des fibres

La stabilité dimensionnelle en température peut être améliorée par introduction locale d'asymétrie dans la séquence d'empilement (Radford et Diefendorf, 1993). La Figure 1-19 montre des exemples d'empilement non symétrique dans l'angle du composite visant à rendre une structure en L stable en température. Un choix adéquat de l'empilement local peut effectivement corriger les effets de distorsion thermoélastique pour des pièces fabriquées avec des moules convexes ou concaves (Huang et Yang, 1997a, 1997b; Radford et Diefendorf, 1993). Cette approche peut être aussi couplée à une stratégie de compensation du moule pour produire des pièces à géométrie contrôlée et stables en température (Radford, 2010).

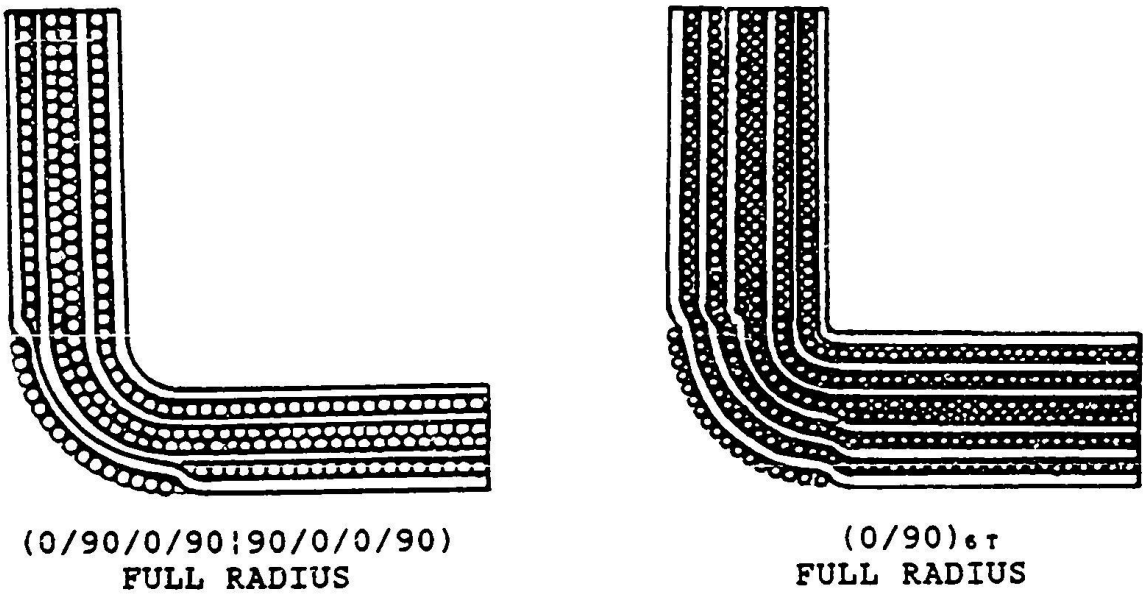

Figure 1-19 : Utilisation d'un empilement non symétrique visant à corriger la distorsion résiduelle (Radford et Diefendorf, 1993).

Utilisation d'une post-cuisson

Au cours de la cuisson, la résine originellement liquide passe dans un premier temps à l'état caoutchouteux puis vitreux. Ces changements d'état s'accompagnent d'une évolution des modules, coefficients de Poisson et coefficients de dilatation thermique du composite (Ersoy et al., 2010a; Ruiz et Trochu, 2005c). Le coefficient de dilatation thermique est notamment plus important à l'état caoutchouteux qu'à l'état vitreux. La distorsion finale d'un composite dépend ainsi fortement de l'historique de cuisson. Par exemple, une température de mise en forme plus basse suivie d'une post cuisson peut réduire la déformation résiduelle de façon significative (cf. Figure 1-20). Si cette procédure peut effectivement réduire la distorsion, l'allongement du temps de cycle associé limite fortement son application en pratique.

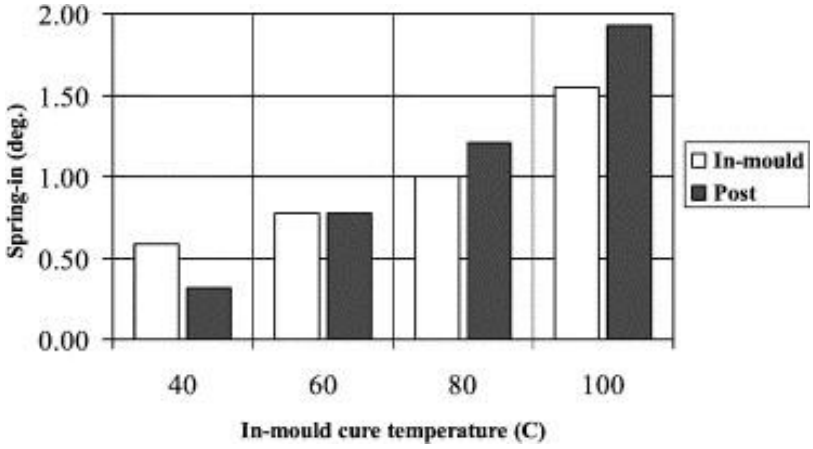

Figure 1-20 : Influence de la température de cuisson sur l'angle de distorsion mesuré avant (In-mould) et après post-cuisson (Post) (Svanberg, 2001).

Modification de la dilatation thermique par ajout de nanoparticules

Depuis quelques années, de nombreux travaux visent à améliorer le comportement des résines par ajout de nanoparticules (nanotubes de carbone, nano-fibres, nano-argiles). Ces particules possèdent en effet des caractéristiques très particulières susceptibles de modifier les performances des résines pour des taux de charge relativement faibles. Par exemples, les nano-fibres de carbone possèdent un coefficient de dilatation thermique négatif. En incorporant ces nano-fibres dans la résine, Hsiao & Gangireddy (2008) ont observé une diminution de la déformation résiduelle de composites verre/polyester de 73% avec un pourcentage de charge en nano-fibres aussi faible que 1.5%. Cette stratégie relativement récente ouvre une nouvelle piste pour corriger la distorsion. Les travaux futurs dans cette direction devront cependant s'assurer que l'incorporation de nano-particules n'engendre pas une augmentation drastique de la viscosité de la résine pouvant nuire à la mise en forme du composite.

CHAPITRE 2 MOTIVATION ET OBJECTIFS

2.1 Motivation et hypothèse

En dehors de leurs propriétés physiques et chimiques intrinsèques, les matériaux composites ont aussi l'avantage de permettre la fabrication de structures de grande taille. Cette caractéristique permet de diminuer le nombre de pièces nécessaires et le temps d'assemblage requis comparativement aux matériaux métalliques. Cet effort de consolidation des pièces structurales mène en revanche à des géométries complexes comportant notamment des brides de fixation ou des nervures de renfort mécanique. Ces éléments de conception se présentent généralement sous la forme d'angles droits nécessitant des faibles rayons de courbure. La Figure 2-1 montre un exemple de pièce réelle comportant des zones fortement courbées. Cette géométrie a été proposée par le partenaire industriel du projet et illustre le type d'application visée pour le développement à long terme du procédé.

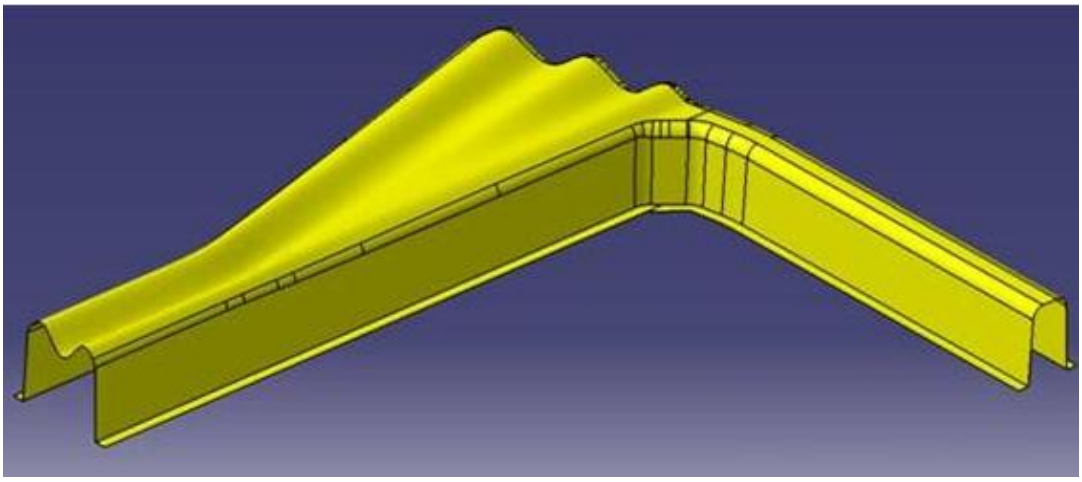

Figure 2-1 : Exemple de géométrie d'une pièce automobile proposée par le partenaire industriel.

Tel que mentionné dans la revue bibliographique, l'injection flexible n'a jusqu'à maintenant été appliquée qu'à des géométries relativement simples: planes ou faiblement courbées. Cependant, le principe de fonctionnement du procédé décrit sur la Figure 1-1 n'impose a priori aucune

restriction quant à la géométrie de la pièce fabriquée. **L'hypothèse principale de ce travail stipule donc que le procédé d'injection flexible peut être utilisé pour la mise en forme de structures complexes comportant notamment des zones de forte courbure.** Avant de formuler les objectifs permettant de valider cette hypothèse, il convient de souligner deux enseignements appris au cours de la recherche bibliographique:

- La mise en forme par les procédés traditionnels peut générer des défauts de fabrication dans les zones de forte courbure. Ce phénomène est principalement dû aux mécanismes de déformation des renforts fibreux et peut être particulièrement important lorsque l'outillage possède une paroi flexible.
- La distorsion d'une pièce composite courbée dépend du procédé de fabrication utilisé et peut être influencée par la qualité de la mise forme. En revanche, aucune étude publiée n'a jusqu'à présent tenté d'étudier l'influence d'éventuels défauts de fabrication sur la déformation résiduelle de façon systématique.

2.2 Objectifs

L'objectif général du projet est d'analyser les caractéristiques spécifiques du procédé d'injection flexible lors de la mise en forme d'une pièce composite haute performance possédant des zones de forte courbure. Le spécimen considéré est représenté sur la Figure 2-2b. Il s'agit d'un panneau rectangulaire possédant deux angles droits (i.e. une géométrie de type marche d'escalier). Le moule « Polyflex II » permettant de fabriquer ce spécimen illustré sur la Figure 2-2a était déjà disponible dans le laboratoire au début de ce projet. En revanche, cet outillage n'avait encore pas été adapté pour permettre une mise en forme robuste par injection flexible. Afin d'atteindre l'objectif principal et éventuellement confirmer l'hypothèse de travail, les quatre objectifs spécifiques suivants ont été identifiés:

- Objectif 1: Développer une procédure de mise en forme robuste permettant de fabriquer la pièce test de manière répétable.
- Objectif 2: Mettre au point des méthodes expérimentales simples et peu onéreuses pour caractériser la qualité de mise en forme générale (variations d'épaisseur, répartition fibres/matrice) et la stabilité dimensionnelle des pièces fabriquées.

- Objectif 3: Identifier les paramètres de fabrication gouvernant la qualité de mise en forme du composite dans les zones courbées.
- Objectif 4: Analyser la spécificité éventuelle du procédé eu égard à la distorsion résiduelle des pièces fabriquées.

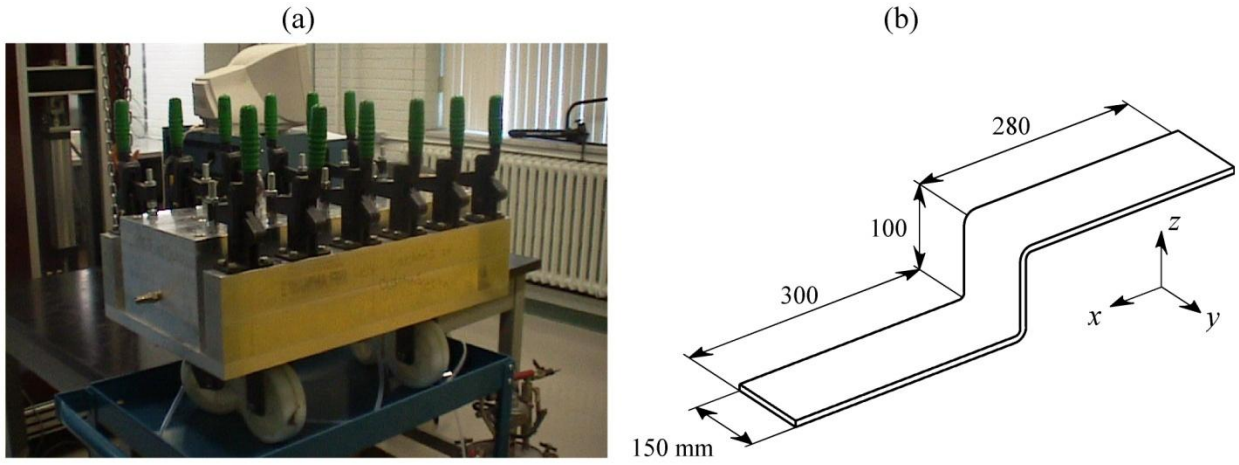

Figure 2-2 : Moule de deuxième génération “Polyflex II” (a) et géométrie de la pièce associée (b).

Les différents objectifs ont été réalisés à travers 3 articles présentés dans les chapitres suivants. Le premier article publié dans la revue *Polymer Composites* présente la procédure de fabrication développée ainsi que les méthodes utilisées pour caractériser les défauts de fabrication. Les premières fabrications réalisées permettent notamment d’illustrer le comportement spécifique des parties courbées et l’importance de la phase de préformage. Le deuxième article analyse la déformation du renfort fibreux au cours du cycle de production pour mieux comprendre les mécanismes de création des défauts. Ce travail a été soumis à *International Journal of Material Forming*. Le dernier article, soumis à la revue *Composites Part A: Applied Science and Manufacturing,* étudie la distorsion des pièces fabriquées. Ce travail cherche notamment à isoler les différentes sources de déformation résiduelle afin d’évaluer si le procédé a une influence sur le tolérancement géométrique de la pièce finale.

CHAPITRE 3 ARTICLE 1: EXPERIMENTAL STUDY OF FLEXIBLE INJECTION TO MANUFACTURE PARTS OF STRONG CURVATURE

Philippe Causse [1], Edu Ruiz and François Trochu

Department of Mechanical Engineering and Chair on Composites of High Performance, Centre de recherche en plasturgie et composites (CREPEC), École Polytechnique de Montréal, P.O. Box 6079, Station "Centre-Ville", Montreal, Canada, H3C 3A7

[1] *Corresponding author's Email: trochu@polymtl.ca*

3.1 Abstract

Flexible injection (FI) is a new process for the manufacture of high performance composites, which consists of injecting a thermosetting resin through a fibrous reinforcement contained in the lower chamber of a double cavity mold. Resin is injected in the lower cavity, which is sealed by a membrane, and then a compaction fluid is injected in the upper chamber to compress the reinforcement. This new composite manufacturing technique, which allows a limited and controlled deformation of the flexible membrane during processing, was shown to be very effective in reducing filling times in the case of planar or slightly curved geometries. In the present study, flexible injection is applied to strongly curved parts, namely here a composite rectangular panel with two 90° corners. After setting up an experimental procedure to produce the stair-shaped components out of fiberglass and vinylester resin, longitudinal cross-sections of the parts are analyzed to assess the quality of the final product in both the flat and curved zones. This characterization method allows detecting manufacturing defects such as thickness gradients or resin-rich zones. Such defects are likely to induce geometrical deformations of the component and may decrease its mechanical performance. Therefore they ought to be minimized to improve the overall quality of the part. Modifications of the manufacturing procedure are proposed in this paper to decrease the importance of process-induced defaults and improve the performance of the flexible injection.

3.2 Introduction

Over the past decades, fiber reinforced thermoset composites have become popular in many demanding applications. Among the multiple manufacturing techniques available to process these advanced materials, *Liquid Composite Molding* (LCM) processes have received much attention because of their ability to fabricate composite structures of complex shape at lower cost than traditional autoclave processing. The two principal LCM techniques, *Resin Transfer Molding* (RTM) and *Vacuum Assisted Resin Infusion* (VARI), have been adapted over the years to devise new process variants such as *Compression Resin Transfer Molding* (CRTM), SCRIMP or *Liquid Resin Infusion* (LRI) for faster and more reliable manufacturing. However, despite an important amount of experimental and theoretical work in this area, none of these techniques is suited for high volume production because of relatively long cycle times. For this reason, a new approach called *Flexible Injection* (FI) was devised recently for fast manufacturing of thermoset matrix composites [1, 2].

3.2.1 Flexible Injection

Flexible Injection is a closed mold technique, in which a rigid mold is separated into two cavities by a flexible membrane. The main stages of the manufacturing cycle are schematically presented in Figure 3-1 and described as follows:

(1) A fibrous preform is placed in the bottom cavity and a flexible membrane is laid upon the bottom half of the mold, which is then closed with an upper mold half.

(2) A volume of resin is injected in the lower cavity (injection chamber), which inflates the membrane until it reaches the upper wall of the cavity.

(3) A pressurized fluid is introduced in the upper cavity (compaction chamber), which imposes through the membrane a compaction pressure on the fiber bed and the resin. As a result, this completes the impregnation of the fiber bed.

(4) After mold filling, the part is cured under constant pressure of the compaction fluid.

(5) Finally, vacuum is applied in the compaction chamber to remove the fluid, the mold is opened, and the part is demolded.

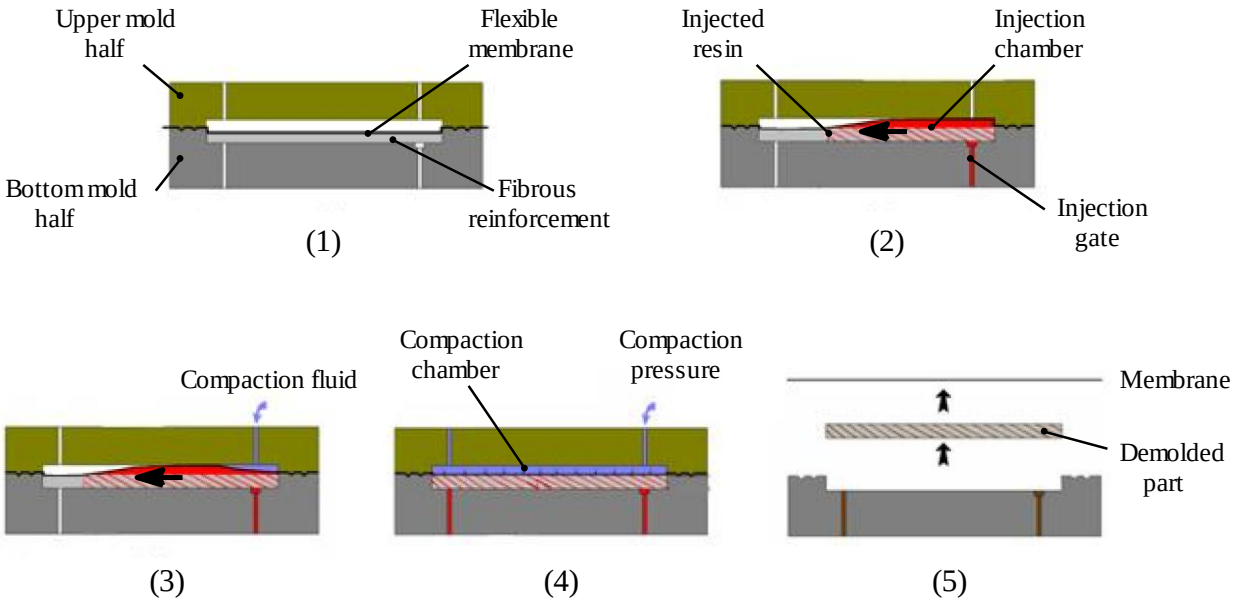

Figure 3-1 : Main steps of the *Flexible Injection* process.

Flexible injection was proven to be a very effective way not only to reduce filling times in the case of simple (planar or slightly curved) geometry [1, 2], but also to improve part quality thanks to the through-thickness consolidation of the composite provided by the compaction fluid. Further process development is of paramount importance in order to evaluate the potential of this new approach for complex geometries, especially in the case of curved parts.

During flexible injection, the final shape of the part is the result of a consolidation process of the saturated fiber bed between a rigid tool and a flexible membrane. This kind of consolidation can also be found in other composite manufacturing techniques such as VARI or autoclave processing. When working with a flexible tool, it often turns out to be difficult to manufacture curved parts of consistent quality [3]. Among all the possible curved geometries, angle-bent shapes such as L-brackets, C-channels or T-stiffeners are special cases of interest. Such typical features being common components in many complex structures, their fabrication has indeed been the topic of numerous investigations and resulted in many scientific or technical publications. Although most of the scientific studies were conducted on parts processed in autoclave, the particular defects observed in the curved areas are very often encountered in other manufacturing processes.

3.2.2 Bibliography

In an extensive experimental study on autoclave processing of L-shaped parts, Hubert and Poursartip [4] showed that sharply curved regions were prone to exhibit manufacturing defects such as voids, fiber wrinkles or resin pockets. Fiber wrinkling and fiber bridging are typical phenomena appearing when one tries to drape plies of continuous fibers into a curved tool [5, 6]. Jain et al. [7] observed that fiber bridging occurs at the corner of L-shaped laminates produced on a female mold. This phenomenon leading to the formation of a resin-rich zone on the mold side was not observed with a male tool. Wisnom et al. [8] reported a corner thickening behavior in concave tools due to fiber bridging. Feih and Shercliff [9] observed that fiber buckling could generate resin pockets in the corner of L-parts. Finally, Oakeshott [10] obtained different qualities of corners depending on fiber orientation : fibers parallel to the L shape led to part thinning and to the creation of resin-rich zones, whereas for fibers perpendicular to the curved profile, no significant thickness variations were observed, although this led to important fiber misalignments.

The absence of visible manufacturing defects does not necessarily guarantee a perfectly homogeneous product. Naji and Hoa [11] studied the influence of resin cure on the quality of thick L-shaped composites and noticed that the use of the recommended curing cycle led to part thickening and to the appearance of gradients in fiber volume fraction in the corners of the part. The authors also proposed a modified curing procedure that could significantly reduce the observed variations [12]. Image analysis performed by Wiersma et al. [13] showed that parts produced on a male mold were thinner, but had an homogeneous fiber volume fraction through the thickness, whereas parts made on a female mold were thicker and exhibited an inhomogeneous fiber/matrix distribution. Hubert and Poursartip [4] explained these specific behaviors in curved sections by an heterogeneous consolidation pressure and local modifications of the compaction response due to fiber orientation. They also found that thickness variations in the corners were greatly influenced by the curvature of the mold (convex or concave). Such behavior had been previously reported by Mallon et al. [14] during the processing of thermoplastic composites formed with a diaphragm. Yang et al. [15] showed that the use of caul sheets could eliminate corner thickness variations by improving the pressure distribution imposed in the curved regions. Such correction was found to be effective only if the caul plates were

sufficiently rigid and adequately dimensioned. The stiffness of the caul sheets was shown by Fernlund et al. [16] to have a strong influence on consolidation in the corners.

Several authors have used numerical modeling to understand the specific behavior of curved sections during consolidation. Hubert et al. [17] developed a 2D finite element model to simulate the autoclave processing of angle-shaped laminates with a convex tool. They found that the consolidation of curved sections was mostly dictated by the shear behavior of the fiber bed with high shear modulus resulting in important corner thickening. Based on a similar approach, the influence of shear behavior was also outlined by Li and Tucker [18]. These authors suggested that the combination of low shear modulus and convex tooling could lead to the formation of wiggles at the corners of the part, but no experimental observation did support their numerical results. However, this hypothesis is consistent with the fiber wrinkling mechanism mentioned above. Recently, Li et al. [19, 20] used a 2D consolidation model to study the manufacture of cornered laminates. These two studies confirm that composite consolidation in curved regions is mainly governed by the shear behavior of the fiber bed. In particular, the stacking sequence has a direct influence on the thickness variations in curved areas as it affects the deformation mode of the fiber bed. These conclusions were well supported by experimental observations.

3.2.3 Outline

The experimental study of manufacturing defects in curved composite specimens was carried out in this paper for stair-shaped rectangular composite samples made by flexible injection process. Firstly, the fibrous reinforcement was preformed in a separate tool. After manufacturing, the quality of the parts was evaluated by analyzing the uniformity of the specimen consolidation in the straight and curved sections.

This paper begins by presenting the experimental setup, and then describes the fabrication of the samples including the preforming procedure of the dry reinforcement. The consolidation of the specimens was studied by image analysis. Preliminary compaction tests were also conducted to select appropriate fiber volume fractions for the test parts, after which a plan of experiments is devised to fabricate a series of test parts by flexible injection. Finally, cross-sections of the

specimens are analyzed to evaluate the uniformity of composite consolidation in several regions of interest: (1) horizontal and vertical straight sections; (2) areas of convex or concave curvatures.

3.3 Experimental setup

The manufacturing experiments were performed with the aluminum mold shown in Figure 3-2a. This setup was designed to process the stair-shaped part of Figure 3-2b. The part consists of three planar sections separated by two right-angled corners. Figure 3-3 shows a schematic representation of the tool. The two mold halves are separated by a flexible membrane cut out from a planar sheet of fluoroelastomer VITON from DuPont (thickness 1/32'', hardness 75 A). A silicone gasket is glued on the top mold around the periphery of the cavity to improve sealing in both cavities. Because of the through-thickness asymmetry of the fabrication process, the two curved regions must be distinguished: with respect to the vertical closing axis of the mold, the top curved area is associated with a convex rigid tool, and the bottom curved section to a concave rigid tool. The radii of curvature of the rigid tool side are respectively 3 mm for the convex corner and 5 mm for the concave corner. It is interesting to note that the central flat region is parallel to the mold closing axis. In the case of RTM, this configuration is not really feasible and could lead to preform shearing during closure of the tool. This problem does not exist in flexible injection, since the overall cavity is thicker than the fiber bed.

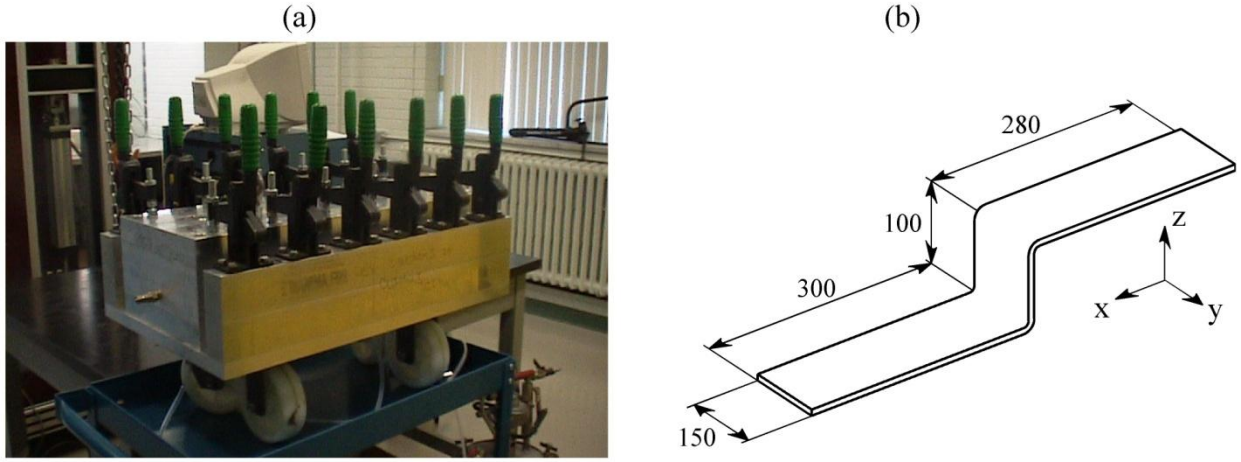

Figure 3-2 : Implementation of flexible injection process for curved parts: (a) experimental aluminum mold; (b) geometry of the part (dimensions are in mm).

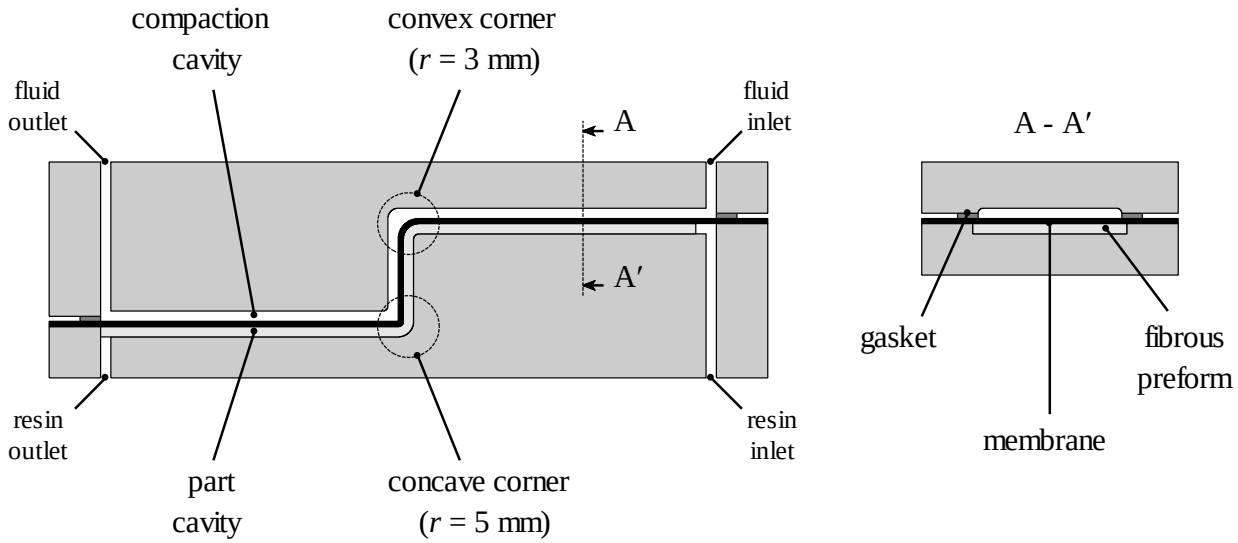

Figure 3-3 : Schematic view of the mold configuration.

3.4 Methodology

This section presents the materials used in the experiments and describes the fabrication and testing procedures followed to manufacture the stair-shaped composite specimens. This research aims to evaluate manufacturing defects in the flat sections and in the corners of the test parts.

3.4.1 Materials

The resin used to manufacture the composite parts was a vinyl ester resin DERAKANE 411-350 from Ashland Inc. The cure initiator was methylethylketone peroxide MEKP 925-H from Norox (1.25 phr) and promoter was cobalt naphtenate 12% (0.1 phr). A gel time retarder, 2-4 pentanedione (0.08 phr), was used to adjust the gel time to approximately two hours. The fibrous reinforcement was an E glass non-crimp stitched fabric Roviply (+45˚, 400 g/m^2 // -45˚, 400 g/m^2 // random mat, 225 g/m^2) from Chomarat (France).

3.4.2 Preforming

Because of the sharp corners of the part, it is nearly impossible to lay up several plies of the dry fabric into the mold prior to closing. For ease of handling, the fiber bed must be preformed to the desired shape before laying it into the cavity. For that purpose, the fabric already contains an epoxy binder (20 g/m^2) that requires a hot (200°C) preforming mold. Because of the lack of such equipment, a simple preforming procedure was devised at room temperature. First, a small quantity of the thermoset system (same formulation than previously stated) was sprayed on both sides of each fabric ply with a pressure gun. The plies were then stacked between two folded aluminum plates and full vacuum was drawn in the cavity (see details in Figure 3-4). Calibrated plastic sheets shown in Figure 3-4b allowed adjusting the vertical dimension L_p of the two plates. A self-hardening modeling clay was applied with a radius gauge in the corners to modify the radii of curvature. After application of the vacuum pressure, the preform was left overnight to cure at room temperature.

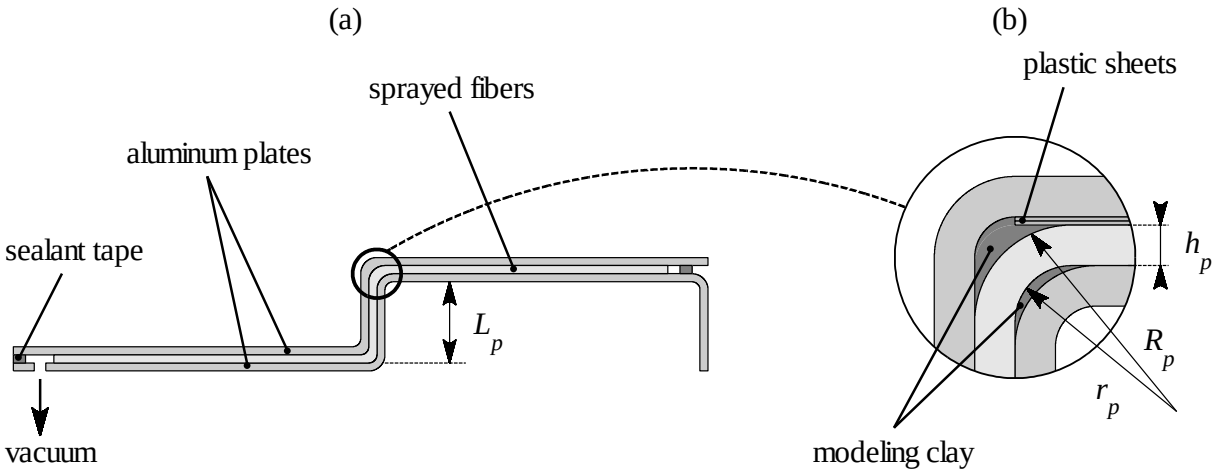

Figure 3-4 : Schematics of the preforming procedure.

The procedure described above was used to prepare large preforms (650 mm wide) with 4 plies of fabric. Such a preform is shown in Figure 3-5a after demolding. These preforms are fairly rigid and easy to manipulate. Each preform was subsequently cut into smaller samples having the dimensions of the final part (see Figure 3-5b).

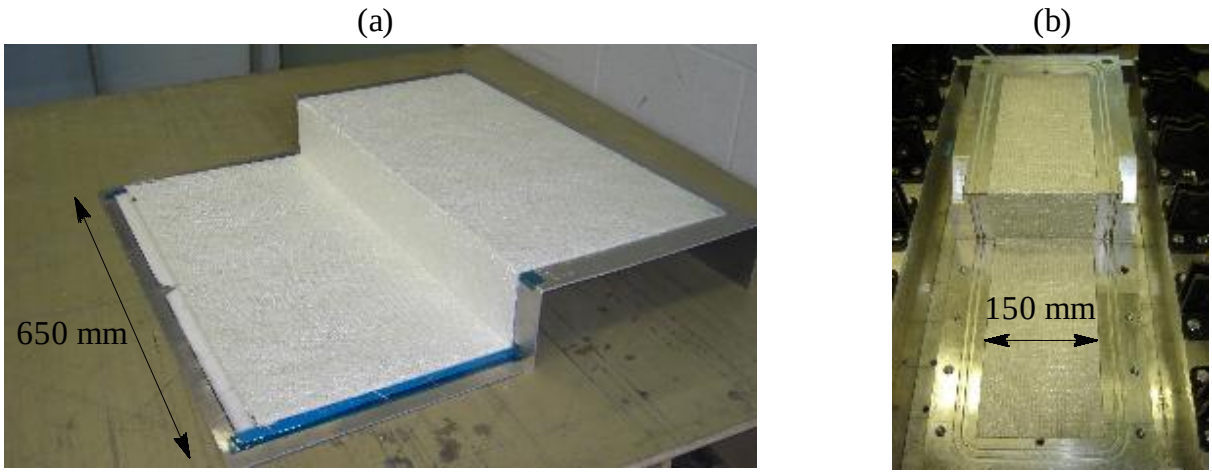

Figure 3-5 : Preparation of the fiber bed: (a) demolding of the large preform; (b) small preform cut to the required dimensions and laid into the bottom mold.

3.4.3 Fabrication

Firstly, the components of the thermoset system were manually mixed and the compound was degassed during 15 minutes under vacuum. After closing both mold halves, a vacuum of 5 kPa was drawn in the part and compaction cavities (see Figure 3-3). Resin was then injected under pressure with a pneumatic gun Semco model 250-A. After calculating the resin loss in the inlet tube, this device allowed controlling the injected quantity of resin with an accuracy of about 2.5%. All the experiments were carried out at room temperature (between 20.5ºC and 22ºC) with a resin injection pressure p_i = 2 bars. After injecting the resin in the part cavity, a fluid was injected in the compaction chamber. The pressure of the compaction fluid, silicone oil from Dow Corning 200 with a viscosity of 100 cSt at 25ºC, was controlled with a pressure tank. The parts were then cured overnight under constant compaction pressure (p_c) of 6 bars.

3.4.4 Compaction tests

The compaction behavior of the fiber bed was characterized by conducting compression and relaxation tests with a MTS testing machine. The results of the compaction tests displayed in

Figure 3-7a will be discussed in more detail in the sequel. Samples were flat squares of 100 mm × 100 mm made of 3 plies of preformed Roviply fabric. The testing sequence selected consisted of a constant speed loading stage (5 mm/min) followed by two hours of relaxation at constant thickness. The experiments were carried out for thicknesses ranging from 2 to 2.7 mm. For each condition, 3 tests were carried out to evaluate the repeatability of the results.

3.4.5 Part analysis

After demolding, the central region of each part was cut into three samples with an approximate width of 35.5 mm following the pattern of Figure 3-6a. The surfaces of the cut specimens were polished with waterproof aluminum oxide sandpaper of increasing grit from 220 to 1200. A scanner Canon CanoScan was used to obtain images of six longitudinal cross-sections (two cross-sections for each sample). Two types of scans were carried out to get images of the whole cross section with a resolution of 1200 dpi and of the two corner areas with a resolution of 4800 dpi (see Figure 3-6b). In order to increase the contrast between the part and the background, the samples were placed on an adhesive tape and a white paint was brushed onto the surface of the tape. Image analysis was subsequently performed with a Matlab code created for this purpose. By comparing luminosity levels, the program automatically detects the pixels located on the edges of the part and generates a precise thickness profile of the cross-section being analyzed.

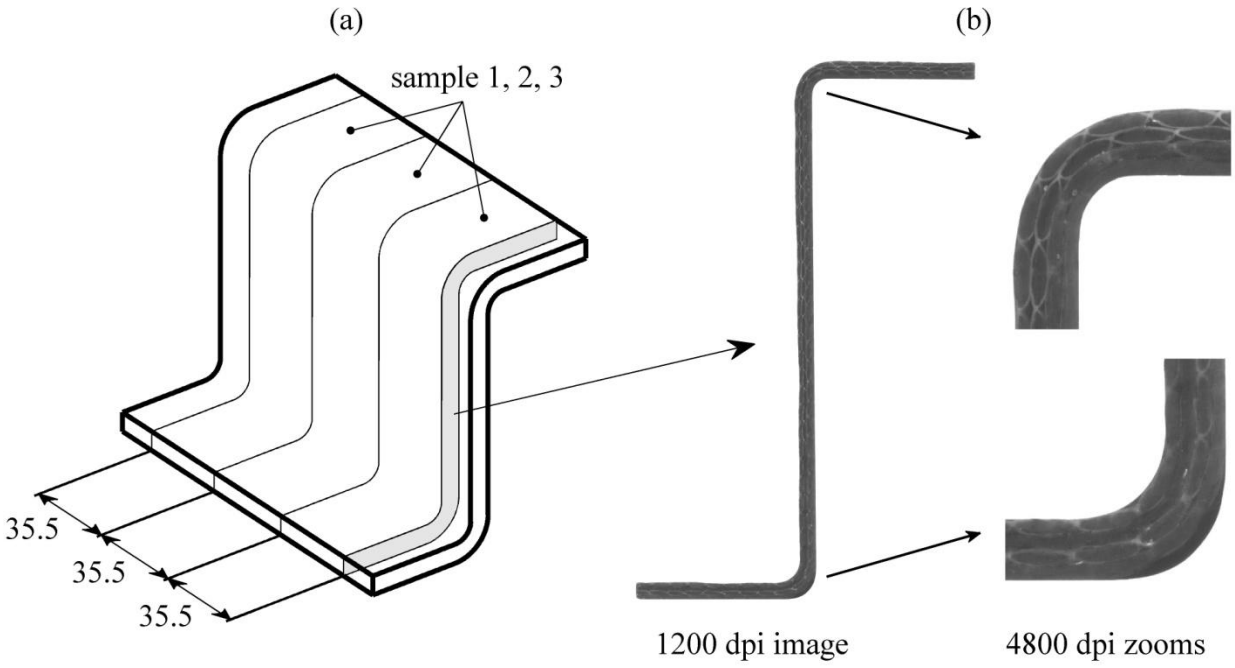

Figure 3-6 : Sample preparation for image analysis: (a) cutting pattern (dimensions in mm); (b) typical scanned images.

3.5 Plan of experiments

3.5.1 Compaction behavior

Characterization of the mechanical response of the fiber bed is required prior to conducting the manufacturing experiments. The goal is to select appropriate values of fiber volume fraction for the composite specimens fabricated by flexible injection. The compaction test procedure (constant speed loading followed by constant thickness relaxation) was indeed selected to reproduce the mechanical load experienced by the fiber bed during manufacturing. Figure 3-7a shows the mean relaxation curves obtained from the compaction tests. In this case, the time origin is taken at the beginning of the relaxation stage (i.e. after compaction at constant speed) so that the compaction curves do not appear in this figure. As expected, the relaxation phenomenon is particularly important during the first minutes of testing. Indeed, it is well known that for short manufacturing times, such a viscoelastic behavior cannot be ignored [21]. However, after two hours of relaxation, the stress decay becomes very small so that the preform may be considered to

have reached equilibrium. Stress values recorded at the end of the relaxation stage were used to construct the long-term compaction curve of Figure 3-7b, in which experimental results were fitted with a classical power law relating the effective stress σ_f applied on the fibers to the fiber volume fraction V_f [22]:

$$\sigma_f = A \times V_f^B \tag{3.1}$$

Note that the fiber volume fraction V_f in the above equation is scaled between 0 and 1 and the compaction stress is given in MPa. Several factors such as the resin saturation of the fiber bed, the number of plies or the compaction speed affect the mechanical response of the fibrous reinforcement under compaction. A complete characterization of fiber compaction is out of the scope of the present study. However, the compaction model (3.1) was used as a first approximation to describe the behavior of the dry fibers during preforming and of the saturated preform during manufacturing.

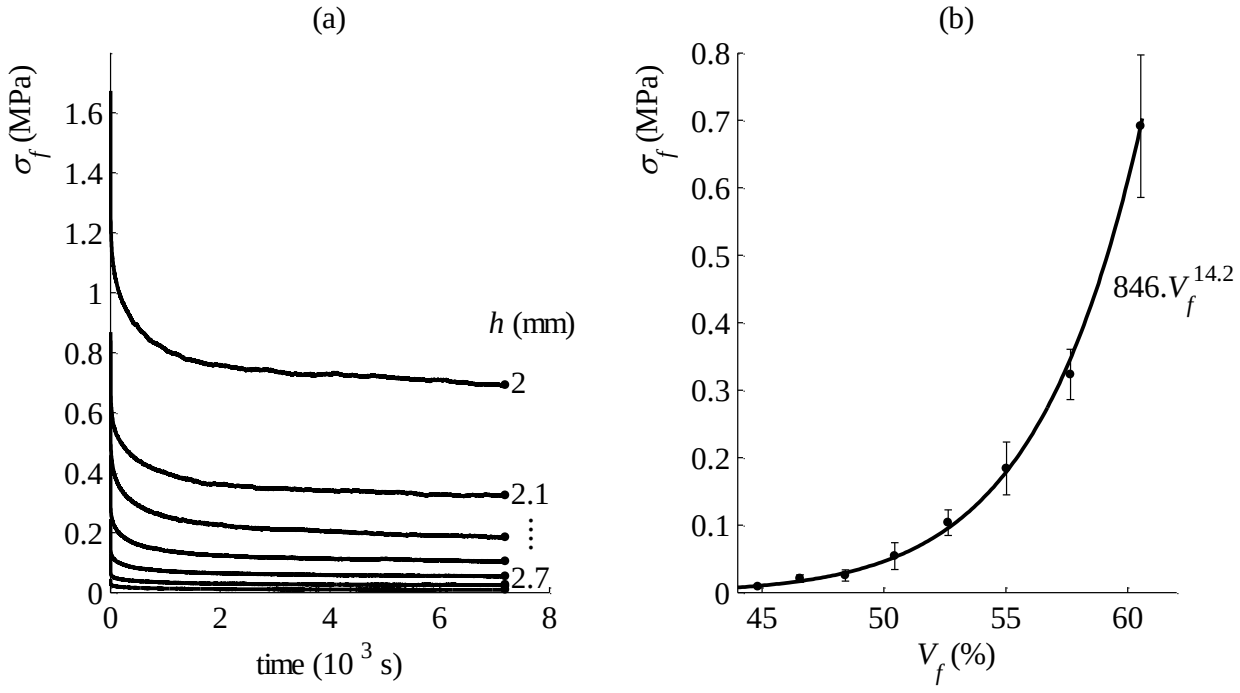

Figure 3-7 : Preform mechanical response: (a) relaxation results; (b) long-term compaction curve. (The fiber volume fraction V_f is scaled between 0 and 1 in the equation of the compaction model.)

3.5.2 Selection of fiber volume fractions

The thermosetting matrix used for the experiments exhibits a low viscosity and a relatively long gel time at room temperature. It is then assumed that consolidation is reached before resin gellation. When the resin flow stops, the internal pressure becomes constant in the cavity (i.e. hydrostatic pressure). At this stage, following Terzaghi's law [23] the compaction pressure p_c is in equilibrium with the effective stress σ_f in the fiber bed and the resin pressure p_r:

$$p_c = \sigma_f + p_r \tag{3.2}$$

Since the part is composed of flat sections, the effective stress in the fibers is assumed to be given by the compaction model of equation (3.1), which was used to evaluate the range of fiber volume fractions achievable with the compaction pressure considered. Figure 3-8 illustrates Terzaghi's law by plotting the effective stress imposed on the fiber bed as a function of the fiber volume fraction as described by equation (3.1). For the compaction pressure of 0.6 MPa used during the manufacturing, three fiber volume fractions V_f are considered. Each V_f results in a different resin pressure to equilibrate the compaction pressure. As a matter of fact, if the resin pressure is too high, the effective stress on the fiber is low and at the limit no stress is imposed to the fibers. This means that the fibers are no longer in contact with the membrane. Therefore, resin will accumulate above the preform. On the other hand, the fiber volume fraction is limited to a value for which the effective stress is significantly lower than the compaction pressure so that the resin pressure remains sufficiently large to give an acceptable low level of porosity in the part. From the reading of the long-term compaction curve, three values of fiber volume fraction were selected in Figure 3-8 to cover a wide range of compaction levels:

- low compaction with V_{f1} = 47.5%, σ_{f1} = 22 kPa,
- medium compaction with V_{f2} = 52.1%, σ_{f2} = 82 kPa,
- high compaction with V_{f3} = 57.6%, σ_{f3} = 347 kPa.

The mass of resin injected was controlled to obtain the desired fiber volume fraction. The mass m_i of the injected resin was calculated by volume conservation inside the cavity assuming a constant thickness throughout the part and a fully saturated fiber bed (without voids). The mass of injected resin is given by the following expression:

$$m_i = \left(\frac{\rho_{fs}\rho_r}{\rho_g} \frac{1-V_f}{V_f} - \rho_{bs} \right) S_p \tag{3.3}$$

where S_p is the area of the preform, ρ_g the glass density, ρ_r the resin density, ρ_{fs} the fiber preform surface density and ρ_{bs} the preform binder surface density.

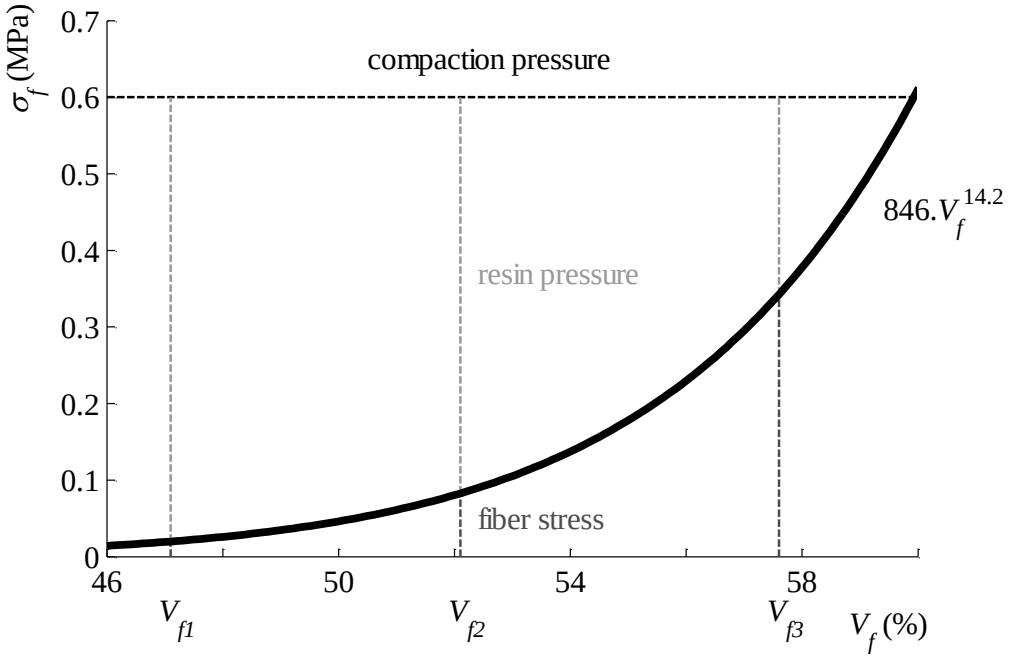

Figure 3-8 : Selection of the fiber volume fractions for the composite specimens fabricated by flexible injection. (The fiber volume fraction V_f is scaled between 0 and 1 in the equation of the compaction model.)

The complete experimental test plan included the preparation of 4 large preforms labeled A to D for a total of 13 parts produced. The manufacturing parameters used for each fabrication are summarized in Table 3.1. Each part was weighed to determine the mass of resin injected. The fiber volume fraction was determined based on the assumptions mentioned above. The small differences observed between the measured fiber volume fractions and the targeted values demonstrate the efficiency of the procedure used to control the mass of resin injected. The only poorly controlled parameter here was the binder content because of the manual spraying procedure.

Table 3.1 : Summary of the manufacturing test plan

Preform	preforming geometry (mm)				L_p	binder content (wt %)	part	V_f (%)	
	convex corner		concave corner						
	r_p	R_p	r_p	R_p				targeted	measured
A	3	6	2	5	100	2.36	a	52.1	52.4
							b	52.1	52.4
							c	52.1	52.3
							d	52.1	52.4
B	3	6	2	5	100	4.24	a	47.5	47.8
							b	52.1	52.0
							c	57.6	57.3
C	2	5	1	4	100	3,25	a	47.5	47.8
							b	52.1	52.2
							c	57.6	57.3
D	3	6	1	4	101	2,88	a	47.5	48.2
							b	52.1	52.4
							c	57.6	58.2

3.6 Cross-section analysis

We begin by studying the consolidation of flat sections, then of the convex corner and finally, of the concave corner. The analysis is straightforward in the flat sections, which are consolidated quite uniformly. However, this is not the case in the curved areas as will be described later.

3.6.1 Consolidation of flat sections

To compare the quality of consolidation in the different straight sections, the thickness of the specimen was estimated by image analysis in the five regions defined in Figure 3-9a. Zones I and V are respectively located in the top and bottom flat sections, and zones II, III, IV in the central flat section of the part. Each zone is 20 mm long with approximately 1000 measurement points. The analysis was repeated for the six longitudinal cross-sections, and the results averaged to obtain the mean part thickness at each location. Typical results are reported in Figure 3-9b for parts with the three different fiber volume fractions considered. In every case, the observed mean thickness is close to the targeted value represented by the dashed line. Overall, there is no

discernable trend. Therefore the thickness can be considered as constant between the different zones, despite a standard deviation of 0.1 mm inside each measurement zone.

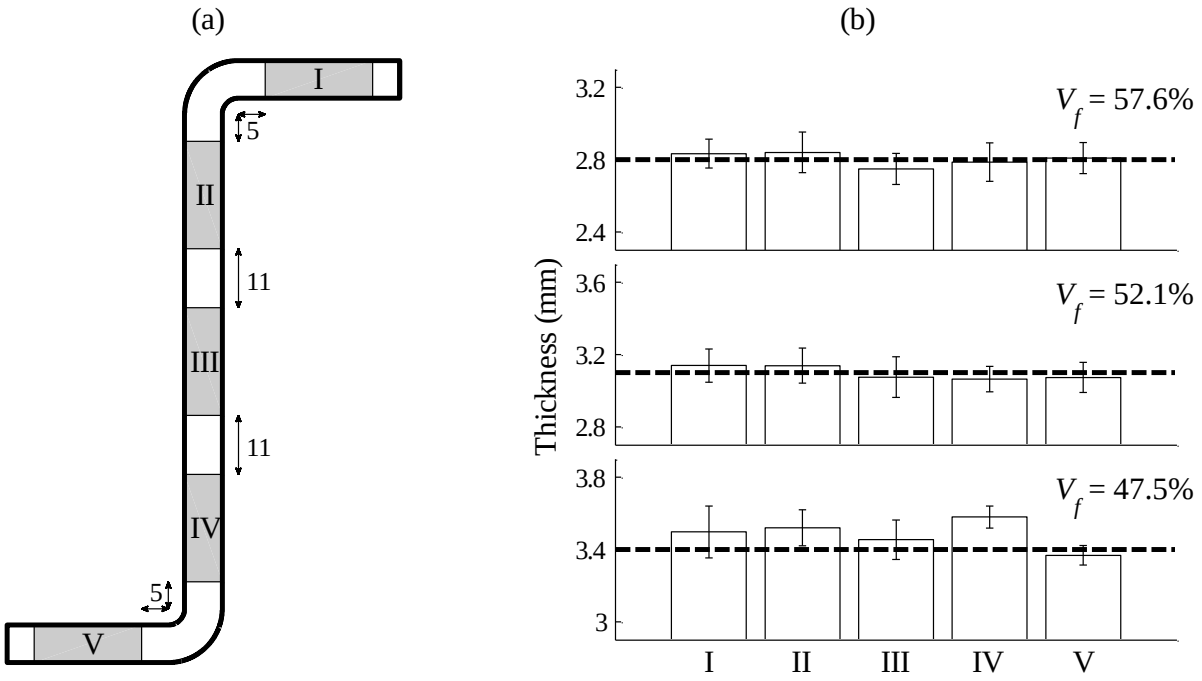

Figure 3-9 : Thickness of flat sections: (a) regions analyzed; (b) typical results.

Figure 3-10 shows typical zoomed images of flat regions, in which surface profiles obtained by image analysis appear clearly on both sides of the part. As seen in this image, the surface finish of the part differs greatly depending on the side considered. On the mold side, the surface finish is quite satisfactory with an almost perfectly straight profile. However, on the membrane side, the hard fibers can penetrate the soft elastomeric material, thus resulting in a rather rough surface finish. Moreover, the presence of stitching threads introduces local variations in the preform architecture. These heterogeneities affect in turn the compaction behavior of the fiber bed and explain the observed thickness variability. Such behavior is inherent to processes with flexible tooling and this effect can only be diminished by using more homogeneous preforms. One could also suggest that a more uniform thickness could be achieved with a stiffer material for the membrane, although this option would probably limit the membrane deformability and could possibly compromise the overall efficiency of the process.

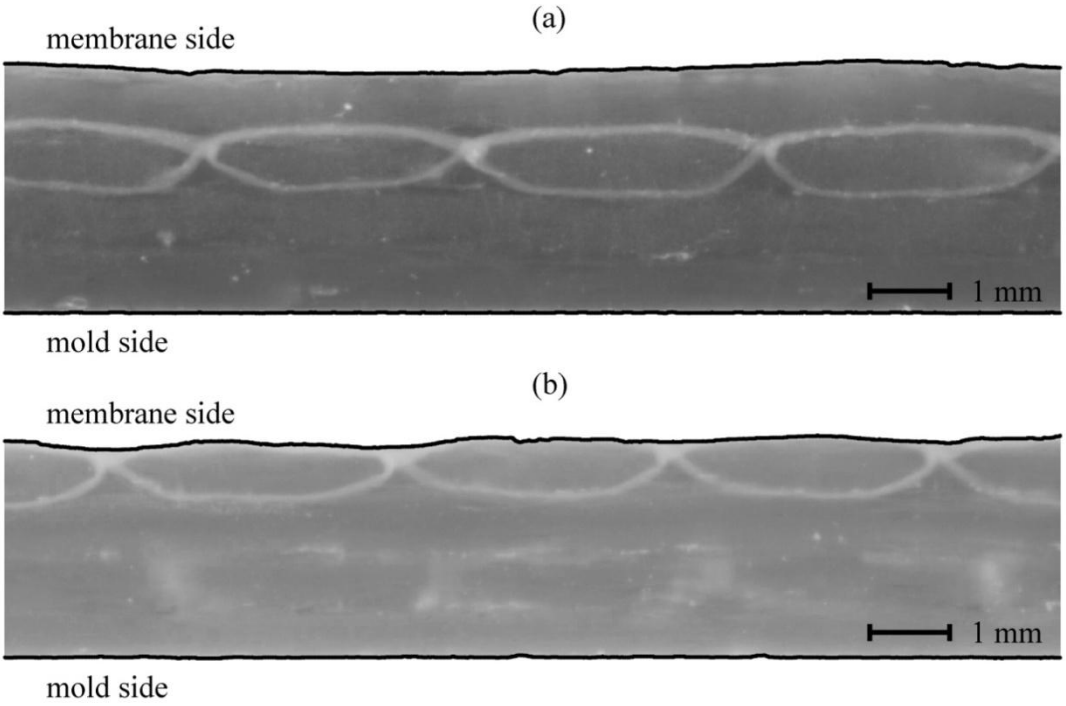

Figure 3-10 : Typical micrographs showing the difference in surface finish observed on the mold and membrane sides: (a) V_f = 52.1%; (b) V_f = 57.6%.

The complete results on the flat sections are reported in Table 3.2. Over the 65 zones considered, only six cases exhibit a difference larger than 0.1 mm between the observed thickness and the targeted value. Considering the intrinsic variability of the fabric material, the process provides a remarkably homogeneous consolidation of the flat sections. It is worth noticing than the central straight section is well consolidated even if it is parallel to the mold closing axis. This gives an advantage to flexible injection as compared to processes like compression RTM or RTM with articulated tooling, which usually lead to a non uniform consolidation of flat sections for parts of complex shape.

Table 3.2 : Summary of thickness analyses in flat sections

Part	Targeted thickness (mm)	Measured thickness ± 1 standard deviation (mm)				
		zone I	zone II	zone III	zone IV	zone V
Aa	3.10	3.13 ± 0.11	3.15 ± 0.10	3.03 ± 0.10	3.04 ± 0.12	3.04 ± 0.11
Ab	3.10	3.14 ± 0.09	3.14 ± 0.10	3.08 ± 0.11	3.06 ± 0.07	3.07 ± 0.08
Ac	3.10	3.18 ± 0.08	3.14 ± 0.09	3.14 ± 0.12	3.07 ± 0.08	3.05 ± 0.08
Ad	3.10	3.18 ± 0.06	3.14 ± 0.07	3.05 ± 0.06	3.04 ± 0.11	3.03 ± 0.11
Ba	3.10	3.03 ± 0.10	3.17 ± 0.08	3.14 ± 0.07	3.14 ± 0.11	3.05 ± 0.15
Bb	2.80	2.83 ± 0.08	2.84 ± 0.11	2.75 ± 0.09	2.79 ± 0.11	2.81 ± 0.09
Bc	3.40	3.39 ± 0.09	3.53 ± 0.16	3.43 ± 0.10	3.50 ± 0.16	3.35 ± 0.09
Ca	2.80	2.80 ± 0.10	2.84 ± 0.12	2.76 ± 0.08	2.80 ± 0.09	2.77 ± 0.08
Cb	3.10	3.21 ± 0.07	3.18 ± 0.21	3.12 ± 0.07	3.15 ± 0.06	3.05 ± 0.04
Cc	3.40	3.50 ± 0.14	3.52 ± 0.10	3.45 ± 0.11	3.58 ± 0.06	3.37 ± 0.05
Da	2.80	2.83 ± 0.09	2.75 ± 0.11	2.76 ± 0.09	2.79 ± 0.09	2.76 ± 0.09
Db	3.10	3.05 ± 0.07	3.17 ± 0.08	3.15 ± 0.07	3.29 ± 0.07	3.15 ± 0.07
Dc	3.40	3.41 ± 0.06	3.47 ± 0.06	3.47 ± 0.07	3.54 ± 0.03	3.41 ± 0.07

3.6.2 Consolidation of the convex corner

The geometry of the preforming tool has an immediate effect on the quality of the composite specimen in the convex corner. This influence will be studied by using three different preforming tools: one at the exact dimensions of the part, one with a sharper curvature and one with a small geometrical defect. The other important parameter is the fiber volume fraction V_f. As explained earlier, three values of V_f will be considered: a small, a medium and a large V_f.

Initially, the geometry of the preforming tool was set to match the dimensions of the manufacturing mold with a central height L_p = 100 mm of the stair-shaped part and an inner radius of the convex corner r_p = 3 mm. Since the preforming thickness was estimated to be 3.06 mm with the compaction model, the outer radius of the preforming mold was adjusted to 6 mm in order to obtain an almost constant thickness at the corner. In order to assess part variability, this configuration was employed to prepare preform A, which was used to fabricate 4 test parts with the same targeted medium fiber volume fraction V_f = 52.1%. Typical cross-sections of the convex

corner are shown in Figure 3-11. Visual inspection of these images reveals no detectable manufacturing defects in the convex corner of the part.

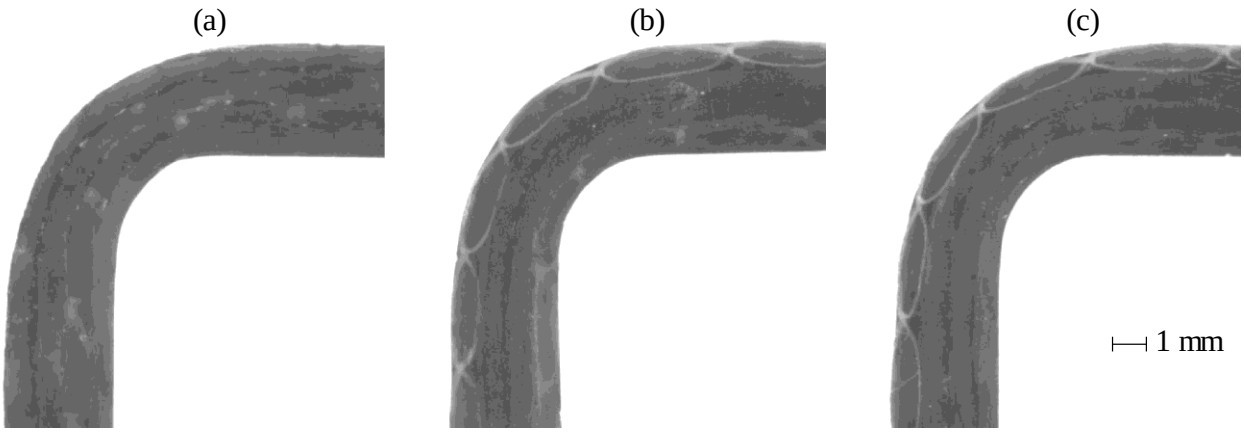

Figure 3-11 : Typical images of the convex corner for the medium fiber volume fraction V_f = 52.1% with the initial preforming geometry: (a) Part Aa; (b) Part Ab; (c) Part Ac.

To characterize more precisely the lay-up quality, mean thickness profiles around the corner of the parts were obtained by image analysis. The results are reported in Figure 3-12 for the 4 parts mentioned above. Firstly, note that there are no significant differences between the parts. Hence, taking into account the natural variability of the fiber material, the repeatability of the experiments can be considered as acceptable. In the straight sections, the profiles are almost perfectly flat and close to the targeted thickness. A slight increase in thickness seems to appear in the vicinity of the corner, but this effect is too small to be distinguished from the local variations discussed in the previous section. In the corners of the parts, a substantial decrease in thickness is observed in the 4 studied parts. This clearly shows that the curved convex region exhibits a different behavior during consolidation as compared to the flat sections.

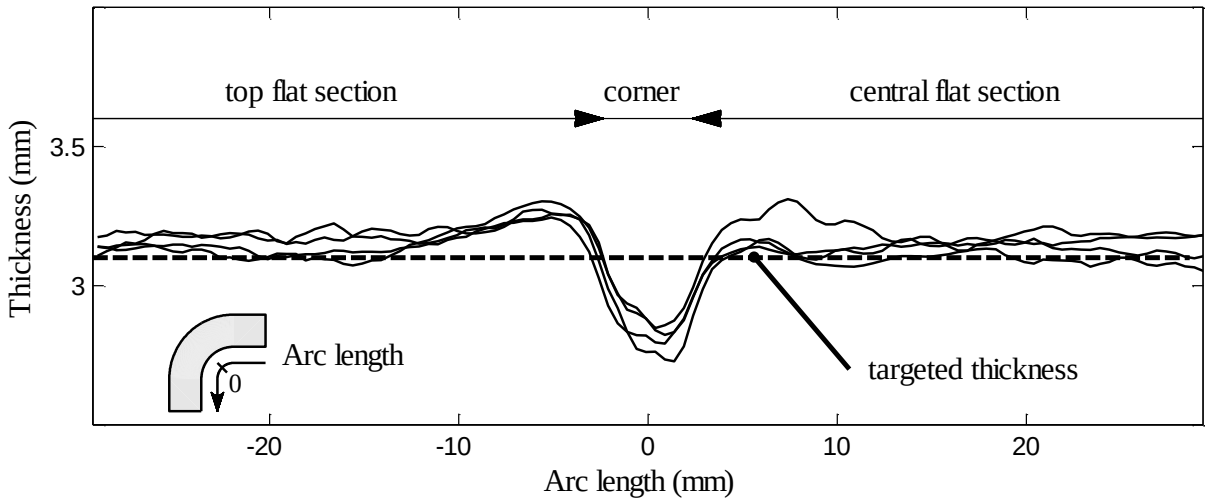

Figure 3-12 : Thickness profiles of 4 parts manufactured at the medium compaction level with the initial preforming geometry (i.e., parts Aa to Ad).

To further investigate the consolidation behavior in the curved convex region, preform B was prepared with the same preforming conditions as preform A, but was used to process parts with three different fiber volume fractions (see Table 3.1). The corresponding thickness profiles of parts Ba to Bc are reported in Figure 3-13. As indicated on this scaled drawing, the thickness of the three parts is lower in the curved area. The thinning phenomenon in the corner becomes more important for lower fiber volume fractions. The difference in consolidation behavior observed between the straight and curved regions is probably due to the presence of inextensible fibers oriented at 45° from the tangential curvature direction. As mentioned before, the fibers were preformed in a mold with a nearly constant thickness cavity. When the preform is demolded, it experiences an increase in thickness because the pressure is relieved (i.e spring-back behavior). In the curved regions, this elastic spring-back is likely to be hindered by the fibers which cannot accommodate a change in length. This mechanism would explain the marked thinning observed in the corner at low fiber volume fraction when the preform is close to a stress-free state. For higher fiber volume fractions, the corner becomes harder to consolidate than the rest of the part, because the fibers in the curved area resist compaction. This specific behavior in the curved region tends to attenuate thinning of the corner for a part with a high fiber volume fraction.

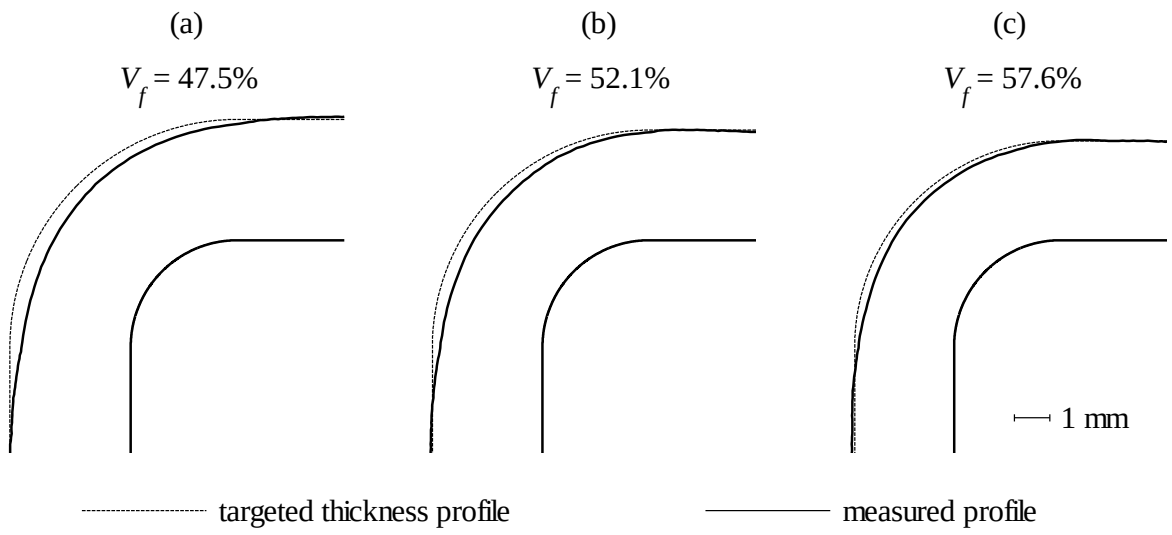

Figure 3-13 : Influence of fiber volume fraction on the consolidation of the convex corner: (a) Part Ba; (b) Part Bb; (c) Part Bc.

In an attempt to improve the thickness uniformity of the parts, preform C was prepared with a modified preforming geometry. The radii of the preforming tool were adjusted to 2 mm and 5 mm for the inner and outer radii respectively (see Figure 3-4 and Table 3.1). This mold configuration also creates a cavity with a nearly constant thickness, but with a sharper corner so that more fibers are squeezed in the curved area. Thickness profiles of the three parts manufactured with the preform C are represented in Figure 3-14. As seen in these parts, modifying the geometry of the preforming mold influences significantly the consolidation of the corner region. At low fiber volume fraction, the curved section is slightly thinner than the rest of the part, but this effect is less important than previously observed. The corner thinning disappears and no noticeable variation can be observed for medium and high fiber volume fractions. Consequently, adapting the preforming geometry helps in reducing the thickness variations in the final part.

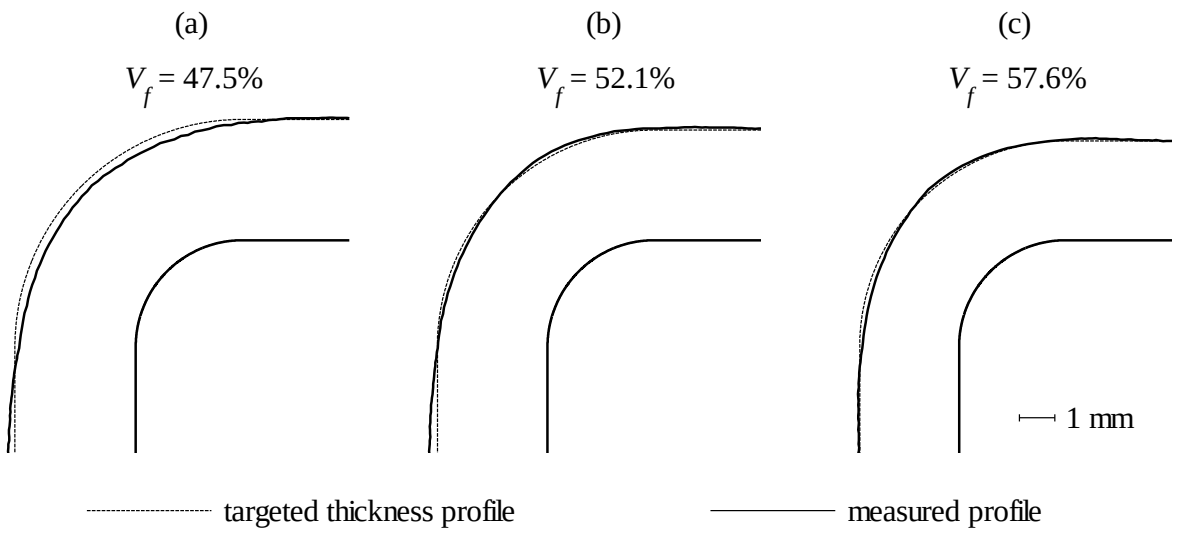

Figure 3-14 : Influence of preforming radii on the consolidation of the convex corner:

(a) Part Ca; (b) Part Cb; (c) Part Cc.

In order to assess the importance of the preform global dimensions, a dimensional error was intentionally introduced when preparing preform D. The central length L_p was adjusted to be 1 mm longer that the manufacturing mold (see Figure 3-4 and Table 3.1). As shown in Figure 3-15, this preform imperfection leads to the creation of a resin-rich region between the mold and the fibers. At low fiber volume fraction, a large resin accumulation is observed in the corner and in the top straight section, because the effective stress in the preform is not large enough to compress the fibers and push them against the tool. When the level of compaction increases, the fibers are forced against the tool, hence decreasing the size of the resin-rich zone. At high fiber volume fraction, Figure 3-15c shows only a minor resin accumulation in the corner. In the case presented here, the preforming mold was badly dimensioned on purpose. Within the framework of an industrial application, it seems obvious to recommend to use a preforming tool of the same geometry as the manufacturing mold. However, improper preform dimensions could also result from a difference in temperature of the preforming tool and the manufacturing mold. Indeed, the coefficient of thermal expansion of the reinforcing fibers is much lower than that of the metallic material used in the tool. In the case of a large part, preforming at a temperature significantly different from that of the manufacturing process would certainly lead to a serious mismatch between the preform and the mold.

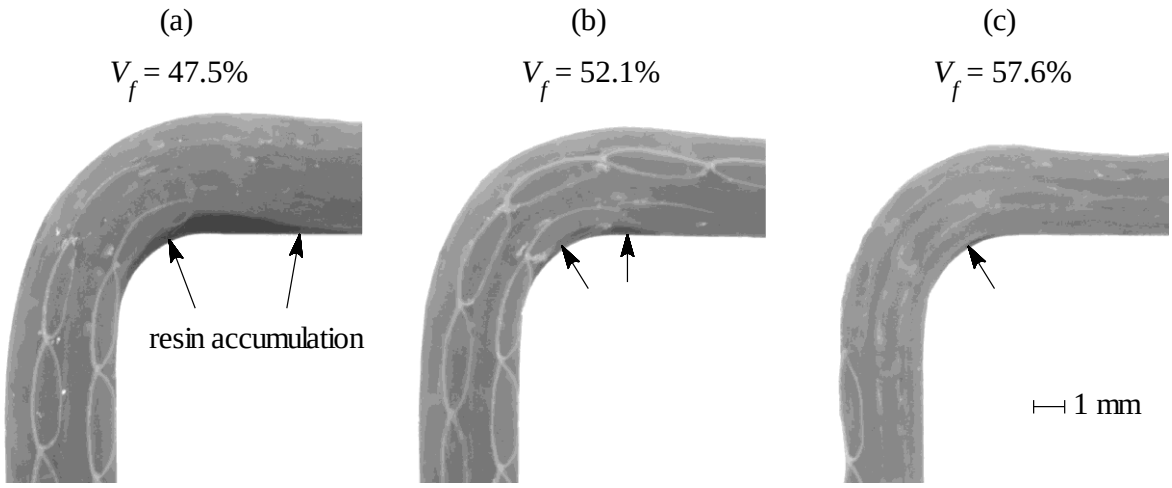

Figure 3-15 : Resin-rich zones in the convex corner induced by poor preform dimensioning: (a) Part Da; (b) Part Db; (c) Part Dc. Arrows indicate resin accumulation.

3.6.3 Consolidation of the concave corner

The methodology of the previous section was applied to evaluate the consolidation of the concave corner region. The influence of the preforming tool was studied by using two different tools: one at the exact dimensions of the part and one with a sharper corner. Three different fiber volume fractions were also considered as before: a small, medium and large V_f.

First, the radii of the preforming tool were set to 5 mm for the outer radius and 2 mm for the inner radius. This configuration matches the geometry of the manufacturing mold on the rigid tool side and creates a nearly constant preforming thickness. These parameters were used for the preparation of preforms A and B (see Table 3.1). Visual inspection of the 4 first parts manufactured with the medium fiber volume fraction indicates the presence of an important defect in the curved region. As shown in Figure 3-16, the fibers tend to bridge over the corner and a resin accumulation is created between the mold and the preform.

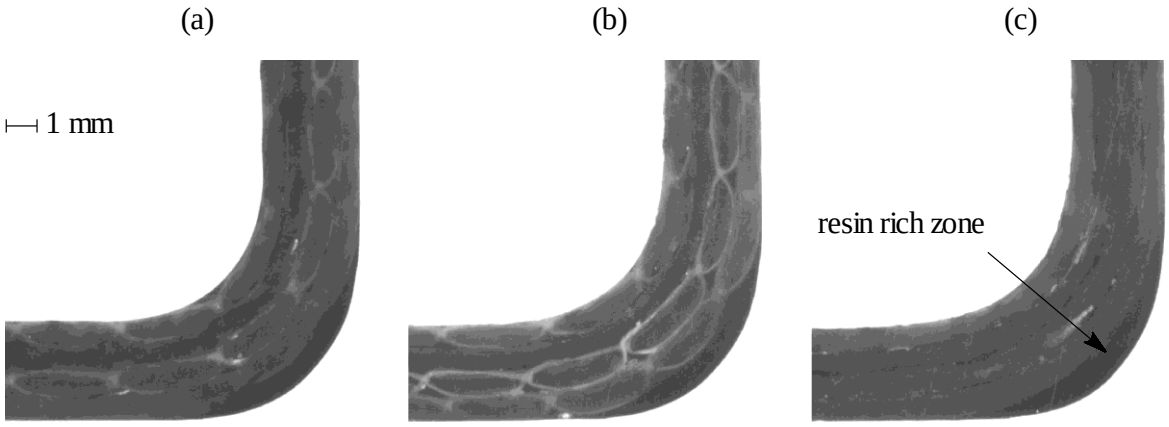

Figure 3-16 : Typical images of the concave corner for the medium fiber volume fraction V_f = 52.1% with the initial preforming geometry: (a) Part Aa; (b) Part Ab; (c) Part Ac.

As seen in Figure 3-17, increasing the targeted fiber volume fraction barely changes the size of the resin-rich region. Even at the largest compaction level, the stress applied on the preform is not sufficient to push it against the mold because stiff fibers resist deformation in the curved area. Figure 3-17a also shows that a second type of manufacturing defect appears at low fiber volume fraction. Since the membrane is cut out from a planar sheet, it does not bend easily in the curved region. When the fiber volume fraction is low, the stress applied on the membrane is not sufficient to properly stretch it and the membrane bridges over the corner without touching the fibers. Consequently, the open gap between the preform and the membrane is filled with resin and a resin-rich zone is created in the concave corner. This undesirable phenomenon disappears when the level of compaction increases, because the membrane is flexible enough to be deformed and comes in contact with the fibers when sufficient stress is applied. However, the use of a membrane with the same geometry as the part to be produced would certainly improve the efficiency of the process. Developing such three-dimensional membranes represents a key step for future applications of flexible injection to more complex geometries.

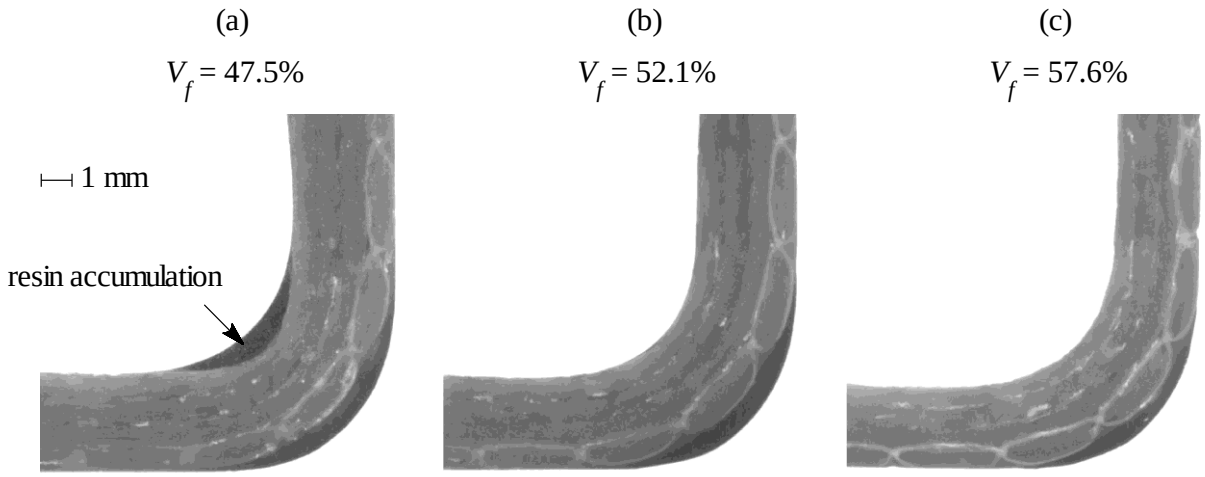

Figure 3-17 : Influence of fiber volume fraction on the consolidation of the concave corner: (a) Part Ba; (b) Part Bb; (c) Part Bc.

Preforms C and D were prepared with a modified preforming tool with a sharper corner region. The inner radius was 1 mm and the outer radius 4 mm so that the thickness of the preforming cavity remains constant (see Table 3.1). As seen in Figure 3-18, the size of the resin-rich zone between the fibers and the mold is much reduced with the adapted preforming geometry. However, a significant resin-rich zone remains on the membrane side at low fiber volume fraction because of bag bridging (see Figure 3-18a). As previously observed, this effect disappears when the fiber volume fraction increases because in this case the resin pressure is lower and the membrane is then allowed to come in direct contact with the fiber bed. On the other hand, the level of compaction has little effect on the resin accumulated on the tool side, because fiber bridging in the concave corner inhibits the consolidation of the preform.

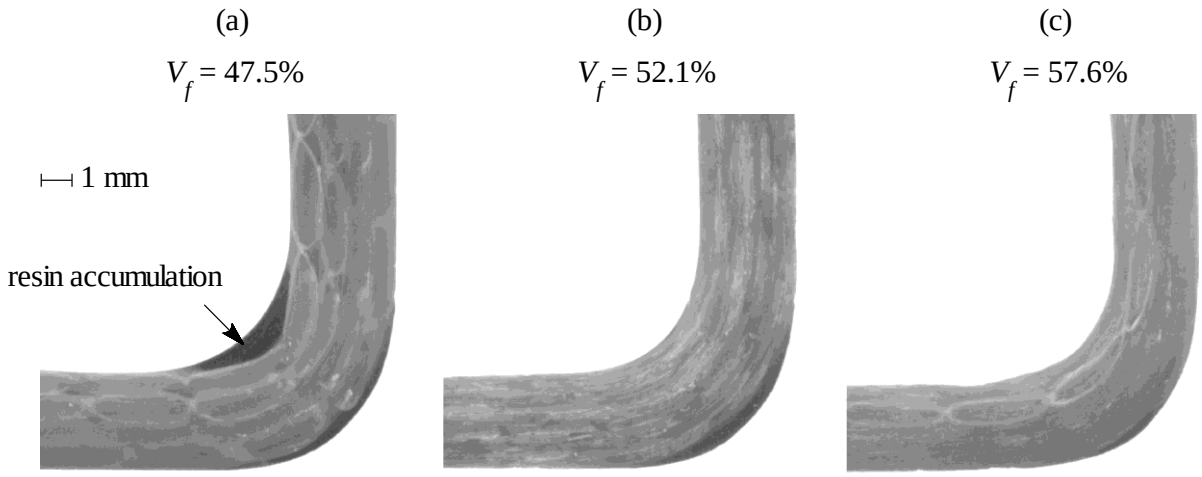

Figure 3-18 : Images of the concave corner obtained with the modified preforming geometry: (a) Part Ca; (b) Part Cb; (c) Part Cc.

3.7 Conclusion

Flexible injection is a promising new technology for rapid manufacturing of complex composite structures with low content of voids. In the present paper, this approach was adapted to manufacture strongly curved parts. A series of stair-shaped components made out of glass fiber and vinyl ester resin have been produced by flexible injection with a specially devised experimental setup. Longitudinal cross-sections of the fabricated parts have been inspected visually and studied by image analysis to assess the efficiency of this new manufacturing technique in terms of part quality. Consolidation of the composite specimens was studied in detail in the flat sections and in the convex and concave corners. The following conclusions can be drawn:

- Flexible injection allows achieving a uniform consolidation of the flat sections along any direction. In particular, this manufacturing technique can efficiently process parts having straight sections parallel to the mold closing axis.
- Curved regions are prone to create manufacturing defects such as resin-rich zones or to exhibit thickness gradients. This difficulty comes from the presence of stiff fibers along the curved profile that change the compaction behavior of the fiber bed.

- The consolidation of the fibrous preform strongly depends on the geometry of the manufacturing tool, mainly for convex or concave corners.
- Dimensional accuracy of preform and membrane were found to be key factors in order to prevent the creation of resin-rich zones in curved areas.
- The preforming stage has a direct influence on the lay-up quality in corners. The use of an adapted preforming strategy can help reducing thickness variations and limit resin accumulations.
- Low fiber volume fractions tend to create resin accumulations. A larger fiber volume fraction creates an effective stress in the preform, strong enough to ensure contact between the membrane and the fiber bed and prevent resin accumulation on the membrane side.

The present study shows that there is no intrinsic limitation to the manufacture of parts of strong curvature by flexible injection. The preparation of the fibrous preform is a key stage for successful manufacturing of composite structures with strongly curved zones. Further investigations could study more thoroughly the influence of the geometry of the preforming tool, of the forming pressure and of the compaction pressure on the quality of the final parts.

3.8 Acknowledgements

The authors are grateful to Dr. John Owens, from General Motors Global Research Laboratory, Detroit, USA, for advice concerning this investigation. The authors also thank S. Boutier and D. Coste from Chomarat for providing the fabrics used in this investigation.

3.9 References

1. E. Ruiz, L.R. Briones, É. Allard, and F. Trochu, in *9th Int. Conf. on Flow Pro. in Comp. Mat. (FPCM9)*, Montréal, Canada (2008).

2. F. Trochu, S. Soukane, and B. Touraine, in *9th Int. Conf. on Flow Pro. in Comp. Mat. (FPCM9)*, Montréal, Canada (2008).

3. C.C. Hiel, M. Sumich, and D.P. Chappell, *J. Compos. Mater.*, **25**, 854 (1991).

4. P. Hubert and A. Poursartip, *J. Compos. Mater.*, **35**, 2 (2001).

5. K. Potter, *Compos. Part A*, **33**, 677 (2002).

6. K.D. Potter, M. Campbell, C. Langer, and M.R. Wisnom, *Compos. A*, **36**, 301 (2005).

7. L.K. Jain, B.G. Lutton, Y.-W. Mai, and R. Paton, *J. Compos. Mater.*, **31**, 696 (1997).

8. M.R. Wisnom, M.I. Jones, and G.F.J. Hill, *Adv. Compos. Letters*, **10**, 171 (2001).

9. S. Feih and H.R. Shercliff, *Compos. A*, **36**, 397 (2005).

10. J.L. Oakeshott, *Plast. Rubb. Compos.*, **32**, 104 (2003).

11. M.I. Naji and S.V. Hoa, *J. Reinf. Plast. Compos.*, **18**, 702 (1999).

12. M.I. Naji and S.V. Hoa, *J. Compos. Mater.*, **34**, 1710 (2000).

13. H.W. Wiersma, L.J.B. Peeters, and R. Akkerman, *Compos. A*, **29**, 1333 (1998).

14. P.J. Mallon, C.M. O'Bradaigh, and R.B. Pipes, *Composites*, **20**, 48 (1989).

15. S.Y. Yang, C.K. Huang, and C.B. Wu, *J. Adv. Mater.*, **27**, 37 (1996).

16. G. Fernlund, J. Griffith, R. Courdji, and A. Poursartip, *Compos. A*, **33**, 411 (2002).

17. P. Hubert, R. Vaziri, and A. Poursartip, *Int. J. Numerical Methods Eng.*, **44**, 1 (1999).

18. M. Li and C.L. Tucker III, *Compos. A*, **33**, 877 (2002).

19. Y. Li, M. Li, Z. Zhang, and Y. Gu, *Polym. Compos.*, **30**, 1510 (2009).

20. Y. Li, M. Li, Y. Gu, and Z. Zhang, *Appl. Compos. Mater.*, **16**, 101 (2009).

21. S. Bickerton, M.J. Buntain, and A.A. Somashekar, *Compos. A*, **34**, 431 (2003).

22. F. Robitaille and R. Gauvin, *Polym. Compos.*, **19**, 198 (1998).

23. T.G. Gutowski, T. Morigaki, and Z. Cai, *J. Compos. Mater.*, **21**, 172 (1987).

Contract grant sponsors: General Motors (GM) of Canada; Canada; Research Chair Program; National Science and Research Council of Canada (NSERC); Center for applied Research on Polymers and Composites; (CREPEC); Canadian Foundation for Innovation (CFI).

CHAPITRE 4 ARTICLE 2: INFLUENCE OF PREFORMING ON THE QUALITY OF CURVED COMPOSITE PARTS MANUFACTURED BY FLEXIBLE INJECTION

Philippe Causse [1], Edu Ruiz and François Trochu

Department of Mechanical Engineering and Chair on Composites of High Performance, Centre de recherche en plasturgie et composites (CREPEC), École Polytechnique de Montréal, P.O. Box 6079, Station "Centre-Ville", Montreal, Canada, H3C 3A7

[1] *Corresponding author's Email: philippe.causse@polymtl.ca*

4.1 Abstract

Flexible Injection is a new processing technique for the manufacture of advanced composites made of continuous reinforcing fibers and thermosetting polymer matrix. The primary objective of this new process is to provide faster and less expensive manufacturing than traditional methods like autoclave processing or Resin Transfer Molding. The present paper investigates the effectiveness of the proposed method to produce composite structures possessing sharp corners. A specially devised setup is used to manufacture out of glass fibers and vinyl ester resin a series of Z-shaped parts with small radii. The quality of the fabricated parts is assessed to detect possible defects induced by the manufacturing process. Each stage of the production cycle is analyzed thoroughly to develop a simplified finite element model reproducing the fiber bed behavior during processing. Parametric studies are conducted to evaluate the impact of processing conditions on the quality of final products. The combination of numerical simulations and experimental observations demonstrates clearly the importance of the preforming stage. At the same time, it provides useful insights on the physical phenomena occurring during Flexible Injection.

KEYWORDS: Liquid Composite Molding (LCM), Flexible Injection (FI), curved composite, fiber preforming, manufacturing defects.

4.2 Introduction

Fiber reinforced thermoset composites possess remarkable specific properties, which make them particularly attractive to design lightweight primary structures. For example, high performance composites have successfully replaced metallic materials in highly demanding aeronautical applications. These progresses were made possible through significant effort to develop and master manufacturing processes such as autoclave processing. Nowadays, there is a growing demand to improve existing methods or develop new processes capable of producing more complex components of consistent quality and at reduced cost. Over the past decades, Liquid Composite Molding (LCM) processes such as Resin Transfer Molding (RTM) have drawn much attention because of their ability to process parts of complex geometry and for their potential for automation. Recently, a novel LCM technique called Flexible Injection was proposed to allow faster manufacturing of high performance parts [1,2]. As shown in Figure 4-1, this new process is a closed mold technique which uses a flexible device (i.e., an elastomeric membrane) to modify the geometry of the tool during processing. The membrane is placed between the two mold halves and divides the overall cavity into two separate chambers. The lower cavity is called the injection cavity, and the top one is referred to as the compaction cavity. The manufacturing cycle of Flexible Injection includes the following steps (see Figure 4-1):

(1) A fibrous preform is placed inside the bottom mold cavity, the membrane is laid upon it and the mold is closed.

(2) A liquid thermoset resin is injected under pressure in the injection cavity. The resin impregnates the fibers, inflates the membrane and flows in the open gap created above the preform. After the required amount of resin has been injected so as to achieve a set fiber volume content, the injection cavity is filled up only partially at the end of the injection stage.

(3) A second fluid, called the compaction fluid, is injected in the compaction cavity above the membrane. By squeezing the membrane back on the preform, this fluid forces the resin to flow through the preform, which completes the impregnation of the fiber bed.

(4) The part is cured under constant compaction pressure.

(5) The compaction fluid is evacuated from the cavity and the part is demolded.

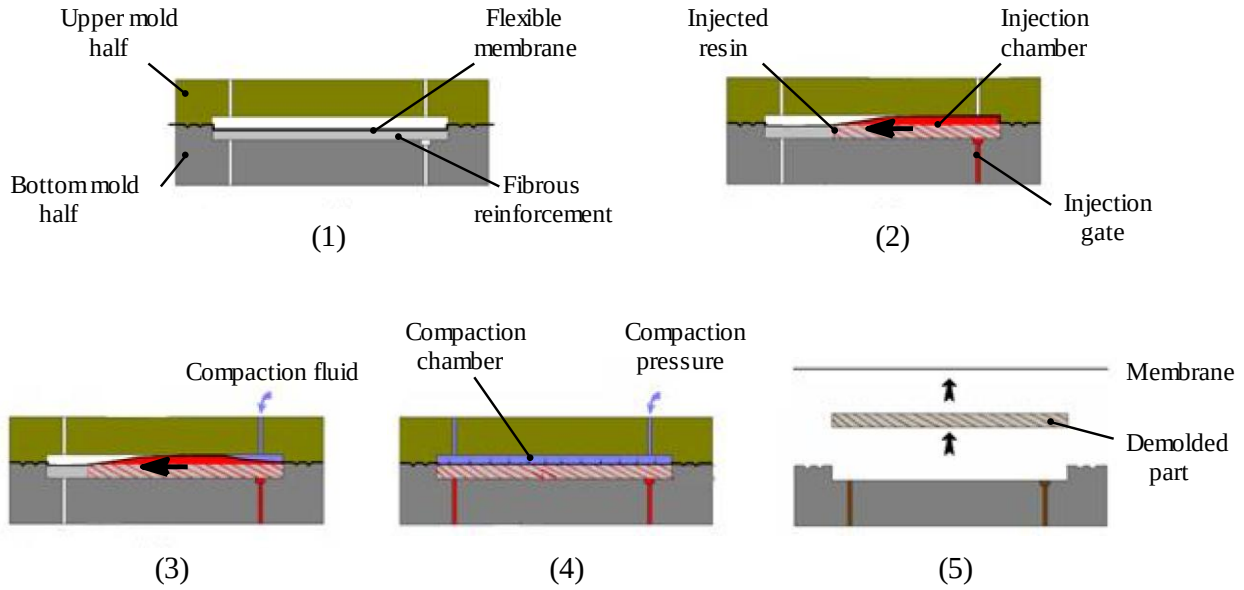

Figure 4-1 : Overview of the Flexible Injection process.

In Flexible Injection, the resin starts to flow through the open gap above the preform, after which a transverse impregnation of the fiber bed takes place. This specific filling pattern was shown to effectively reduce the filling time compared to classical RTM [1,2]. A second advantage is the application of a compaction pressure during cure to ensure proper consolidation and hence a low void content of the final product. However, preliminary work for parts of curved geometry showed that manufacturing defects such as resin rich areas and thickness gradients could be created in zones of small curvature radii [3]. It was also suggested that the geometry and the mechanical response of the preform were key factors that ultimately affect the quality of the component in strongly curved regions.

As explained by Hubert and Poursartip [4], understanding the influence of process parameters on the quality of final parts has been a major concern in autoclave processing. For parts of complex shape, it can be difficult to produce structures of consistent quality. Curved areas are indeed prone to generate manufacturing defects that have an impact on product performance. This limitation mainly comes from the behavior of the reinforcing fibers which tend to wrinkle or bridge over curved sections [5-7]. This type of fiber deformation can in turn affect the resin flow

and create unwanted resin rich zones, as observed for example by Feih and Shercliff [8] and Jain et al. [9]. In the scientific literature, the issue of composite processing in curved parts is commonly tackled by studying simple angled shapes such as L-brackets. This geometry possesses the double advantage of being easily implemented at laboratory scale and of reproducing closely the behavior of parts with flanges and ribs.

Several parameters have been shown to influence the quality of curved composites such as fiber orientation [10,11], geometry of the tool (convex or concave) [10,12], curvature radius [13] or curing cycle [14,15]. Numerical modeling has proved to be a useful way to understand the consolidation behavior of curved laminates [16-18]. These parametric studies have shown that the shear behavior of the fiber bed has a major influence on the thickness in curved areas after composite consolidation. Caul sheets or rubber pressure pads can help to get rid of corner thickness variations as reported by Yang et al. [19] and Fernlund et al. [20]. However, Gu et al. [21] showed that the efficiency of such devices depends strongly on their flexibility and geometry to ensure that an even pressure is transferred from the bagging to the composite. By selecting an appropriate pressure concentration device, Brillant and Hubert [22] were able to produce composites of small radius out of the autoclave with a consolidation pressure as low as the atmospheric pressure. In the RTM process, thickness gradients are not expected to appear since both sides of the tool are rigid. However, the use of a fixed cavity does not guarantee a perfectly homogeneous fiber/matrix distribution in the final product especially in curved areas. Resin rich zones have indeed been observed in the corners of sharply bent structures [23,24]. Such defect is due to a tight packing of the fibers against the convex sections of the mold, leaving an open gap between the fiber bed and the concave side of the tooling. This effect is inherent to fibrous reinforcements, but some studies conducted by Holmberg and Berglund [25] and Arndt [26] suggested that it could be diminished by preforming the fibers in a separate tool with a slightly different geometry from that of the processing mold.

The objective of this paper is to understand the cause of processing defects during the manufacture of strongly curved parts by Flexible Injection. The experimental procedure followed to manufacture the test specimens is first presented. The deformation of the fiber bed during the

production cycle is then analyzed in details for the simple case of a planar geometry and a compaction model is proposed to reproduce the experimental results. After defining an appropriate range of fiber volume fractions for the study, a first series of parts is manufactured to illustrate the specific behavior of curved shapes. The analysis of fiber deformation is further extended to the two-dimensional case and a finite element model is developed to simulate the manufacturing experiments. Finally, the new software tool is used to conduct parametric studies in order to identify the key parameters that control the quality of the final composite. The comparison of numerical predictions with experimental results provides an insight on the causes of the observed manufacturing defects.

4.3 Manufacturing experiments

4.3.1 Setup

The laboratory mold used to conduct the manufacturing experiments is shown in Figure 4-2a. This setup was machined from an aluminum block and is equipped with a manual clamping system. The mold was designed to produce the stair-shaped component schematically drawn in Figure 4-2b. This test specimen is a rectangular panel with two curved zones (90º corners). By convention, the *x*-axis shown in Figure 4-2b corresponds to the 0º direction of the laminate.

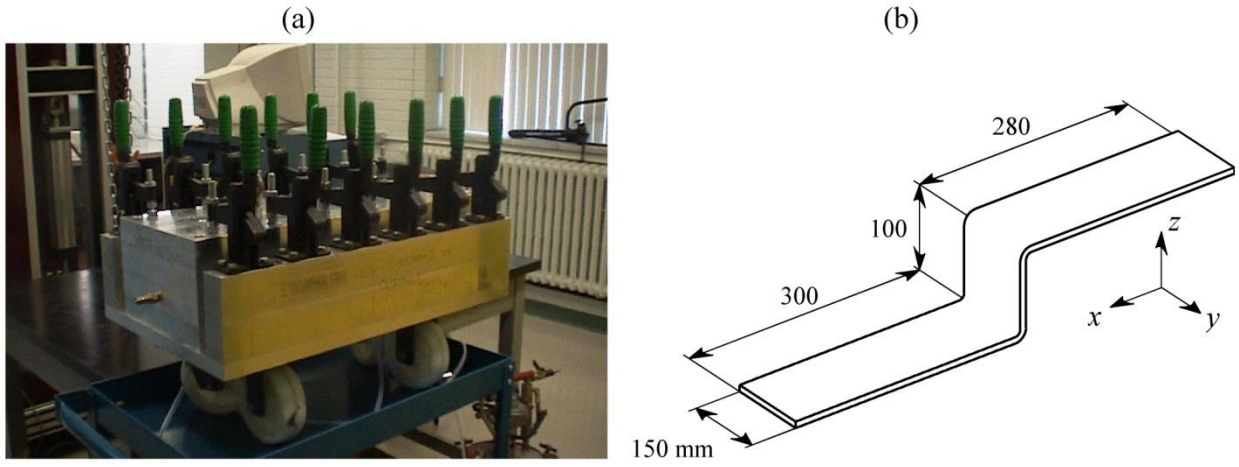

Figure 4-2 : Flexible Injection mold (a) and corresponding test part (b).

4.3.2 Materials

The composite specimens were made out of glass fibers and vinyl ester resin. The matrix was DERAKANE 411-350 from Ashland Inc. The resin formulation included:

- a cure initiator methylethylketone peroxide MEKP 925-H from Norox (1.25 phr);
- a promoter cobalt naphtenate 12% (0.1 phr);
- a gel time retarder 2-4 pentanedione (0.08 phr).

With the above described formulation, the thermoset system exhibits a gel time of approximately two hours for the manufacturing conditions selected in this investigation.

The reinforcement was a quasi-unidirectional E glass fabric Saeruni from Saertex with a surface density of 970 $g.m^{-2}$. As shown in Figure 4-3b, this fabric is not perfectly unidirectional since it includes some fibers oriented at 90º. These stabilizing bundles account for approximately 8% of the total fabric weight.

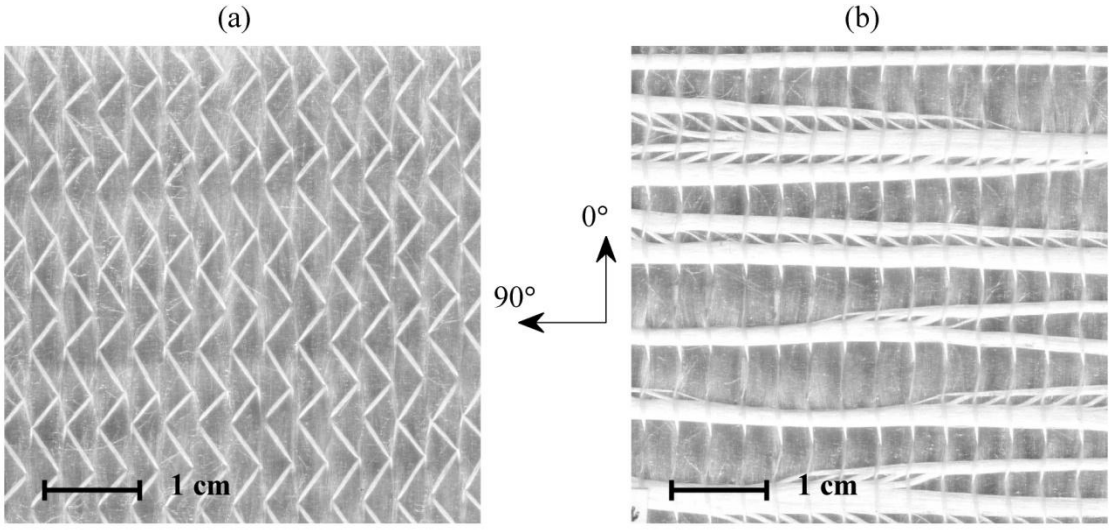

Figure 4-3 : Glass fiber fabric Saeruni used in the study: (a) top view; (b) bottom view.

Before injection, the fibrous reinforcement was preformed to the desired shape in the preforming tool depicted in Figure 4-4. The two halves of the preforming tool were obtained by metal folding. Their geometry was adjusted with calibrated plastic sheets and by applying self-hardening modeling clay with a radius gauge in the different corners. This manipulation allowed controlling the inner and outer preforming radii r_p and R_p of both corners as illustrated in Figure 4-4b. A small amount of vinyl ester resin was manually sprayed as thermosetting binder on each fabric ply. The reinforcement was then placed between the two preforming plates and vacuum was drawn in the cavity to impose a preforming pressure p_p on the stacking. After closing the preforming tool and establishing the vacuum pressure, the preform was left overnight to cure at room temperature. This preforming procedure was used to prepare semi-rigid fibrous samples having a width of 650 mm and reproducing the stair shape of the manufacturing mold. These large preforms were finally cut for processing into smaller specimens (matching the dimensions of the test part). All the manufacturing experiments presented in this study were carried out with a unidirectional stacking consisting of 5 plies oriented along one of the fabric's principal directions, namely 0º or 90º (see Figure 4-3).

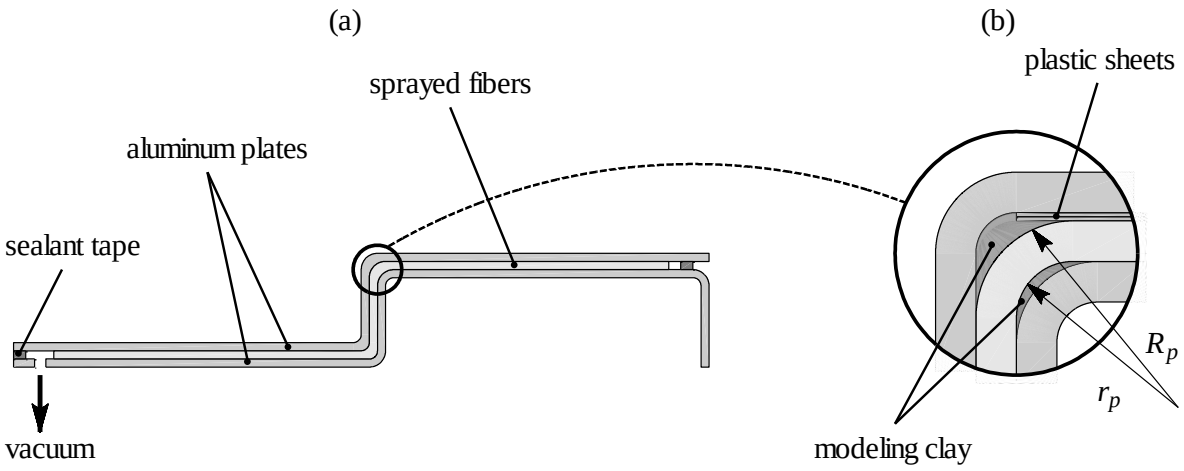

Figure 4-4 : Schematic representation of the preforming tool.

4.3.3 Processing

Figure 4-5 shows the mold configuration at the beginning of the processing cycle. As seen in the transverse cross-section A-A', the compaction cavity is slightly narrower than the injection cavity to pinch off the edges of the preform and prevent fiber wash-out during injection. The flexible membrane was cut out from a sheet of fluoroelastomer VITON from DuPont (thickness 1/32", hardness 75 A). As indicated in. Figure 4-5, two different curved regions exist in the part. The upper curved zone (with the membrane on the outside edge) is called the convex corner, and the lower curved zone is the concave corner. After preforming, the fibrous reinforcement was set in the cavity of the mold as shown in Figure 4-5. The fabrication stage followed the previously described standard procedure for Flexible Injection. Firstly, the resin and fluid outlets were connected to catch pots and vacuum was drawn in both the injection and compaction cavities. Resin was then injected at constant pressure with a Semco pneumatic gun model 250-A. The compaction fluid was silicone oil Dow Corning 200 with a viscosity of 100 cSt at 25ºC. The injection of the fluid was controlled with a simple pressure tank. All the experiments in the present study were carried out at room temperature (21±1ºC) with a constant injection pressure (p_i = 200 kPa) and constant compaction pressure (p_c = 600 kPa). Because of the relatively long gel time of the thermoset system, the parts were cured at least 6 hours before demolding.

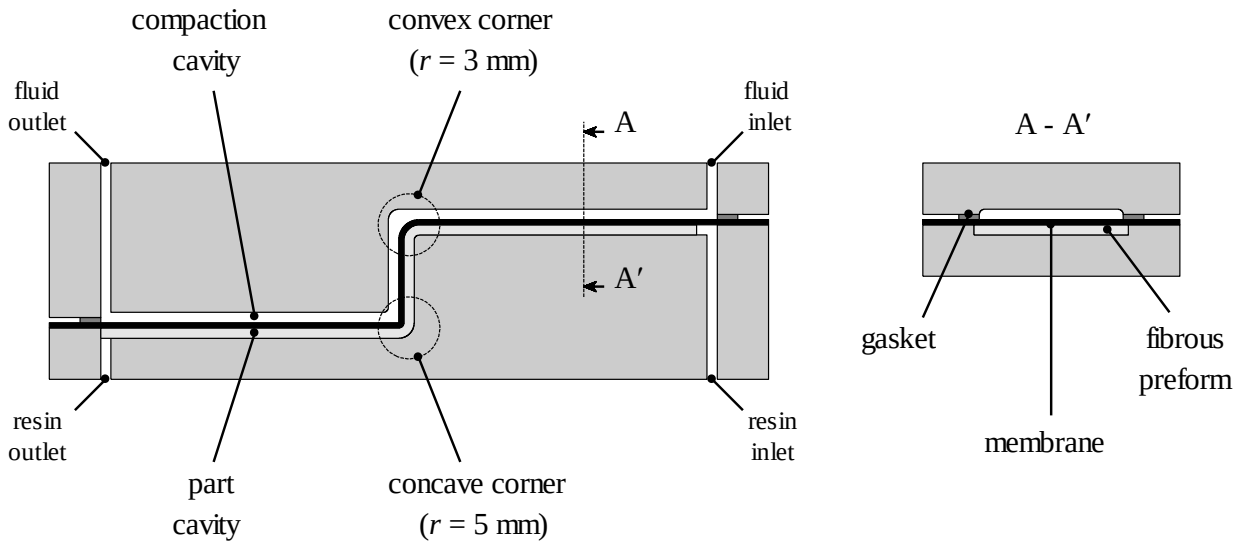

Figure 4-5 : Mold configuration prior to injection.

4.4 Analysis of fiber deformation: the planar geometry case

In Flexible Injection, the mechanical response of the fiber bed plays a key role because the final shape of the part is the result of the consolidation of the saturated reinforcement. Therefore, it is necessary to analyze the deformation of the fibers during the whole production cycle in order to understand how the geometry of the part is generated. In the present section, this analysis is carried out in the case of a planar geometry. The following three main fabrication stages will be considered: (1) preforming; (2) preform demolding; (3) processing. Figure 4-6 schematically describes the evolution of the thickness h and the effective compressive stress σ_f applied on the fibers during the production cycle. At each stage, these parameters depend on the boundary conditions imposed on the fiber bed and on its mechanical behavior. This load history is detailed in the sequel.

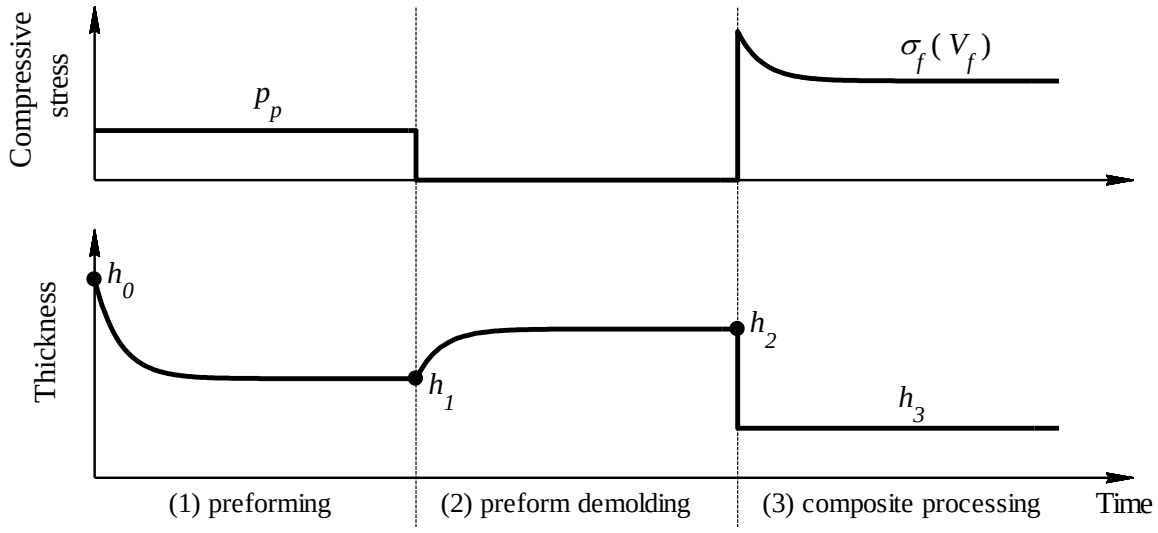

Figure 4-6 : Schematic representation of the mechanical load on the fiber bed during the three stages of the fabrication cycle.

4.4.1 Preforming

During preforming the reinforcement is subjected to the constant compressive stress of the preforming pressure p_p. Since engineering fabrics are viscoelastic materials, the complete

stacking experiences a gradual decrease in thickness from its initial height h_0 to a long term equilibrium state h_1. To quantify this phenomenon, compressive creep tests were performed with a MTS testing machine equipped with parallel plates. Samples consisting of five plies of unpreformed fabric (100×100 mm) were subjected to a constant speed load sequence (5 mm/min) until the desired stress was reached. The load was then maintained during two hours. The tests were repeated three times for two values of stress. Results reported in Figure 4-7 show that most of the change in thickness occurs during the first minutes of testing. For the two compressive stresses considered, the thicknesses reached at the end of the test were respectively:

- h_1 = 3.63±0.03 mm for σ_f = 30 kPa;
- h_1 = 3.16±0.05 mm for σ_f = 100 kPa.

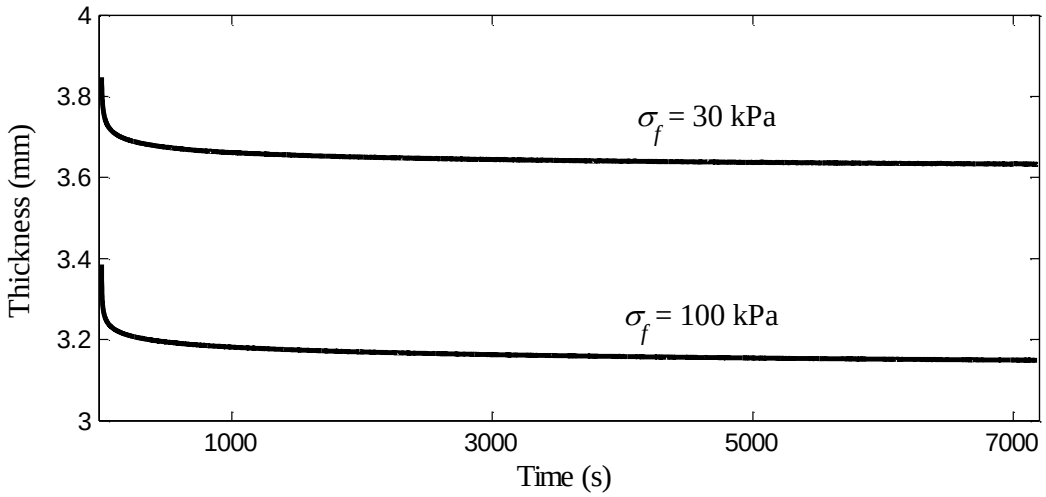

Figure 4-7 : Creep behavior of the unpreformed fiber fabric.

4.4.2 Preform demolding

When the preform is demolded, its thickness gradually increases. This phenomenon is called elastic springback. After sufficient time for creep recovery, the thickness stabilizes at a new equilibrium value denoted h_2 (see Figure 4-6), which is the natural thickness of the preform. This parameter was evaluated by applying a small compressive stress of 1 kPa on preformed samples and compared to the natural thickness of the pristine fabric h_0. Results reported in Figure 4-8a

show that the preforms are significantly thinner than the unpreformed fabric. Such a difference may be explained by viscoelastic effects such as nesting and by the presence of a cured binder that rigidifies the preform and hinders the rearrangement of the fibers. As seen in Figure 4-8a, increasing the preforming pressure from 30 kPa to 100 kPa only slightly reduces the natural thickness of the preform. However, the preforming pressure has a larger impact on the elastic springback represented by the difference $\Delta h = h_2 - h_1$ (see Figure 4-8b).

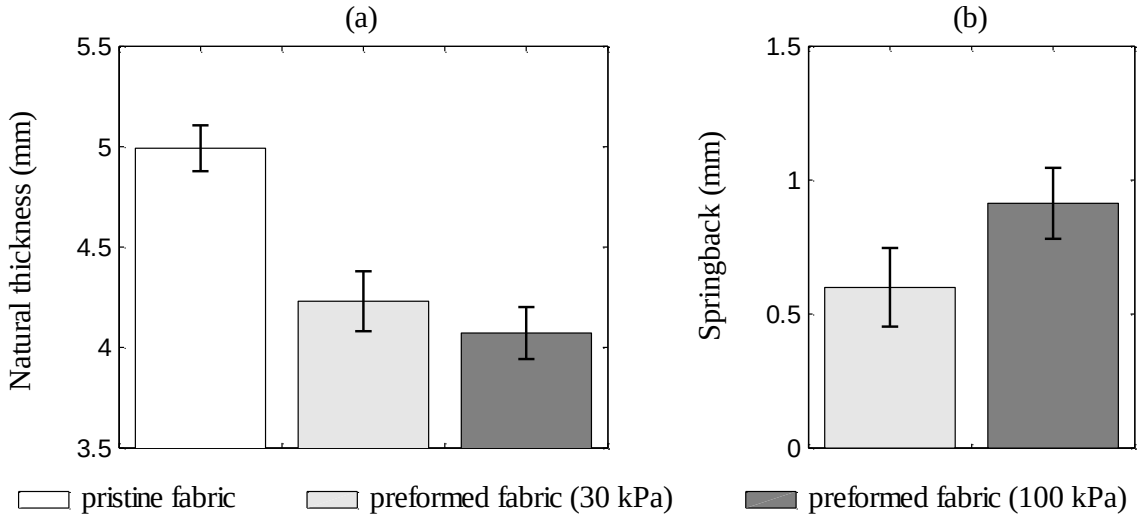

Figure 4-8 : Effect of the preforming pressure on the natural thickness of the fabric and on the elastic springback of the preform.

4.4.3 Processing

Impregnation of the fiber bed by the liquid resin is a complex phenomenon involving flow of the resin through the porous preform, flow of the fluid in the compaction chamber, deformation of the flexible membrane and compaction of the fiber bed. Understanding all the effects of the mechanical load imposed on the fibers during the processing stage would be a daunting task because of the strong coupling existing between all these phenomena. In the present case, however, the resin has a low viscosity and its gel time is much longer than the impregnation time. Therefore, it can be assumed that the resin flow inside the cavity is over long before gel occurs. At the limit, the entire processing stage can be simply viewed as a through-thickness compression

of the preform to a final thickness h_3 (see Figure 4-6). Assuming a perfect impregnation of the fibers (i.e., no void), h_3 can be determined by volume conservation inside the cavity as a function of the mass m_i of resin injected:

$$h_3 = \frac{1}{\rho_r}\left(\frac{m_i}{S_p} + \rho_{bs}\right) + \frac{\rho_{fs}}{\rho_g} \tag{4.1}$$

where S_p is the area of the preform, ρ_g the glass density, ρ_r the resin density, ρ_{fs} the fiber preform surface density and ρ_{bs} the preform binder surface density.

To approximate the mechanical response of the fiber bed during processing, relaxation tests were carried out on preformed and unpreformed fabric samples for thicknesses ranging from 2.8 to 3.6 mm. Typical relaxation curves are shown in Figure 4-9 for a preforming pressure of 100 kPa. As already seen during the creep experiments, the viscoleastic behavior of the fabric is particularly strong at the beginning of the test. For the lowest thickness considered (i.e., 2.8 mm), relaxation is still present, though strongly weakened after 2 hours of testing.

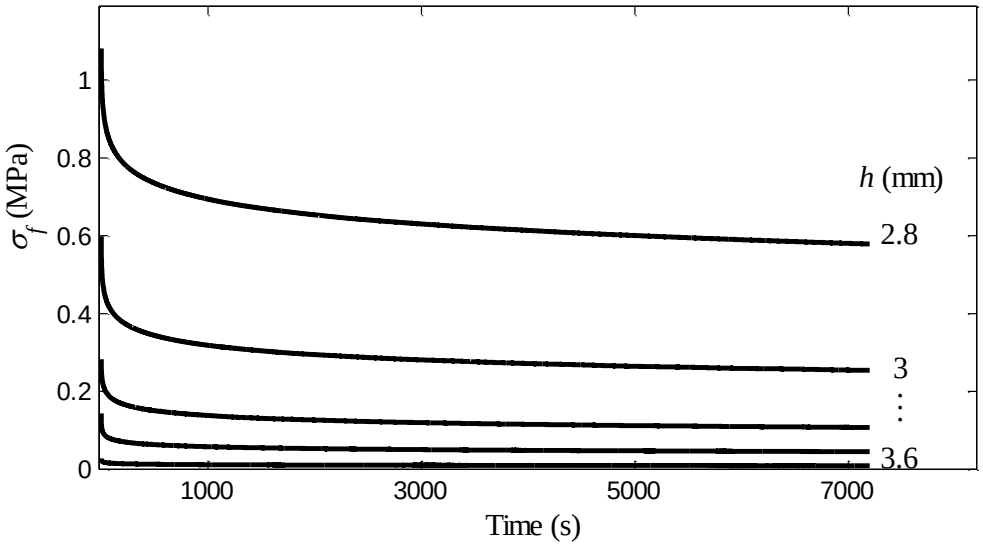

Figure 4-9 : Relaxation curves of the preformed fabric (5 plies, p_p = 100 kPa).

Stress values recorded after 2 hours of relaxation were used to construct a long term compaction curve describing the compressive behavior of the preform in its relaxed state. Results are reported in Figure 4-10 for both the raw fabric and the preformed samples. Preforming changes significantly the mechanical response of the fiber bed. Preforms become indeed much harder to compact than the unpreformed fabric when the effective stress exceeds the preforming pressure. This behavior is not surprising since the cured binder is likely to impede fiber motion during compaction. Moreover, the preforming pressure has a strong impact on the compaction behavior since for a given fiber volume fraction, the effective stress is always higher for preforms prepared under 30 kPa compared to samples prepared under 100 kPa.

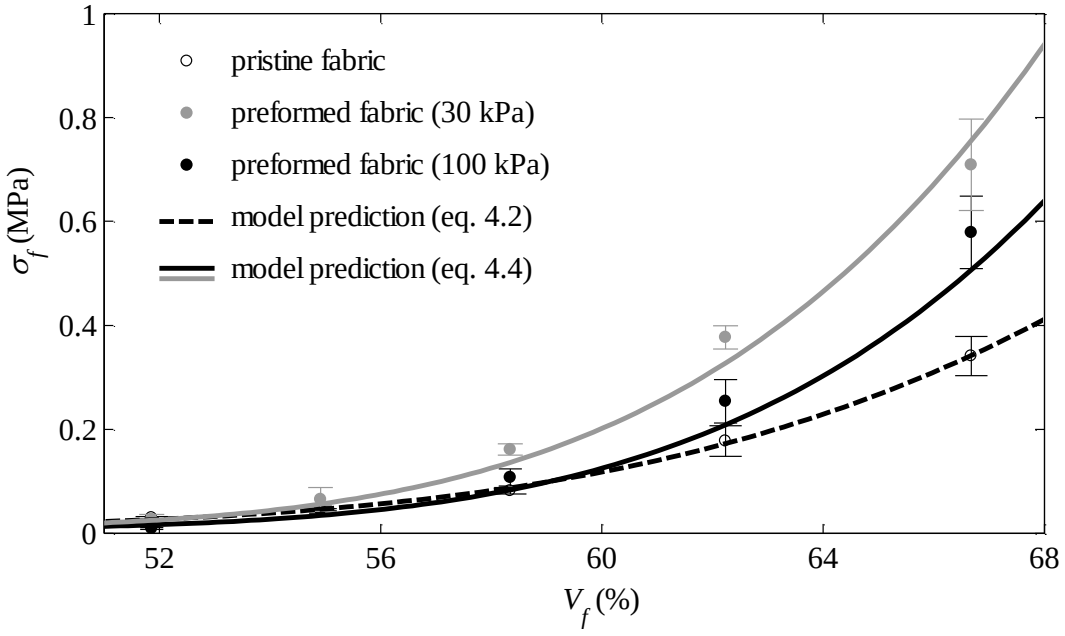

Figure 4-10 : Long term compaction behavior of the fiber bed (relaxed fibers after 2 hours compaction at constant thickness).

4.4.4 Compaction behavior modeling

Two different compaction models were used to reproduce the behavior of the pristine and preformed fabrics and take into account the influence of the preforming pressure on the

compaction curve. Firstly, the results obtained for the unpreformed samples were interpolated by the following equation (dashed line in Figure 4-10):

$$\sigma_f = -E_0.\varepsilon_T + A_0.\left(-\varepsilon_T\right)^{B_0} \tag{4.2}$$

where E_0, A_0 and B_0 are fitting parameters and ε_T is the logarithmic through-thickness strain defined as :

$$\varepsilon_T = \ln\left(\frac{h}{h_0}\right) \tag{4.3}$$

where we remind that h_0 is the natural thickness of the pristine fabric.

Typical compaction models for fiber fabrics usually express the effective stress as a function of the fiber volume fraction. In the present study however, the effective stress was related to the logarithmic strain, because one of our subsequent goals is to implement the compaction model in a commercial finite element software.

A second model was used to represent the compaction of the preformed fabric. The objective of this approach is to provide a compaction law that accounts for the effect of the preforming pressure p_p on the mechanical response of the fibrous reinforcement. The behavior of the preformed fabric was thus modeled with the following modified version of the compaction law (solid lines in Figure 4-10):

$$\sigma_f = -E_2.\left(\varepsilon_T - \varepsilon_2\right) + A_2.\left(-\varepsilon_T + \varepsilon_2\right)^{B_2} \tag{4.4}$$

where E_2, A_2 and B_2 are fitting parameters and ε_2 is the logarithmic strain corresponding to the natural thickness of the fabric after preforming. This term had to be introduced because preforms are thinner than the pristine fabric so that the effective stress must be zero when $\varepsilon_T = \varepsilon_2$. Furthermore, ε_2 must be a function of p_p to introduce dependence on the preforming pressure in the compaction model. To do so, it is assumed that the compaction curves of the pristine and preformed fabrics cross each other at the preforming conditions (pressure p_p, strain ε_1). The

preforming strain ε_1 is related to the thickness h_1 reached at the end of the preforming stage (see Figure 4-6) through equation (4.3):

$$\varepsilon_1 = \ln\left(\frac{h_1}{h_0}\right) \tag{4.5}$$

and satisfies:

$$p_p = -E_0.\varepsilon_1 + A_0.(-\varepsilon_1)^{B_0} \tag{4.6}$$

After calculating ε_1 with the above equation, the strain ε_2 is deduced from the relation:

$$p_p = -E_2.(\varepsilon_1 - \varepsilon_2) + A_2.(-\varepsilon_1 + \varepsilon_2)^{B_2} \tag{4.7}$$

The values of the fitting parameters obtained during the analysis are summarized in Table 4.1. As seen in Figure 4-10, this modeling approach satisfactorily describes the experimental results for the two values of preforming pressure considered. Moreover, an interesting feature of the proposed model is that a compaction law of the preformed fabric can be derived from the set of parameters A_i, B_i and E_i for any value of the preforming pressure.

Table 4.1 : Fitting parameters used in compaction models

	E_i (MPa)	A_i (MPa)	B_i
Pristine fabric (i = 0)	0.047	8	5.9
Preforms (i = 2)	0.055	44	5.8

4.4.5 Selection of fiber volume fractions

Knowledge of the fiber bed compaction behavior is essential for successful implementation of Flexible Injection. During consolidation, a constant compaction pressure p_c is applied on the resin saturated preform. Assuming that the membrane is perfectly flexible, this pressure balances the

pressure of the resin p_r and the effective stess σ_f on the fiber bed according to Terzaghi's law [27]:

$$p_c = \sigma_f(V_f) + p_r \tag{4.8}$$

Sufficient pressure must be maintained on the resin to make sure that the preform is well impregnated in order to get an acceptable void content in the final part. Consequently, the target value of the fiber volume fraction must be selected to ensure that the effective stress on the preform is significantly lower than the compaction pressure. In the present study, three values of fiber volume fraction were used in the manufacturing experiments:

- low compaction for V_{f1} = 53%,
- medium compaction for V_{f2} = 60%,
- high compaction for V_{f3} = 64%.

Considering the compaction behavior of the preform shown in Figure 4-10, the highest value of fiber volume fraction could be questionable for a real application with the compaction pressure of 600 kPa used in this study. Indeed, this situation is likely to result in a very low resin pressure and thus in a possibly important void content. This value was nevertheless chosen because the present work focuses on fiber deformation, one of the main objectives being to study the largest possible range of compaction levels. If impregnation quality were a primary concern, a fiber volume fraction of 64% would probably require a compaction pressure higher than 600 kPa.

4.5 Experimental analysis of corner quality for preforming with part geometry

A first series of parts was manufactured with the fiber volume fractions previously selected to illustrate the specific behavior of the curved sections and observe possible manufacturing defects in these areas. Two unidirectional fibrous preforms (samples A and B) with different fabric orientations (i.e., 0º and 90º) were prepared for these preliminary experiments. These specimens were obtained with an initial preforming tool reproducing the geometry of the processing mold (see Figure 4-5). The inner radius of the preforming tool was thus adjusted to 3 mm in the convex

corner and the outer radius was set to 5 mm in the concave corner. As reported in Table 4.2, the two other radii were selected to create a preforming cavity of almost constant thickness. Table 4.2 also shows that the binder content is not perfectly controlled because of the manual spraying process, but this parameter remains relatively low (< 4% wt). Three parts labeled 1, 2 and 3 were manufactured from each large preform. For each part, the mass of resin injected was calculated from equation (4.1) according to the desired fiber volume fraction. After demolding, the parts were weighted and the actual fiber content was calculated using the same relation. As seen in Table 4.2, the fiber volume fraction of the part is relatively well controlled considering the simple injection gun used for the fabrication. After demolding, the central sections of the parts were cut out and polished. Images of longitudinal cross-sections were obtained with a scanner Canon CanoScan. The observed results for the two types of curved areas are discussed in the following paragraphs.

Table 4.2 : Processing conditions used during the first series of manufacturing experiments

Preform	Fabric orientation	Preforming pressure (kPa)	Preforming geometry (mm)				Binder content (wt %)	Part	V_f (%)	
			Convex		Concave					
			r_p	R_p	r_p	R_p			target	Real
A	0º	100	3	6.5	1.5	5	3.27	A1	53	53.2
								A2	60	59.7
								A3	64	63.5
B	90º	100	3	6.5	1.5	5	2.21	B1	53	53.3
								B2	60	60.1
								B3	64	64.3

4.5.1 Convex corner

Figure 4-11 shows cross-sectional images of the convex corner of the parts. In all cases, the distribution of fibers inside the composite seems relatively homogeneous and no resin rich zone is visible. However, significant corner thickness variations appear when the fabric is oriented in the 0º direction. A corner thinning behavior is observed for the specimen manufactured with the fiber volume fraction of 53%, whereas the part with fiber volume fraction of 64% exhibits a marked corner thickening. The part manufactured at a medium fiber content V_f = 60% does not show significant thickness variations. These observations show that fibers oriented at 0º locally change the compaction behavior of the preform by limiting thickness changes in the curved region. Such behavior is caused by the extreme stiffness of the fibers that follow the curvature of the part. This fact was already reported several times in autoclave processing [10,13,14]. This effect does not exist when the fabric is oriented at 90º, because the longitudinal stiffness of the preform is much smaller. In this case, the flat and curved sections behave quite in the same way and an almost constant thickness profile is obtained for all the fiber volume fractions considered. However, the part manufactured at V_f = 64% shows localized thickness drops occurring in both the flat and curved sections. This behavior is caused by the fiber bundles which locally penetrate the soft material of the membrane. This effect could certainly be attenuated with a fabric made out of thinner bundles or by increasing the hardness of the membrane material. Note that this was already proposed in the rubber pressure molding technique by Sharma et al. [28].

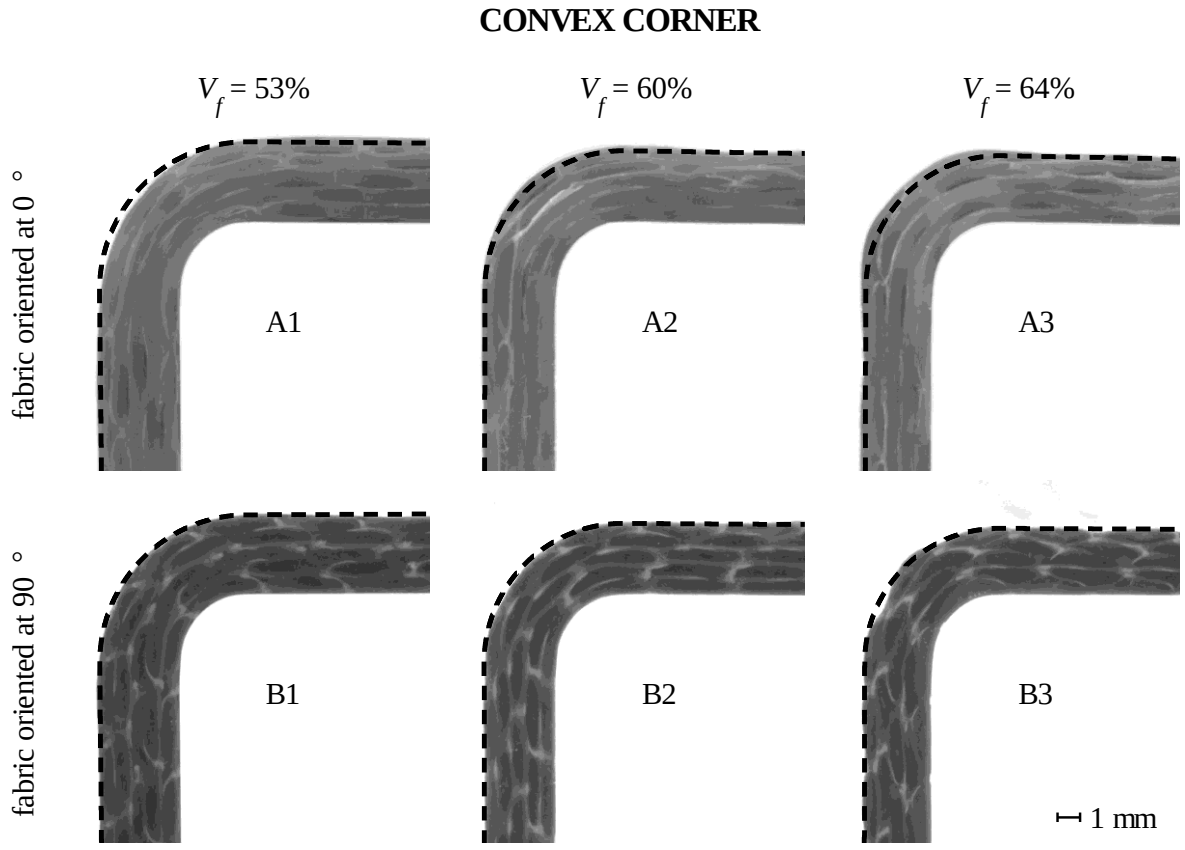

Figure 4-11 : Influence of fiber orientation on the quality of the convex corner for parts manufactured with the initial geometry of the preforming tool (dashed lines represent the targeted constant thickness profiles).

4.5.2 Concave corner

As seen in Figure 4-12, a completely different behavior is observed in the concave corner. Two different types of resin rich zones are visible on the cross-sections of the parts. The first kind of resin accumulation referred to as DEF1 is located on the inner side of the corner. Such defect is caused by an inappropriate membrane geometry and appears only for the lowest fiber volume fraction. Under such circumstances, there is little difference between the resin pressure and the compaction pressure so that according to Terzaghi's law (4.8), the effective stress acting on the membrane is too low to deform it from its initial planar geometry to the tightly bent shape required in the corner. Consequently, the membrane bridges over the corner and the open gap between the preform and the membrane is filled by pure resin. When the fiber volume content

increases, the compaction pressure becomes sufficiently higher than the resin pressure. This allows the compaction pressure to push the resin out of the corner area and forces the membrane against the fibers. Hence, the membrane induced resin rich zone disappears.

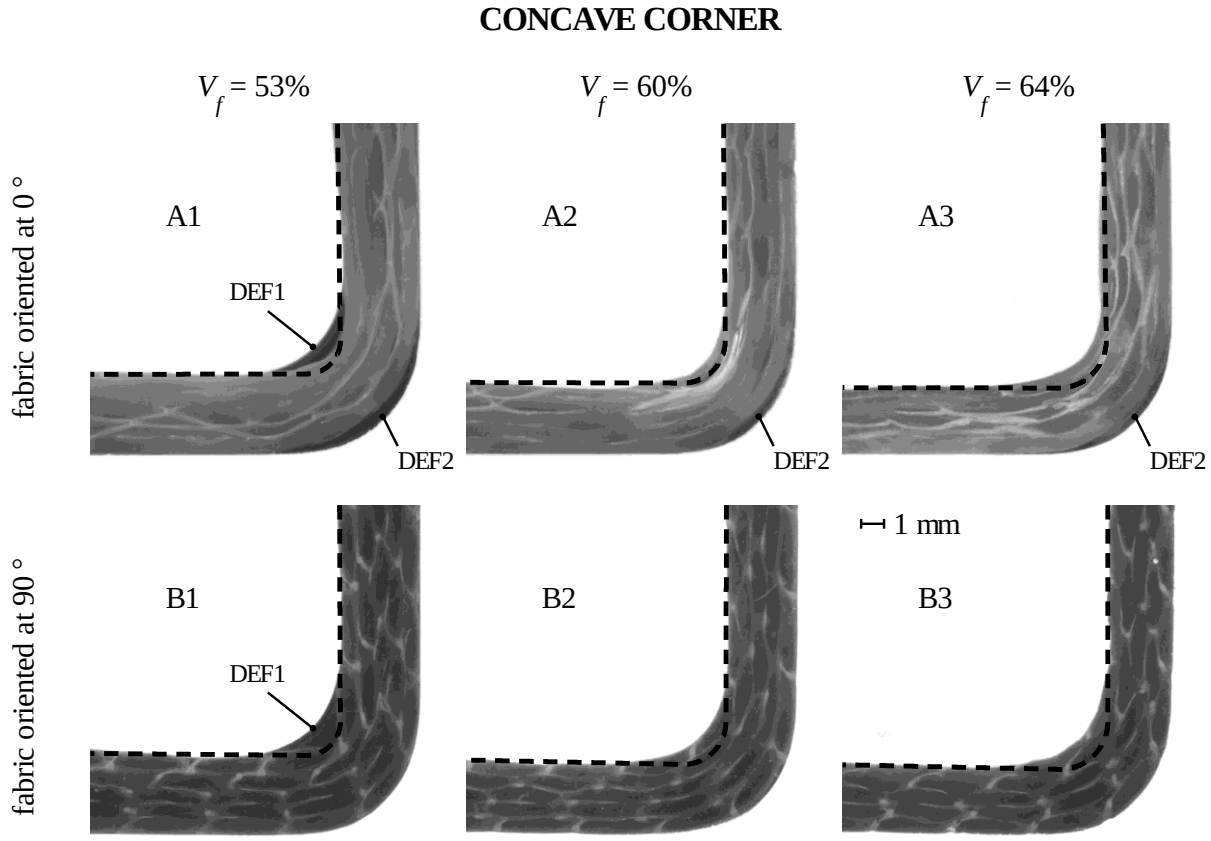

Figure 4-12 : Typical images showing different types of resin rich zones observed in the concave corner of parts processed with the initial preforming geometry (dashed lines represent the targeted constant thickness profiles).

Figure 4-12 also shows that a second type of resin accumulation exists in the parts processed with the fabric oriented at 0º. This defect labeled DEF2 is located on the outside of the corner between the preform and the mold wall. As already mentioned, the effective stress on the preform is low for a fiber volume fraction of 53% and the preform can be considered to be in an almost stress free state. Consequently, the existence of such preform induced resin rich zones suggests that the initial preforming geometry creates specimens that do not match precisely with the shape of the

mold in the concave corner (when the fibers are oriented at 0º). Furthermore, increasing the effective stress on the preform for a larger fiber volume content does not eliminate this defect. As observed in the convex corner, it seems that stiff fibers resist compaction in the curved area. This results in a completely different behavior between the flat sections of the part and the corner regions. No outer resin rich zone appears with fibers oriented at 90º. This suggests that fabric orientation changes the preforming behavior and hence affects the geometry of the fiber bed after preforming. In all the cases presented in Figure 4-12, the concave corner region is far from exhibiting the targeted thickness. This observation is somehow surprising for the parts oriented at 90º, for which one would expect an easier compaction as in the convex corner. This phenomenon will require further investigation, but could possibly be explained by the presence of stabilizing fibers in the 0º direction (see Figure 4-3b).

Using a flexible membrane reproducing the curvature of the part would probably eliminate membrane induced resin accumulations (DEF1). The manufacture of such device is feasible with existing rubber processing technology, but is out of the scope of the present study. Consequently, the remainder of this paper will focus on two types of defect: resin rich zones (DEF2) and thickness gradients arising from an imperfect geometry of the preform.

4.6 Analysis of fiber deformation in curved areas

From the observations of the first fabricated parts, it appears that compaction behavior in curved areas and preforming conditions play a key role in the generation of manufacturing defects. In this section, the deformation of the fiber bed in curved regions is analyzed during the different stages of the production cycle (refer to Figure 4-6). Starting from experimental observations of corner preforming, a multi-step finite element model is proposed to reproduce the deformation of the fibers during the whole fabrication process.

4.6.1 Preforming

During preforming, the planar fabric plies are forced to adopt a curved shape between two rigid tools. In that sense, the preforming procedure can be compared with the mold closing stage in RTM. For tightly bent shapes, it has been observed that fibers tend to become more compacted in the corners of the tools, thus leaving an open gap between the fibers and the outer radius. This phenomenon illustrated schematically in Figure 4-13 can be quantified by comparing the thickness h_c in the center of the curved area with the thickness h of the flat section through the following ratio:

$$r_h = \frac{h_c}{h} \tag{4.9}$$

Note in Figure 4-13 that the outer preforming radius R_p does not come into contact with the fiber bed, and hence does not affect the placement of the fibers in the corner as long as:

$$R_p \leq r_p + h.\frac{r_h - \sqrt{2}}{1-\sqrt{2}} \tag{4.10}$$

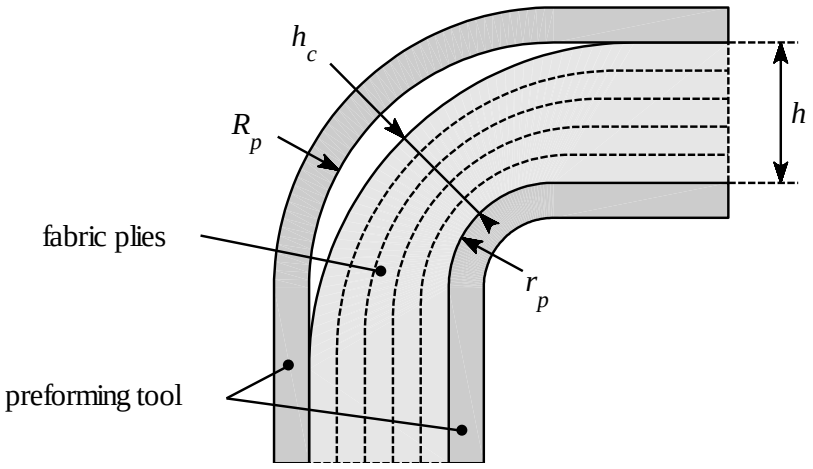

Figure 4-13 : Schematic representation of fiber rearrangement during corner preforming.

Few studies have investigated the influence of the preforming conditions on the thickness ratio r_h. Gao and Young [23] analyzed cross-sectional images of angled parts manufactured with RTM and observed a decrease of r_h for larger cavity thickness and lower fiber volume fraction. The latter finding was recently confirmed by Dong [24], who also showed that the thickness ratio was strongly dependent on the inner radius of the mold with smaller radii resulting in increased corner thinning of the reinforcement.

Experimental observations of corner preforming

In order to investigate the behavior of the fabric used in this study, a simple apparatus was designed to reproduce the conditions of corner preforming. The setup consists of two right-angled brackets mounted on a MTS testing machine. It was used to compress samples consisting of 5 plies of fabric (50×50 mm). Typical images of the stacking deformation during progressive closure of the setup are shown in Figure 4-14. The photographs show the deformations in the corner zone of the fabric plies at 90º (left) and 0º (right) when the cavity thickness decreases from 8 to 3 mm. As expected, fibers oriented at 90º conform more easily to the curved geometry of the tool, whereas fibers oriented at 0º tend to resist bending, thus resulting in important corner thinning of the stacking.

To quantify this corner thinning phenomenon, hot glue was injected in the gap between the fibers and the outer mold after closure of the setup. Prior to this manipulation, a thin plastic tape was placed in the center of the outer fabric ply to protect the fibers. After solidification of the hot glue, the setup was opened and the thickness of the adhesive measured with a depth gauge micrometer. The fiber bed thickness in the center of the corner was thus indirectly evaluated. This procedure was used to characterize fabric stacking oriented at 0º and was repeated for three different internal radii (1.25, 3.5 and 6.5 mm) and thicknesses ranging from 3 to 5 mm. In all cases, the outer radius R_p was sufficiently small to ensure that inequality (4.10) was verified. The results are reported in Figure 4-15, which plots the thickness ratio r_h as a function of the cavity thickness for the three curvature radii considered. Note the important corner thinning occuring

when the setup is closed to the natural thickness of the stacking h_0 = 5 mm. Moreover, the thickness ratio decreases with the inner preforming radius. The corner thinning effect decreases when the fabric is further compacted. For the larger radius studied (i.e., 6.5 mm), thickness ratios larger than 1 are even observed for cavity thicknesses of 3 and 3.5 mm.

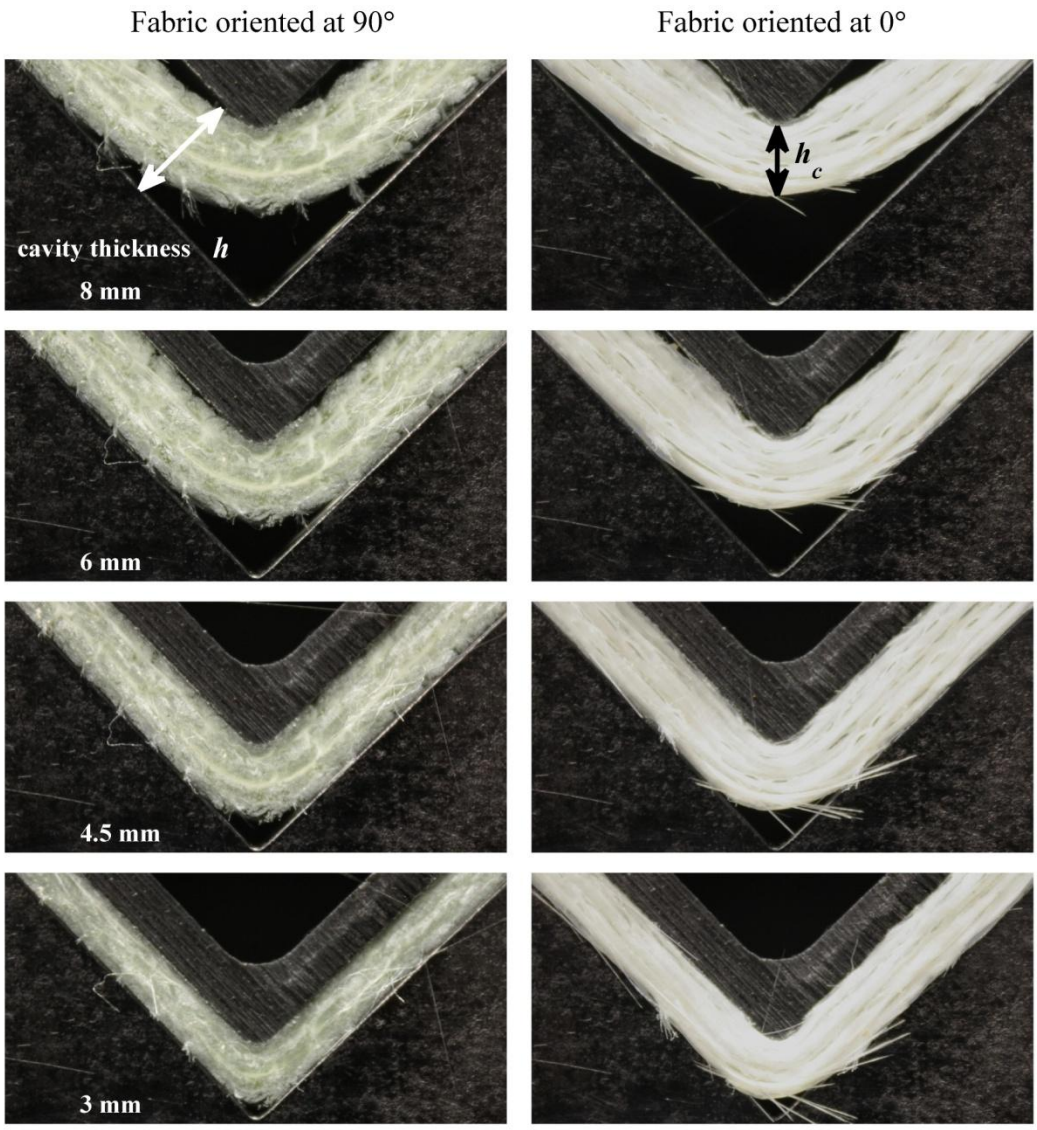

Figure 4-14 : Illustration of corner preforming behavior of the Saeruni fabric with an inner radius of 1.25 mm. For the fabric oriented at 90º, fibers are perpendicular to the cross-section, while for the fabric oriented at 0º, the fibers are parallel to the cross-section.

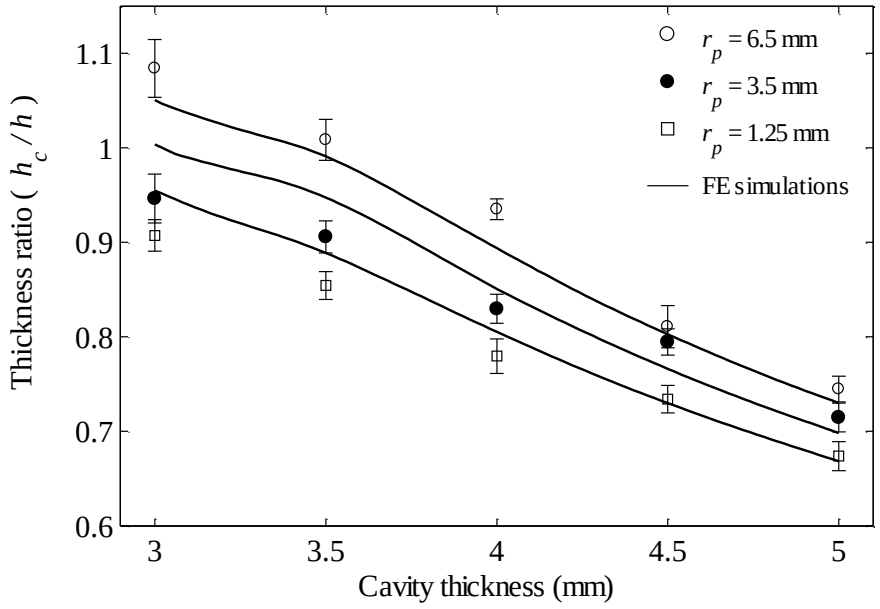

Figure 4-15 : Influence of the inner preforming radius and cavity thickness on the geometry of the corner section (fabric oriented at 0º).

Finite Element Modeling

Modeling corner prefoming is a difficult exercise since it involves large displacements and complex deformation mechanisms such as fiber bundle bending and compaction, interply slip and sliding of the fabric against the walls of the tool. In the present study, a simplified 2D plane strain model was developed with ANSYS software to reproduce the corner preforming experiment with the fibers oriented at 0º. As shown in Figure 4-16, the initial geometry of the fiber bed is described by three parameters: the flat arm thickness h_0, the inner radius r_{in} and the outer radius r_{out}. These parameters are related to the thickness ratio r_h through the equation:

$$r_{out} = r_{in} + h_0 . \frac{r_h - \sqrt{2}}{1 - \sqrt{2}} \tag{4.11}$$

The basic assumption consists of considering the corner preforming experiment starting for the larger inner radius and the larger cavity in a stress free state, on which the initial geometry is constructed. Parameters h_0 and r_{in} were consequently set to 5 mm and 6.5 mm respectively. Parametric studies were conducted for initial thickness ratio r_h between 0.72 and 0.76 in order to

obtain the best fit of the experimental results. For each ratio value, the outer radius of the preform r_{out} was deduced from equation (4.11).

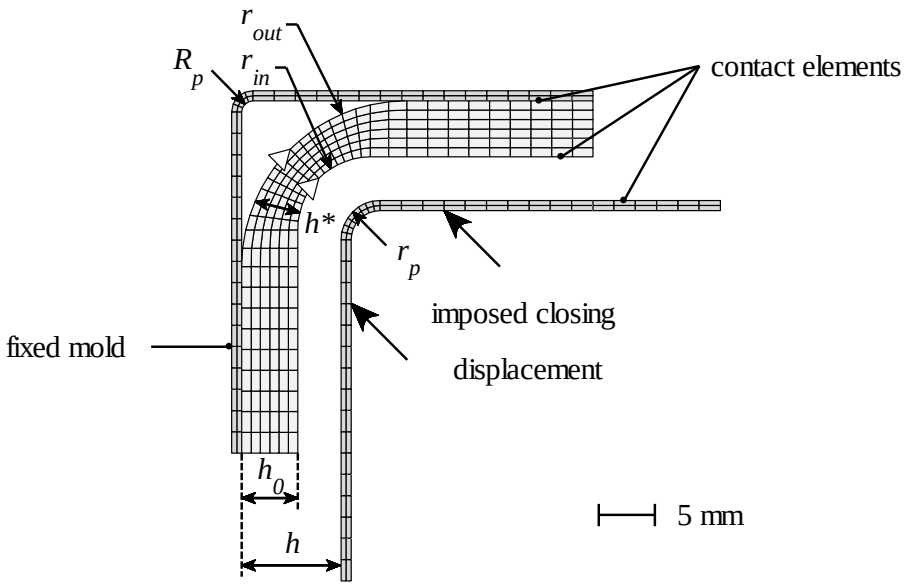

Figure 4-16 : Finite element model used to reproduce the corner preforming experiment.

Figure 4-16 also shows the boundary conditions used for the simulations. The outer mold is fixed while a displacement is imposed on the inner part of the tool. Nodes located in the center of the preform corner are restricted to through-thickness displacements. Both molds and the preform are meshed with quadratic elements and contact elements are placed between the preform and the tools. A friction coefficient of 0.25 was determined by placing a fabric sample on an inclined aluminum plane and measuring the angle for which sliding started to occur. The molds were modeled as very rigid isotropic bodies (E = 1000 GPa, ν = 0.3) and the fabric stacking was modeled as a homogeneous orthotropic material. The compaction law for pristine fabric (4.2) was used to describe the transverse behavior of the fibers, but it was modified before implementation in the simulation software. By convention, a compressive stress is considered negative and the sign of the equation was inverted. Rewriting the compaction law in terms of thickness h of the stacking gives the following expression for the through-thickness stress σ_T :

$$\sigma_T = E_0.\ln\left(\frac{h}{h_0}\right) - A_0.\left[-\ln\left(\frac{h}{h_0}\right)\right]^{B_0} \tag{4.12}$$

The above equation is only valid for a stacking of initial thickness h_0 = 5 mm and for $h \leq h_0$. To avoid using any undefined function in the calculations, the compaction law was extended to the case where $h > h_0$ by considering only the first linear term:

$$\sigma_T = E_0.\ln\left(\frac{h}{h_0}\right) \text{ when } h > h_0 \tag{4.13}$$

Figure 4-16 shows that the initial thickness h^* in the model varies along the arc length of the fiber bed and is lower in the curved area than the natural thickness h_0. For each element of the model, the parameter h^* was calculated according to its position relative to the corner. Since the initial geometry is supposed to be stress free, the compaction law was shifted by a factor $-\sigma^*$ to ensure that $\sigma_T = 0$ when $h = h^*$. After such modification, the transverse constitutive law becomes:

$$\sigma_T = E_0.\ln\left(\frac{h}{h_0}\right) - A_0.\left[-\ln\left(\frac{h}{h_0}\right)\right]^{B_0} - \sigma^* \text{ when } h \leq h_0 \tag{4.14}$$

$$\sigma_T = E_0.\ln\left(\frac{h}{h_0}\right) - \sigma^* \text{ when } h > h_0 \tag{4.15}$$

with

$$\sigma^* = E_0.\ln\left(\frac{h^*}{h_0}\right) - A_0.\left[\ln\left(\frac{h_0}{h^*}\right)\right]^{B_0} \tag{4.16}$$

Note also that the constitutive law must be expressed as a function of the through-thickness true strain ε_T, which is calculated from the actual initial thickness h^* as follows:

$$\varepsilon_T = \ln\left(\frac{h}{h^*}\right) \tag{4.17}$$

Substituting equation (4.17) in (4.14) and (4.15) gives the following final form of the transverse constitutive law:

$$\sigma_T = E_0.(\varepsilon_T - \varepsilon^*) - A_0.(-\varepsilon_T + \varepsilon^*)^{B_0} - \sigma^* \text{ when } \varepsilon_T \leq \varepsilon^* \tag{4.18}$$

$$\sigma_T = E_0.(\varepsilon_T - \varepsilon^*) - \sigma^* \text{ when } \varepsilon_T > \varepsilon^* \tag{4.19}$$

with

$$\varepsilon^* = \ln\left(\frac{h_0}{h^*}\right) \tag{4.20}$$

The longitudinal and shear behavior of the stacking were modeled using linear relationships:

$$\sigma_L = E_L.\varepsilon_L \tag{4.21}$$

$$\sigma_{LT} = G_{LT}.\varepsilon_{LT} \tag{4.22}$$

where the longitudinal modulus E_L was calculated from the initial fiber volume V_{f0} and the modulus of glass fibers E_g as follows:

$$E_L = V_{f0}.E_g = 27 \text{ GPa} \tag{4.23}$$

The shear modulus G_{LT} was varied from 0.02 MPa to 0.2 MPa through parametric studies to fit the experimental results.

The fiber bed constitutive law (equations (4.18), (4.19), (4.21) and (4.22)) was implemented in the finite element software *via* a fortran USERMAT subroutine. Solid lines in Figure 4-15 show the simulation results for the best values of the initial thickness ratio (r_h = 0.73) and shear modulus (G_{LT} = 0.08 MPa) obtained during the analyses. As can be seen, the model is able to reproduce the observed experimental trends, but overpredicts the thickness ratio for low values of cavity thickness and preforming radius. However, the comparison remains quite satisfying considering the numerous simplifying assumptions.

Figure 4-17 shows the through-thickness stress distribution predicted by the model for a cavity thickness of 3 mm and three different preforming radii in the inner corner. Decreasing this radius forces the fabric to adopt a sharply bent geometry and creates a highly compacted zone in the corner. By changing the geometry and the stress state of the fabric before cure of the binder, the prefoming conditions are then likely to affect the properties of the resulting preform.

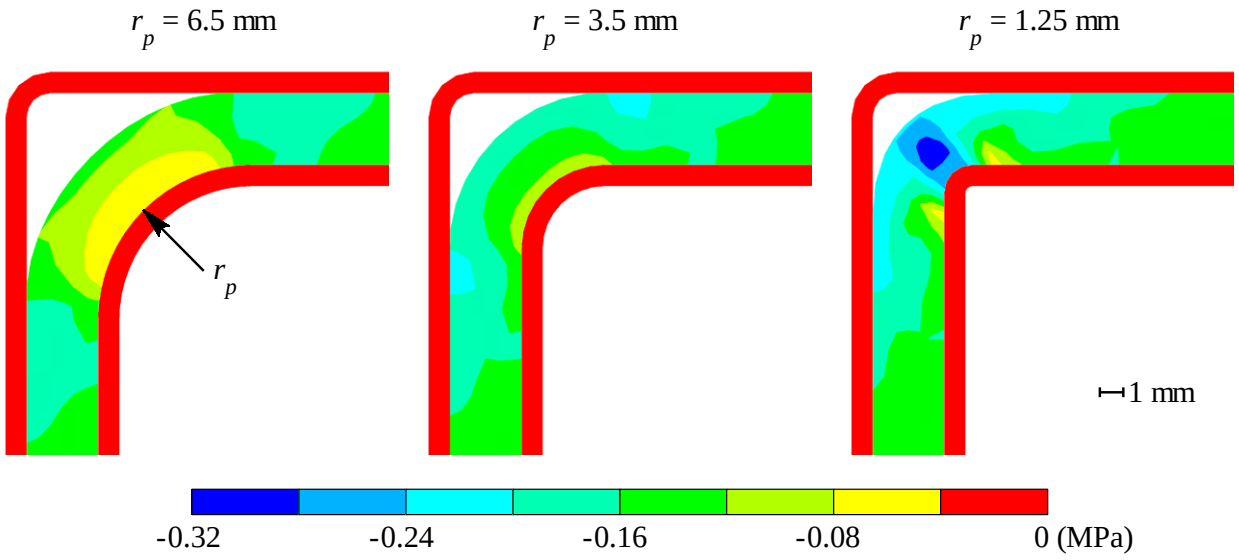

Figure 4-17 : Simulated through-thickness stress during corner preforming (fabric oriented at 0º, cavity thickness h = 3 mm).

4.6.2 Preform demolding

Impact of binder cure on fiber bed shear behavior

It was previously shown that preforming has an impact on the planar compaction behavior of the fiber bed. Cure of the thermoset binder also changes the overall shear response of the preform since intimately bound fabric plies are not allowed to slip freely relatively to each other. To illustrate this change in behavior, three point bending tests were carried out on pristine and preformed fabrics (width 40 mm, span 50 mm). The test sequence was a simple constant speed ramp at 5 mm/min. Resulting force-displacement curves reported in Figure 4-18 show that

preformed samples resist to bending whereas no significant rigidity can be observed with the unpreformed fabric.

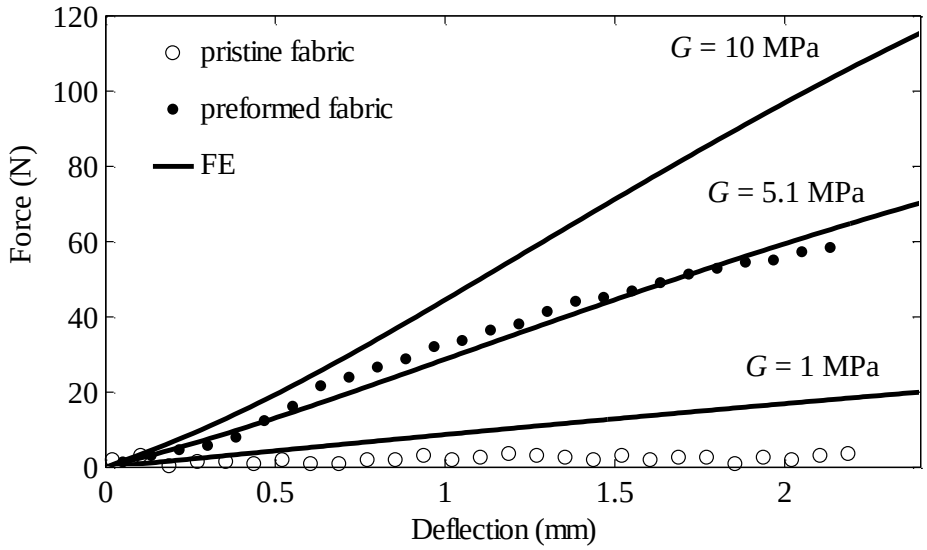

Figure 4-18 : Influence of preforming on the flexural behavior of the reinforcement in three point bending test (fabric oriented at 0°).

The impact of binder cure on the shear modulus of the fiber bed was evaluated through parametric numerical studies. A finite element model was first developed to reproduce the three point bending test. The model is similar to the one presented in the previous section, but uses unrelaxed versions of the compaction parameters E_i, A_i and B_i since no relaxation was involved during the experiments. Finally, the shear modulus G_{LT} was varied from 0.1 MPa to 10 MPa to get the best representation of the experimental results obtained with the preformed sample. As seen in Figure 4-18, a bending force matching the experiments was predicted with a shear modulus of 5.1 MPa. This represents an increase by a factor 50 compared to the shear modulus of unpreformed fabric determined previously. Note that no attempt was made to characterize the influence of the preforming pressure on the shear modulus and a unique value was used in subsequent simulations regardless of the preforming conditions.

Numerical simulation of elastic springback in curved areas

In the flat sections of the parts, the change in interply slip behavior does not really alter the springback of the preform after demolding. In curved sections however, the limited shear deformation of the preform implies a change in geometry because stiff fibers along the curvature of the part cannot accommodate a change in length during thickness recovery. As seen in the photograph of Figure 4-19a, this results in a demolded preform that does not retain a right-angled shape. The springback of the stair-shaped preform was predicted by numerical simulation. The first stage consisted of simulating the preforming step as described in the previous section for a final thickness of the flat section corresponding to the preforming pressure. In the second part of the analysis, the mechanical properties of the fiber bed were modified to reproduce the effect of binder cure. The shear modulus was changed from 0.08 MPa to 5.1 MPa and the transverse constitutive law (equations (4.18) and (4.19)) was replaced by:

$$\sigma_T = E_2.(\varepsilon_T - \varepsilon_2) - A_2.(-\varepsilon_T + \varepsilon_2)^{B_2} - \sigma^* \text{ when } \varepsilon_T \leq \varepsilon_2 \quad (4.24)$$

$$\sigma_T = E_2.(\varepsilon_T - \varepsilon_2) - \sigma^* \text{ when } \varepsilon_T > \varepsilon_2 \quad (4.25)$$

where ε_2 was derived for each element by considering its through-thickness strain/stress state (ε_1/σ_1) predicted at the end of the preforming step. Following the procedure presented for the planar case, this parameter was computed to verify:

$$\sigma_1 = E_2.(\varepsilon_1 - \varepsilon_2) - A_2.(-\varepsilon_1 + \varepsilon_2)^{B_2} - \sigma^* \quad (4.26)$$

After changing the preform properties, a zero-displacement condition was imposed on the inner central node and the preforming tools were removed from the model so that the preform could adapt freely to the new set of boundary conditions without external load. An example of predicted demolded geometry is given in Figure 4-19b which shows that the shape of the demolded preform corresponds to the experimental observation.

(a) (b)

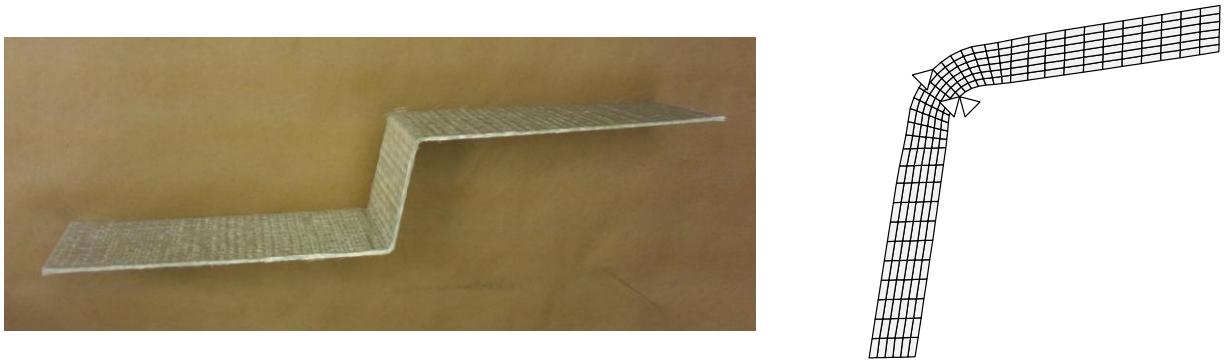

Figure 4-19 : Elastic springback of a stair-shaped preform: (a) typical shape of a demolded preform; (b) example of predicted geometry (r_p = 3.5 mm, p_p = 100 kPa).

4.6.3 Processing

Before processing, the preform is first manually laid in the mold cavity and forced to conform to the stair-shaped geometry. In the simulation, this stage was reproduced by applying a small draping force on the extremities of the preform (see Figure 4-20a). In the all the cases studied, a draping force of 18 N was found sufficient to bring the preform into contact with the tool. Finally, a constant pressure was applied on the outer nodes of the preform to simulate processing. Since the membrane and the resin were not included in the model, the planar compaction model (4.4) was used to calculate the processing pressure required to reach the targeted fiber volume fraction.

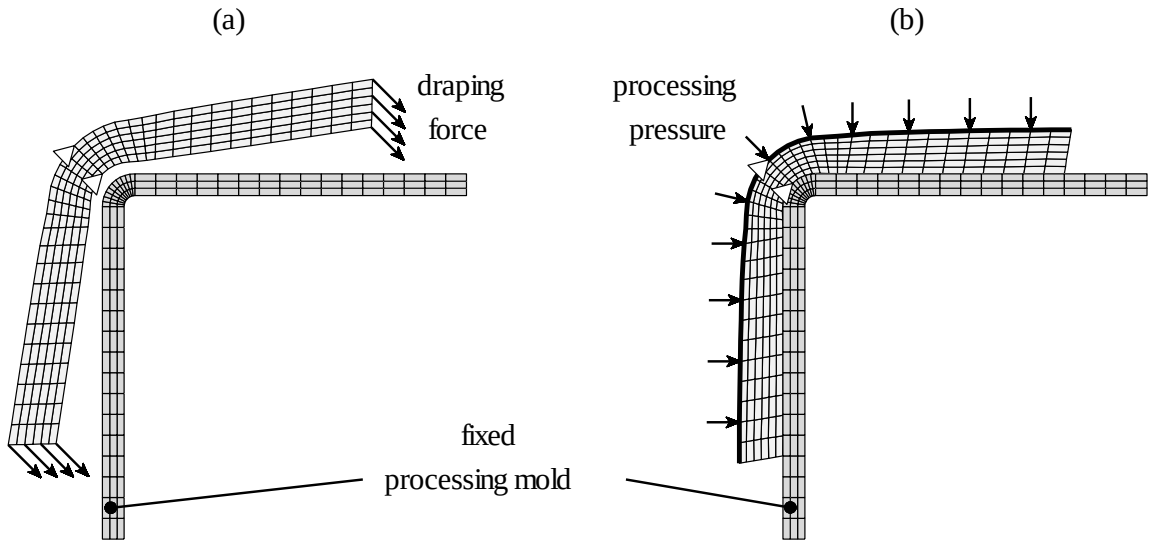

Figure 4-20 : Simulation of the processing stage: (a) placement of the preform in the processing tool; (b) application of the processing pressure.

As a first validation test, the finite element model was used to replicate the fabrication of the parts with a 0º fabric orientation (parts A1 to A3 in Table 4.2). Contour plots of the predicted through-thickness stress are drawn in Figure 4-21. The predictions compare favorably with the experimental observations (refer to Figure 4-11 and Figure 4-12). At low fiber volume fraction, the convex corner is significantly more compacted than the rest of the part. The corner thinning phenomenon is slightly overestimated compared to the experiments. This affects also the flat regions in the vicinity of the corner. When the fiber volume fraction increases, the compressive stress in the corner is barely changed, whereas flat sections away from the curved area are adequately compacted. As observed during the experiments, corner thinning disappears for a fiber volume fraction of 60%. Corner thickening appears finally when V_f = 64%.

In the concave region, an open gap is predicted between the fibers and the mold, which is in agreement with the preform induced resin rich zone (DEF2) observed on the parts. The stress distribution in the concave corner is quite different from the convex case. At low fiber volume fraction, an important stress concentration is predicted in the curved region. When the level of compaction increases, flat sections of the part are forced toward the mold. As a reaction, fibers

located on the inner side of the corner tend to move away from the tool because deformation is quite limited in the longitudinal direction. As a result, the concave corner becomes less compacted than the flat sections for a fiber volume fraction of 64%. Overall, the main difference between the simulations and the experiments concerns the inner radius of the concave corner. The predicted thickness in the center of the concave corner is indeed lower than expected. This suggests that the model does not perfectly reproduce the elastic springback of the preform at such location.

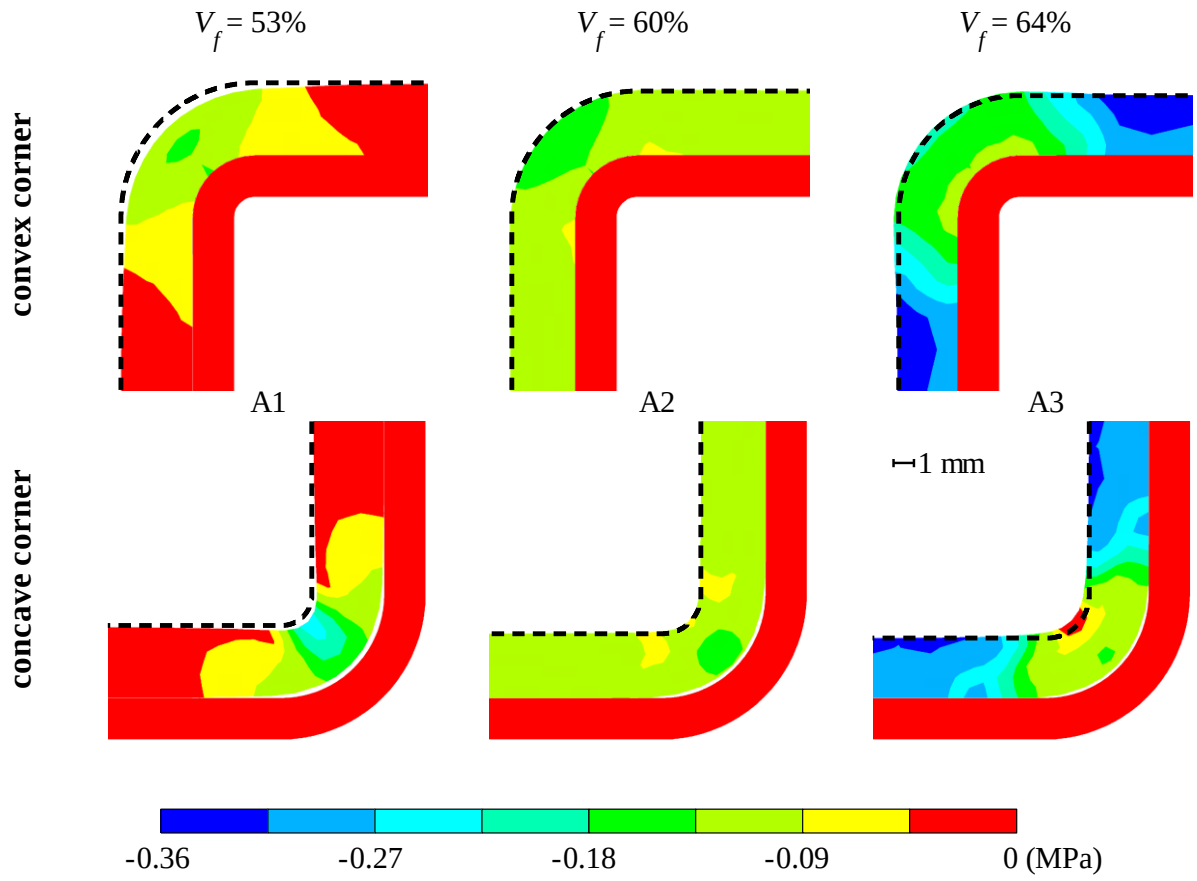

Figure 4-21 : Predicted through-thickness stress distribution in the corners of parts manufactured with the initial preforming geometry (dashed lines represent targeted constant thickness profiles).

Numerical results presented in Figure 4-21 are in rather good agreement with the layup quality observed in the first parts fabricated. However, one must keep in mind that the development of the model is based on several important assumptions that might jeopardize its predictive ability from a quantitative point of view. Among the main limitations of the approach, one can mention:

- the use of an initial stress free geometry of significant curvature;
- an homogeneous representation of the fabric stacking unable to capture adequately physical phenomena such as interply slip;
- constitutive laws that do not take time dependence into account (although constructed from experimental relaxed data);
- no membrane deformation nor resin flow is taken into account;
- the combination of orthotropic behavior of the fiber bed with large deformations may lead to poor conservation of the material principal directions during the treatment of geometrical nonlinearities.

Notwithstanding the above comments, the proposed model helps to investigate the deformation mechanisms occurring during Flexible Injection. Thanks to this analysis, explanation could be proposed for the observed experimental results.

4.7 Influence of preforming conditions on corner quality

In this section, parametric studies are conducted to analyze the effects of the geometry of the prefoming tool in the corners and of the preforming pressure upon the quality of the test part. The objective is to understand how manufacturing defects are generated and propose corrective strategies to eventually eliminate them. This matter was addressed through numerical studies and with a second series of nine fabrications. This second set of parts was manufactured from three large prefoms with fabric oriented at 0º that were prepared under different preforming conditions. The processing parameters are summarized in Table 4.3. Firstly, preforms C and D were obtained using modified preforming tool geometries. In both cases, the preforming radii were selected to ensure that inequality (4.10) was verified. As a result, the main parameter of interest of preforms C and D is the inner preforming radius r_p. Finally, preform E was prepared with the initial

preforming geometry (same as preforms A and B), but with a reduced preforming pressure of 30 kPa.

Table 4.3 : Summary of the second series of manufacturing experiments

Preform	Fabric orientation	Preforming pressure (kPa)	Preforming geometry (mm)				Binder content (wt %)	Part	V_f (%)	
			Convex		Concave					
			r_p	R_p	r_p	R_p			target	Real
C	0º	100	4	6.5	4	5	3.27	C1	53	53.4
								C2	60	60.1
								C3	64	63.4
D	0º	100	1	3	1	3	3.75	D1	53	53.2
								D2	60	60.1
								D3	64	63.2
E	0º	30	3	6.5	1.5	5	2.37	E1	53	53.3
								E2	60	60.4
								E3	64	64.6

4.7.1 Change in the inner preforming radius

Convex corner

The influence of the preforming geometry in the convex corner region was investigated numerically by varying the inner preforming radius r_p from 1 to 4 mm. The simulations were conducted with a small outer prefoming radius (R_p = 1 mm) to ensure that the fibers did not come in contact with the outer preforming tool in the curved region. Figure 4-22 shows the predicted through-thickness stress distributions in the convex corner for the different cases studied. It should be reminded that the processing tool has a radius of 3 mm. The case with r_p = 3 mm was thus already discussed in the previous section. The results of Figure 4-22 show that the preforming radius has a noticeable impact on the layup quality and on the stress distribution in

the corner of the composite. For a preforming radius of 4 mm (hence larger than the mold radius), a highly compacted zone is created on the inner side of the curved region, because the fiber bed and the mold first come in contact in the middle of the corner. This situation also affects the flat regions in the vicinity of the corner. For the low fiber volume fraction of 53%, a small open gap is predicted between the fibers and the mold, which may result in the creation of another type of resin rich zone. Increasing the fiber volume fraction eliminates this defect, but these regions resist compaction and thickening is predicted at the junctions of flat and curved sections for a fiber volume fraction of 64%. On the other hand, using a preforming radius smaller than the mold radius may generate a resin accumulation on the inner side of the convex corner. With a preforming radius of 2 mm, a small gap is predicted between the fibers and the mold. This defect become more important when the radius is further decreased to 1 mm. This is similar to the preform induced resin rich zones (DEF2) already observed in the concave corner. Furthermore, the size of these resin accumulations remains almost constant for all the fiber volume fractions considered. Overall, the arrangement of the fibers in the curved region remains virtually unchanged regardless of the effective stress imposed on the reinforcement.

Figure 4-23 shows experimentally observed cross-sections of the convex corner for the two extreme values discussed above. A good agreement exists with the predictions although quantitative differences may be noticed. For a preforming radius of 4 mm, an increase in thickness occurs in the transition regions between the flat arms and the corner, but this effect concerns a wider zone than expected. For the lowest fiber volume fraction, a thin resin rich zone (DEF3) seems to exist as predicted in these regions, although the observed defect is rather small and can hardly be confirmed. With a preforming radius of 1 mm, resin rich zones (DEF2) are clearly visible in the corner for all the fiber volume fractions considered. However, the observed defect is smaller than predicted. This tends to confirm that the model underestimates the springback of the inner radius. Finally, note that an air bubble is visible in the resin rich zone for the fiber volume fraction of 64%. This is not surprising since a very low resin pressure is expected in that case as discussed previously.

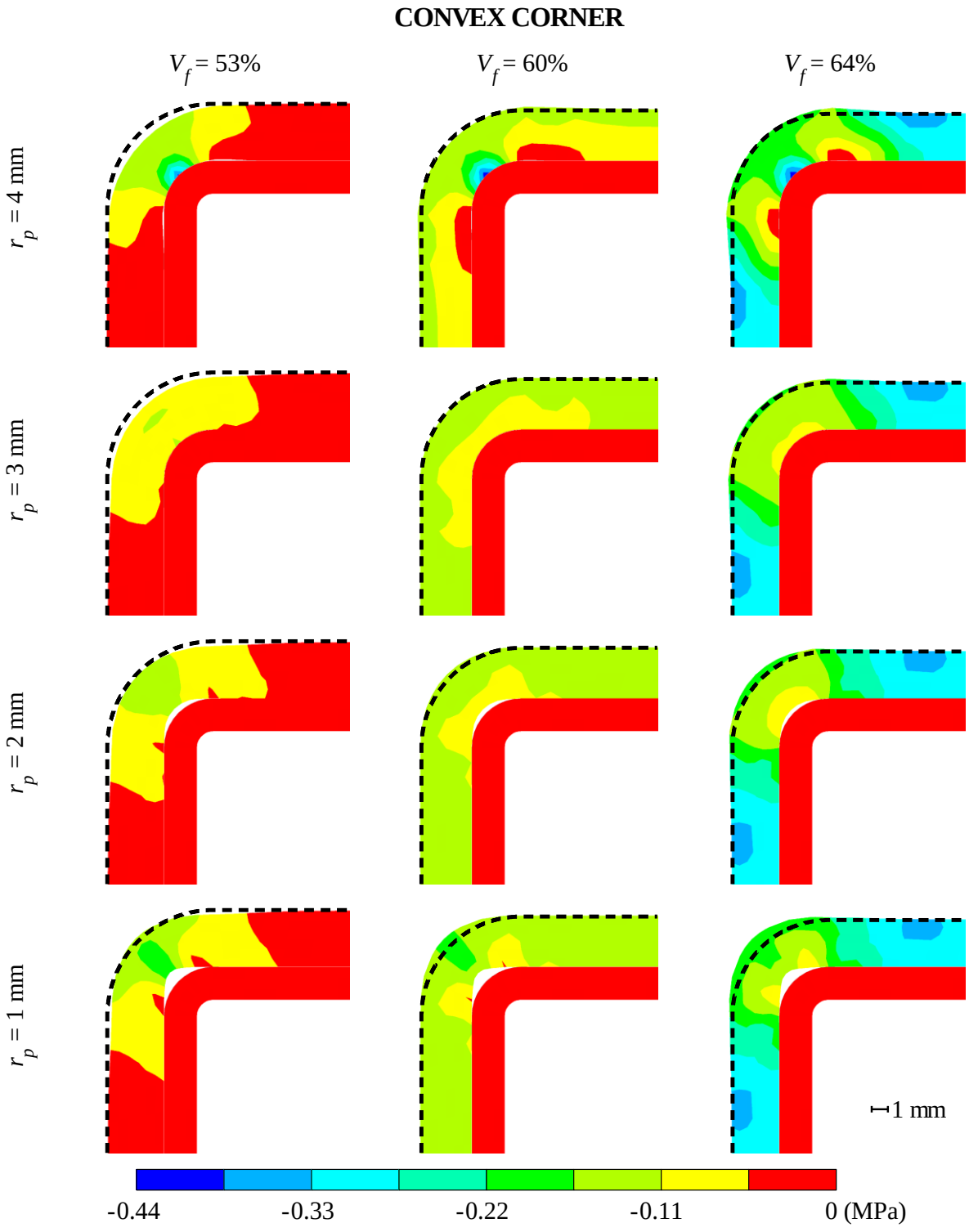

Figure 4-22 : Through-thickness stress distribution predicted by numerical simulation in the convex corner for different preforming and processing conditions (dashed lines represent perfect thickness profiles).

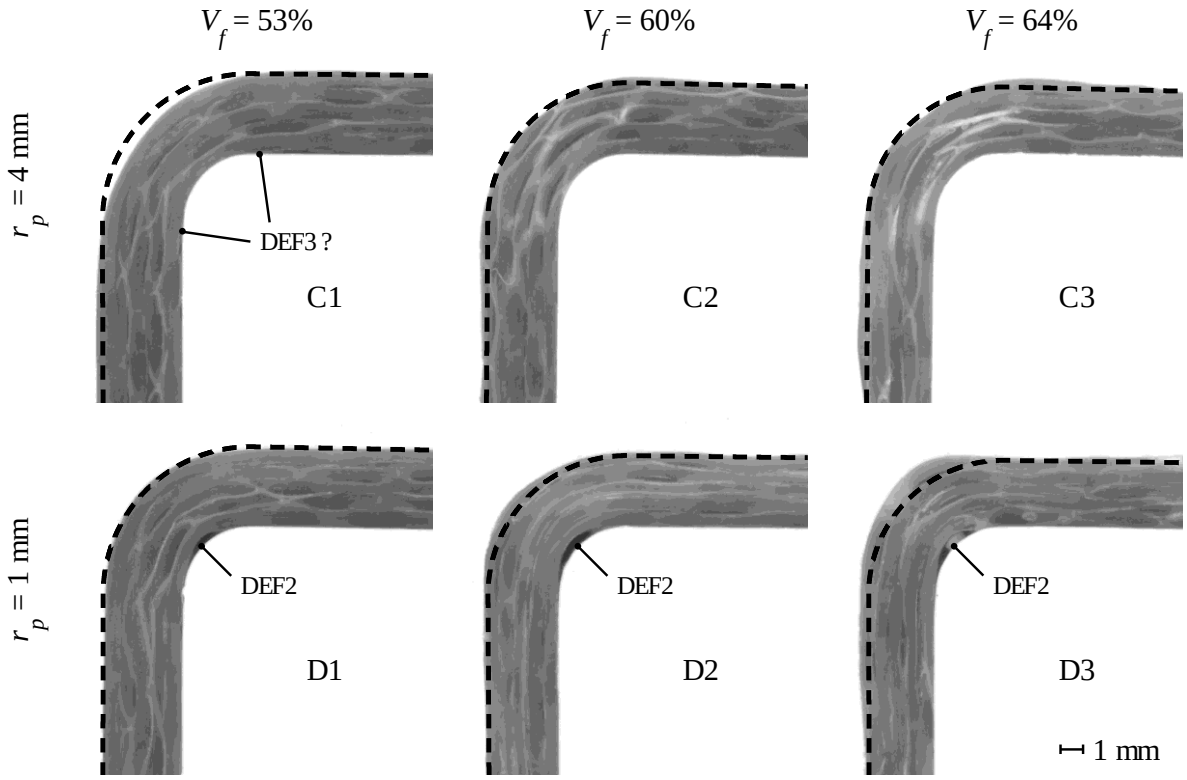

Figure 4-23 : Typical images of the convex corner of parts manufactured for two different inner preforming radii r_p = 1 mm and r_p = 4 mm.

Concave corner

A similar approach was used to study the influence of the preforming radius in the concave corner. Figure 4-24 presents contour plots of the through-thickness stress for all the cases studied. With a preforming radius of 4 mm, an important gap is created between the preform and the mold, which results in a large resin rich zone (DEF2). Decreasing the preforming radius gradually decreases the size of the defect by forcing the fiber bed in the corner. For the lowest prefoming radius of 1 mm, the fibers come in contact with the curved region of the mold and the defect disappears almost entirely. As observed for the first fabricated parts, increasing the fiber volume fraction reduces the compaction on the inner side of the corner for all the radii considered. Moreoever, the inner shape of the corner gets further apart from the targeted geometry of the part. Finally, note that the effective stress on the preform increases with the

targeted fiber volume fraction, but this barely changes the geometry of the fiber bed in the curved region. As in the case of the convex corner, this suggests that an efficient prefoming technique for Flexible Injection must preform the fiber bed in the curved regions to the expected shape of the final part.

Figure 4-25 confirms that the experimentally observed cross-sectional images of the test parts manufactured with different preforming radii are consistent with the results of the numerical investigation. With an inner preforming radius of 4 mm, a large resin rich zone (DEF2) appears on the outer side of the corner for all the fiber volume fractions considered. As predicted by the simulations, this defect is eliminated when r_p is reduced to 1 mm. With such preforming radius, a membrane induced resin rich zone (DEF1) is created for the lowest fiber volume fraction as already observed in the first parts. Once again, the main difference between the simulations and the experiments concerns the inner side of the corner, the elastic springback of the preform being more important than predicted in this area. Finally, it is particularly interesting to note that a preforming radius of 1 mm allows processing a strongly curved part without apparent defects for a fiber volume fraction of 60%. As a matter of fact, the use of a concave rigid mold is known to constitute a difficult case for composite manufacturing processes using flexible tooling (like autoclave processing for example) because fibers tend to bridge over such areas.

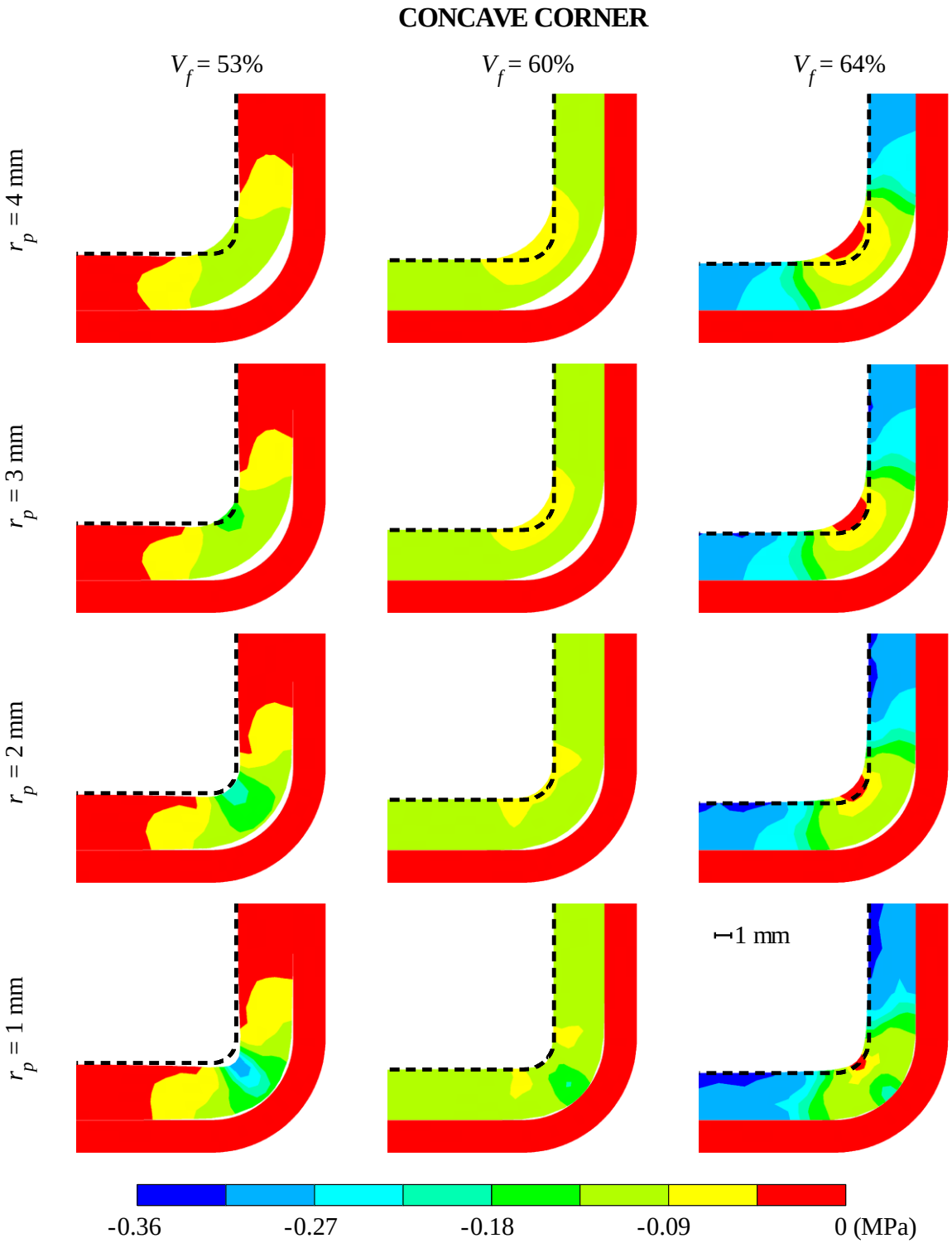

Figure 4-24 : Through-thickness stress distribution predicted by numerical simulation in the concave corner for different preforming and processing conditions (dashed lines represent perfect thickness profiles).

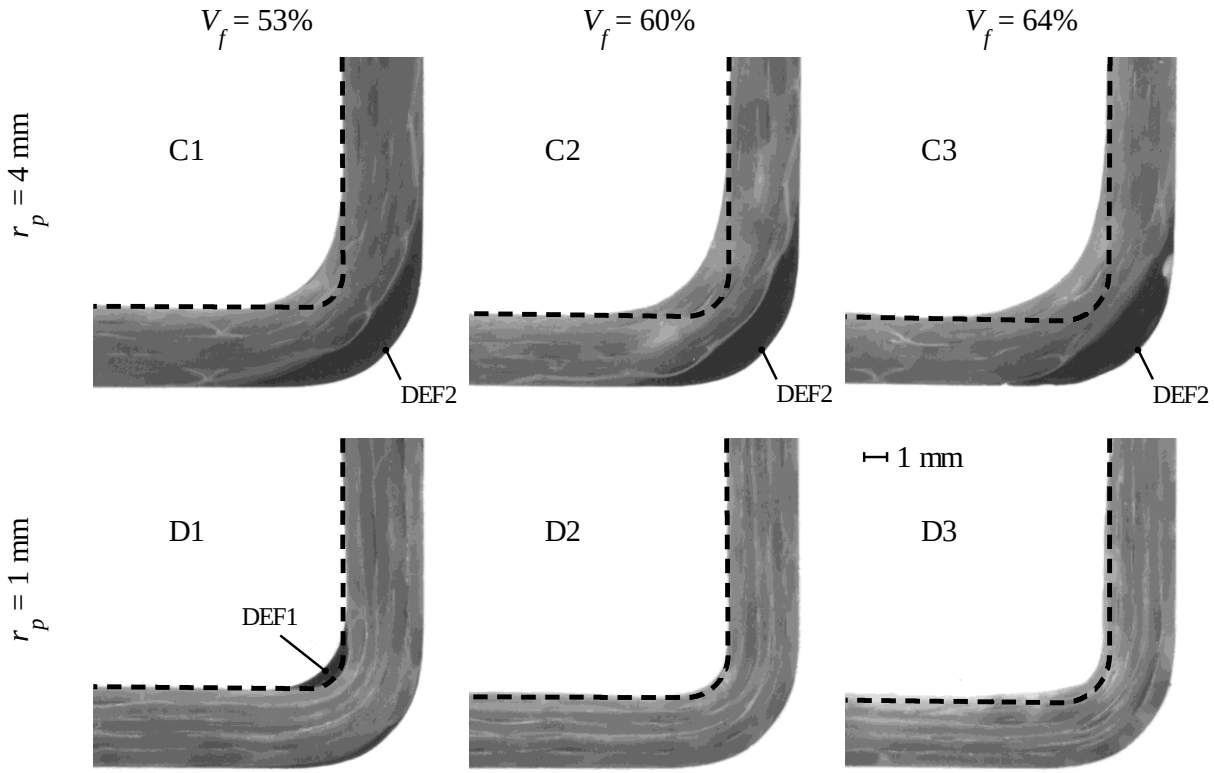

Figure 4-25 : Layup quality observed in the concave corner for two different inner preforming radii r_p = 1 mm and r_p = 4 mm.

4.7.2 Change in the preforming pressure

During preforming, the applied pressure governs the thickness of the stacking. The geometry of the prefom in the curved region is then likely to be affected by a change in preforming pressure. Figure 4-26 shows thickness profiles predicted by the model with the initial preforming tool geometry for various preforming pressures. In the convex corner, decreasing the preforming pressure reduces the corner thinning that occurs at low fiber volume fraction. With a preforming pressure of 30 kPa, an almost constant thickness profile is indeed predicted for V_f = 53%. However, decreasing the prefoming pressure exacerbates corner thickening for larger fiber volume fractions. In such case, a higher prefoming pressure should be recommended in order to get a more homogeneous thickness. For example, the model predicts that a uniform thickness can be obtained for a fiber volume fraction of 64% with a p_p = 300 kPa.

In the concave corner, increasing the preforming pressure forces the fiber bed to take a smaller radius on the outer side of the curved area. The preform induced resin rich zone DEF2 can thus be eliminated with p_p = 300 kPa. Such prefoming pressure seems well adapted for high fiber volume fractions, but may not be appropriate for lower values, since important corner thinning is predicted for V_f = 53%. In the cases presented here, decreasing the preforming pressure to 30 kPa is not recommended, because this results in a larger resin rich zone and important corner thickening for high fiber volume contents.

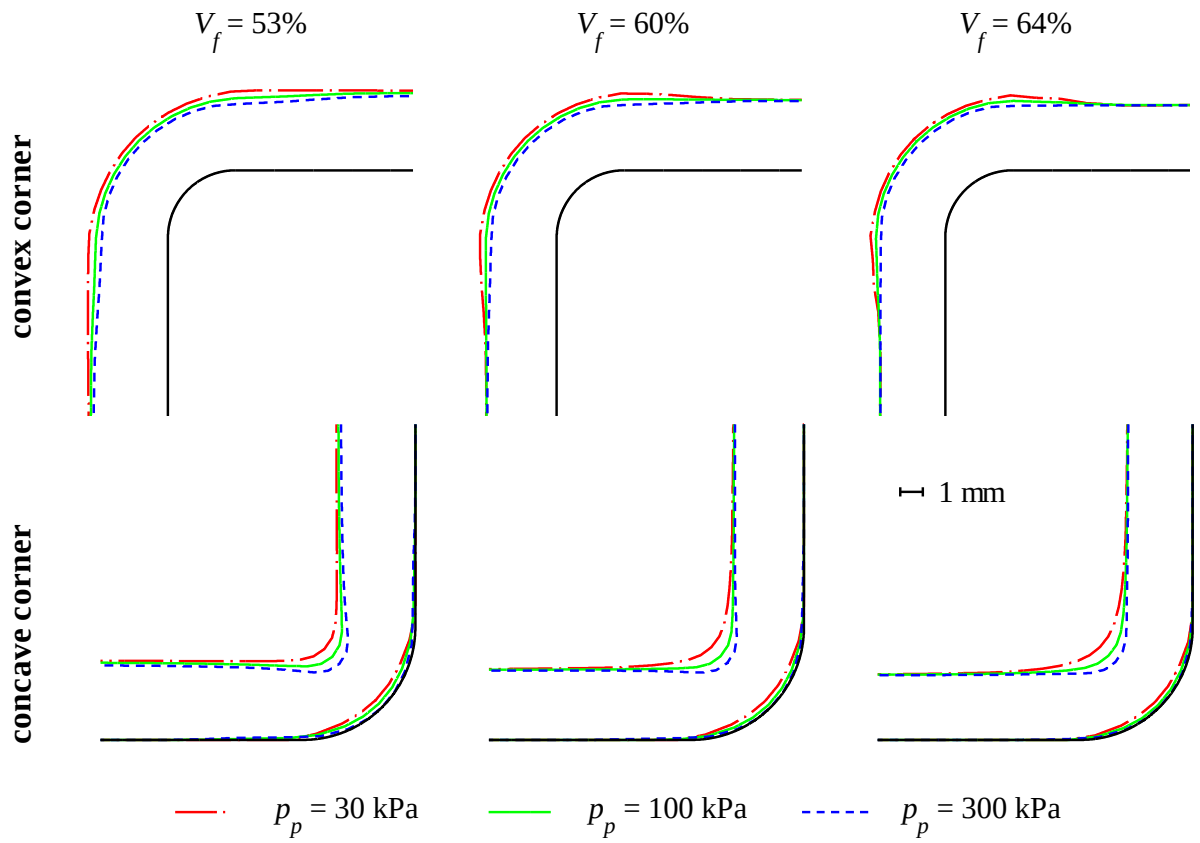

Figure 4-26 : Predicted thickness profiles in the curved regions with the initial prefoming tool geometry for three preforming pressures of 30, 100 and 300 kPa.

The preforming pressure used in this study is limited by the atmospheric pressure. Consequently, the influence of this parameter was only investigated experimentally with a reduced value of 30 kPa. Corresponding cross-sectionnal images are reported in Figure 4-27. As expected, no

significant corner thinning is observed in the convex corner for a fiber volume fraction of 53%. When the fiber content increases, corner thickening gradually develops. However, the experimentally observed layup for a fiber volume fraction of 64 % is slightly different than the numerical prediction. A marked corner thickening appears, but the phenomenon is limited to the corner and does not affect the flat sections close to the curved area. This difference could be due to local fiber wrinkling on the outer side of the corner, because of the important effective stress applied on the preform. Finally, the experiments confirm that reducing the preforming pressure is not appropriate with the preforming geometry studied here, since this results in larger manufacturing defects in the concave corner.

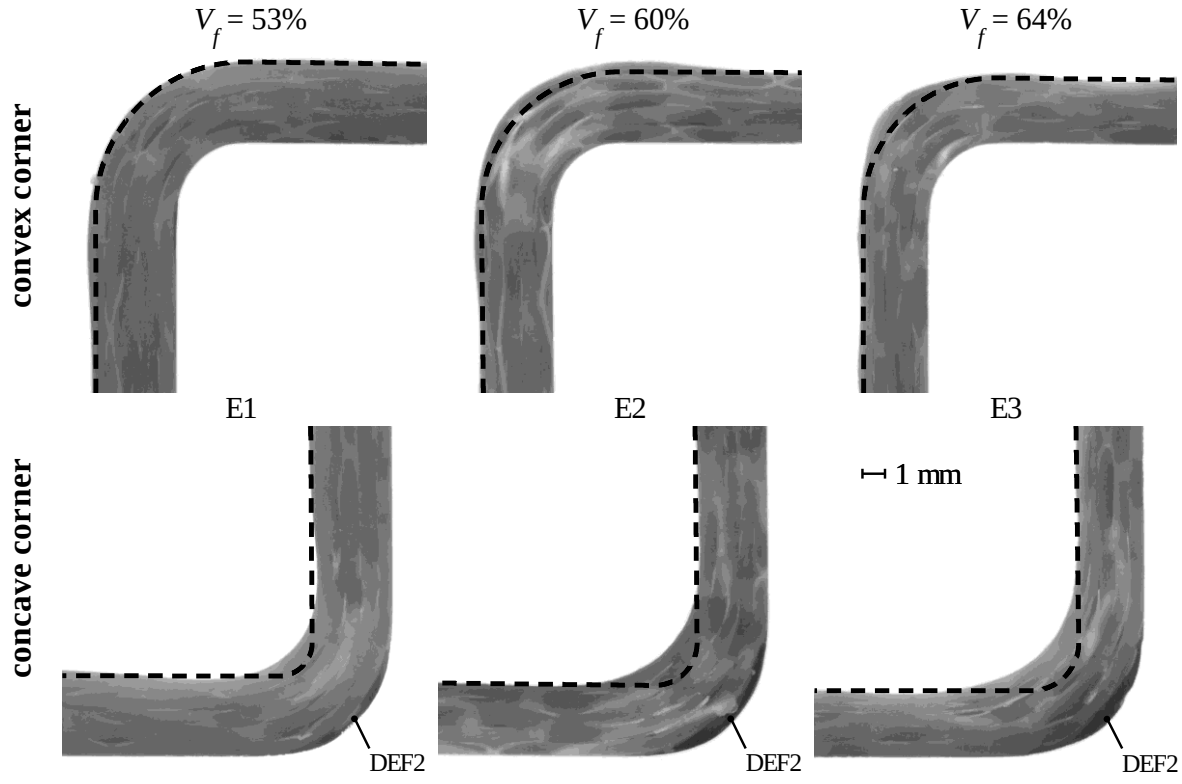

Figure 4-27 : Typical images of curved regions obtained with the initial preforming geometry for a reduced preforming pressure of 30 kPa.

4.8 Summary and conclusions

Flexible Injection possesses an interesting potential for the fast manufacturing of high performance composite parts. However, the flexibility of the processing tool can create problems when tightly bent structures need to be produced. The goal of this paper was to investigate the specific features of Flexible Injection in the manufacture of curved shapes. The approach consisted of analyzing separately the different stages of the production cycle: preforming, release from the preforming tools and processing. Simple characterization tests were used to build a multi-step finite element model reproducing the behavior of the fibrous preform during the fabrication process. Numerical simulations were then used to identify the important processing parameters that control the quality of the final product and understand the mechanisms that generate manufacturing defects. The predictions of the finite element model were compared with the experimental observations provided by manufacturing a series of curved parts with a specially devised setup. This investigation lead to the following conclusions:

- The quality of curved composites manufactured by Flexible Injection depends on the initial geometry of the fibrous preform, on its mechanical behavior and on the geometry of the processing tool (i.e., convex or concave).
- The consolidation of curved sections is limited by the presence of reinforcing fibers in the curvature direction.
- The geometry of the fiber bed after preforming is influenced by the specific bending behavior of fiber bundles, which tend to become more compacted when conformed to a strongly curved shape.
- The use of a prefoming binder changes the mechanical response of the fiber bed by limiting fiber rearrangement and interply slip. Such preforming strategy notably affects the one-dimensional compaction and shear behavior of the preform.
- With an appropriate prefoming strategy, Flexible Injection allows manufacturing tightly bent composites with a high fiber volume fraction without important manufacturing defects.

- Predicting the optimum prefoming conditions for a given application is a complex task, which requires extensive material characterization and a precise knowledge of the preform behavior during the entire manufacturing cycle.

Finally, the experimental results presented in this work were obtained by laboratory procedures involving manual handling (e.g., during preforming). This might not be perfectly representative of a fully automated industrial application. However, the above conclusions on the physics of the process should remain valid. For example, braiding or 3D weaving technologies have the ability to produce fibrous preforms of complex shapes. Using these methods in conjunction with Flexible Injection will require a thorough knowledge of the fiber bed behavior during preforming and processing. Moreover, recently proposed advanced modeling techniques [29] and characterization methods [30] could also be used to study the interply slip phenomenon. Such works could possibly bring interesting contributions in the future, not only for Flexible Injection, but also for other composite manufacturing processes.

4.9 Acknowledgements

The authors would like to thank Dr. John Owens, from General Motors Laboratory, Detroit, USA, for his advises regarding the orientation of the research, and General Motors (GM) of Canada, Safran, the Canada Research Chair program and the National Science & Research Council of Canada (NSERC) for their financial contributions. The support of “Centre de recherche en plasturgie et composites” (CREPEC) and of the “Consortium de recherche et d’innovation en aérospatiale du Québec” (CRIAQ) for the research infrastructure of the Chaire sur les Composites à Haute Performance (CCHP) at École Polytechnique de Montréal are also gratefully acknowledged. Finally, the authors would like to thank Hermann Kreyenschulte for his efficient help in the manufacturing experiments.

4.10 References

1. Ruiz E, Briones LR, Allard É, Trochu F (2008) Flexible Injection: A Novel LCM Technology for Low Cost Manufacturing of High Performance Composites. Part I: Experimental Investigation. Proceedings FPCM9, 34

2. Trochu F, Soukane S, Touraine B (2008) Flexible Injection: A Novel LCM Technology for Low Cost Manufacturing of High Performance Composites. Part II: Numerical Model. Proceedings FPCM9, 35

3. Causse P, Ruiz E, Trochu F (2011) Experimental study of flexible injection to manufacture parts of strong curvature. Polym Compos 32 (6):882-895

4. Hubert P, Poursartip A (1998) A Review of flow and compaction modelling relevant to thermoset matrix laminate processing. J Reinf Plast Compos 17 (4):286-318

5. Boisse P, Hamila N, Vidal-Salle E, Dumont F (2011) Simulation of wrinkling during textile composite reinforcement forming. Influence of tensile, in-plane shear and bending stiffnesses. Compos Sci Technol 71 (5):683-692

6. Wisnom MR, Jones MI, Hill GFJ (2001) Interlaminar tensile strength of carbon fibre-epoxy - Specimen size, layup and manufacturing effects. Adv Compos Lett 10 (4):171-177

7. Potter K (2002) Beyond the pin-jointed net: Maximising the deformability of aligned continuous fibre reinforcements. Compos Part A: Appl Sci Manuf 33 (5):677-686

8. Feih S, Shercliff HR (2005) Quality assessment of curved composite components in peel joint structures. Compos Part A: Appl Sci Manuf 36 (3):397-408

9. Jain LK, Lutton BG, Mai Y-W, Paton R (1997) Stresses and Deformations Induced during Manufacturing. Part II: A Study of the Spring-In Phenomenon. J Compos Mater 31 (7):696-719

10. Hubert P, Poursartip A (2001) Aspects of the Compaction of Composite Angle Laminates: An Experimental Investigation. J Compos Mater 35 (1):2-26

11. Oakeshott JL, Lemoine D (1998) Experimental study of spring forward in cured laminated U-channels made from unidirectionally reinforced carbon fibre-epoxy prepregs. Plast Rubber Compos Process Appl 27 (4):190-199

12. Wiersma HW, Peeters LJB, Akkerman R (1998) Prediction of Springforward in Continuous-Fibre/Polymer L-Shaped Parts. Compos Part A: Appl Sci Manuf 29 (11):1333-1342

13. Li Y, Li M, Gu Y, Zhang Z (2009) Numerical and experimental study on the effect of lay-up type and structural elements on thickness uniformity of L-shaped laminates. Appl Compos Mater 16 (2):101-115

14. Naji MI, Hoa SV (1999) Curing of thick angle-bend thermoset composite part: curing cycle effect on thickness variation and fiber volume fraction. J Reinf Plast Compos 18 (8):702-723

15. Naji MI, Hoa SV (2000) Curing of thick angle-bend thermoset composite part: curing process modification for uniform thickness and uniform fiber volume fraction distribution. J Compos Mater 34 (20):1710-1755

16. Hubert P, Vaziri R, Poursartip A (1999) A two-dimensional flow model for the process simulation of complex shape composite laminates. Int J Numer Methods Eng 44 (1):1-26

17. Li M, Tucker III CL (2002) Modeling and simulation of two-dimensional consolidation for thermoset matrix composites. Compos Part A: Appl Sci Manuf 33 (6):877-892

18. Li Y, Li M, Zhang Z, Gu Y (2009) Numerical analysis of parametric effects on consolidation of angle-bended composite laminates. Polym Compos 30 (10):1510-1516

19. Yang SY, Huang CK, Wu CB (1996) Influence of processing on quality of advanced composite tools. J Adv Mater 27 (3):37-44

20. Fernlund G, Griffith J, Courdji R, Poursartip A (2002) Experimental and numerical study of the effect of caul-sheets on corner thinning of composite laminates. Compos Part A: Appl Sci Manuf 33 (3):411-426

21. Gu Y, Li M, Li Y, Zhang Z (2010) Pressure transfer behaviour of rubber mould and the effects on consolidation of L-shape composite laminates. Polym Polym Compos 18 (3):167-174

22. Brillant M, Hubert P (2010) Out-of-autoclave processing of complex shape laminates. SAMPE 2010 "New Materials and Processes fo a New Economy", electronic proceedings

23. Gao Z-S, Young W-B (2002) Study of the bending induced gap in fiber preforming of woven fiber mats. Polym Compos 23 (2):239-248

24. Dong C (2011) Model development for the formation of resin-rich zones in composites processing. Compos Part A: Appl Sci Manuf 42 (4):419-424

25. Holmberg JA, Berglund LA (1997) Manufacturing and performance of RTM U-beams. Compos Part A: Appl Sci Manuf 28 (6):513-521

26. Arndt RD (1991) Fabric preforming for structural reaction injection molding. Proceedings of the Annual ASM/ESD Advanced Composites Conference, 35-40

27. Gutowski TG, Morigaki T, Cai Z (1987) The Consolidation of Laminate Composites. J Compos Mater 21 (2):172-188

28. Sharma SD, Kar KK, Kumar P, Kar KK (2006) Surface roughness of fiber reinforced plastic laminates fabricated using rubber pressure molding technique. Polym Compos 27 (5):504-512

29. Chen Q, Boisse P, Park CH, Saouab A, Breard J (2011) Intra/inter-ply shear behaviors of continuous fiber reinforced thermoplastic composites in thermoforming processes. Compos Struct 93 (7):1692-1703

30. Vanclooster K, Lomov SV, Verpoest I (2010) Inter-ply and tool-ply friction measurement of woven reinforced thermoplastic composites at forming conditions. Proceedings TEXCOMP 10, 381-388

CHAPITRE 5 ARTICLE 3: SPRING-IN BEHAVIOR OF CURVED COMPOSITES MANUFACTURED BY FLEXIBLE INJECTION

Philippe Causse [1], Edu Ruiz and François Trochu

Department of Mechanical Engineering and Chair on Composites of High Performance, Centre de recherche en plasturgie et composites (CREPEC), École Polytechnique de Montréal, P.O. Box 6079, Station "Centre-Ville", Montreal, Canada, H3C 3A7

[1] *Corresponding author's Email: philippe.causse@polymtl.ca*

5.1 Abstract

This paper investigates the manufacturing distortion of curved composite parts manufactured by a new Liquid Composite Molding (LCM) process called Flexible Injection (FI). This technique uses a deformable tool to speed up the fabrication but may generate manufacturing defects when strongly curved shapes are processed. The goal of the study is to evaluate the impact of such heterogeneities on the dimensional stability of the product. Curved components were first manufactured with varying processing conditions to achieve a wide range of layup quality. The shape stability of the samples was then recorded as a function of temperature to measure the thermoelastic component of distortion and experimental results were compared with predictions made by two modeling techniques. Under certain conditions, manufacturing defects can significantly affect the distortion behavior. This suggests that a robust preforming procedure is of primary importance to produce curved parts by Flexible Injection with a high level of repeatability.

KEYWORDS: A. Polymer-matrix composites (PMCs), B. Defects, B. Residual/internal stress, Flexible Injection (FI)

5.2 Introduction

Fiber reinforced thermoset composites are high performance materials well suited for advanced applications demanding a certain combination of properties such as light weight, high strength and corrosion resistance for example. This advantage comes from the association of two different constituents, each fulfilling a specific function: the reinforcing fibers and the polymer matrix. Processing of these materials inevitably generates residual stresses that can significantly affect the performance of the manufactured part. For thick components, the magnitude of residual stresses can even be sufficient to induce matrix cracking and delamination [1]. In the case of thin-walled structures, this worst case scenario is unlikely, but partial relief of the residual stresses after demolding can cause significant manufacturing distortions potentially resulting in out-of-tolerance product. In particular, curved composites usually experience an increase of their curvature. This phenomenon illustrated in Figure 5-1 for a typical L-bracket is commonly referred to as spring-in. Extensive experimental and theoretical work has been accomplished to understand the underlying physics of spring-in. The three following causes of distortion have been indentified:

- mismatch in the thermal expansion behavior of the fibers and matrix;
- volumetric shrinkage of the resin during polymerization;
- tool/part interaction during processing.

The spring-in angle exhibited by a right-angled thermoset composite is typically comprised between 1º and 2º. Several experimental techniques have been used to measure this deformation. Simple approaches have been devised such as drawing the shape of the part on paper [2], stamping the part on a reference paper [3] or analyzing scanned images [4] and photographs [5, 6]. More complex and expensive techniques also exist using coordinate measuring machines [7-9] or specially designed experimental setups involving laser beams and reflecting mirrors [8, 10]. In certain cases, the geometry of the sample may have an impact on the precision of the measure. For example, Albert and Fernlund [4] showed that the apparent spring-in measured on L-brackets could be greatly affected by small warpage of the flat sections surrounding the curved region. Adequately measuring the overall amount of distortion is critical, but this does not give

information on the relative contribution of each source of deformation. To overcome this limitation, Radford and Rennick [10] proposed an interesting approach to separate the total deformation into a thermoelastic and a non thermoelastic contributions. The procedure consists of recording the shape of the structure versus temperature to isolate reversible effects due to differential thermal expansion. Measuring such thermoelastic spring-in can provide valuable additional data to understand the physical phenomenon and validate the predictions of computer models.

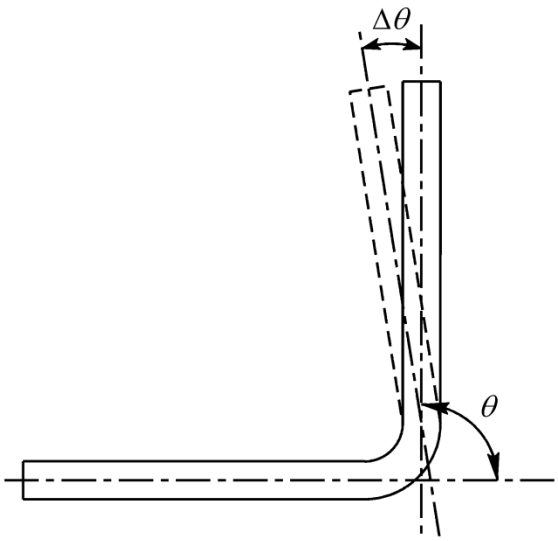

Figure 5-1 : Illustration of the spring-in phenomenon for an L-shaped composite part.

When tight dimensional tolerances are required, anticipating manufacturing distortions is of primary importance to apply corrective strategies such as compensated mold design. First attempts to predict the amount of spring-in were done by deriving simple analytical formulas based on geometrical relations and linear elasticity [11, 12]. This approach remained popular in the scientific literature and was directly used by several authors or slightly modified to introduce temperature dependency in the expression of the thermal expansion [3, 13] or to take into account local heterogeneity in the composite [8]. On the other hand, several investigations have studied the spring-in by the finite element method either with commercial software [2, 6, 9, 14-18] or

purposely written codes [19-22]. At any rate, an efficient predictive method should be able to reproduce the exact contribution of each cause of distortion.

Residual deformations are strongly dependent on the fiber/matrix distribution inside the composite. For example, through-thickness fiber volume fraction gradients can cause warpage in flat sections [23] and thus modify the apparent spring-in of angled shapes manufactured on convex or concave tooling [24]. Morever, curved structures with small radii may exhibit manufacturing defects such a resin accumulations [25-28] or thickness variations [25, 29, 30]. Some studies suggested that resin rich regions [9, 31] or corner thickness gradients [8, 19] could significantly affect the magnitude of distortions. However, Dong [28] recently pointed out that no published work has yet attempted to systematically assess the potential impact of defects on the amount of spring-in.

Flexible Injection is a new Liquid Composite Molding technology currently under development at École Polytechnique de Montréal [32, 33]. This method uses a deformable tool to speed up the filling compared to classical RTM. Like in many composite manufacturing processes, defects may appear when strongly curved parts are processed [34]. The main objective of the study is to quantify the impact of local defects on the residual distortion of L-shaped composites made by Flexible Injection. For that purpose, a series of curved composites was manufactured under varying processing conditions. The thermoelastic behavior of the specimens is then analyzed and the results are compared with the predictions of different modeling techniques. Numerical parametric studies are also presented to widen the scope of the investigation and discuss further the possible impact of manufacturing defects.

5.3 Experimental

5.3.1 Manufacturing of test samples

The curved composite specimen studied in this investigation is the stair-shaped rectangular panel shown in Figure 5-2. This test part consists of three flat sections delimited by two simple curved areas (i.e., 90º corners). The samples were manufactured by implementing the Flexible Injection technology on a specially designed laboratory mold.

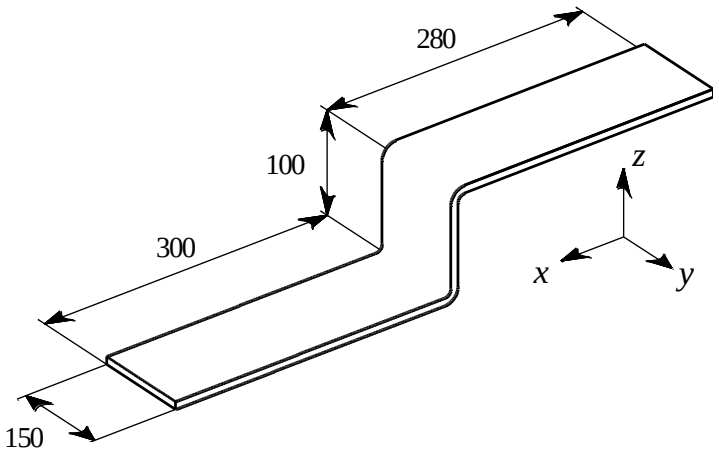

Figure 5-2 : Geometry of the curved composite specimen (dimensions in mm).

Setup and procedure

Figure 5-3 shows a schematic view of the processing tool at the beginning of the manufacturing cycle. The setup consists of two aluminum mold halves separated by a flexible membrane cut out from a planar sheet of VITON (thickness 1/32”, hardness 75A). This device divides the mold chamber into two separate cavities. The bottom cavity is called the injection chamber and contains the fibrous preform. The top cavity is called the compaction chamber and is originally empty before processing. Flexible Injection is an asymmetric process since one side of the part is formed on a rigid metallic mold, while the other is in contact with a flexible elastomeric membrane. Consequently, the two curved regions of the stair-shaped part correspond to different

mold configurations. As indicated in Figure 5-3, the top corner is associated with a convex rigid mold, while the lower one is a concave rigid mold corner.

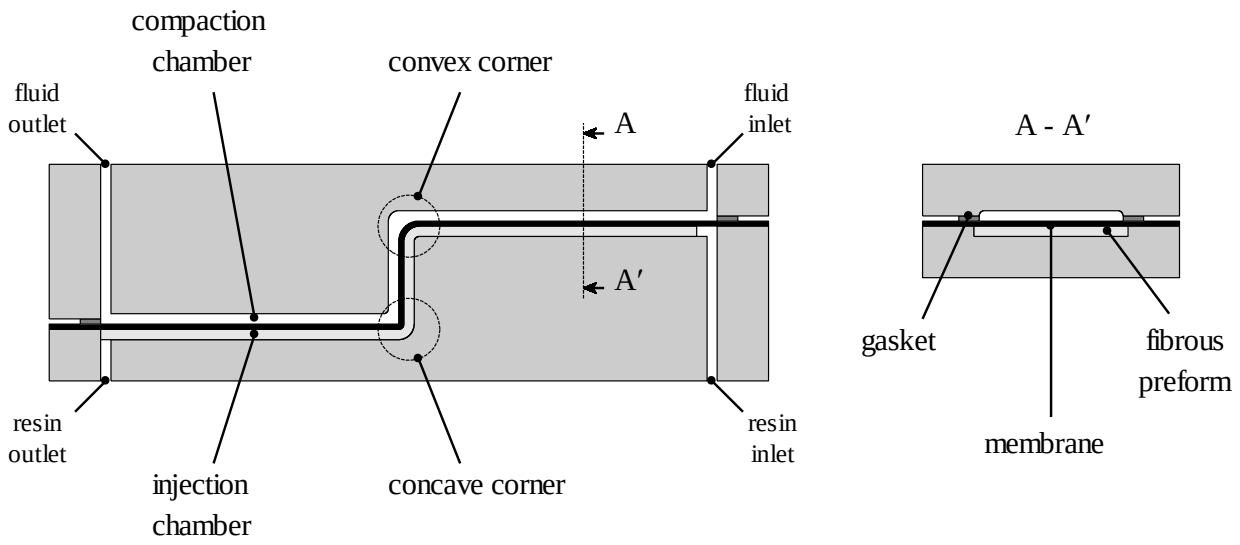

Figure 5-3 : Schematic representation of the manufacturing setup.

This manufacturing setup was used to fabricate the test specimens according to the following procedure:

- Fluid and resin outlets were connected to catchpots and vacuum was drawn in both chambers of the mold.
- A controlled volume of liquid thermoset resin was injected in the injection chamber with a pneumatic gun Semco model 250A.
- After closing of the resin inlet, a compaction fluid (silicone oil Dow Dorning 200 of viscosity 100 cSt at 25ºC) was injected under constant pressure in the compaction chamber.
- Both fluid and resin outlets were closed and the part was cured while maintaining the compaction fluid at constant compaction pressure.
- After polymerization of the resin, the compaction fluid was removed from the cavity, the setup was opened and the final part demolded.

The fabrication of the test parts was conducted at room temperature with a constant injection pressure of the resin of 200 kPa and a constant compaction pressure of 600 kPa.

Materials

Resin was DERAKANE 411-350 from Ashland Inc. The formulation also included a cure initiator (methylethylketone peroxide MEKP 925-H from NOROX at 1.25 phr), a promoter (Cobalt Naphtenate 12% at 0.1 phr) and a gel time retarder (2-4 pentanedione at 0.08 phr). Such a formulation allows room temperature cure with a gel time of two hours. Reinforcement was an E glass quasi-unidirectional fabric Saeruni from SAERTEX. The fabric possesses approximately 92% of the fibers oriented in the 0º direction and 8% in the 90º direction to stabilize the structure and facilitate handling. These 90º bundles can be seen in Figure 5-4b. Before processing, the fibers were preformed by using a small amount of the vinyl ester resin as thermosetting binder and compacting the stacking between two rigid plates reproducing the desired stair shape. Details of the preforming procedure described in [34] can be found in Appendix A.

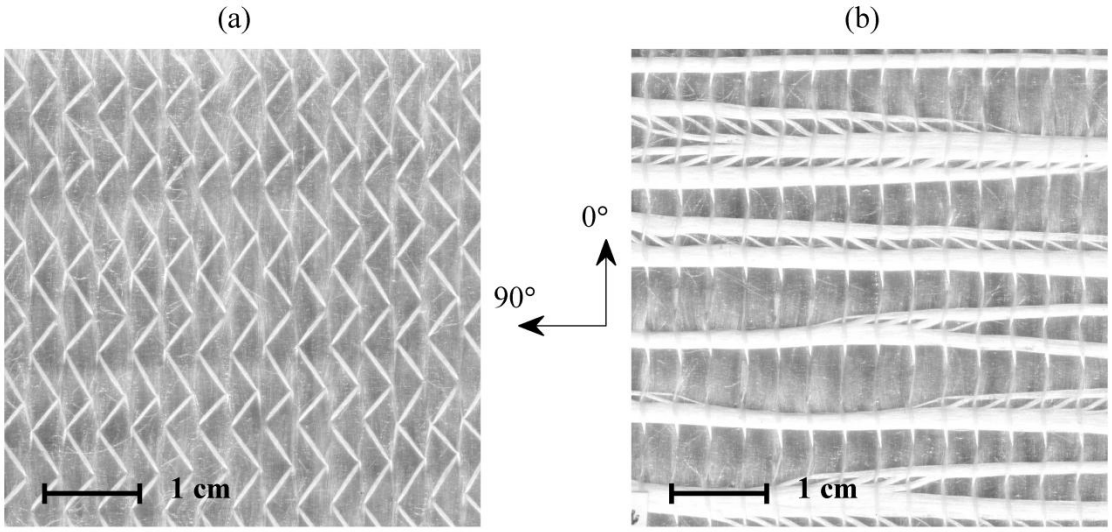

Figure 5-4 : Architecture of the glass fabric Saeruni: (a) top view; (b) bottom view.

Manufacturing experiments

The manufacturing experiments comprised the preparation of 4 large fibrous preforms labeled A to D. These samples had a width of 650 mm and consisted of five plies of fabric oriented at 0º (i.e., the 0º direction indicated in Figure 5-4 is aligned with the *x* axis of Figure 5-2). The preforms were prepared with different prefoming mold geometry and preforming pressure in order to modify the placement of the fibers in the curved regions. The influence of the preforming conditions on the quality of the final part was investigated in [35] and is not the topic of the present study. Each large preform was subsequently cut into smaller samples to manufacture three parts labeled a,b and c with the fiber volume fractions V_{fa} = 53%, V_{fb} = 60% and V_{fc} = 64%. These fiber contents were achieved by carefully controlling the amount of resin injected during fabrication.

5.3.2 Analysis of the fabricated parts

After demolding, the central section of the test part was cut into three smaller Z-shaped samples as illustrated in Figure 5-5a. The cut out surfaces were polished with waterproof aluminum oxide sandpaper and images of these cross-sections were obtained with a scanner CanoScan 5600F to assess the corner layup quality (see Figure 5-5b). A second type of image was used to study the distortion behavior of the part. Firstly, the samples were post-cured free standing as recommended by the manufacturer (i.e., 2 hours at 120ºC). Black dots were then glued along the cross-sections to serve as markers for image analysis. A typical cross-sectional image with 15 markers is shown in Figure 5-5c.

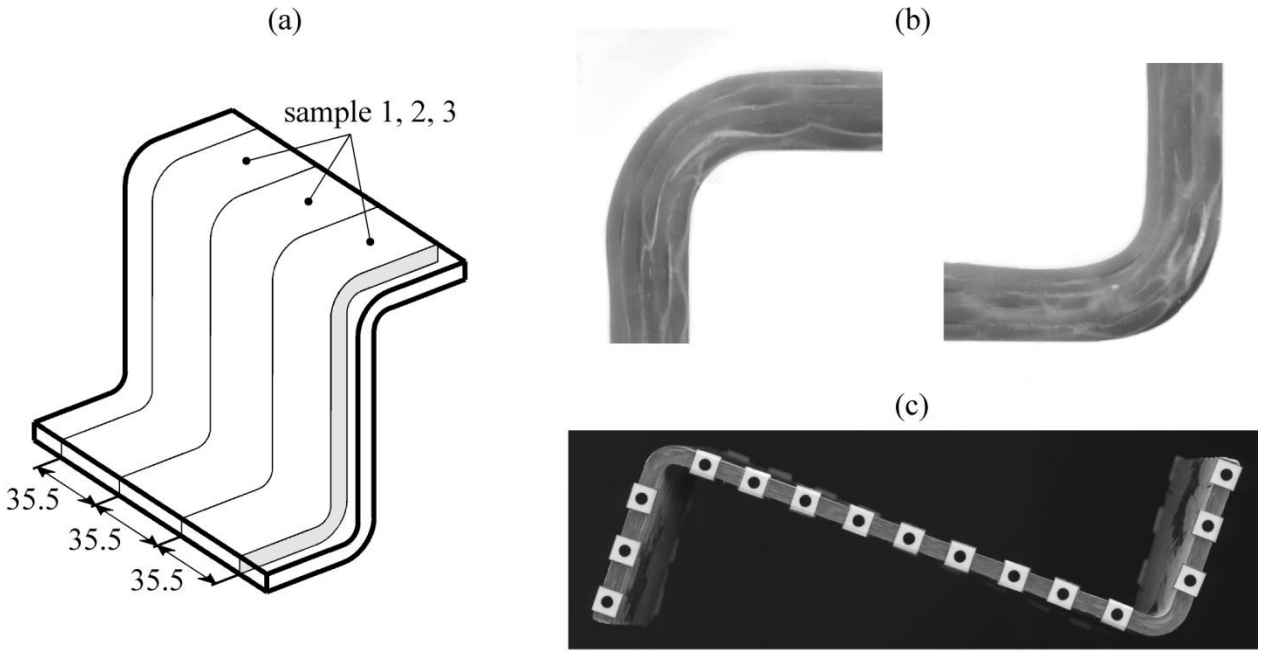

Figure 5-5 : Analysis of the part: (a) cutting pattern; (b) typical corner images for layup characterization; (c) cross-section with markers for distortion analysis.

Characterization of corner layup quality

Two types of manufacturing defects can be observed in the corners of the parts: thickness gradients and resin rich zones that can be located on the inner side or on the outer side of the curvature. Such defects were experimentally quantified by fitting a parametric description of the L structure on the cross-sectional images of the corners. The proposed ideal geometry shown in Figure 5-6a is described by five parameters: the flat arm thickness h and 4 radii denoted r_{in}, $r_{f,in}$, r_{out} and $r_{f,out}$. The corresponding thickness of the composite region in the center of the corner is demoted h_c. This approach allows reproducing the main manufacturing defects observed on the real parts. An inner (respectively outer) resin rich zone is represented when $r_{f,in} \neq r_{in}$ (respectively $r_{f,out} \neq r_{out}$). A corner thickness gradient in the curved composite region is obtained when $r_{f,out} \neq r_{f,in} + h$. An example of part with defect is given in Figure 5-6b, in which an inner resin rich zone is observed in the corner. The geometric parameters defining the corner layup of manufactured parts are summarized in Table 5.1. Note the large variety of manufacturing defects observed in the test specimens.

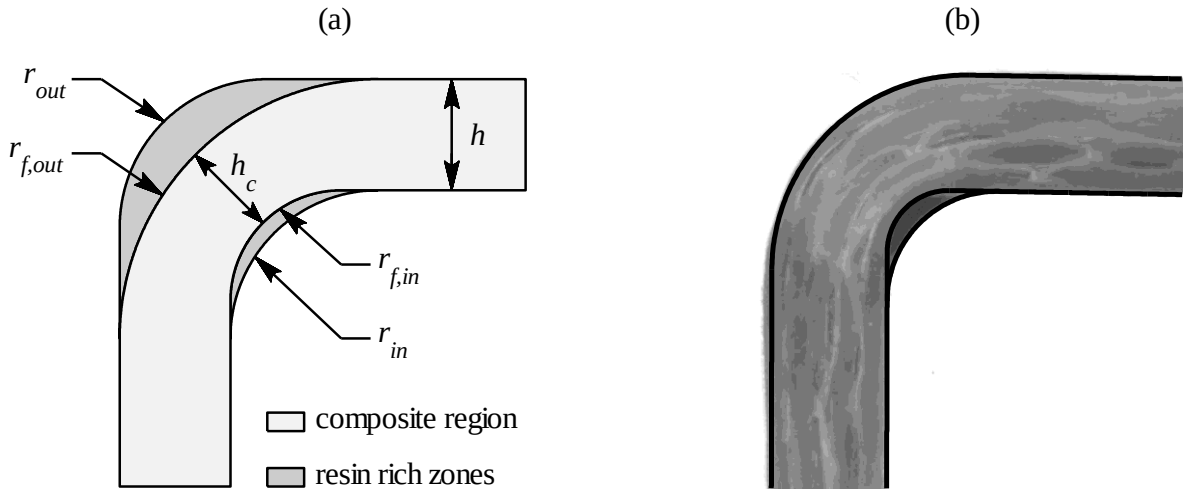

Figure 5-6 : Parametric representation of manufacturing induced defects: (a) ideal geometry; (b) example of real part with inner resin accumulation.

Table 5.1 : Geometric parameters describing the corner quality of the test specimens (dimensions in mm)

Part	h	Convex corner				Concave corner			
		r_{in}	$r_{f,in}$	r_{out}	$r_{f,out}$	r_{in}	$r_{f,in}$	r_{out}	$r_{f,out}$
Aa	3.52	3	3	7.69	7.69	4.58	4.58	5	9.06
Ab	3.12	3	3	6.46	6.46	5.67	5.67	5	8.86
Ac	2.9	3	3	6.14	6.14	6.89	6.89	5	9.26
Ba	3.52	3	3	7.05	7.05	3.63	2.36	5	6.58
Bb	3.12	3	3	5.88	5.88	3.13	3.13	5	5.92
Bc	2.9	3	3	5.12	5.12	4.38	4.38	5	6.12
Ca	3.52	3	3	6.30	6.30	3.69	3.69	5	6.82
Cb	3.12	3	3	4.97	4.97	4.39	4.39	5	6.54
Cc	2.9	3	3	4.79	4.79	5.60	5.60	5	7.04
Da	3.52	3	2.49	6.40	6.40	2.93	1.35	5	5
Db	3.12	3	2.38	5.32	5.32	2.48	2.48	5	5
Dc	2.9	3	2.27	5.30	5.30	3.69	3.69	5	5

Measurement of the thermoelastic spring-in

The thermoelastic spring-in was measured by recording the change in shape of the parts during a simple cool down experiment. The procedure consisted of heating the sample at 90ºC for 1 hour. The specimen was then quickly removed from the oven and placed on the scanner. Cross-sectional images (Figure 5-5c) were subsequently recorded for 50 minutes. This measurement time was largely sufficient to cool down the part to room temperature (22ºC). The first scanned image was taken less than 10 seconds after removal from the oven and was assumed to represent the sample in its initial state (i.e., uniform temperature T = 90ºC). At the beginning of the experiment, an image was recorded every 12 s. The elapsed time between 2 scans was then progressively increased to reach 70 s at the end of the test. Overall, one measurement corresponds to a series of 57 images that were automatically treated with an image analysis code developed with MATLAB. This program uses luminosity contrasts to detect the boundaries of each black marker and interpolate the position of its center.

A total of 4 markers surrounding the curved area (2 on each flat arm) were used to measure the evolution of the composite angle during cool down. As shown in Figure 5-7, the procedure consisted of recording the angle θ_m defined by two straight lines passing through the markers centers. This method can detect very small changes in angle but may be affected by warpage of the flat sections. Such measurement artifact is schematically illustrated in Figure 5-7. If the flat arms of the L shape bend inwards with a uniform curvature κ, then the measured angle θ_m depends on the relative position of the markers and is related to the real central angle θ of the corner through the equation:

$$\theta_m = \frac{\kappa L}{2} + \theta \tag{5.1}$$

where L is the total flat arm length defined by the set of 4 markers considered:

$$L = l_1 + l_2 + l_3 + l_4 \tag{5.2}$$

Note that a minus sign would be introduced in equation (5.1) if the curvature of the flat sections was oriented in the opposite direction (i.e., flat arms bending outwards of the L shape).

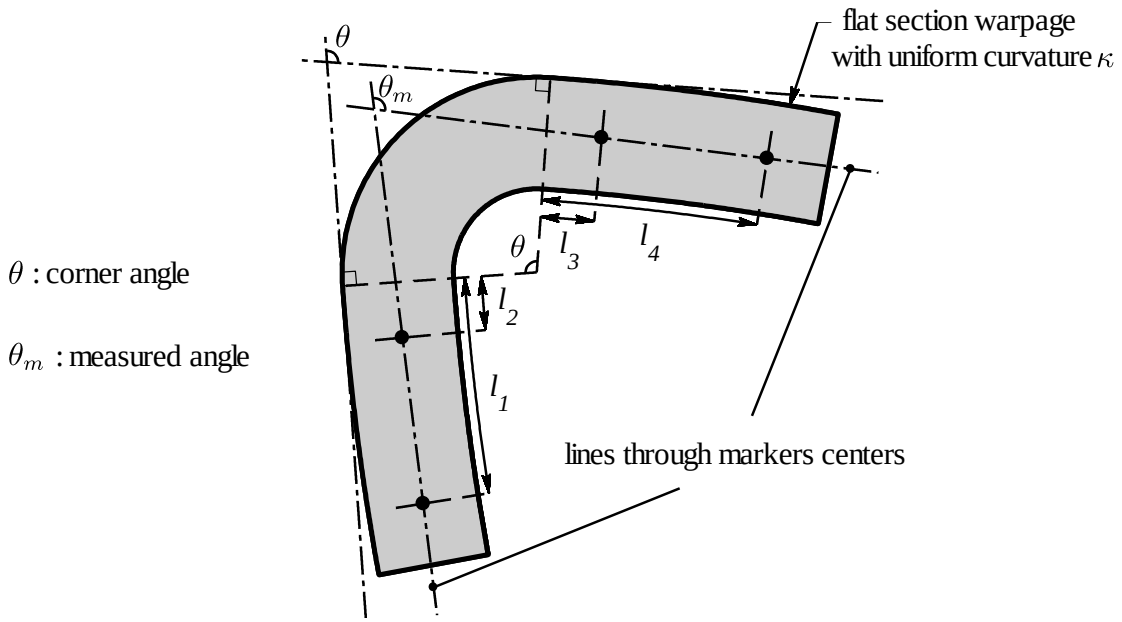

Figure 5-7 : Influence of flat section warpage on the measured central angle.

Figure 5-8 shows the typical changes in angle $\Delta\theta_m$ of the convex corner measured during the cool down procedure. These results were recorded during the same experiment with different sets of 4 markers for varying total flat arm length. This parameter has a clear impact on the result since the measured values increase with *L*. An opposite behavior was observed in the concave corner of the component. This shows that a convex up curvature develops from the mold side to the membrane side during cool down of the part. Such arm bowing effect can be caused by a small asymmetry of the stacking sequence or by through-thickness fiber volume gradients. Although the origin of this warpage was not studied here, its effects were corrected to extract the real spring-in angle of the curved structure. Raw results were first interpolated with the following expression (solid lines in Figure 5-8):

$$\theta_m = \theta_0 + \Delta\theta_{total}\left(1 - e^{\frac{-t}{\tau}}\right) \tag{5.3}$$

where θ_0, $\Delta\theta_{total}$ and τ are fitting parameters.

Overall changes in angle $\Delta\theta_{total}$ obtained for the cool down experiment shown in Figure 5-8 are reported in Figure 5-9. As can be seen, the results are in agreement with the linear relationship

proposed by equation (5.1). The corrected value of the change in angle was finally determined by extrapolating the data at $L = 0$ (see Figure 5-9).

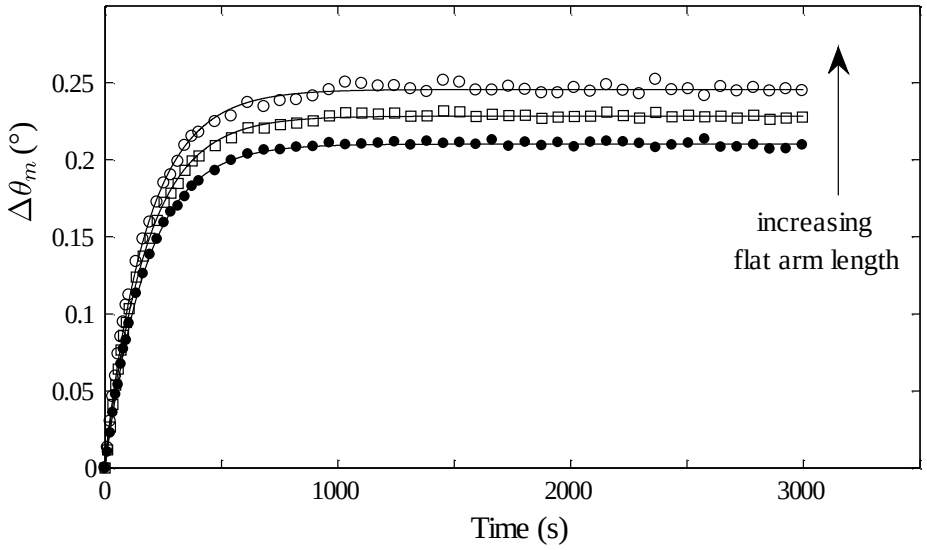

Figure 5-8 : Influence of total flat section length on the measured distortion during cool down of the part (results recorded during the same experiment, symbols represent different sets of 4 markers used for image analysis).

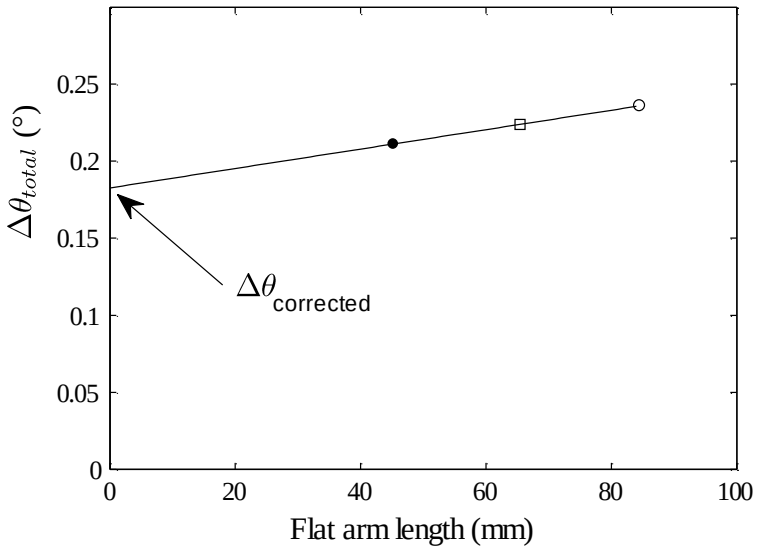

Figure 5-9 : Correction of the arm bowing effect: extrapolation of the real spring-in angle (results corresponding to the experiment presented in Figure 5-8).

5.4 Prediction of the thermoelastic spring-in

This section presents two different techniques to predict the amount of thermoelastic spring-in experienced by an L-shaped composite. Though different in nature, the two approaches share the same basic simplifying assumption: the stabilizing bundles (see Figure 5-4b) are neglected and the fabric is considered to be perfectly unidirectional with all fibers oriented in the 0º direction. Furthermore, given the range of temperature used in the thermoelastic characterization (22-90ºC) and the glass transition temperature of the post-cured resin (120ºC), the properties of the resin are considered constant (i.e., independent of temperature).

5.4.1 Analytical approach

Following the approach proposed by Nelson and Cairns [11] and Radford and Diefendorf [12], the thermoelastic spring-in S_{th} of a curved composite of central angle θ can be estimated by the closed form solution:

$$S_{th} = \frac{\Delta\theta}{\theta} \times \frac{1}{\Delta T} = \frac{\left(\alpha_i - \alpha_t\right)}{1 + \alpha_t \Delta T} \tag{5.4}$$

which can be linearized into:

$$S_{th} = \frac{\Delta\theta}{\theta} \times \frac{1}{\Delta T} = \alpha_i - \alpha_t \tag{5.5}$$

where ΔT is the change in temperature, α_i the in-plane coefficient of thermal expansion (CTE) and α_t the through-thickness CTE.

Under the assumption of unidirectionality discussed above, α_i and α_t correspond respectively to the longitudinal CTE α_L and transverse CTE α_T, which can be estimated by the following expressions proposed by Schapery [36]:

$$\alpha_L = \frac{E_f \alpha_f V_f + E_m \alpha_m \left(1 - V_f\right)}{E_f V_f + E_m \left(1 - V_f\right)} \tag{5.6}$$

$$\alpha_T = \left(1 + \nu_m\right)\alpha_m \left(1 - V_f\right) + \left(1 + \nu_f\right)\alpha_f V_f - \alpha_L \nu_{LT} \tag{5.7}$$

with

$$\nu_{LT} = V_f \nu_f + (1 - V_f)\nu_m \tag{5.8}$$

where V_f is the fiber volume fraction, E, α and v are Young's modulus, CTE and Poisson's ratio of the constituents (f stands here for the fibers and m for the matrix).

An analytical expression of the thermoelastic spring-in is finally obtained by substituting equations (5.6) to (5.8) in (5.5). Such prediction only depends on the fiber volume fraction and the properties of the constituents. The materials properties used as input in the model are summarized in Table 5.2. These data come from the supplier except for Poisson's ratio and the CTE of the matrix, which were not given in the material data sheet. Poisson's ratio v_r was taken from Ziehl [37] and the CTE α_r was estimated experimentally by measuring the change in diameter of cylindrical samples of pure resin for temperature varying from 22ºC to 90ºC.

Table 5.2 : Material properties of Derakane 411-350 and Saeruni glass fabric

	Resin	Fibers
Young's Modulus (GPa)	3.2	73
Poisson's ratio	0.35	0.18
CTE (10^{-6}/ºC)	67	5

5.4.2 Numerical modeling

The analytical method presented above assumes a perfect layup quality and constant properties throughout the composite. In order to take into account observed manufacturing defects in the spring-in analysis, a 2D plane strain finite element model of an L-shaped composite was developed with ANSYS. The geometry of the model is based on the five parameters introduced in Figure 5-6. A typical finite element mesh in the most general case with two resin rich zones and a corner thickness variation in the composite region is shown in Figure 5-10. Zones of pure

resin are considered as an isotropic linear elastic material while the composite region is modeled as a transversely isotropic material. In the latter case, the fiber volume fraction is first calculated for each element according to its relative position in the structure. Coefficients of thermal expansion and Poisson's ratio are then computed by equations (5.6) to (5.8).

The other elastic properties are approximated with the Halpin-Tsai equations [38]. A simple law of mixture is thus used to estimate the longitudinal modulus E_L:

$$E_L = V_f E_f + (1 - V_f) E_m \tag{5.9}$$

The shear modulus G_{LT} is calculated by the following expression:

$$G_{LT} = G_m \frac{1 + \xi_{G_{LT}} \eta_{G_{LT}} V_f}{1 - \eta_{G_{LT}} V_f} \tag{5.10}$$

where the parameter $\xi_{G_{LT}}$ follows the empirical relation proposed by Hewitt and de Malherbe [39]:

$$\xi_{G_{LT}} = 1 + 40 V_f^{10} \tag{5.11}$$

and:

$$\eta_{G_{LT}} = \frac{G_f - G_m}{G_f + \xi_{G_{LT}} G_m} \tag{5.12}$$

The shear moduli of the fibers and of the matrix are calculated from the data of Table 5.2 by the classical conversion formulas of isotropic elasticity.

Similarly, the transverse modulus E_T is deduced from:

$$E_T = E_m \frac{1 + \xi_{E_T} \eta_{E_T} V_f}{1 - \eta_{E_T} V_f} \tag{5.13}$$

with

$$\xi_{E_T} = 2 + 40.V_f^{10} \tag{5.14}$$

$$\eta_{E_T} = \frac{E_f - E_m}{E_f + \xi_{E_T} E_m} \tag{5.15}$$

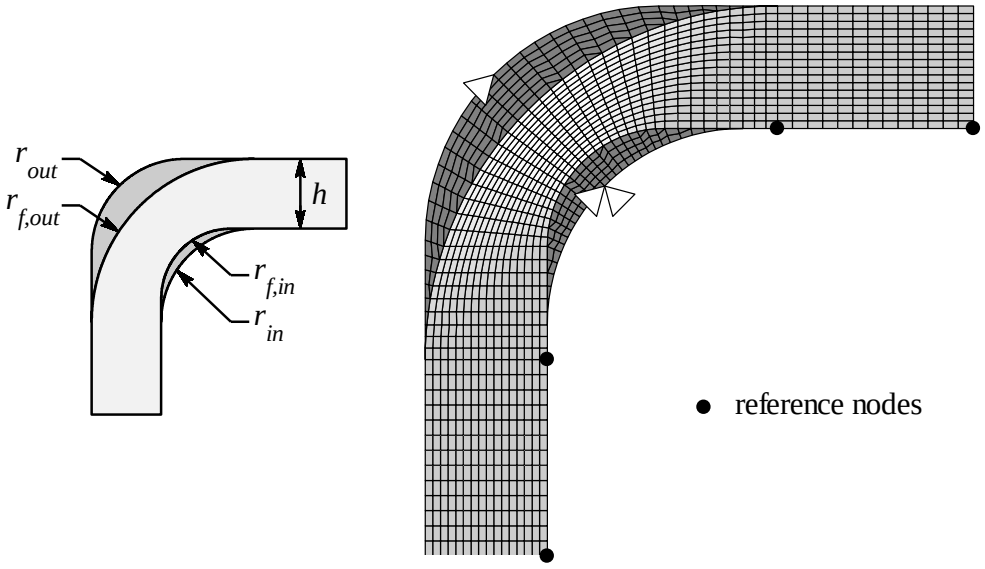

Figure 5-10 : Finite element model including manufacturing defects (lighter colors indicate higher fiber volume contents).

Boundary conditions are applied on the axis of symmetry of the model. As indicated in Figure 5-10, a zero-displacement condition is imposed on the central inner node while the central outer node is limited to through-thickness displacements only. Finally, a uniform temperature change corresponding to the experimental conditions ΔT = -68ºC is applied to the model and the thermoelastic spring-in is deduced from the resulting displacements of 4 reference nodes located in the flat regions of the L shape.

5.5 Results and discussion

This section discusses the impact of the manufacturing quality on the distortion behavior of the curved structure. Experimental values of the thermoelastic spring-in are first compared with the

predictions of the models for parts possessing corner thickness variations and resin rich zones. Numerical simulations are also used to evaluate the influence of the composite stiffness and discuss the possible consequences on the overall amount of manufacturing distortion.

5.5.1 Influence of thickness gradients on the thermoelastic spring-in

The following section analyses the case with corner thickness gradients (i.e., $r_{f,out} \neq r_{f,in} + h$), but without resin rich zone (i.e., $r_{in} = r_{f,in}$ and $r_{out} = r_{f,out}$). Such situation is observed experimentally in the convex corner of parts A_i, B_i and C_i (see Table 4.1). To quantify the magnitude of the manufacturing defect, the thickness ratio r_t is introduced:

$$r_t = \frac{h_c}{h} \tag{5.16}$$

which compares the thickness in the center of the corner h_c with the flat arm thickness h. With the parametric representation of the curved shape, the thickness ratio can then be calculated by the following equation:

$$r_t = \frac{\left(r_{f,out} - r_{f,in}\right)\left(1-\sqrt{2}\right)}{h} + \sqrt{2} \tag{5.17}$$

Figure 5-11 plots the thermoelastic spring-in as a function of the thickness ratio for the three fiber volume fractions considered. Firstly, it can be noted that a rather important variability exists in the experimental results. This can be attributed to the measurement method employed, but may also likely be caused by the intrinsic variability of the fibrous reinforcement. Indeed, the position of the stabilizing bundles is not perfectly homogeneous (see Figure 5-4b). This feature can change the amount of fibers oriented at 90º in the corner of the component and hence have an impact on the local coefficients of thermal expansion.

Despite the observed scattering, a clear trend appears in the results with the absolute amount of thermoelastic distortion increasing with the thickness ratio. This observation is not surprising since an increase in thickness ratio results in a lower fiber volume fraction in the corner of the

composite, and consequently in a larger difference between the longitudinal and transverse CTEs. Obviously, the analytical modeling approach is unable to capture such phenomenon since the predicted distortion only depends on the targeted fiber volume fraction. A better representation is obtained in the numerical simulations although the predicted distortion is more important that the measured value for all the cases studied. This difference may be caused by an initial error in the input data or can also be explained by the assumption of a perfectly unidirectional laminate. A more realistic model of the reinforcement structure would be required in future investigation.

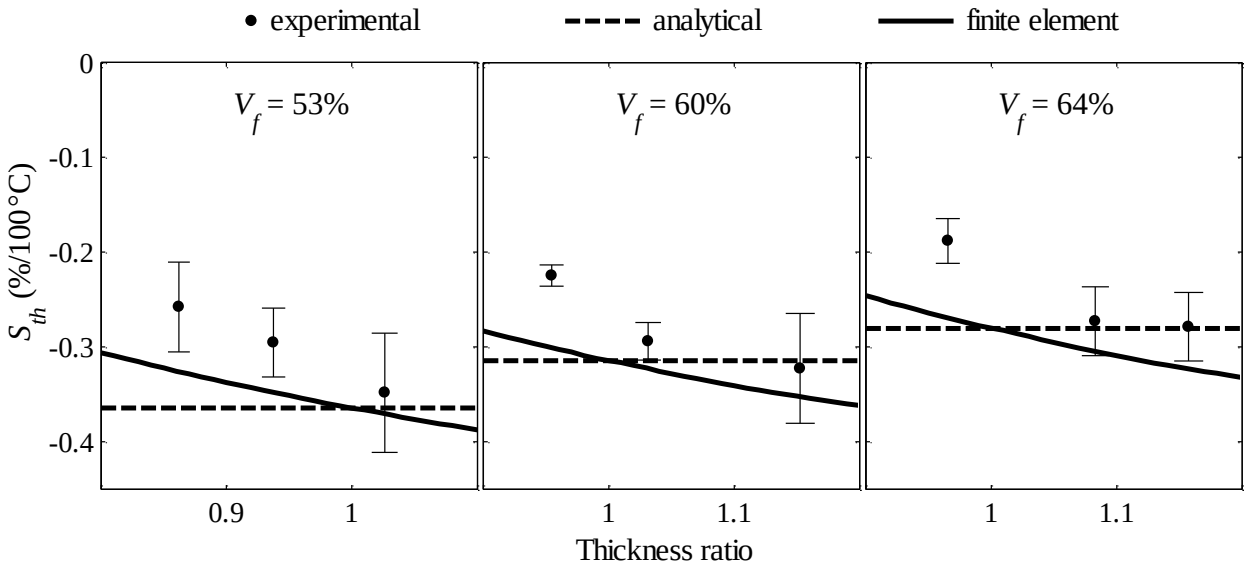

Figure 5-11 : Effect of corner thickness gradients on the thermoelastic spring-in.

5.5.2 Influence of resin rich zones on the thermoelastic spring-in

Regions of pure resin possess a much larger coefficient of thermal expansion than the rest of the composite. When the temperature changes, this type of manufacturing defect influences the deformation of the structure by creating zones of stress concentration. This effect is illustrated in Figure 5-12, which compares the longitudinal stress distribution inside the curved structure for different corner layup quality during a uniform cool down. The three cases presented possess the same composite region with h = 3.12 mm, $r_{f,in}$ = 3 mm and $r_{f,out} = r_{f,in} + h$, which corresponds to a uniform fiber volume fraction of 60%. The size of the inner resin rich area considered is

characterized by a radius difference $\Delta r = r_{in} - r_{f,in} = 1$ mm. Similarly, the outer resin rich zone studied corresponds to $\Delta r = r_{f,out} - r_{out} = 1$ mm. As seen in the contour plot, these manufacturing defects locally introduce compressive stresses in the composite region and thus modify the thermoelastic response of the structure. An inner resin rich zone tends to increase the thermoelastic spring-in while an outer accumulation lowers the amount of distortion.

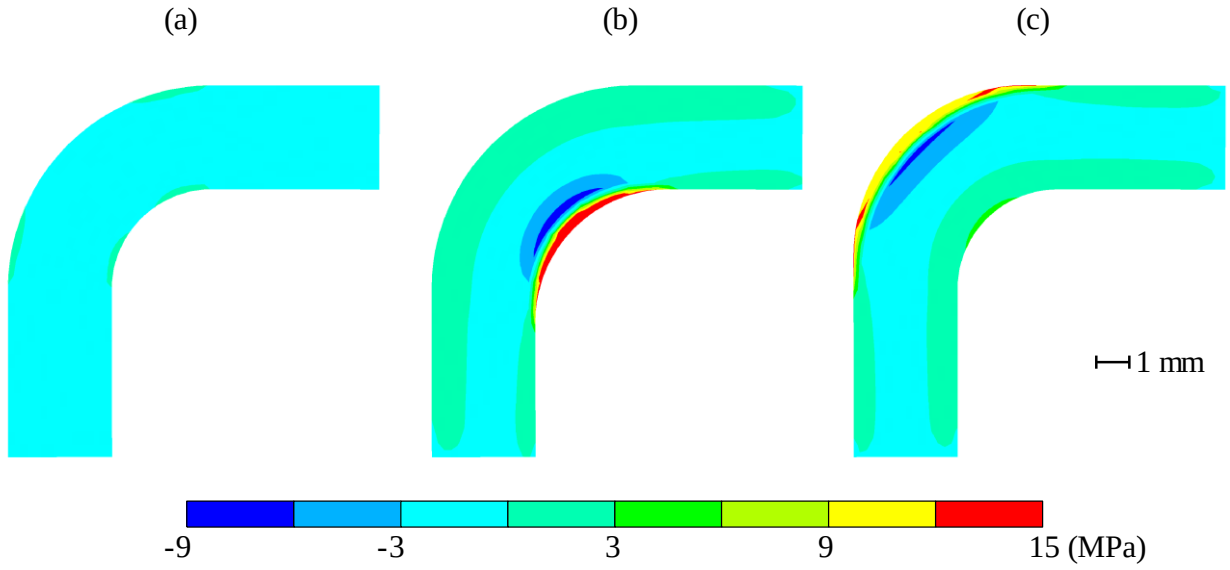

Figure 5-12 : Predicted longitudinal stress distribution during uniform cool down ($\Delta T = -68^{o}C$) for different corner qualities: (a) perfect lay-up; (b) inner resin rich zone; (c) outer resin rich zone.

Figure 5-13 presents experimental values of the thermoelastic spring-in for parts with significant resin rich areas. Cases with an inner accumulation correspond to the convex corners of parts Di and samples with an outer resin rich zone come from the concave corners of parts Ai (see Table 5.1). The results obtained strongly support the numerical investigation discussed above. For all the fiber volume fractions considered, the thermoelastic spring-in is indeed between 2 and 3 times larger for the inner resin rich zone. This observation cannot be reproduced by the analytical model, while finite element simulations performed with the real layup quality give a fairly good prediction of the measured distortion. It appears that a small manufacturing defect located in the

corner of the specimen can have an important impact on the shape stability of the entire structure. However, note that the analyses presented here are purely elastic even though thermosetting resins are known to exhibit a viscoelastic behavior. With the stress distribution presented in Figure 5-12, zones of pure resin experience an important tensile stress that may relax over time. Consequently, curved composites with resin rich zones may have a complex time dependent distortion behavior. Such phenomenon remains however out of the scope of the current investigation.

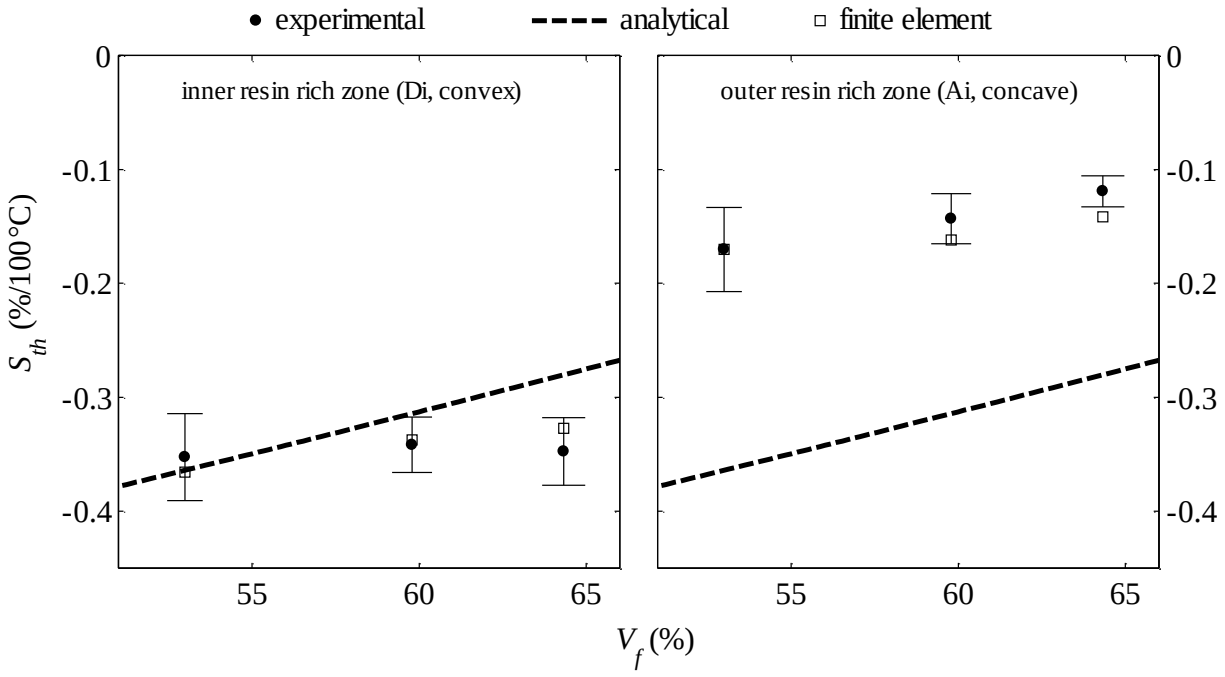

Figure 5-13 : Impact of resin rich zones on the thermoelastic spring-in.

5.5.3 Influence of composite thickness

The cavity of the mold was designed to produce parts made of 5 plies of the selected fabric. This technical constraint inevitably limits the scope of the experimental study. However, numerical modeling can bring here a useful contribution by allowing to investigate situations that are not directly accessible experimentally. For example, parametric studies can be conducted by varying the number of fabric plies to evaluate the influence of the stiffness of the composite specimen on

the distortion behavior. Figure 5-14 shows the predicted thermoelastic spring-in of a curved part with corner thickness gradient. No noticeable difference is observed for the different numbers of plies investigated. This suggests than the thickness ratio r_t is good indicator of the impact of layup quality on distortion when no resin rich zone is present on the structure.

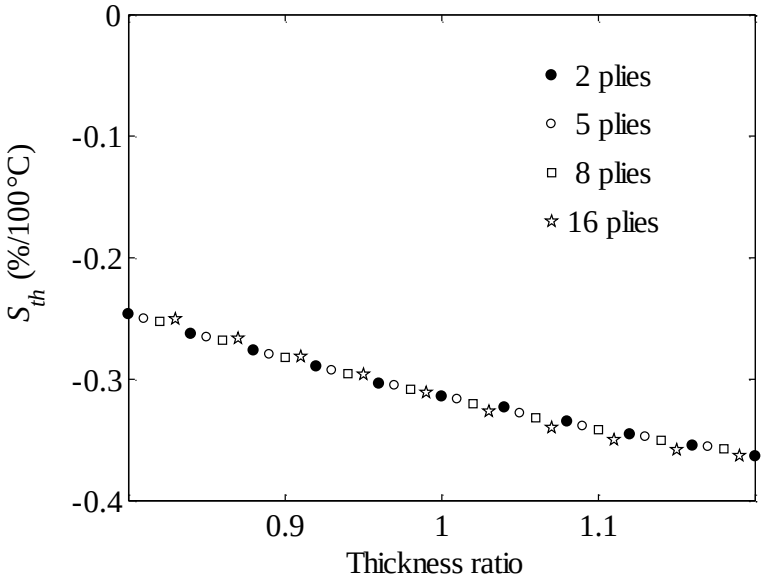

Figure 5-14 : Thermoelastic spring-in predicted by finite element simulations for different numbers of plies.

As previously discussed, resin rich zones generate stress concentration in the composite when the temperature changes. The subsequent impact on the shape of the part consequently depends on the stiffness of the specimen. This effect is shown in Figure 5-15, which summarizes the results of parametric studies for different numbers of fabric plies. This analysis was carried out for an internal radius $r_{f,in}$ = 3 mm and a constant fiber volume fraction in the composite (i.e, $r_{f,out} = r_{f,in} + h$). The size of the different resin rich zones was quantified by the difference in radius Δr already introduced in the previous section. As expected, the distortion does not depend on the number of plies when the layup of the composite is perfect. It can also be verified that the predicted spring-in in such case corresponds to the analytical solution (though the latter is not plotted in the figure). When the composite is made of 2 fabric plies, the structure is thin and rather flexible. In that case, resin rich zones have a large influence on the thermoelastic distortion. For example, the

predicted spring-in is almost zero for a fiber volume of 66% and an outer resin rich zone with $\Delta r = r_{f,out} - r_{out} = 2$ mm. When the number of plies increases, the structure becomes more rigid and is hence less affected by defects. For a composite made of 8 plies, resin rich zones with a radius difference of 2 mm have almost no impact on the shape stability.

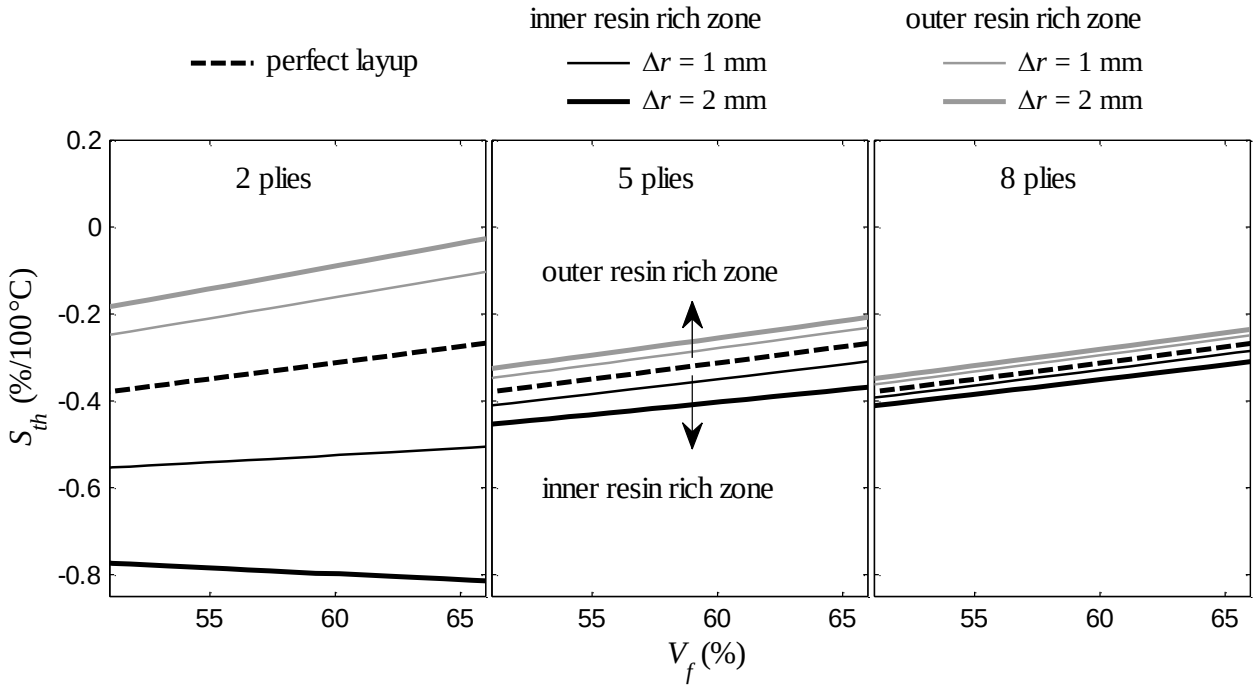

Figure 5-15 : Influence resin rich zones on the predicted thermoelastic spring-in for different numbers of plies.

Figure 5-16 shows examples of predicted longitudinal stress in the corner for an inner resin accumulation ($\Delta r = 2$ mm, $V_f = 60\%$). For a 2-ply composite, the manufacturing defect generates a through-thickness gradient and the outer plies of the curved region experience important tensile stress. When 8 fabric plies are used, the stress in the composite region is barely affected by the presence of the resin rich zone. However, this does not mean that the defect is harmless for the structure. The resin pocket is still submitted to important tensile stress and may constitute a crack initiation site that can threaten the overall mechanical performance of the specimen.

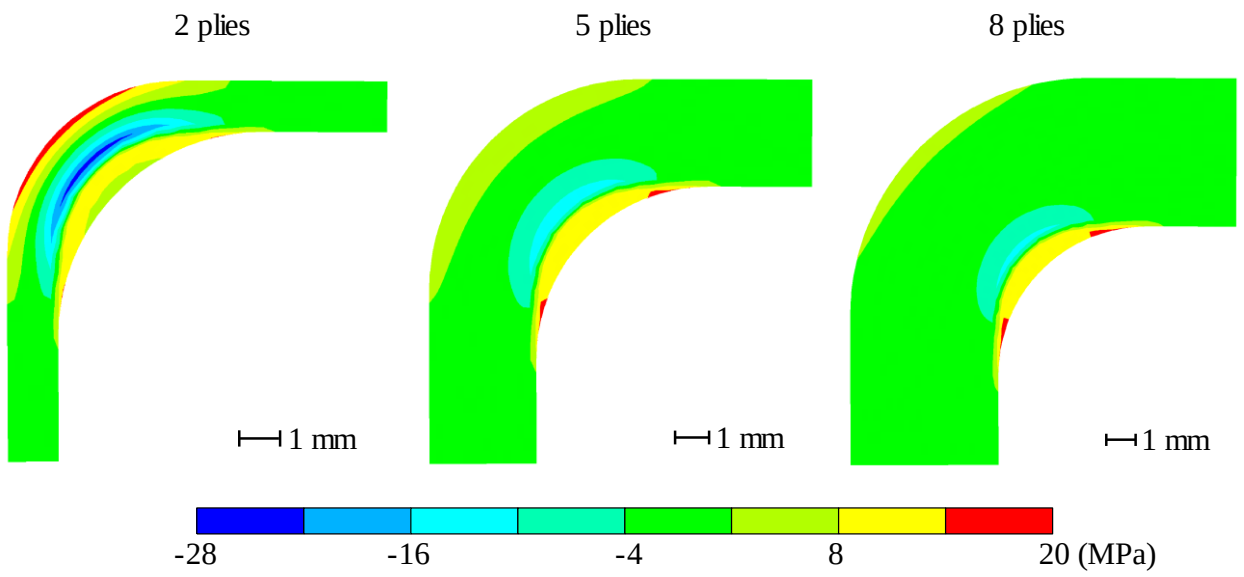

Figure 5-16 : Impact of the number of plies on the predicted longitudinal stress distribution during uniform cool down (ΔT = -68ºC) for an inner resin rich area $\Delta r = r_{in} - r_{f,in}$ = 2 mm.

5.5.4 Impact on the overall amount of distortion

The composite components studied in this work are relatively thin (around 3 mm) and were processed with a massive aluminum setup that constitutes an important heat sink to evacuate the energy generated by the exothermic reaction. The maximum temperature reached during processing is then assumed to be only slightly above room temperature. This assumption has two implications on the overall amount of residual deformation experienced after demolding. Firstly, the thermoelastic distortion due to CTE mismatch should be very low since there is almost no cool down of the part before demolding. Moreover, the commonly accepted tool/part interaction mechanism in autoclave processing appears to be negligible since there is no significant thermal expansion of the tooling during processing. Hence, as a fist approximation, chemical shrinkage of the resin can be considered as the only source of manufacturing distortion.

In an attempt to characterize the overall deformation of the fabricated parts, cross-sectional images of the samples (Figure 5-5b) were analyzed with an in-house MATLAB code. This

program detects the edges of the part located on the mold side and subsequently calculates the angles of the structure. Results are reported in Figure 5-17 for the series of parts Ai and Di, which possess resin rich zones (concave corner for Ai and convex corner for Di). It is reminded that the thermoelastic spring-in of these samples was shown to be drastically affected by the layup quality (see Figure 5-13). A very different behavior is observed in the overall amount of distortion since no significant effect of the resin rich zones is observed. This observation is somewhat unexpected because thermal expansion and cure shrinkage are distortion sources that act through the same deformation mechanisms. Both phenomena indeed constitute a differential volume change between the fibers and the matrix. This is why some authors introduced an effective coefficient of thermal expansion [2, 6] to treat the two contributions simultaneously. This analogy does not seem possible in the cases presented in Figure 5-13 and Figure 5-17.

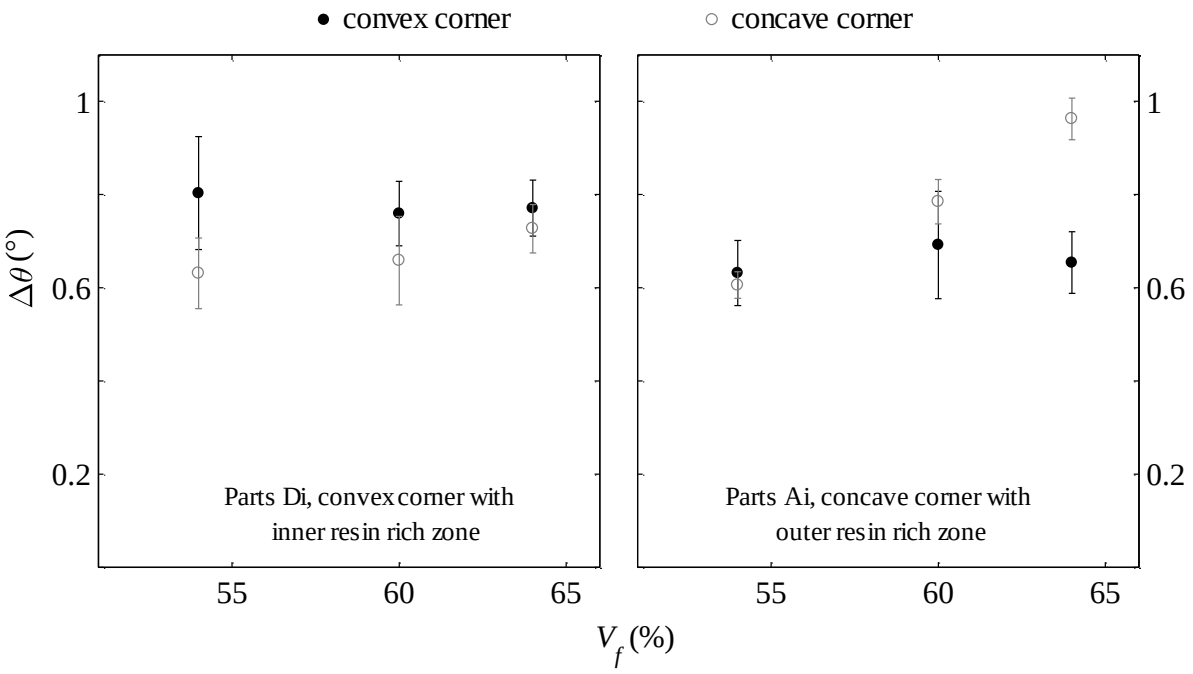

Figure 5-17 : Demolded distortion of parts possessing a resin rich zone.

Two reasons can be proposed to explain the low impact of resin rich zones on the distortion induced by cure shrinkage. As already mentioned, relaxation phenomena may induce a stress decay and a progressive deformation in time. Moreover, since most of the shrinkage occurs when the matrix is in the rubbery state, the resin rich zones may be too flexible to generate significant

stress concentration in the composite. This second hypothesis is supported by Figure 5-18, which shows the thermoelastic spring-in predicted for different layup qualities and a resin modulus ranging from 1 MPa to 3.2 GPa. With a matrix modulus below 100 MPa, the layup quality has virtually no impact on the thermoleastic spring-in. This suggests that resin rich zones can only affect the distortion when the resin is in the glassy state and could explain the lack of experimental trend observed in Figure 5-17. However, note that this analysis does not intent to estimate precisely the cure induced distortion. It is indeed well acknowledged that residual stress development when the resin is in the rubbery state is a complex process involving gradual evolution of the mechanical and physical properties and relaxation [40, 41]. Further investigation is then required to validate the proposed interpretation. For that purpose, future work should focus on high temperature manufacturing with different resin/fibers systems. This would allow studying parts with different relative contributions to the overall distortion. Moreover, modeling the viscoelastic properties as a function of glass transition temperature will be required for precise thermoelastic analysis and further processing optimization [42]. Such an investigation could also benefit from more precise measurement techniques to eventually lower the experimental variability.

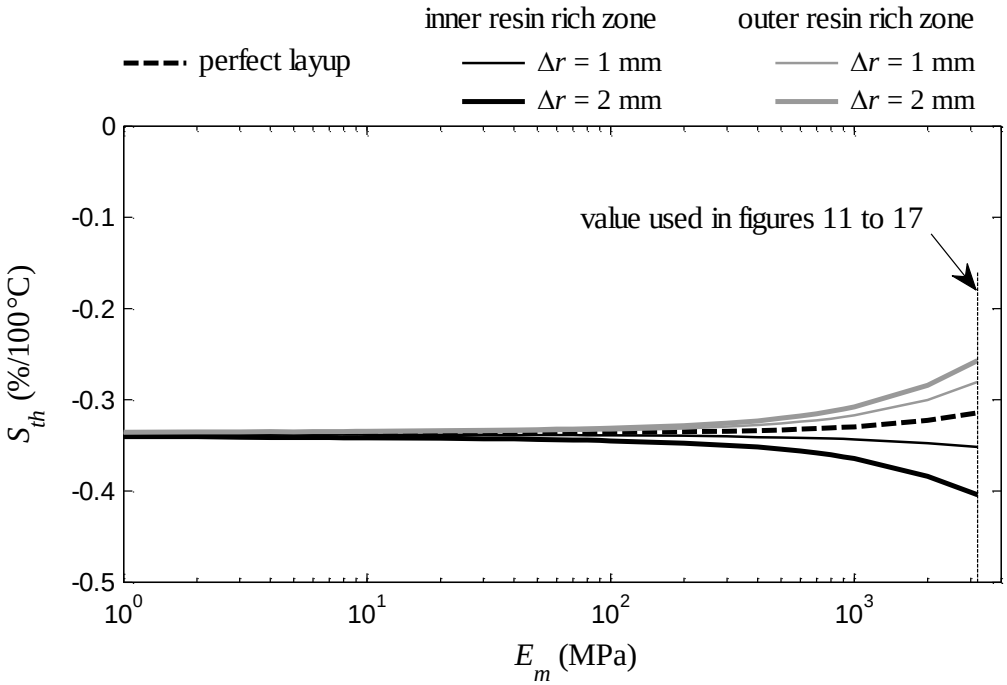

Figure 5-18 : Influence of resin modulus on the predicted thermoelastic spring-in.

A last remark is worth mentioning about the data presented in Figure 5-17. In the concave corner, the demolded distortion seems to increase with the fiber volume fraction. This trend is not really marked for parts Di, but is rather significant for parts Ai, which possess an outer resin rich zone. This defect is created by fiber bridging over curved areas as illustrated in Figure 5-19. In such a configuration, the application of the compaction pressure may generate tensile in-plane stress on the fibers located on the inner side of the corner. This mechanism was previously described in autoclave processing [43] and could explain the observed increase in spring-in since a higher fiber volume fraction is associated with a more important effective stress on the fiber bed. Analyzing such fiber stresses and estimating their possible impact on the residual deformation would also be valuable for further development of Flexible Injection.

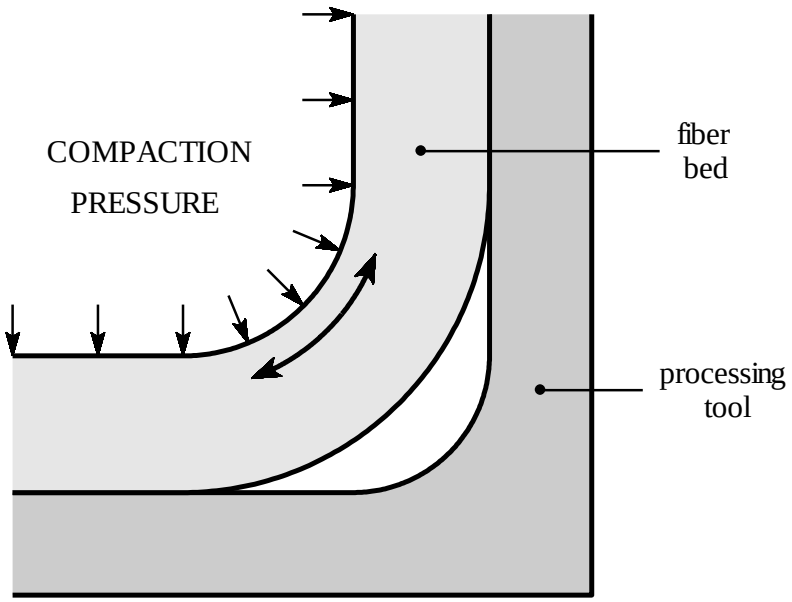

Figure 5-19 : Possible mechanism generating in-plane stresses during fiber bridging over a concave corner.

5.6 Conclusions

This paper investigates the influence of manufacturing defects on the distortion of curved thermoset composites. A series of stair-shaped components was first manufactured by a new LCM process called Flexible Injection. These samples were prepared for various preforming conditions, which resulted in different layup quality in the corners of the parts. Two types of defects were typically observed in curved areas: thickness gradients and resin rich zones. These defects were then quantified by analyzing cross-sectional images of the fabricated parts. Moreover, the change in shape of the specimens was recorded during a simple cool down experiment to characterize the thermoleastic spring-in behavior of the structure. Experimental observations were subsequently compared with predictions made by an analytical model and numerical simulations. Results show that the manufacturing quality can impact the thermoelastic distortion through different mechanisms depending on the type of defect. Firstly, thickness gradients change locally the fiber volume fraction and in turn modify the coefficients of thermal expansion in the corners of the composite specimens. Secondly, resin rich zones constitute regions of higher CTE that create stress concentration on one side of the curved area. Consequently the relative impact of such defects decreases when the overall stiffness of the structure increases.

Preliminary results also indicate that the impact of the manufacturing quality may be different for the residual deformation induced by chemical shrinkage. This cause of distortion seems indeed less affected by resin accumulations, because most of the volumetric shrinkage occurs in a flexible rubbery state. Further investigation would be necessary to confirm this hypothesis and study the influence of fiber stress resulting from consolidation of the preform. The issue of mechanical performance could also be addressed since manufacturing heterogeneity is expected to impact the overall strength and fatigue behavior of the composite. Finally, note that although the present study focused on Flexible Injection, the conclusions may also be valid for other processes that experience similar manufacturing problems such as RTM or autoclave processing.

5.7 Acknowledgements

The authors would like to thank Dr. John Owens, from General Motors Laboratory, Detroit, USA, for advice on the general research orientation, and General Motors (GM) of Canada, the Canada Research Chair program and the National Science & Research Council of Canada (NSERC) for their financial contributions. The support of “Centre de recherche en plasturgie et composites” (CREPEC) and of “Consortium de recherche et d’innovation en aérospatiale du Québec” (CRIAQ) for the research infrastructure of the Chaire sur les Composites à Haute Performance (CCHP) at École Polytechnique de Montréal is also gratefully acknowledged.

5.8 Appendix A. Fiber preforming

The setup used to prepare the fibrous reinforcement is schematically shown in Figure 5-20. This preforming tool is made of two aluminum plates obtained by metal folding. Self-hardening modeling clay was applied with a radius gauge in the corners of the plates to adjust the different radii of curvature r_p and R_p. A small amount of vinyl ester resin was first manually sprayed on each fabric ply with a pressure gun. The reinforcement was then placed between the two preforming plates and vacuum was drawn in the cavity to impose a preforming pressure p_p on the stacking. After closing the preforming tool, the preform was left overnight to cure at room temperature while the vacuum pressure was maintained inside the cavity. This procedure was used to prepare semi-rigid fibrous preforms under controlled preforming conditions (r_p, R_p and p_p).

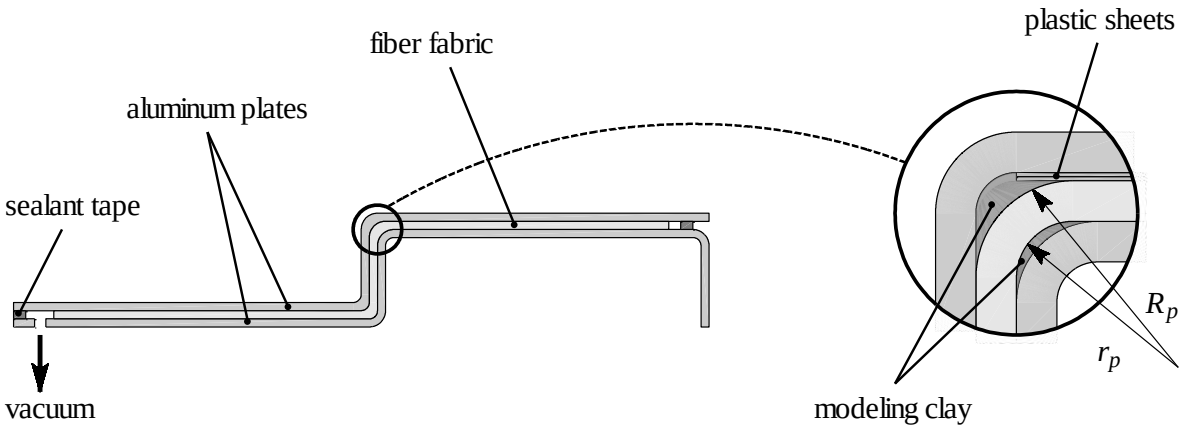

Figure 5-20 : Schematic representation of the preforming tool.

5.9 References

1. Ruiz E, Trochu F. Numerical analysis of cure temperature and internal stresses in thin and thick RTM parts. Compos Part A: Appl Sci Manuf 2005;36(6):806-826.

2. Hsiao K-T, Gangireddy S. Investigation on the spring-in phenomenon of carbon nanofiber-glass fiber/polyester composites manufactured with vacuum assisted resin transfer molding. Compos Part A: Appl Sci Manuf 2008;39(5):834-842.

3. Yoon KJ, Kim J-S. Effect of thermal deformation and chemical shrinkage on the process induced distortion of carbon/epoxy curved laminates. J Compos Mater 2001;35(3):253-263.

4. Albert C, Fernlund G. Spring-in and warpage of angled composite laminates. Compos Sci Technol 2002;62(14):1895-1912.

5. Darrow Jr DA, Smith LV. Isolating components of processing induced warpage in laminated composites. J Compos Mater 2002;36(21):2407-2419.

6. Bapanapalli SK, Smith LV. A linear finite element model to predict processing-induced distortion in FRP laminates. Compos Part A: Appl Sci Manuf 2005;36(12):1666-1674.

7. Yang SY, Huang CK, Chen CC. Effect of processing on precision of composite panels. Mater Manuf Process 2003;18(5):769-781.

8. Salomi A, Garstka T, Potter K, Greco A, Maffezzoli A. Spring-in angle as molding distortion for thermoplastic matrix composite. Compos Sci Technol 2008;68(14):3047-3054.

9. Oakeshott JL. Warpage of carbon-epoxy composite channels. Plast Rubber Compos 2003;32(3):104-113.

10. Radford DW, Rennick TS. Separating sources of manufacturing distortion in laminated composites. J Reinf Plast Compos 2000;19(8):621-641.

11. Nelson RH, Cairns DS. Prediction of dimensional changes in composite laminates during cure. In: 34th International SAMPE Symposium. Reno, NV, USA, 1989. p. 2397-2410.

12. Radford DW, Diefendorf RJ. Shape Instabilities in Composites Resulting from Laminate Anisotropy. J Reinf Plast Compos 1993;12(1):58-75.

13. Ersoy N, Potter K, Wisnom MR, Clegg MJ. Development of spring-in angle during cure of a thermosetting composite. Compos Part A: Appl Sci Manuf 2005;36(12):1700-1706.

14. Wang J, Kelly D, Hillier W. Finite element analysis of temperature induced stresses and deformations of polymer composite components. J Compos Mater 2000;34(17):1456-1471.

15. Svanberg JM, Holmberg JA. Prediction of shape distortions. Part II. Experimental validation and analysis of boundary conditions. Compos Part A: Appl Sci Manuf 2004;35(6):723-734.

16. Clifford S, Jansson N, Yu W, Michaud V, Manson JA. Thermoviscoelastic anisotropic analysis of process induced residual stresses and dimensional stability in real polymer matrix composite components. Compos Part A: Appl Sci Manuf 2006;37(4):538-545.

17. Dong C. Modeling the process-induced dimensional variations of general curved composite components and assemblies. Compos Part A: Appl Sci Manuf 2009;40(8):1210-1216.

18. Ersoy N, Garstka T, Potter K, Wisnom MR, Porter D, Stringer G. Modelling of the spring-in phenomenon in curved parts made of a thermosetting composite. Compos Part A: Appl Sci Manuf 2010;41(3):410-418.

19. Wiersma HW, Peeters LJB, Akkerman R. Prediction of Springforward in Continuous-Fibre/Polymer L-Shaped Parts. Compos Part A: Appl Sci Manuf 1998;29(11):1333-1342.

20. Zhu Q, Geubelle PH, Li M, Tucker Iii CL. Dimensional accuracy of thermoset composites: Simulation of process-induced residual stresses. J Compos Mater 2001;35(24):2171-2205.

21. Johnston A, Vaziri R, Poursartip A. A Plane Strain Model for Process-Induced Deformation of Laminated Composite Structures. J Compos Mater 2001;35(16):1435-1469.

22. Fernlund G, Rahman N, Courdji R, Bresslauer M, Poursartip A, Willden K, Nelson K. Experimental and numerical study of the effect of cure cycle, tool surface, geometry, and lay-up on the dimensional fidelity of autoclave-processed composite parts. Compos Part A: Appl Sci Manuf 2002;33(3):341-351.

23. Radford DW. Cure Shrinkage Induced Warpage in Flat Uni-Axial Composites. J Compos Technol Res 1993;15(4):290-296.

24. Radford DW. Volume fraction gradient induced warpage in curved composite plates. Compos Eng 1995;5(7):923-934.

25. Hubert P, Poursartip A. Aspects of the Compaction of Composite Angle Laminates: An Experimental Investigation. J. Compos. Mater. 2001;35(1):2-26.

26. Gao Z-S, Young W-B. Study of the bending induced gap in fiber preforming of woven fiber mats. Polym Compos 2002;23(2):239-248.

27. Feih S, Shercliff HR. Quality assessment of curved composite components in peel joint structures. Compos Part A: Appl Sci Manuf 2005;36(3):397-408.

28. Dong C. Model development for the formation of resin-rich zones in composites processing. Compos Part A: Appl Sci Manuf 2011;42(4):419-424.

29. Naji MI, Hoa SV. Curing of thick angle-bend thermoset composite part: curing cycle effect on thickness variation and fiber volume fraction. J. Reinf. Plast. Compos. 1999;18(8):702-723.

30. Li Y, Li M, Gu Y, Zhang Z. Numerical and experimental study on the effect of lay-up type and structural elements on thickness uniformity of L-shaped laminates. Appl Compos Mater 2009;16(2):101-115.

31. Dong C, Zhang C, Liang Z, Wang B. Dimension variation prediction for composites with finite element analysis and regression modeling. Compos Part A: Appl Sci Manuf 2004;35(6):735-746.

32. Ruiz E, Briones LR, Allard É, Trochu F. Flexible Injection: A Novel LCM Technology for Low Cost Manufacturing of High Performance Composites. Part I: Experimental Investigation. In: Proceedings FPCM9. Montréal, Canada, 2008. p. 34.

33. Trochu F, Soukane S, Touraine B. Flexible Injection: A Novel LCM Technology for Low Cost Manufacturing of High Performance Composites. Part II: Numerical Model. In: Proceedings FPCM9. Montréal, Canada, 2008. p. 35.

34. Causse P, Ruiz E, Trochu F. Experimental study of flexible injection to manufacture parts of strong curvature. Polym Compos 2011;32(6):882-895.

35. Causse P, Ruiz E, Trochu F. Analysis of Fiber Preforming for Improved Manufacturing of Curved Parts by Flexible Injection. In: Proceedings ICCM18. Jeju island, Korea, 2011. p.

36. Schapery RA. Thermal Expansion Coefficients of Composite Materials Based on Energy Principles. J Compos Mater 1968;2(3):380-403.

37. Ziehl PH. Development of a damage based design criterion for fiber reinforced vessels. Ph.D. thesis, The University of Texas at Austin, 2000.

38. Halpin JC, Kardos JL. HALPIN-TSAI Equations: a review. Polym Eng Sci 1976;16(5):344-352.

39. Hewitt RL, de Malherbe MC. An Approximation for the Longitudinal Shear Modulus of Continuous Fibre Composites. J Compos Mater 1970;4:280-282.

40. Ruiz E, Trochu F. Thermomechanical Properties during Cure of Glass-Polyester RTM Composites: Elastic and Viscoelastic Modeling. J Compos Mater 2005;39(10):881-916.

41. Ersoy N, Garstka T, Potter K, Wisnom MR, Porter D, Clegg M, Stringer G. Development of the properties of a carbon fibre reinforced thermosetting composite through cure. Compos Part A: Appl Sci Manuf 2010;41(3):401-409.

42. Ruiz E, Trochu F. Comprehensive thermal optimization of liquid composite molding to reduce cycle time and processing stresses. Polym Compos 2005;26(2):209-30.

43. Potter KD, Campbell M, Langer C, Wisnom MR. The generation of geometrical deformations due to tool/part interaction in the manufacture of composite components. Compos Part A: Appl Sci Manuf 2005;36(2 SPEC ISS):301-308.

CHAPITRE 6 DISCUSSION GÉNÉRALE ET RECOMMANDATIONS

Ce dernier chapitre effectue une synthèse générale du travail réalisé. L'approche adoptée, les principaux enseignements et les limitations du projet sont tout d'abord discutés. Des recommandations pour la suite des travaux sont alors formulées.

6.1 Discussion générale

L'objectif de ce travail était d'étudier la spécificité du procédé d'injection flexible lors de la mise en forme de pièces fortement courbées. La méthodologie adoptée pour atteindre cet objectif a privilégié une approche expérimentale. Cette décision a été motivée par deux raisons principales. Tout d'abord, les travaux précédents ont clairement illustré la difficulté de modéliser les différents phénomènes physiques impliqués. Les principales avancées dans le développement du procédé ont en effet été obtenues jusqu'à maintenant par une analyse expérimentale. Par ailleurs, la chaire CCHP est à l'heure actuelle le seul laboratoire utilisant cette technique de fabrication, il donc primordial de recueillir un maximum d'observations expérimentales en vue de proposer des solutions de développement à court terme. L'archivage des observations effectuées contribue de plus à constituer une base de données pouvant s'avérer utile pour les futurs travaux de caractérisation ou de modélisation. Par exemple, certains échantillons fabriqués au cours de la thèse sont actuellement analysés par pyrolyse de la matrice et par tomographie afin d'évaluer les mécanismes de formation des porosités.

Le moule de fabrication « Polyflex II » a été le principal outil de recherche utilisé au cours du projet. La géométrie correspondante est relativement simple (pas de double courbure) mais est cependant représentative d'applications réelles comme les pièces comprenant des brides de fixation. Le fait que la partie centrale de la cavité soit parallèle à la direction de fermeture a notamment permis de vérifier qu'une telle configuration était envisageable avec le procédé d'injection flexible. La mise en place de la méthodologie de fabrication a nécessité deux étapes principales: l'adaptation du moule pour l'injection flexible et le développement de la procédure

de préformage. Une membrane flexible en fluoroelastomère a tout d'abord été sélectionnée. Ce choix a été motivé par la bonne compatibilité chimique et la faible déformation permanente du matériau. La principale limitation de la membrane est sa forme plane qui n'adopte pas naturellement la géométrie du moule. Comme discuté dans la thèse, ceci peut entraîner la formation de zones riches en résine sur la partie concave à faible taux de fibres. Il est aussi possible que la force nécessaire pour déformer la membrane limite la contrainte effectivement transmise au renfort dans les parties courbées. Cependant, la bonne imprégnation visuelle des spécimens fabriqués suggère une pression de résine élevée et donc une flexibilité suffisante de la membrane. La configuration de la cavité sélectionnée a par ailleurs démontré que la membrane pouvait être utilisée pour assurer l'étanchéité dans les deux chambres du montage. Cet avantage permet d'éliminer les résidus de résine sur le plan de joint (le « flash ») et de se passer d'éléments d'étanchéité comme des joints toriques. Le développement de la procédure de préformage a été une étape décisive pour la réussite des fabrications. Les inconvénients de la méthodologie proposée sont principalement: le nombre de manipulations manuelles nécessaires, le mauvais contrôle de la densité surfacique d'agent liant et la force de fermeture du montage limitée par la pression atmosphérique. Malgré ces inconvénients, l'analyse des pièces fabriquées (notamment au chapitre 3) fait état d'une répétabilité satisfaisante de la mise en forme.

Afin de simplifier la mise en œuvre du procédé, des conditions de fabrication simplifiées et ne représentant pas nécessairement une application industrielle haute performance ont été choisies. Les expériences ont ainsi été réalisées à température ambiante avec des pressions d'injection et de compaction constantes. Il apparaît raisonnable de supposer que ces paramètres n'ont que peu d'influence sur le comportement des parties courbées. L'utilisation d'une température de fabrication plus élevée aurait cependant permis d'obtenir une distorsion plus importante et une séparation plus aisée des différentes sources de déformation résiduelle.

Pour limiter les coûts, des matériaux peu dispendieux (fibres de verre et résine vinylester) ont été utilisés. Dans le cadre de l'étude de la mise en forme d'une pièce courbée, ce choix n'introduit a priori aucune limitation spécifique et il est raisonnable de penser que des résultats similaires auraient été obtenus avec des fibres de carbone et une résine époxy par exemple. Cependant, il

convient de souligner que la formulation de la résine a été ajustée pour obtenir un temps de gel d'environ 2 heures et un temps total de fabrication dépassant 6 heures. Ces conditions de fabrication sont bien évidemment incompatibles avec l'objectif principal de réduction du temps de cycle total. L'utilisation d'une résine plus réactive peut avoir deux impacts sur les conclusions du travail. Tout d'abord, un temps de gel plus court entraîne une relaxation moins importante du renfort. Au moment du gel de la résine, la contrainte effective sur la préforme est alors plus importante et la pression sur la résine moins élevée. Pour les taux volumiques de fibres considérés dans le projet, il est donc probable qu'une résine plus réactive engendre une moins bonne qualité d'imprégnation. Il se peut aussi que la résine se solidifie avant que l'équilibre de consolidation ne soit atteint. Dans une telle situation, des variations d'épaisseur pourraient être observées y compris sur les parties planes des pièces.

Au cours du projet, les analyses ont principalement porté sur la partie centrale de la pièce incluant les deux angles. Les parties planes restantes (environ 25 cm) n'ont pas été étudiées mais peuvent faire l'objet de travaux futurs (pour une analyse du taux de vide par exemple). Différentes techniques ont été développées pour caractériser la qualité des pièces. Les méthodes proposées reposent sur l'utilisation d'un simple scanner optique et ont donc l'avantage d'être peu couteuses. Grâce aux différents codes d'analyse d'images développés avec le logiciel MATLAB, des profils d'épaisseur continus plus précis et moins dépendants de l'utilisateur que les techniques de mesure par micromètre couramment utilisée dans la littérature ont été obtenus. Cette approche a aussi permis de caractériser précisément les défauts de fabrication à l'aide de la représentation géométrique simplifiée proposée au chapitre 5. Un désavantage de la méthode reste cependant le temps de préparation des échantillons. Un soin particulier doit en effet être observé au cours de la phase de découpe et de polissage afin d'obtenir des résultats exploitables. L'analyse d'image a aussi été utilisée pour quantifier la distorsion des sections courbées. L'utilisation de série de marqueurs a permis d'enregistrer l'évolution de la forme générale de la pièce et de corriger les effets du gauchissement sur la distorsion des parties courbées. L'expérience de refroidissement possède cependant deux désavantages. Le temps de mesure est tout d'abord relativement long. Cette contrainte a nécessité un long programme de mesure pour caractériser chaque coupe longitudinale (6 par pièce) de tous les spécimens analysés. De plus, la mesure ne donne qu'une valeur totale de l'angle de distorsion entre deux températures de référence. La procédure ne peut

donc pas détecter d'éventuels effets non linéaires dus à la dépendance de la dilatation à la température.

Bien qu'ayant privilégié un approche expérimentale, ce travail de thèse à aussi eu recours a des modèles simplifiés. Cette démarche visait principalement à faciliter la compréhension des observations expérimentales et à identifier les phénomènes importants devant être pris en compte lors de futurs travaux de modélisation plus raffinés. Le modèle de déformation fibreuse présenté au chapitre 4 a notamment illustré l'importance de comprendre l'influence de l'agent liant sur le comportement mécanique du renfort. L'essai de caractérisation du préformage courbé utilisé pour construire la géométrie initiale du modèle a par ailleurs permis une caractérisation très rapide du renfort fibreux. La réalisation d'un essai ne demande en effet que quelques minutes ce qui constitue une nette amélioration comparativement aux méthodes de caractérisation des régions riches en résine proposées auparavant pour le procédé RTM. Dans le chapitre 5, la comparaison des résultats expérimentaux avec les prédictions des modèles de distorsion a permis de bien illustrer le possible impact des défauts de fabrication. Le modèle paramétrique incluant ces hétérogénéités n'a pas la vocation d'être développé ultérieurement pour inclure les effets du retrait chimique par exemple. Les différentes études paramétriques réalisées ont cependant clairement montré l'importance de bien contrôler la qualité de mise en forme dans le cadre d'une étude du phénomène de distorsion.

De façon générale, ce travail de thèse a tâché de comprendre les caractéristiques spécifiques du procédé d'injection flexible lors de la mise en forme d'une structure courbée. Le travail a ainsi identifié l'influence majeure des mécanismes de déformation de la membrane et du renfort fibreux. Par ailleurs, la méthodologie générale utilisée au cours du projet peut servir de base à d'autres études plus approfondies dans le futur. Dans cette optique, la section suivante présente une série de recommandations pour le développement à venir.

6.2 Recommandations

6.2.1 Membrane flexible

Pour éviter la formation de zones riches en résine dues à la membrane flexible, il est primordial que cette dernière puisse adopter facilement la forme exacte de la pièce. Il est donc conseillé de développer des membranes tridimensionnelles possédant une géométrie bien contrôlée. Cette recommandation a déjà été mise en pratique pour la fabrication de panneaux auto-raidis (Rifay, 2010). La Figure 1-1 montre la membrane tridimensionnelle conçue pour la mise en forme d'un panneau plan avec raidisseur de type oméga en forme de croix. Grâce à ce dispositif, la pièce considérée a pu être fabriquée avec succès.

Figure 6-1 : Membrane flexible tridimensionnelle développée pour la mise en forme de panneaux auto-raidis.

Dans le futur, il serait aussi intéressant d'étudier la déformation de la membrane au cours du cycle de fabrication. Tel qu'illustré schématiquement sur la Figure 6-2, la membrane doit adopter deux positions limites au cours de la mise en forme. À l'injection, elle doit se plaquer sur la partie supérieure de la cavité pour permettre l'écoulement de la résine au dessus de la préforme. À l'étape de consolidation, la membrane doit par la suite rentrer en contact avec la partie supérieure de la préforme. Pour la forme en U illustrée sur la Figure 6-2, ces deux positions limites impliquent une déformation planaire pouvant être importante. Un futur projet pourrait viser à

optimiser les paramètres de conception des membranes (épaisseur et rigidité) pour autoriser la déformation nécessaire. Une telle étude serait aussi utile afin de connaître la contrainte requise pour déformer la membrane et estimer la pression effectivement transmise à la résine. Le développement de membranes possédant des propriétés variables dans le plan serait aussi une piste d'étude intéressante. Les membranes pourraient par exemple être plus rigides dans les zones fortement courbées pour assurer une meilleure consolidation à la manière des coussinets de pression déjà utilisés en autoclave.

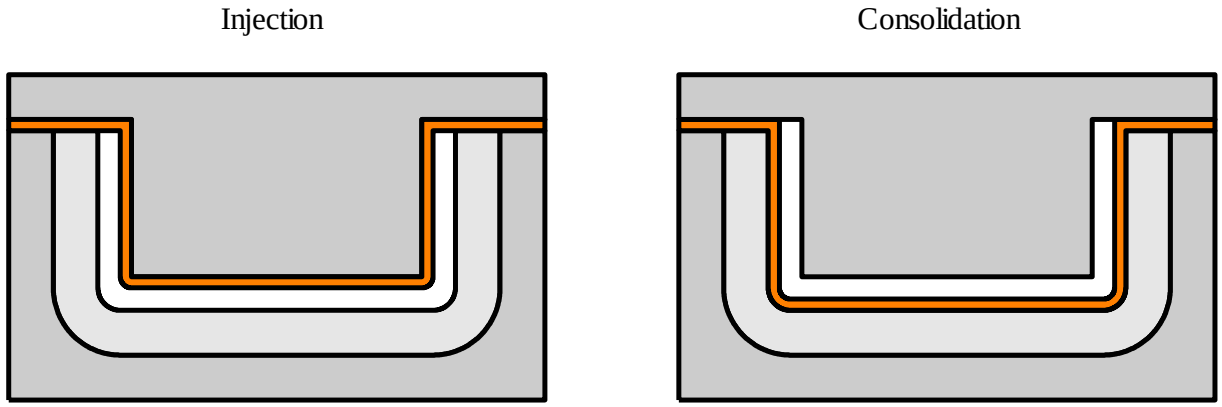

Figure 6-2 : Positions limites idéales de la membrane lors de la mise en forme d'un canal en U.

6.2.2 Préforme fibreuse

Préparation de la préforme

A l'avenir, il est recommandé d'évaluer des procédures de préformage pouvant être implémentées au niveau industriel. Les deux options envisageables sont le préformage sous presse par utilisation d'un agent liant et l'utilisation de techniques textiles. La première solution se rapproche de la procédure de préformage utilisée dans cette thèse. Au cours des travaux futurs, il serait intéressant d'utiliser des presses de préformage permettant un meilleur contrôle du déplacement (et donc de la cavité de préformage) et de la pression appliquée. Par ailleurs, la résine thermodurcissable devra être remplacée par des agents liants spécialement développés pour le préformage des tissus. Un premier pas a déjà été fait dans cette direction avec l'utilisation

d'adhésifs pouvant être polymérisés par rayonnement ultra-violet (Rifay, 2010). D'autres produits commerciaux restent encore à évaluer afin de déterminer une solution optimale pour l'injection flexible. Les techniques textiles telles que le tressage ou le tissage tridimensionnel peuvent apporter de nouvelles opportunités pour le développement du procédé. Les futurs travaux devront notamment déterminer si ces méthodes sont compatibles avec l'injection flexible en termes de cadence de production.

Modélisation du comportement

Le modèle éléments finis présenté au chapitre 4 peut servir de base au développement de futurs outils pour la simulation de la mise en forme avec un préformage par agent liant. Le modèle de compaction proposé peut par exemple être directement utilisé. En revanche, la représentation du cisaillement à travers l'épaisseur reste à améliorer. Les futurs modèles devront notamment inclure une meilleure représentation du glissement inter-plis et du couplage entre la flexion et la compaction transverse des torons. Dans le cas d'un préformage par technique textile, une attention particulière devra être portée à la représentation de l'architecture des fibres afin de représenter l'ondulation des mèches de façon réaliste. Les outils numériques et les techniques de caractérisation récemment proposés pour l'étude du drapage peuvent servir de point de départ à ces futurs projets.

6.2.3 Autre recommandations

Conditions de fabrication

Les futures expériences devraient utiliser différents couples résine/fibres ainsi qu'une température de mise en forme plus élevée. Les pièces fabriquées permettront ainsi une étude plus poussée des différentes sources de distorsion.

Amélioration des techniques de caractérisation

Des améliorations peuvent être apportées aux méthodes de caractérisation par analyse d'images développées dans la thèse. La préparation des échantillons pour l'analyse du profil d'épaisseur

pourrait par exemple être simplifiée en utilisant une fine couche de peinture colorée sur la surface de la pièce afin de faciliter la détection des points frontières. Pour la mesure de la distorsion, l'échantillon pourrait être placé dans une enceinte thermique possédant une paroi transparente et le scanner pourrait être remplacé par un appareil photo à haute résolution. Cette modification permettrait d'enregistrer plus précisément l'évolution de la distorsion en fonction de la température.

Autres formes particulières

Le présent travail a démontré que l'injection flexible pouvait être appliquée à des pièces comportant des angles droits simples. D'autres cas géométriques particuliers doivent encore être étudiés en vue de la fabrication de structures plus générales. La Figure 6-3 propose trois situations pouvant faire l'objet de travaux futurs. Les formes nervurées en T sont courantes dans les applications structurales. Cette géométrie est a priori relativement défavorable pour l'injection flexible. En effet, la fabrication de ce type de pièce ne semble envisageable qu'avec une membrane reproduisant le T, et donc une nervure mise en forme entre 2 parois flexibles. La faisabilité d'une telle fabrication devra être étudiée dans les travaux futurs. Des pièces possédant des variations d'épaisseur (continue ou par saut) devraient aussi être étudiées. Dans ce cas, la géométrie de la chambre de compaction devra possiblement être adaptée pour assurer une répartition homogène de la résine dans le moule.

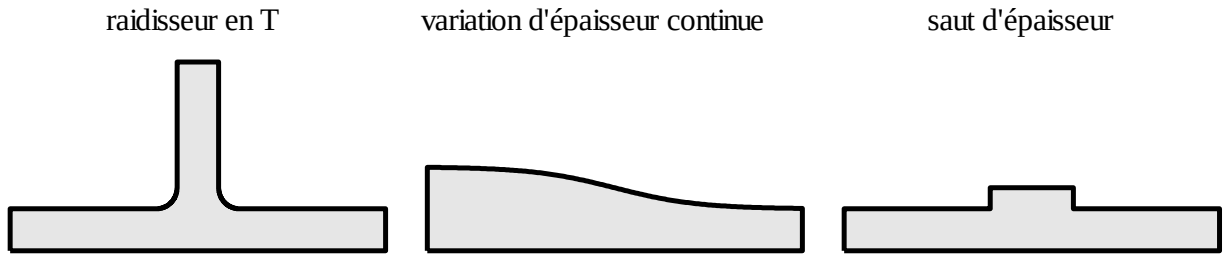

Figure 6-3 : Différentes configurations géométriques pouvant faire l'objet de travaux futurs sur l'injection flexible.

CONCLUSION

L'injection flexible est une nouvelle méthode de fabrication de pièces composites haute performance à matrice thermodurcissable. L'originalité de cette technique réside dans l'utilisation d'une membrane flexible et d'un fluide de compaction permettant d'imposer une déformation contrôlée du moule d'injection au cours de la fabrication. Les premiers travaux de développement réalisés sur des géométries simples ont permis de démontrer le potentiel du procédé en termes de rapidité d'injection et de qualité de l'imprégnation. Au cours de ce projet doctoral, l'injection flexible a pour la première fois été appliquée à des géométries fortement courbées. De façon générale, le projet visait à identifier les paramètres de fabrication critiques permettant une mise en forme robuste.

Un montage expérimental a tout d'abord été développé pour fabriquer une pièce en forme d'escalier possédant deux zones fortement courbées. L'analyse des premières pièces fabriquées a démontré le comportement spécifique des parties courbées lors de la consolidation finale du composite. Des défauts de fabrication comme des gradients d'épaisseur ou des régions riches en résine ont en effet tendance à apparaître dans les zones de forte courbure. Ces problèmes de mise en forme proviennent essentiellement des mécanismes de déformation de la membrane et de la préforme fibreuse. La préparation de la préforme a notamment une influence prépondérante sur la qualité finale de la pièce. L'analyse de la déformation des fibres au cours de cycle de production complet a permis de mieux comprendre le lien entre les conditions de préformage et le placement des fibres dans les zones fortement courbées. Grâce à une sélection adéquate des paramètres de préformage, la pièce test a ainsi pu être fabriquée sans défaut apparent avec un taux volumique de fibres représentatif d'une application haute performance. La dernière partie du travail s'est intéressée à la déformation résiduelle des pièces fabriquées. Cette étape a tâché de quantifier l'impact des défauts de fabrication sur les différentes composantes de la distorsion. Sous certaines conditions, une influence significative de la qualité de mise en forme sur le tolérancement géométrique du produit a ainsi été constatée.

De façon générale, le projet démontre que l'injection flexible ne possède pas de limitation intrinsèque pour la mise en forme de structures fortement courbées. En ce sens, le travail constitue une étape de développement supplémentaire vers l'application du procédé à des pièces réelles de géométries complexes. Malgré plusieurs simplifications de mise en œuvre lors de la réalisation des expériences, la méthodologie et les principales conclusions du travail peuvent être transposées à un cadre plus général. Les travaux futurs de développement à court et long terme bénéficieront des solutions technologiques proposées et des recommandations formulées par ce travail de thèse.

BIBLIOGRAPHIE

Abdellaoui, C. (2008). *Étude expérimentale du contrôle en pression et en température de la fabrication de composites par injection flexible.* Mémoire de maîtrise inédit, École Polytechnique de Montréal, Montréal.

Albert, C., & Fernlund, G. (2002). Spring-in and warpage of angled composite laminates. *Compos Sci Technol, 62*(14), 1895-1912.

Allard, É. (2006). *Analyse expérimentale et optimisation d'un procédé d'injection flexible pour la fabrication rapide des composites.* Mémoire de maîtrise inédit, École Polytechnique Montréal, Montréal.

Arafath, A. R. A., Vaziri, R., & Poursartip, A. (2009). Closed-form solution for process-induced stresses and deformation of a composite part cured on a solid tool: Part II - Curved geometries. *Composites Part A: Applied Science and Manufacturing, 40*(10), 1545-1557.

Arndt, R. D. (1991). Fabric preforming for structural reaction injection molding, *Detroit, MI, USA*.(pp. 35-40): Publ by Springer-Verlag New York Inc.

Bapanapalli, S. K., & Smith, L. V. (2005). A linear finite element model to predict processing-induced distortion in FRP laminates. *Compos Part A: Appl Sci Manuf, 36*(12), 1666-1674.

Bel, S., Boisse, P., & Dumont, F. (2011). Analyses of the Deformation Mechanisms of Non-Crimp Fabric Composite Reinforcements during Preforming. 1-16.

Bickerton, S., Buntain, M. J., & Somashekar, A. A. (2003). The viscoelastic compression behavior of liquid composite molding preforms. *Compos. A, 34*(5), 431-444.

Boisse, P., Hamila, N., Vidal-Salle, E., & Dumont, F. (2011). Simulation of wrinkling during textile composite reinforcement forming. Influence of tensile, in-plane shear and bending stiffnesses. *Compos Sci Technol, 71*(5), 683-692.

Brillant, M., & Hubert, P. (2010). Out-of-autoclave processing of complex shape laminates, *Seattle, WA, United states*.(pp. electronic proceedings): Soc. for the Advancement of Material and Process Engineering.

Briones, L. R. (2005). *Injection flexible dans moule isotherme : conception et analyse d'un nouveau procédé de fabrication de composites.* Mémoire de maîtrise inédit, École Polytechnique de Montréal, Montréal.

Cann, M. T., & Adams, D. O. (2001). Effect of part-tool interaction on cure distortion of flat composite laminates, *Long Beach, CA.*(Vol. 46 II, pp. 2264-2277): Soc. for the Advancement of Material and Process Engineering.

Cao, X., & Lee, L. J. (2003). Control of Shrinkage and Final Conversion of Vinyl Ester Resins Cured in Low-Temperature Molding Processes. *Journal of Applied Polymer Science, 90*(6), 1486-1496.

Capehart, T. W., Muhammad, N., & Kia, H. G. (2007). Compensating Thermoset Composite Panel Deformation using Corrective Molding. *Journal of Composite Materials, 41*(14), 1675-1701.

Cauchois, J.-P. (1997). *R.T.M. process* France: Editions Syntech.

Causse, P., Ruiz, E., & Trochu, F. (2011a). *Analysis of Fiber Preforming for Improved Manufacturing of Curved Parts by Flexible Injection*. Proceedings ICCM18, Jeju island, Korea.

Causse, P., Ruiz, E., & Trochu, F. (2011b). Experimental study of flexible injection to manufacture parts of strong curvature. *Polym Compos, 32*(6), 882-895.

Chen, Q., Boisse, P., Park, C. H., Saouab, A., & Breard, J. (2011). Intra/inter-ply shear behaviors of continuous fiber reinforced thermoplastic composites in thermoforming processes. *Compos Struct, 93*(7), 1692-1703.

Clifford, S., Jansson, N., Yu, W., Michaud, V., & Manson, J. A. (2006). Thermoviscoelastic anisotropic analysis of process induced residual stresses and dimensional stability in real polymer matrix composite components. *Compos Part A: Appl Sci Manuf, 37*(4), 538-545.

Daqoune, T. (2007). *Analyse expérimentale sur des renforts tissés d'un procédé d'injection flexible pour la fabrication rapide des composites* Mémoire de maîtrise inédit, École Polytechnique Montréal, Montréal.

Darrow Jr, D. A., & Smith, L. V. (2002). Isolating components of processing induced warpage in laminated composites. *J Compos Mater, 36*(21), 2407-2419.

Dong, C. (2008). Development of a model for predicting the transverse coefficients of thermal expansion of unidirectional carbon fibre reinforced composites. *Applied Composite Materials, 15*(3), 171-182.

Dong, C. (2009a). Modeling the dimensional variations of composites using effective coefficients of thermal expansion. *Journal of Composite Materials, 43*(22), 2639-2652.

Dong, C. (2009b). Modeling the process-induced dimensional variations of general curved composite components and assemblies. *Compos Part A: Appl Sci Manuf, 40*(8), 1210-1216.

Dong, C. (2011). Model development for the formation of resin-rich zones in composites processing. *Compos Part A: Appl Sci Manuf, 42*(4), 419-424.

Dong, C., Zhang, C., Liang, Z., & Wang, B. (2004a). Assembly dimensional variation modelling and optimization for the resin transfer moulding process. *Modelling and Simulation in Materials Science and Engineering, 12*(3), 221-237.

Dong, C., Zhang, C., Liang, Z., & Wang, B. (2004b). Dimension variation prediction for composites with finite element analysis and regression modeling. *Compos Part A: Appl Sci Manuf, 35*(6), 735-746.

Ersoy, N., Garstka, T., Potter, K., Wisnom, M. R., Porter, D., Clegg, M. (2010a). Development of the properties of a carbon fibre reinforced thermosetting composite through cure. *Compos Part A: Appl Sci Manuf, 41*(3), 401-409.

Ersoy, N., Garstka, T., Potter, K., Wisnom, M. R., Porter, D., & Stringer, G. (2010b). Modelling of the spring-in phenomenon in curved parts made of a thermosetting composite. *Compos Part A: Appl Sci Manuf, 41*(3), 410-418.

Ersoy, N., Potter, K., Wisnom, M. R., & Clegg, M. J. (2005a). Development of spring-in angle during cure of a thermosetting composite. *Compos Part A: Appl Sci Manuf, 36*(12), 1700-1706.

Ersoy, N., Potter, K., Wisnom, M. R., & Clegg, M. J. (2005b). An experimental method to study the frictional processes during composites manufacturing. *Composites Part A: Applied Science and Manufacturing, 36*(11), 1536-1544.

Feih, S., & Shercliff, H. R. (2005). Quality assessment of curved composite components in peel joint structures. *Compos Part A: Appl Sci Manuf, 36*(3), 397-408.

Fernlund, G., Griffith, J., Courdji, R., & Poursartip, A. (2002a). Experimental and numerical study of the effect of caul-sheets on corner thinning of composite laminates. *Compos Part A: Appl Sci Manuf, 33*(3), 411-426.

Fernlund, G., Osooly, A., Poursartip, A., Vaziri, R., Courdji, R., Nelson, K. (2003). Finite element based prediction of process-induced deformation of autoclaved composite structures using 2D process analysis and 3D structural analysis. *Composite Structures, 62*(2), 223-234.

Fernlund, G., Rahman, N., Courdji, R., Bresslauer, M., Poursartip, A., Willden, K. (2002b). Experimental and numerical study of the effect of cure cycle, tool surface, geometry, and lay-up on the dimensional fidelity of autoclave-processed composite parts. *Compos Part A: Appl Sci Manuf, 33*(3), 341-351.

Fu, S., & Radford, D. W. (1999). Effects of lamination angle on the 3-D thermal expansion coefficients. *International SAMPE Technical Conference, 31*, 221-231.

Gao, Z.-S., & Young, W.-B. (2002). Study of the bending induced gap in fiber preforming of woven fiber mats. *Polym Compos, 23*(2), 239-248.

Garstka, T., Ersoy, N., Potter, K. D., & Wisnom, M. R. (2007). In situ measurements of through-the-thickness strains during processing of AS4/8552 composite. *Composites Part A: Applied Science and Manufacturing, 38*(12), 2517-2526.

Goetschel, D. B., & Radford, D. W. (1997). Analytical development of through-thickness properties of composite laminates. *Journal of Advanced Materials, 28*(4), 37-46.

Gu, Y., Li, M., Li, Y., & Zhang, Z. (2010). Pressure transfer behaviour of rubber mould and the effects on consolidation of L-shape composite laminates. *Polym Polym Compos, 18*(3), 167-174.

Gutowski, T. (1997). *Advanced composite Manufacturing*. New York ; Toronto: John Wiley & Sons.

Gutowski, T. G., Morigaki, T., & Cai, Z. (1987). The Consolidation of Laminate Composites. *J. Compos. Mater., 21*(2), 172-188.

Halpin, J. C., & Kardos, J. L. (1976). HALPIN-TSAI Equations: a review. *Polym Eng Sci, 16*(5), 344-352.

Hammond, M. G., & Farrell, K. (1978). GRAPHITE EPOXY COMPOSITE MATERIAL COMPONENTS FOR COMMUNICATIONS SATELLITES. 1392-1404.

Helms, H., & Lambrecht, U. (2007). The potential contribution of light-weighting to reduce transport energy consumption. *International Journal of Life Cycle Assessment, 12*, 58-64.

Hewitt, R. L., & de Malherbe, M. C. (1970). An Approximation for the Longitudinal Shear Modulus of Continuous Fibre Composites. *J Compos Mater, 4*, 280-282.

Hiel, C. C., Sumich, M., & Chappell, D. P. (1991). Curved beam test specimen for determining the interlaminar tensile strength of a laminated composite. *J. Compos. Mater., 25*(7), 854-868.

Holmberg, J. A., & Berglund, L. A. (1997). Manufacturing and performance of RTM U-beams. *Compos Part A: Appl Sci Manuf, 28*(6), 513-521.

Hsiao, K.-T., & Gangireddy, S. (2008). Investigation on the spring-in phenomenon of carbon nanofiber-glass fiber/polyester composites manufactured with vacuum assisted resin transfer molding. *Compos Part A: Appl Sci Manuf, 39*(5), 834-842.

Huang, C. K., & Yang, S. Y. (1997a). Experimental study on the accuracy of advanced composite tools for slanted shapes. *Polymer Composites, 18*(4), 442-452.

Huang, C. K., & Yang, S. Y. (1997b). Study on accuracy of angled advanced composite tools. *Materials and Manufacturing Processes, 12*(3), 473-486.

Hubert, P., & Poursartip, A. (1998). A Review of flow and compaction modelling relevant to thermoset matrix laminate processing. *J Reinf Plast Compos, 17*(4), 286-318.

Hubert, P., & Poursartip, A. (2001). Aspects of the Compaction of Composite Angle Laminates: An Experimental Investigation. *J. Compos. Mater., 35*(1), 2-26.

Hubert, P., Vaziri, R., & Poursartip, A. (1999). A two-dimensional flow model for the process simulation of complex shape composite laminates. *Int J Numer Methods Eng, 44*(1), 1-26.

Islam, M. R., Sjolind, S. G., & Pramila, A. (2001). Finite element analysis of linear thermal expansion coefficients of unidirectional cracked composites. *Journal of Composite Materials, 35*(19), 1762-1776.

Jain, L. K., Hou, M., Ye, L., & Mai, Y.-W. (1998). Spring-in study of the aileron rib manufactured from advanced thermoplastic composite. *Composites Part A: Applied Science and Manufacturing, 29*(8), 973-979.

Jain, L. K., Lutton, B. G., Mai, Y.-W., & Paton, R. (1997). Stresses and Deformations Induced during Manufacturing. Part II: A Study of the Spring-In Phenomenon. *J Compos Mater, 31*(7), 696-719.

Jain, L. K., & Mai, Y.-W. (1996). On Residual Stress Induced Distortions during Fabrication of Composite Shells. *Journal of Reinforced Plastics and Composites, 15*(8), 793-805.

Jain, L. K., & Mai, Y.-W. (1997). Stresses and Deformations Induced during Manufacturing. Part I: Theoretical Analysis of Composite Cylinders and Shells. *Journal of Composite Materials, 31*(7), 672-695.

Jeffreys, D., & Leaney, P. G. (2000). Dimensional control as an integral part of next-generation aircraft development. *Proceedings of the Institution of Mechanical Engineers, Part B: Journal of Engineering Manufacture, 214*(9), 831-835.

Johnston, A., Vaziri, R., & Poursartip, A. (2001). A Plane Strain Model for Process-Induced Deformation of Laminated Composite Structures. *J Compos Mater, 35*(16), 1435-1469.

Karadeniz, Z. H., & Kumlutas, D. (2007). A numerical study on the coefficients of thermal expansion of fiber reinforced composite materials. *Composite Structures, 78*(1), 1-10.

Kelly, A. (2008). Very stiff fibres woven into engineering's future: A long-term perspective. *Journal of Materials Science, 43*(20), 6578-6585.

Kelly, P. A., Umer, R., & Bickerton, S. (2006). Viscoelastic response of dry and wet fibrous materials during infusion processes. *Composites Part A: Applied Science and Manufacturing, 37*(6 SPEC ISS), 868-873.

Li, M., Li, Y., Zhang, Z., & Gu, Y. (2008). Numerical Simulation of Two-Dimensional Flow and Compaction During the Consolidation of Laminated Composites. *Polymer Composites, 29*(5), 560-568.

Li, M., & Tucker III, C. L. (2002). Modeling and simulation of two-dimensional consolidation for thermoset matrix composites. *Compos Part A: Appl Sci Manuf, 33*(6), 877-892.

Li, Y., Li, M., Gu, Y., & Zhang, Z. (2009a). Numerical and experimental study on the effect of lay-up type and structural elements on thickness uniformity of L-shaped laminates. *Appl Compos Mater, 16*(2), 101-115.

Li, Y., Li, M., Zhang, Z., & Gu, Y. (2009b). Numerical analysis of parametric effects on consolidation of angle-bended composite laminates. *Polym Compos, 30*(10), 1510-1516.

Loos, A. C., & Springer, G. S. (1983). CURING OF EPOXY MATRIX COMPOSITES. *Journal of Composite Materials, 17*(2), 135-169.

Mallon, P. J., O'Bradaigh, C. M., & Pipes, R. B. (1989). Polymeric diaphragm forming of complex-curvature thermoplastic composite parts. *Composites, 20*(1), 48-56.

Musselman, M. (2006). *Automotive composites: a design and manufacturing guide* (2nd^{e} éd.). Wheat Ridge, CO: Ray Publishing.

Naji, M. I., & Hoa, S. V. (1999). Curing of thick angle-bend thermoset composite part: curing cycle effect on thickness variation and fiber volume fraction. *J. Reinf. Plast. Compos., 18*(8), 702-723.

Naji, M. I., & Hoa, S. V. (2000). Curing of thick angle-bend thermoset composite part: curing process modification for uniform thickness and uniform fiber volume fraction distribution. *J. Compos. Mater., 34*(20), 1710-1755.

Nelson, R. H., & Cairns, D. S. (1989). Prediction of dimensional changes in composite laminates during cure. *34th International SAMPE Symposium, Reno, NV, USA.*(Vol. 34, pp. 2397-2410): Publ by SAMPE, Covina, CA, USA.

Niggemann, C., Young, S. S., Gillespie, J. W., & Heider, D. (2008). Experimental investigation of the controlled atmospheric pressure resin infusion (CAPRI) process. *Journal of Composite Materials, 42*(11), 1049-1061.

Oakeshott, J. L. (2003). Warpage of carbon-epoxy composite channels. *Plast Rubber Compos, 32*(3), 104-113.

Oakeshott, J. L., & Lemoine, D. (1998). Experimental study of spring forward in cured laminated U-channels made from unidirectionally reinforced carbon fibre-epoxy prepregs. *Plast Rubber Compos Process Appl, 27*(4), 190-199.

Potter, K. (1997). *Resin Transfer Moulding*. London: Chapman and Hall.

Potter, K. (2002). Beyond the pin-jointed net: Maximising the deformability of aligned continuous fibre reinforcements. *Compos Part A: Appl Sci Manuf, 33*(5), 677-686.

Potter, K. D. (2004). Deformation properties of uncured reinforcements - a reappraisal. *International Journal of Materials & Product Technology, 21*(1-3), 4-23.

Potter, K. D., Campbell, M., Langer, C., & Wisnom, M. R. (2005). The generation of geometrical deformations due to tool/part interaction in the manufacture of composite components. *Compos Part A: Appl Sci Manuf, 36*(2 SPEC ISS), 301-308.

Radford, D. W. (1987). *SHAPE STABILITY IN COMPOSITES (ANISOTROPIC).* Ph.D. thesis, Rensselaer Polytechnic Institute, New York.

Radford, D. W. (1993). Cure Shrinkage Induced Warpage in Flat Uni-Axial Composites. *J Compos Technol Res, 15*(4), 290-296.

Radford, D. W. (1995). Volume fraction gradient induced warpage in curved composite plates. *Compos Eng, 5*(7), 923-934.

Radford, D. W. (2010). Balancing mechanisms of distortion to yield distortion-free/shape stable composites. *Journal of Reinforced Plastics and Composites, 29*(12), 1875-1892.

Radford, D. W., & Diefendorf, R. J. (1993). Shape Instabilities in Composites Resulting from Laminate Anisotropy. *J Reinf Plast Compos, 12*(1), 58-75.

Radford, D. W., & Rennick, T. S. (2000). Separating sources of manufacturing distortion in laminated composites. *J Reinf Plast Compos, 19*(8), 621-641.

Rifay, M. (2010). *Fabrication de plaques auto-raidies par injection flexible.* Mémoire de maîtrise inédit, École Polytechnique de Montréal, Montréal.

Robitaille, F., & Gauvin, R. (1998a). Compaction of textile reinforcements for composites manufacturing. I: Review of experimental results. *Polym. Compos., 19*(2), 198-216.

Robitaille, F., & Gauvin, R. (1998b). Compaction of textile reinforcements for composites manufacturing. II: Compaction and relaxation of dry and H_2O-saturated woven reinforcements. *Polymer Composites, 19*(5), 543-557.

Robitaille, F., & Gauvin, R. (1999). Compaction of Textile Reinforcements for Composites Manufacturing. III: Reorganization of the Fiber Network. *Polymer Composites, 20*(1), 48-61.

Ruiz, E., Briones, L. R., Allard, É., & Trochu, F. (2008). *Flexible Injection: A Novel LCM Technology for Low Cost Manufacturing of High Performance Composites. Part I: Experimental Investigation*. Proceedings FPCM9, Montréal, Canada.

Ruiz, E., & Trochu, F. (2005a). Comprehensive thermal optimization of liquid composite molding to reduce cycle time and processing stresses. *Polym Compos, 26*(2), 209-230.

Ruiz, E., & Trochu, F. (2005b). Numerical analysis of cure temperature and internal stresses in thin and thick RTM parts. *Compos Part A: Appl Sci Manuf, 36*(6), 806-826.

Ruiz, E., & Trochu, F. (2005c). Thermomechanical Properties during Cure of Glass-Polyester RTM Composites: Elastic and Viscoelastic Modeling. *J Compos Mater, 39*(10), 881-916.

Ruiz, E., & Trochu, F. (2011). Manufacture of composites by a flexible injection process using a double or multiple cavity mold. US 7,866,969 B2.

Salomi, A., Garstka, T., Potter, K., Greco, A., & Maffezzoli, A. (2008). Spring-in angle as molding distortion for thermoplastic matrix composite. *Compos Sci Technol, 68*(14), 3047-3054.

Schapery, R. A. (1968). Thermal Expansion Coefficients of Composite Materials Based on Energy Principles. *J Compos Mater, 2*(3), 380-403.

Sehanobish, K. (2009). *Engineering plastics and plastic composites in automotive applications* Warrendale, PA: SAE international.

Sharma, S. D., Kar, K. K., Kumar, P., & Kar, K. K. (2006). Surface roughness of fiber reinforced plastic laminates fabricated using rubber pressure molding technique. *Polym Compos, 27*(5), 504-512.

Svanberg, J. M. (2001). An experimental investigation on mechanisms for manufacturing induced shape distortions in homogeneous and balanced laminates. *Composites - Part A: Applied Science and Manufacturing, 32*(6), 827-838.

Svanberg, J. M. (2002). *Predictions of manufacturing induced shape distortions - high performance thermoset composites.* doctoral thesis, Lulea university of technology.

Svanberg, J. M., Altkvist, C., & Nyman, T. (2005). Prediction of shape distortions for a curved composite C-spar. *Journal of Reinforced Plastics and Composites, 24*(3), 323-339.

Svanberg, J. M., & Holmberg, J. A. (2004a). Prediction of shape distortions Part I. FE-implementation of a path dependent constitutive model. *Composites Part A: Applied Science and Manufacturing, 35*(6), 711-721.

Svanberg, J. M., & Holmberg, J. A. (2004b). Prediction of shape distortions. Part II. Experimental validation and analysis of boundary conditions. *Compos Part A: Appl Sci Manuf, 35*(6), 723-734.

Toll, S., & Manson, J. A. (1994). An analysis of the compressibility of fibre assemblies. *Proceedings of the Sixth International Conference on Fibre Reinforced Composites*.

Touraine, B. (2005). *Simulation d'un procédé d'injection sous paroi flexible.* Mémoire de maîtrise inédit, École Polytechnique de Montréal, Montréal.

Trochu, F., Soukane, S., & Touraine, B. (2008). *Flexible Injection: A Novel LCM Technology for Low Cost Manufacturing of High Performance Composites. Part II: Numerical Model*. Proceedings FPCM9, Montréal, Canada.

Twigg, G., Poursartip, A., & Fernlund, G. (2004a). Tool-part interaction in composites processing. Part I: Experimental investigation and analytical model. *Composites Part A: Applied Science and Manufacturing, 35*(1), 121-133.

Twigg, G., Poursartip, A., & Fernlund, G. (2004b). Tool-part interaction in composites processing. Part II: Numerical modelling. *Composites Part A: Applied Science and Manufacturing, 35*(1), 135-141.

Vanclooster, K., Lomov, S. V., & Verpoest, I. (2010). Inter-ply and tool-ply friction measurement of woven reinforced thermoplastic composites at forming conditions.(pp. 381-388).

Wang, J., Kelly, D., & Hillier, W. (2000). Finite element analysis of temperature induced stresses and deformations of polymer composite components. *J Compos Mater, 34*(17), 1456-1471.

Wang, X., Zhang, Z., Xie, F., Li, M., Dai, D., & Wang, F. (2009). Correlated rules between complex structure of composite components and manufacturing defects in autoclave molding technology. *Journal of Reinforced Plastics and Composites, 28*(22), 2791-2803.

Wiersma, H. W., Peeters, L. J. B., & Akkerman, R. (1998). Prediction of Springforward in Continuous-Fibre/Polymer L-Shaped Parts. *Compos Part A: Appl Sci Manuf, 29*(11), 1333-1342.

Wisnom, M. R., Gigliotti, M., Ersoy, N., Campbell, M., & Potter, K. D. (2006). Mechanisms generating residual stresses and distortion during manufacture of polymer-matrix composite structures. *Composites Part A: Applied Science and Manufacturing, 37*(4), 522-529.

Wisnom, M. R., Jones, M. I., & Hill, G. F. J. (2001). Interlaminar tensile strength of carbon fibre-epoxy - Specimen size, layup and manufacturing effects. *Adv Compos Lett, 10*(4), 171-177.

Yang, S. Y., & Huang, C. K. (1997). Curvature Predictions of Flat Advanced Composite Tools Based on Measured Volume Fraction Gradient. *Journal of Advanced Materials, 28*(2), 47-55.

Yang, S. Y., Huang, C. K., & Chen, C. C. (2003). Effect of processing on precision of composite panels. *Mater Manuf Process, 18*(5), 769-781.

Yang, S. Y., Huang, C. K., & Wu, C. B. (1996). Influence of processing on quality of advanced composite tools. *J. Adv. Mater., 27*(3), 37-44.

Yoon, K. J., & Kim, J.-S. (2001). Effect of thermal deformation and chemical shrinkage on the process induced distortion of carbon/epoxy curved laminates. *J Compos Mater, 35*(3), 253-263.

Zahlan, N., & O'Neill, J. M. (1989). Design and fabrication of composite components; the spring-forward phenomenon. *Composites, 20*(1), 77-81.

Zhu, Q., Geubelle, P. H., Li, M., & Tucker Iii, C. L. (2001). Dimensional accuracy of thermoset composites: Simulation of process-induced residual stresses. *J Compos Mater, 35*(24), 2171-2205.

Ziehl, P. H. (2000). *Development of a damage based design criterion for fiber reinforced vessels.* Ph.D. thesis, The University of Texas at Austin, Austin.